RETINAL AND CHOROIDAL OXIMETRY USING SNAPSHOT MULTISPECTRAL IMAGING

Tushar R. Choudhary

Submitted for the Degree of
Doctor of Philosophy
at Heriot-Watt University
on completion of research in the
School of Life Sciences
February 2015

ABSTRACT

The principal aim of the research was to validate and develop a non-invasive multispectral imaging technique of measuring oxygen saturation in retinal and choroidal vasculature. The Image replicating imaging spectrometer (IRIS) snapshot multispectral fundus camera used for retinal imaging, and image analysis protocols used to perform oximetry are described.

In vitro and *in vivo* validation of oximetry techniques was performed. For *in vitro* validation an artificial eye containing blood at varying oxygenation was used. For *in vivo* validation the pig was used as an animal model. The calculated oxygen saturation was compared to blood gas analysis (gold standard) results and was found to be in close agreement.

Retinal oximetry was performed on healthy human subjects. The average oxygen saturation value (± SD) for retinal arterioles and venules were 96.08% ± 1.9% and 68.04% ± 2.1%, respectively.

The application of retinal oximetry technique was explored by conducting human hypoxia trials, in which the effect of acute mild hypoxia on retinal oxygenation and autoregulation was assessed on healthy human subjects. Hypoxic exposure resulted in a decline in both retinal arterial and venous saturation, as well as a significant increase in retinal vessel calibre, suggesting an autoregulatory response.

This thesis also explored the possibility of exploiting fundus reflections to measure the choroidal oxygenation non-invasively. Fundus reflection intensity at two wavelengths, 780 nm and 800 nm (oxygen sensitive and isosbestic) were used to calculate intensity ratio (R), which is directly proportional to the blood oxygenation. A pilot study on 10 healthy humans was conducted. Fundus reflection was recorded at room air (normoxia) and 15% inspired oxygen (mild hypoxia). A significant reduction ($P < 0.001$) in intensity ratio was observed during hypoxia.

To my mom and dad.

ACKNOWLEDGEMENTS

I would like to thank my supervisors Professor Derek Ball and Professor Andy Harvey, for giving me the opportunity to conduct this research and for their patience, support and guidance in helping me complete this work. I would also like to express my gratitude to my past and present colleagues in the Imaging Concepts Group; in particular Alistair Gorman, Javier Fernandez Ramos and Lewis Mackenzie for their excellent Matlab and technical skills that helped me in the course of my research. I would like to thank my clinical collaborator Professor Andrew McNaught for his help and support. I would also like to thank my colleagues Laurence Brewer and Marieke van der Putten to take out time to proofread draft of my thesis.

I am extremely grateful to all the people who participated in the human trial of the research, especially to all my friends whom I unashamedly and repeatedly exploited in the name of science.

I am grateful to my parents Rakesh and Kumud, my sister Vatsala, my brother in law Vishal, my niece Vamika and my brother Himanshu, for their unconditional love and support.

I am also extremely grateful to Vrushali Patil for her love and support during the difficult years of PhD and for sharing her enthusiasm for science, and life, with me.

Tushar Choudhary

February 2015

ACADEMIC REGISTRY
Research Thesis Submission

Name*:*			
School/PGI:			
Version: *(i.e. First, Resubmission, Final)*		Degree Sought (Award **and** Subject area)	

Declaration

In accordance with the appropriate regulations I hereby submit my thesis and I declare that:

1) the thesis embodies the results of my own work and has been composed by myself
2) where appropriate, I have made acknowledgement of the work of others and have made reference to work carried out in collaboration with other persons
3) the thesis is the correct version of the thesis for submission and is the same version as any electronic versions submitted*.
4) my thesis for the award referred to, deposited in the Heriot-Watt University Library, should be made available for loan or photocopying and be available via the Institutional Repository, subject to such conditions as the Librarian may require
5) I understand that as a student of the University I am required to abide by the Regulations of the University and to conform to its discipline.

* *Please note that it is the responsibility of the candidate to ensure that the correct version of the thesis is submitted.*

Signature of Candidate*:*		Date:	

Submission

Submitted By *(name in capitals):*	
Signature of Individual Submitting:	
Date Submitted:	

For Completion in the Student Service Centre (SSC)

Received in the SSC by *(name in capitals):*			
Method of Submission *(Handed in to SSC; posted through internal/external mail):*			
E-thesis Submitted (**mandatory for final theses)**			
Signature:		Date:	

Please note this form should bound into the submitted thesis.

Updated February 2008, November 2008, February 2009, January 2011

DECLARATION

The work presented in this thesis was carried out in Imaging Concepts Group, led by Professor Andy Harvey (University of Glasgow, formerly at Heriot-Watt University, Edinburgh). In the course of this thesis I have acknowledged the contributions to my research made by collaborators. The rest of the work presented here is mine alone.

Important contributions were made in the following areas

- Chapter 2: The IRIS snapshot multispectral fundus camera was constructed by Imaging Concepts Group. The algorithms and software control of the camera was also created by Imaging Concepts Group. Some modifications in the software were made by the author along the course of the research.
- Chapter 3: The model eye was constructed by Imaging Concepts Group and has been used previously for validation purpose for a sequential spectral imaging fundus camera.
- Chapter 4, Chapter 5 and Chapter 6: The algorithms to process and analyse retinal images were created by Imaging Concepts Group. As the project evolved, many important modifications in the algorithms were made by the author with the help from Imaging Concepts Group. Few new algorithms for easy analysis of oximetry data were also created by the author with the help from Imaging Concepts Group.

Tushar Choudhary
February 2015

LIST OF PUBLICATIONS

1. T. Choudhary, D. Ball, J. Fernandez, A. McNaught, A. Harvey, “Assessment of acute mild hypoxia on retinal oxygen saturation using snapshot retinal oximetry” *Invest Ophthalmol Vis Sci.* 2013;54:7538-7543.
2. T. Choudhary, D. Ball, E. Stefansson, A. Harvey, "Choroidal oximetry using fundus (red-eye) reflection", to be submitted in Journal of Biomedical Optics
3. T. Choudhary, D. Ball, J. Fernandez, A. McNaught, A. Harvey, "Hypoxia and autoregulation in retinal vessels", Oximetry Workshop, January 2014, Birmingham.
4. T. Choudhary, D. Ball, E. Stefansson, A. Harvey, "Choroidal Oximetry using red-eye reflection", Oximetry Workshop, January 2014, Birmingham.
5. Lewis E. Mackenzie, T. Choudhary, A. Davies, K. Smith, A. Harvey, "Novel applications of oximetry in systemic and peripheral vasculature", PHOTON14, Institute of Physics, London
6. J. Fernandez, L. Brewer, T. Choudhary, A. Gorman, A. Harvey, "High speed snapshot multispectral imaging", PHOTON14, Institute of Physics, London
7. T. Choudhary, D. Ball, A. Harvey, “The effect of mild hypoxia on retinal oxygen saturation” IOVS 2013; ARVO E-Abstract 103:43.
8. T. Choudhary, D. Ball, A. Harvey, "Vascular Oximetry: the retina and beyond", Feb 2013, SUPA PaLS Meeting, Heriot-Watt University, Edinburgh
9. Andy McNaught, T. Choudhary, ...A. Harvey, "Retinal Oximetry: update", The British Eye Study Group 2013 annual meeting, Alfriston, Sussex
10. T. Choudhary, D. Ball, A. Gorman, A. Harvey, “Comparative measurements of oxygen saturation in the femoral and retinal arteries of pigs”, Oximetry conference, January 2012, Reykjavik, Iceland

CONTENTS

List of Figures

List of Tables

ABBREVIATIONS

c: concentration or haematocrit

CA: ciliary artery

CBF: cerebral blood flow

CCD: charged coupled device

CRA: central retinal artery

CRAO: central retinal artery occlusion

CRVO: central retinal vascular occlusion

D: dioptre

d: distance/path length

DR: diabetic retinopathy

FEP: fluorinated ethylene propylene

FiO_2: fraction of inspired oxygen

fMRI: functional magnetic resonance imaging

FWHM: full-width half maximum

GUI: graphical user interface

Hb: haemoglobin (without any oxygen attached)

HbO_2: oxygenated haemoglobin

I: intensity of light

I_0: intensity of incident light

ICA: internal carotid artery

IOP: intra ocular pressure

IRIS: image replicating imaging spectrometer

I_T: intensity of transmitted light

n: refractive index

OA: ophthalmic artery

OD (λ): optical density (wavelength)

OD: optical density

ODR: optical density ratio

OS: oxygen saturation

PCO_2: pressure of carbon dioxide/ carbon dioxide tension

PO_2: pressure of oxygen/ oxygen tension

POAG: primary open angle glaucoma

RPE: retinal pigment epithelium

RVO: retinal vascular occlusion

sCMOS: scientific complementary metal–oxide–semiconductor

SD: standard deviation

SO_2: oxygen saturation

SPCA: short posterior ciliary artery

T: transmission

VEGF: vascular endothelial growth factor

ε: extinction coefficient of blood

Standard SI-units and metric system prefixes used in the text are not listed here.

Chapter 1

Introduction

1.1. Introduction

This chapter describes anatomy, structure and blood supply of the retina and eye. It also describes in detail some retinal pathologies and retinal oxygenation in health and diseases. An overview of existing retinal oximetry techniques is also given.

1.2. Human Eye

The human eye is an extremely specialised photoreceptive organ. It processes light energy from the environment in specialised nerve cells located in the retina. These cells are called rods and cones, and they produce signals that are relayed to the optic nerve and then to the brain, where the information is processed and interpreted as vision.

1.2.1. Structure of Eye

The eye is roughly a sphere that is 2.5 cm in diameter. The eye is made up of three basic layers known as tunics. They are the fibrous (corneoscleral) outer coat, the uvea or uveal tract (composed of choroid, ciliary body and iris) and the inner neural layer (retina).

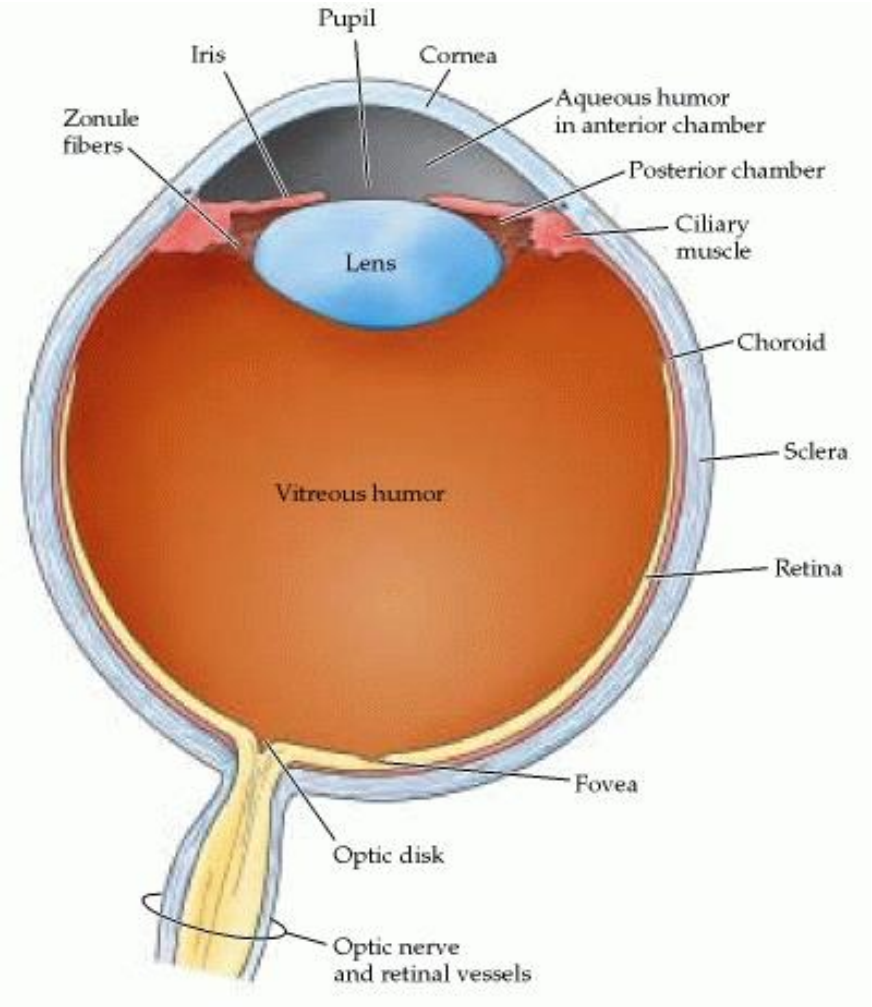

Figure 1.1: The structure of eye [1].

The space between the lens and the cornea is known as the anterior chamber, which is filled with a clear, watery fluid called aqueous humour. The main function of the aqueous humour is to supply nutrients to avascular ocular tissues; posterior cornea, trabecular meshwork as well as the lens. The region between the lens and the iris is the posterior chamber where aqueous humour is produced by the ciliary processes. The space between the lens and the retina is called the vitreous humour or vitreous body filled with a thick, gel like substance. The vitreous humour helps to keep retina in place by pressing it against the choroid. It accounts for about 80% of the volume of the eye. It also maintains the shape of the eye and contains phagocytic cells that remove blood and other debris to provide unobstructed transmission of light.

1.2.2. Retina

The retina (Figure 1.2) is approximately 0.5 mm thick and lines the back of the eye. It is the primary visual receptive tissue consisting of two basic layers: the inner layer is the neurosensory retina with the outer layer comprised of the retinal pigment epithelium (RPE).

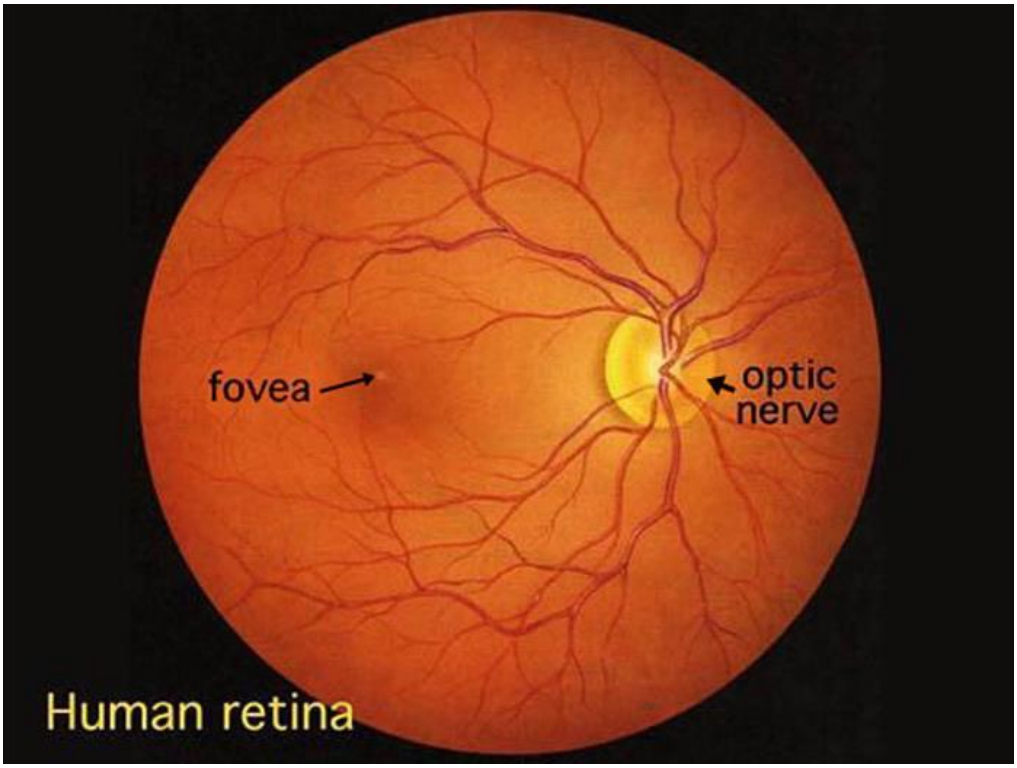

Figure 1.2: Human retina [2].

The retina is a complex, layered structure of interconnected neurons. Photoreceptor cells are a type of retinal neuron which are responsible for the absorption of photons of light. These cells occupy the retinal layer farthest from the incoming light. In the center of the retina is the optic nerve (Figure. 1.2), that appears as an oval white area measuring approximately 3 mm^2. From the center of the optic nerve radiate the major blood vessels of the retina. Area near the optic disc is called macula and is also known as yellow spot. The centre of macula is the fovea which is an oval-shaped, blood-vessel-free reddish spot.

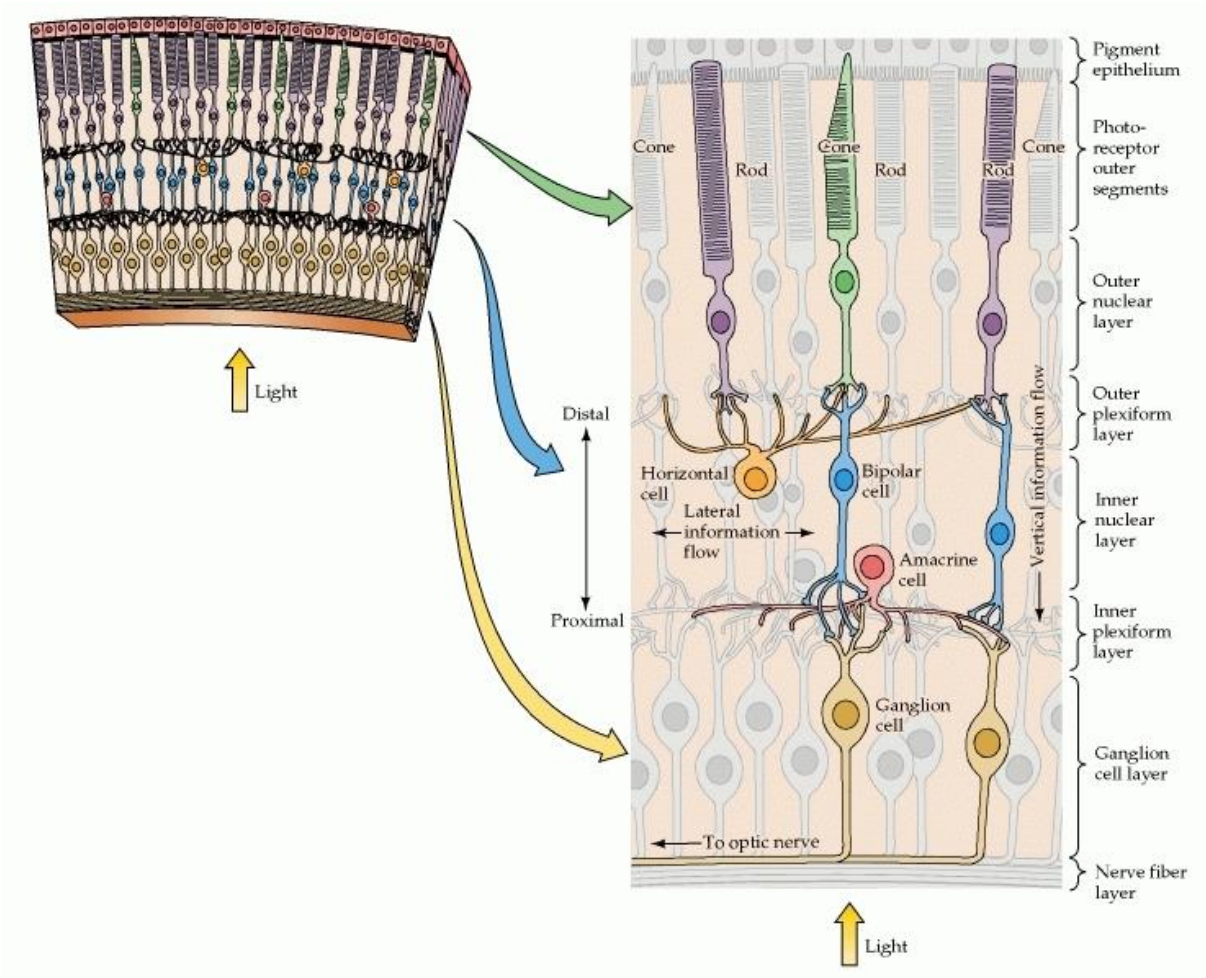

Figure 1.3: Cellular organisation of retina [1].

There are two types of photoreceptor cells in retina, called rods and cones. The retina contains about 120 million rod cells and 6 million cone cells. Their distribution over the retina (Figure. 1.4) is not uniform with the cones present at a low density throughout the retina, with a high concentration in foveal region, whereas rods are present at high concentration throughout most of the retina, with a sharp decline in the fovea. Cones are adapted for photopic (daytime) and colour vision. There are three types of cones: one containing visual pigment most sensitive to blue light, one that is sensitive to green light, and one that is most sensitive to long wavelengths that include red and yellow light. The rods are extremely sensitive to light but provide very low spatial resolution, whereas the cones are comparatively insensitive to light but have very high spatial resolution.

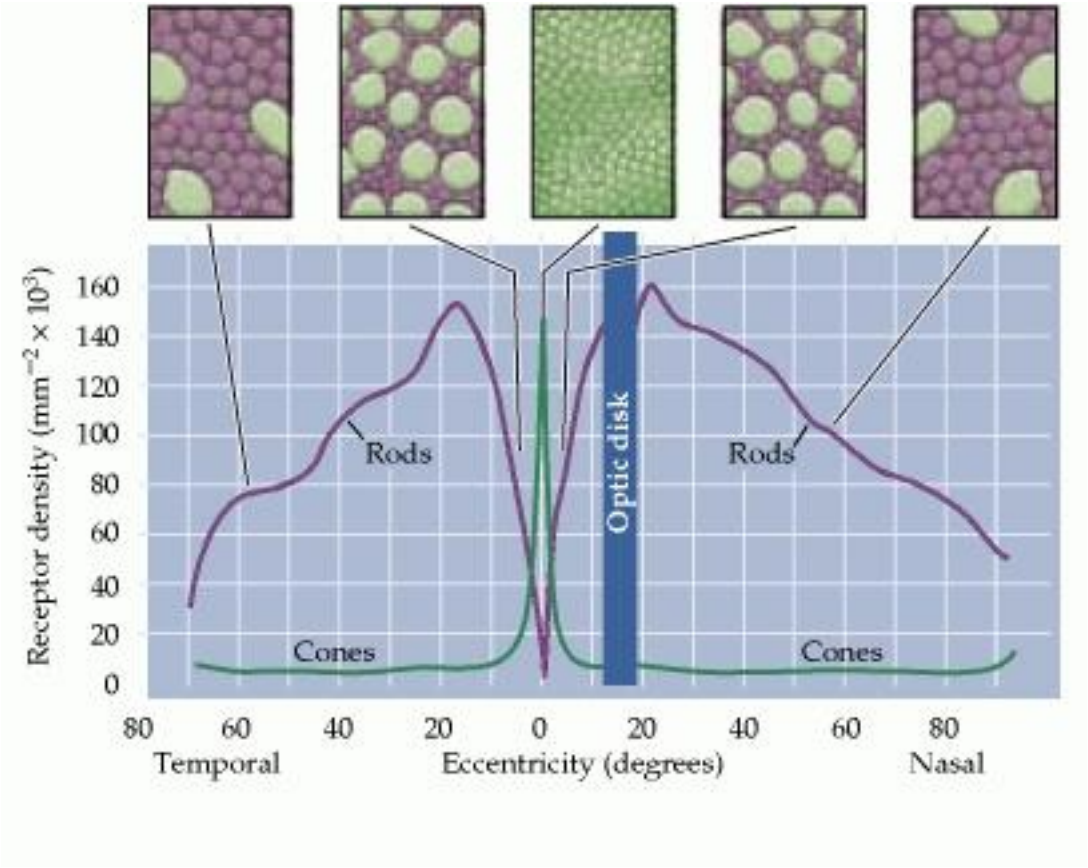

Figure 1.4: The distribution of rods and cones in human retina in the left eye [1].

1.2.3. The Choroid

The choroid is highly vascular, dark brown tissue located between retina and sclera. The main function of the choroid is to supply oxygen and nutrients to the outer retina. Histologically, the choroid can be divided into five layers; Bruch's membrane, the choroiocapillaris, the two vascular layers (Haller's and Sattler's), and the suprachoroid (Figure 1.5)[3]. The average thickness of choroid is approximately 400 μm [4] and its thickness is affected by diurnal variations [5], intraocular pressure (IOP) [6] , refractive state of the eye[7] and the blood flow variations [8].

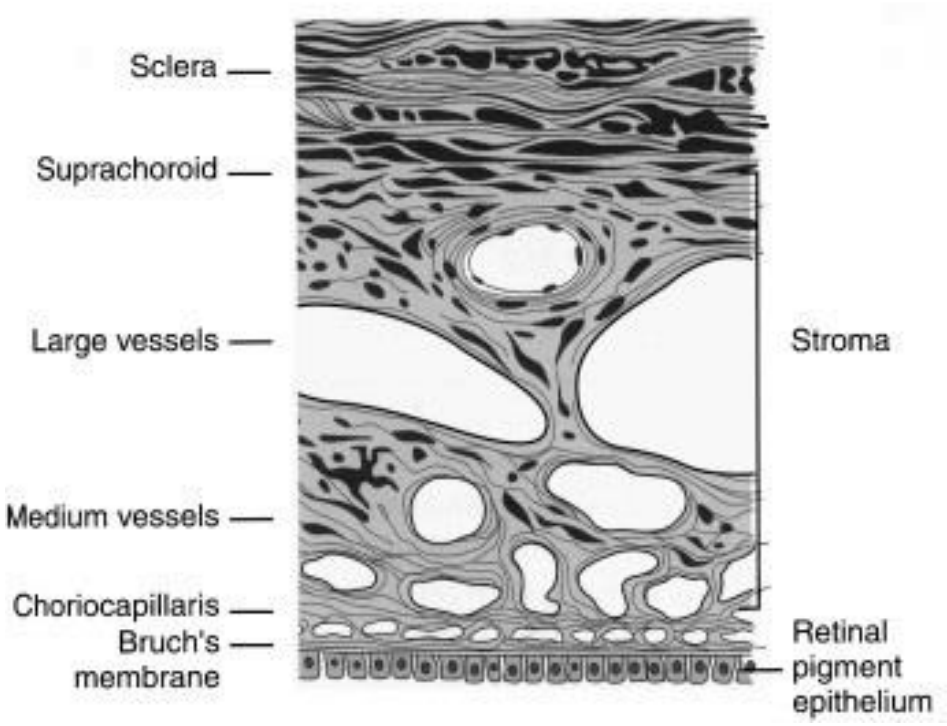

Figure 1.5: A diagram of different layers of choroid [9].

The choriocapillaris is a highly anastomosed network of capillaries, apposed to Bruch's membrane[10], and is thickest at the fovea (10 μm), thinning to about 7 μm in the periphery. The main vascular region of the choroid consists of the outer Haller's layer and the inner Sattler's layer. The Haller's layer consists of large blood vessels and the inner Sattler's layer consists of medium and small arteries and arterioles that feed the capillary network, and veins.

1.3. Blood Supply to the Retina

The retina has high oxygen demand and to meet this high metabolic requirement it is supplied by two vascular systems: the retinal circulation and the choroidal circulation [11]. The choroid supplies the outer layers of the retina including the photoreceptors. The inner layers of the retina including the retinal ganglion cells are supplied by the retinal vessels. Approximately 65% of the oxygen consumed by the retina is delivered by the choroid. Retinal and choroidal blood vessels are both supplied from the ophthalmic artery, which in turn is a branch of the internal carotid artery (see Figure 1.6).

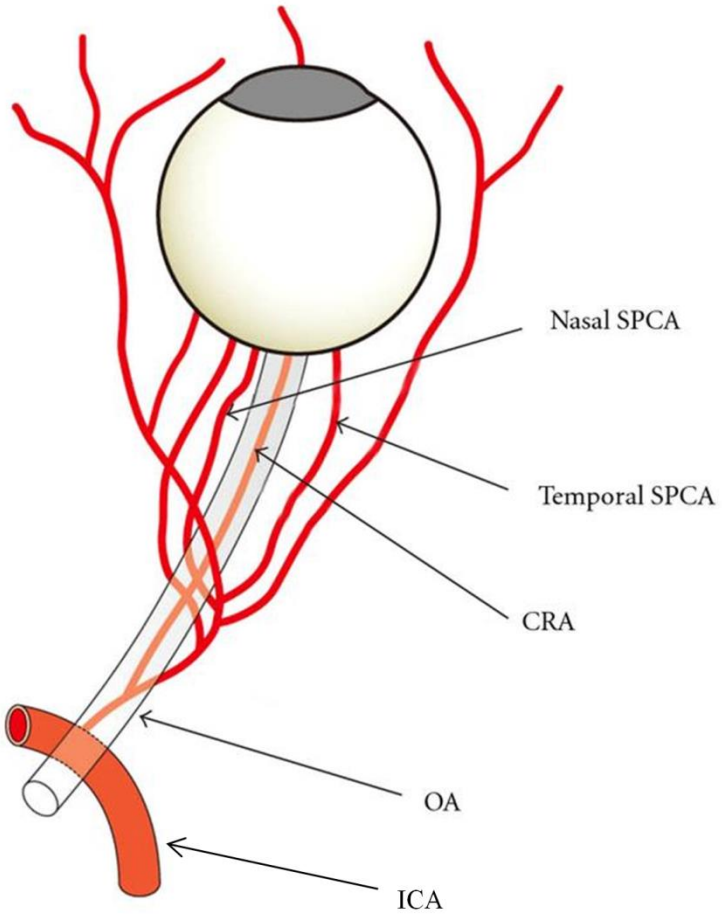

Figure 1.6: The blood supply of the eye. The ophthalmic artery (OA) arises from the internal carotid artery (ICA) and supplies the eye. Central retinal artery (CRA) and ciliary artery (CA) are the branches of ophthalmic artery which supplies to retina and choroid. SPCA (short posterior ciliary artery) [12].

The ophthalmic artery branches into central retinal artery and ciliary arteries. The central retinal artery constitutes the retinal vasculature; it enters the optic disc and branches into four intra-retinal arterioles (Figure 1.7) namely superior, inferior, nasal, and temporal retinal arterioles. These arterioles further bifurcate to form smaller arteriole branches and eventually feed into the capillary bed [13].

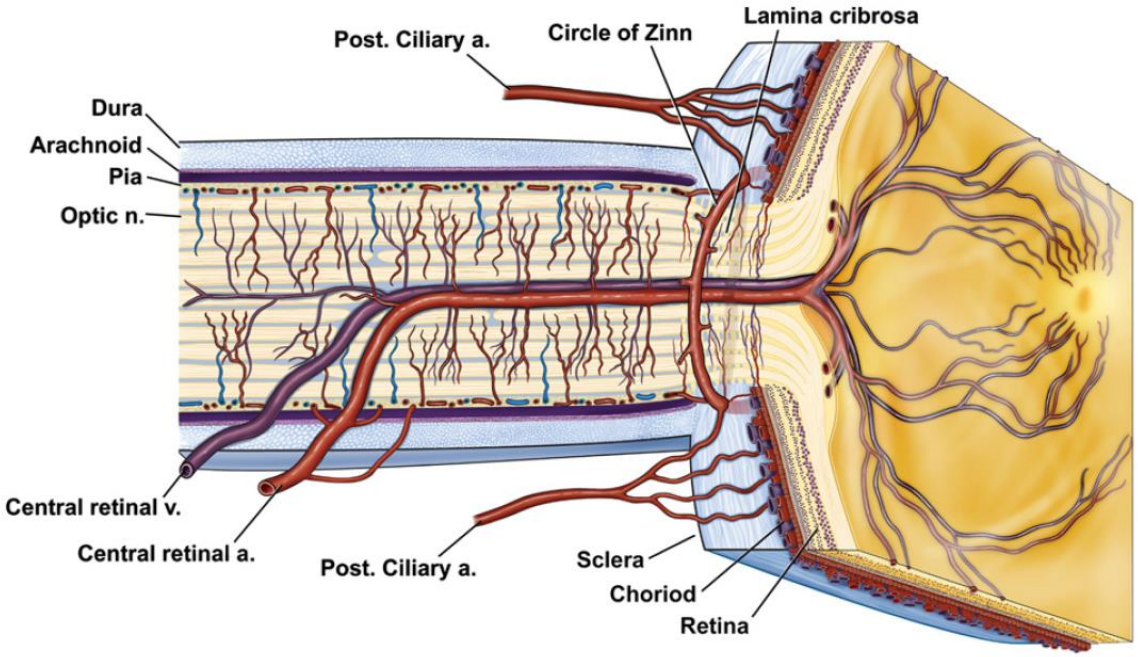

Figure 1.7: Anatomy of ocular circulation (a-artery, b-vein, n-nerve).Cut away drawing along the superioreinferior axis of the human eye through the optic nerve, showing the vascular supply to the retina and choroid. Drawings by Dave Schumick from [14].

Retinal capillaries are 5-7 µm in diameter and are organised into two layer network[13], in the nerve fibre layer and the deeper layer in the inner nuclear layer. Retinal capillaries are more profuse in the macula and spreads across the peripheral retina and are absent in the fovea superficial layer located and capillary free zone across arterioles and venules [15]. The fovea being devoid of retinal capillaries is supplied by choroidal circulation[16], the retina in this region, being very thin facilitates oxygenation from the choroid. The retinal venules collect the deoxygenated blood from the arteriolar capillary network, follows same course as retinal arterioles and drain into central retinal vein. The central retinal vein leaves the eye via the optic disc.

The posterior ciliary, which branches from ophthalmic artery, constitutes the choroidal circulation. The choroid can be divided into five layers; Bruch's membrane, suprachoroidea and three vascular layers of choriocapillaries, Sattler's layer and Haller's layer. Haller's layer comprises of large arteries and veins and Sattler's layer includes medium and small arterioles which supplies to the choriocapillaries [13]. A network of vortex veins drains blood from the choroid which then merges into ophthalmic vein [17].

The retinal blood flow is characterised by a low perfusion rate (approx 40–80 μl/min), a high vascular resistance, a high oxygen extraction and accordingly a high arteriovenous oxygen extraction (30-35%). On the other hand, the choroid shows the highest perfusion rate per gram tissue of all vascular beds within the human body (approximately 1,200–2,000 μl/min), a low vascular resistance, a low oxygen extraction and a low arteriovenous oxygen extraction. Oxygen saturation in retinal arterioles and venules in healthy volunteers is found to be about 92-97% and 58-65% [18, 19]. This suggests that the arteriovenous oxygen saturation difference in retinal circulation is about 30%, whilst in the choroid it is found to be about 3% [20].

Whereas autoregulatory processes exist in retinal blood vessels there is a limited degree of autoregulation in choroidal blood vessels [21-23]. Autoregulation of blood flow, through metabolic regulation, can be defined as the capacity of an organ or tissue to regulate its blood supply according to its metabolic need [23-25]. Whereas the retinal circulation is sensitive to changes in blood oxygenation, the choroid appears to be unresponsive to variations in oxygen availability [26, 27]. Retinal autoregulation of blood flow is the result of the interaction of myogenic and metabolic mechanisms via the release of vasoactive substances and adaptation of the vascular tone of arterioles and capillaries [25]. The retina can respond to physiological variations in perfusion pressure, blood gases, intraocular pressure, and as well as to visual stimulation like flicker stimulation and light/dark transition. Hypoxia induces vasodilation of retinal vessels, which increases retinal blood flow[28-34]; a response that can also be observed in the cerebral circulation [35, 36]. The retinal circulation can actively autoregulate the blood flow for a wide range of perfusion pressure [37-39]. Retinal blood flow has been reported to increase during visual stimulation such as light/dark transition[40, 41] and flicker stimulation [21, 42-44].

Choroidal circulation is insensitive to change in partial pressure of oxygen but reacts towards changes in partial pressure of CO_2 [26, 27]. Choroidal circulation reacts in exactly the opposite way to retinal circulation when exposed to light/dark transition. Studies reported that there is a decrease in choroidal flow in dark, and the flow increased when it was exposed to light [45, 46]. Flicker stimulation has no effect on choroidal blood flow [47].

1.4. Retinal Pathologies

1.4.1. Diabetic Retinopathy

Diabetic retinopathy is an ocular complication associated with both type I and type II diabetes mellitus [48]. Diabetic retinopathy (DR) is a prime cause of blindness in developed countries. Diabetes is one of the leading causes of blindness in people of working age in the UK [49]. According to a recent study there are 4,200 people in England who are blind due to diabetic retinopathy and this number increases by 1,280 each year [50]. DR is characterised by hyperglycaemia, basement membrane thickening[51], pericyte loss, microaneurysms, intra retinal microvascular anomalies[52] and preretinal neovascularisation [53, 54]. It advances slowly from an early stage to an advanced vision threatening stage and is classed into early, middle and advanced levels.

Hyperglycaemia seems to be a key factor in the aetiology of diabetic retinopathy. Hyperglycaemia is linked with a variety of biological consequences identified in the progression of diabetic retinopathy such as glucose transport, basement membrane thickening, pericyte loss, blood characteristics [55]. Studies in animal models such as the streptozotocin rat suggest that long-term hyperglycaemia is essential to evoke changes to the retinal vasculature[56]. Vascular endothelial growth factor (VEGF) plays an early role in the onset of diabetic retinopathy. VEGF is clearly elevated in retinal tissues of patients with diabetes [57, 58]. VEGF is a strong angiogenic factor capable of stimulating endothelial cells to degrade extracellular eye matrix, migrate, proliferate and form tubes [59, 60]. Recent studies show that it also acts as a survival factor for newly formed vessels [61].

The microvascular abnormalities and capillary damage in DR eventually leads to poor distribution of blood, which results in retinal tissue hypoxia. It is still not well understood whether microvascular damage leads to tissue hypoxia or tissue hypoxia occurs before any microvascular damage. Diabetic retina with only few microaneurysms present was also found to be hypoxic [62]. Hyperoxia has been demonstrated to reverse some effects of DR, emphasising the importance of hypoxia in the pathogenesis of DR [63].

1.4.2. Glaucoma

Glaucoma is an optic neuropathy of unknown aetiology which is characterised by structural change in optic nerve and visual field defects [64]. Glaucoma is one of the leading causes of blindness in the western world. Increased intraocular pressure (IOP) is one of the main risk

factor for glaucoma. Impaired ocular blood flow regulation is gaining popularity as other major risk factor for glaucoma[65] as many patients with glaucoma have normal or low IOP [64]. Till date the accepted form of treatment for glaucoma remains IOP reduction as it not only reduces mechanical pressures but may also increase blood flow [65]. The effect of intraocular pressure on glaucoma can be attributed to mechanical stress[66] and also explained via the effects of intraocular pressure on ocular blood flow [23]. In retina, the difference between arterial and venous pressure is the perfusion pressure. In the eye, the venous pressure is roughly equal to the intraocular pressure [67], hence a high intraocular pressure with a low systemic blood pressure will result in reduced blood flow[68] and in turn to hypoxia in the retinal tissue. However relation between ocular perfusion pressure and blood flow in the eye is complex [23]. Studies also suggest evidence of hypoxia in the optic nerve head and in the retina in glaucomatous eye [69]. Many population based studies have shown that low ocular perfusion pressure is a risk factor for prevalence, incidence and progression of glaucoma [70, 71].

1.4.3. Retinal Vascular Occlusion

Retinal vascular obstructive disease is a condition where an obstruction in the blood vessels of the retina occurs. The retinal occlusions can be broadly divided into artery occlusion or vein occlusion. Retinal vein occlusions are much common than artery occlusion. Both retinal arterial and venular occlusions can be further sub-divided into central occlusion or branch occlusion, depending on the site.

1.4.3.1. Central Retinal Vein Occlusion (CRVO)

Central retinal vein occlusion is a common retinal vascular disorder which presents with sudden onset of vision loss and characterised by retinal hemorrhages, tortuous retinal veins, cotton-wool spots, macular edema, and optic disc edema [72]. Central retinal vein occlusion is caused as a result of a thrombus in the central retinal vein. CRVO results in retinal ischemia, hypoxia and neovascularisation. The incidence of CRVO increases with age, hypertension, cardiovascular diseases, diabetes, high IOP and history of glaucoma [73, 74]. There is a reduced blood flow in the retina in patients with CRVO [75]. Reduction in blood flow to the retina as result of CRVO affects the inner retinal oxygenation [76]. Currently, the treatment for CRVO includes laser photocoagulation, systemic steroids, anticoagulants, antiplatlet drugs [77]. Except for laser photocoagulation, there is no clear evidence that any other treatment is effective in CRVO [78].

1.4.3.2. Central Retinal Artery Occlusion

Central retinal artery occlusion (CRAO) is the occlusion of the central retinal artery which results in vision loss. CRAO is the ocular equivalent to the cerebral stroke [79]. The most common cause of CRAO is an embolus blocking the retinal artery[80], or could also caused by an occlusive thrombus at the level immediately posterior to the lamina cribrosa [81]. CRAO generally affects older patients over 60 years of age[82] and the incidence of disease is associated with atherosclerosis, systemic hypertension and diabetes [83]. The symptoms of CRAO are usually sudden, painless dramatic loss of vision, although some vision can be improved within a few hours of the initial onset [84]. A study on a primate animal model demonstrated no permanent damage to retina by ischemia up to about 97 min due to retinal artery occlusion [85]. The study also showed that long CRAO and ischemia resulted in more extensive and irreversible damage to retina.

1.5. Motivation Behind Retinal Oximetry

Historically imaging of the fundus began more than one and a half century ago, when Charles Babbage invented the first direct ophthalmoscope in 1845 [86, 87]. The credit for inventing the modern ophthalmoscope goes to von Helmholtz, who independently reinvented it in 1851 [88]. Present day fundus cameras are based on the work of Helmholtz. Helmholtz ophthalmoscope (figure 1.8) used a naked candle as the illumination source. Notable improvements were made in the image quality by Gerloff [89] in 1891, who used flash powder illumination, and by Dimmer[90] in 1899 who switched to carbon arc illumination.

Figure 1.8: Early Model of Helmholtz ophthalmoscope, 1851 [91].

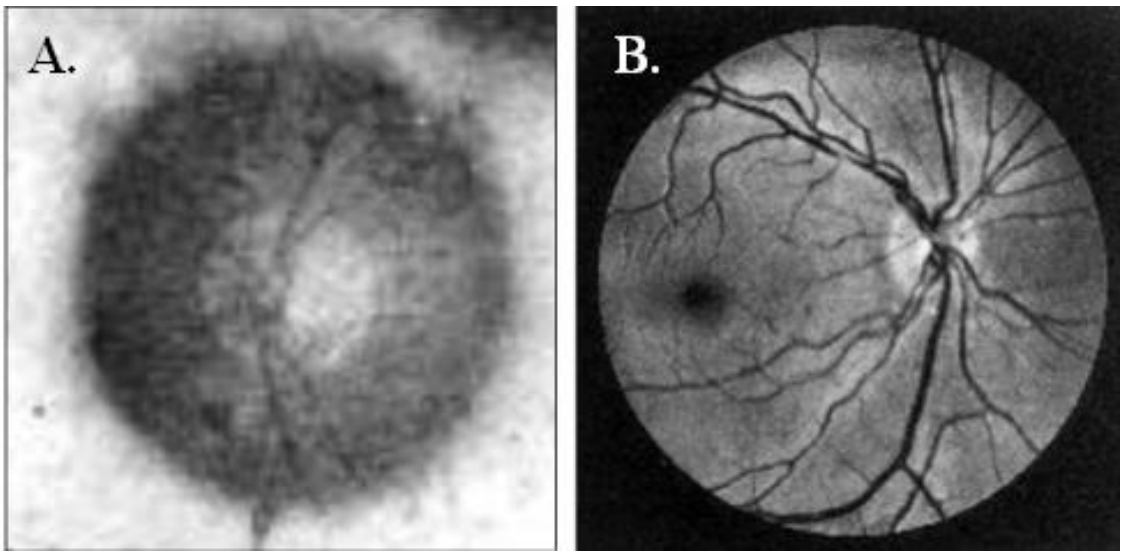

Figure 1.9: (A) Retinal photograph by Gerloff [89] and (B) Retinal photograph taken by Dimmer's fundus camera [90].

Since then, with the advancements in imaging and technology, retinal imaging became one of the most important tools in diagnosing eye pathologies and preventing many blinding eye diseases by early diagnosis. If one looks back at the very first attempt made to image the retina, by the French physician Jean Mery [92], for which he immersed a live cat in water and

demonstrated that, its retinal vessels are visible from the outside, to now, the whole field has grown tremendously. With the introduction of new technologies like fluorescein angiography, optical coherence tomography and spectral imaging, it is possible to not only look at the structural features of retina but to assess its function as well. Non-invasive oximetry using spectral imaging provides us with the tool to perform functional imaging of the retina.

Retinal tissue has a high oxygen demand and an adequate oxygen supply is required for normal function [93, 94]. To meet this high oxygen demand the retina is supplied by two circulations. Retinal blood supply is unique in feature because it supplies the whole of the retina without obscuring or disturbing the vision. The retina can respond to physiological variations in oxygen saturation; for example, reduced oxygen saturation can rapidly affect the retinal metabolism triggering local vasodilatation, and increased blood flow [95]. Abnormal retinal tissue oxygenation has been shown to contribute or associated with retinal diseases such as, proliferative diabetic retinopathy, glaucoma, retinal vascular occlusion and retinopathy of prematurity [63, 96]. Furthermore, tissue oxygen consumption is partly reflected by the arterio-venous difference in oxygen saturation and may provide an objective measure of disease severity in inner retinal disease, such as glaucoma [97].

Retinal oximetry represents a significant development in understanding the normal retinal circulation and physiology as well as pathologies of vision threatening diseases like diabetic retinopathy, glaucoma, vascular occlusions and other diseases.

1.5.1. Retinal Oxygenation in Health

As already described in the section above (Blood Supply to Retina) the retina has dual circulation- choroidal and retinal. In healthy individuals oxygen saturation in retinal arterioles and venules is found to be about 92-97% and 58-65% respectively [18, 19] with an arteriovenous oxygen saturation difference of about 30%. The arteriovenous oxygen saturation difference provides details of the oxygen consumption and metabolic activity of the healthy retina. Retinal oxygenation and blood flow is altered in many diseases and in light/dark transitions and in neural stimulus like flickering light.

The retinal oxygen consumption is increased in dark than in light [98]. Oxygen saturation in retinal vessels is higher in dark than in light [99], as in the dark, photoreceptors in the outer retina consume more oxygen [100, 101]. Similarly, Flicker light stimulation is known to increase the metabolic demand of the inner retina [102-104]. Retinal venous oxygen

saturation is increased by flicker light stimulation[105] along with retinal vessel diameters, which indicates increased blood flow.

In these diseases, retinal circulation does not properly respond to hypoxia, flicker stimulation or dark adaptation [13, 23, 25]. Improved understanding of the retinal oxygenation and effect of light/dark, flicker stimulation etc in healthy retina will improve our understanding of retinal oxygenation and functions in normal healthy individuals, therefore provides a route to developing an understanding of these disease mechanisms and potentially for clinical diagnosis.

1.5.2. Retinal Oxygenation in Diseases

1.5.2.1. Retinal Oxygenation in Diabetic Retinopathy

Tissue hypoxia plays a vital role in the progression of diabetic retinopathy although exact mechanism is yet to be known [63]. The very first attempt to measure retinal oxygenation in patients with diabetes was by Hickam et al. in 1959 [106]. Since then many studies assessed retinal oxygenation in diabetic retinopathy and found that venous oxygen saturation is significantly higher in diabetic retinopathy as compared to normal healthy subjects [107-110]. Another study of retinal oxygenation in diabetic patients reported an increased arteriovenous oxygen saturation difference in patients with diabetes [111]. The increased oxygen saturation in retinal venules in diabetic retinopathy can be explained by poor distribution of oxygen by capillaries, shunting of blood through preferential channels and bypassing non-perfused capillaries in the capillary network [110]. This explanation also supports the role of hypoxia in the progression of diabetic retinopathy.

Studies demonstrating benefits of supplemental oxygen in diabetic retinopathy by reporting improved contrast sensitivity [112], improved colour vision defects [113], and improved rod sensitivity [114] provides further evidence of role of hypoxia in diabetic retinopathy.

As described in section above (Retinal Oxygenation in Health), the retinal oxygen consumption is increased in dark. Dark adaptation is altered in diabetic retina and during dark adaptation diabetic retina becomes hypoxic and exacerbate the retinopathy, the effect can be reversed by administration of oxygen [115]. Another study reported that prevention of dark adaptation in diabetic retinopathy reversed or slowed the progression of diabetic retinopathy when compared with untreated eye [116]. In diabetic patients, flicker responses of retinal vessels are abnormally reduced [117-119]. The reduction in flicker response increased with

the severity of retinopathy [117]. Another study reported increased venous saturation in healthy control with flicker stimulation and this effect was less prominent in patients with diabetic retinopathy [120].

Measurement of retinal oxygen saturation in diabetic retinopathy provides us with the detailed information of amount of oxygen delivered to retina and the consumption. Thus by monitoring arteriolar and venular oxygen saturation we can monitor the progression of the different stages of the disease and plan effective course of treatment.

1.5.2.2. Retinal Oxygenation in Glaucoma

There is growing evidence in support of abnormal oxygenation and vascular hypothesis in the pathogenesis of glaucoma [121]. When patients with glaucoma were treated with hyperbaric oxygen, a treatment independent of IOP regulation, they showed improved visual field outcomes when compared with the control [122]. Non-invasive retinal oximetry studies have demonstrated that glaucomatous visual field defects are associated with increased venular oxygen and decreased arteriovenous oxygen saturation difference in retinal oxygen saturation [123-125]. The results from these studies suggest that retinal oxygen metabolism is affected in the glaucoma and the decreased arteriovenous difference in severe glaucoma may be related to lower oxygen consumption secondary to neuropathy [125].

The widely accepted form of treatment for glaucoma is by IOP reduction which works by reducing mechanical pressures and as result increasing blood flow [65], which improves the oxygenation in retina. More studies of retinal oximetry in glaucoma will help us understand the disease progression. It will definitely be useful in monitoring of the disease if not diagnosis.

1.5.2.3. Retinal Oxygenation in Retinal Vascular Occlusion

Retinal vascular occlusions (CRVO and CRAO) occur by blocked retinal vessels leading to ischemia and tissue hypoxia. Treatment in form of scatter photocoagulation of ischemic hypoxic areas has been shown to restore local retinal pO_2 [126]. Photocoagulation decreases oxygen consumption in outer retina by destroying the photoreceptors. Retinal oximetry studies shows decreased venous oxygen saturation in CRVO eyes than in fellow eyes and there is considerable variability within and between CRVO eyes [127], whereas retinal arteriolar saturation remains unaffected. In another case study of CRAO, low retinal arteriolar oxygen saturation 30h after the vision loss was reported in the affected eye [128]. A month

later, even after the treatment, the eye remained blind, but the perfusion and retinal oxygenation was reported to be normal by retinal oximetry.

In another study, the variation of retinal vascular oxygen content in an acute experimental model of retinal vein occlusion was demonstrated to induce an immediate decrease in retinal vascular oxygen content [129]. This study demonstrated that vascular occlusion can directly affect oxygen content in the affected vascular segment and oximetry measurements may provide vital information about the acuity of RVO. Retinal hypoxia may play an important role in RVO and retinal oximetry may be a reliable indication of the severity of the occlusion.

1.6. Retinal Oximetry

Retinal oximetry is the measurements of oxygen saturation of blood in retinal vessels. Retinal oximetry can be broadly classified in two categories namely invasive and non-invasive.

1.6.1. Invasive Measurements

Invasive techniques mostly include oxygen sensitive probes that are placed above the retina or may even penetrate the retina [101, 130, 131]. Other invasive techniques to measure oxygenation includes phosphorescence quenching [132-134] and functional magnetic resonance imaging (fMRI) [135]. Due to invasive nature of these techniques, they have been used mainly in animal and are unsuitable for use in humans. Most of the useful information on retinal oxygenation comes from these invasive studies done on animals.

1.6.2. Non-invasive Measurements

A non-invasive measurement of retinal oximetry is based on the concept that light absorption by blood depends on the blood oxygen saturation (SO_2) and wavelength (λ) of light. In blood haemoglobin (Hb) is one of the strongest absorbers of light. Haemoglobin is the oxygen carrying molecule of blood located in red blood cells. It carries about 97% of the oxygen in blood; 3% is dissolved in plasma. Haemoglobin exists in two states: oxygenated (HbO_2) and deoxygenated (Hb) haemoglobin. Oxygenated and deoxygenated haemoglobin have different colour and absorption characteristics. The absorption characteristics of blood can be given by extinction coefficients of haemoglobin [136] shown in the figure below.

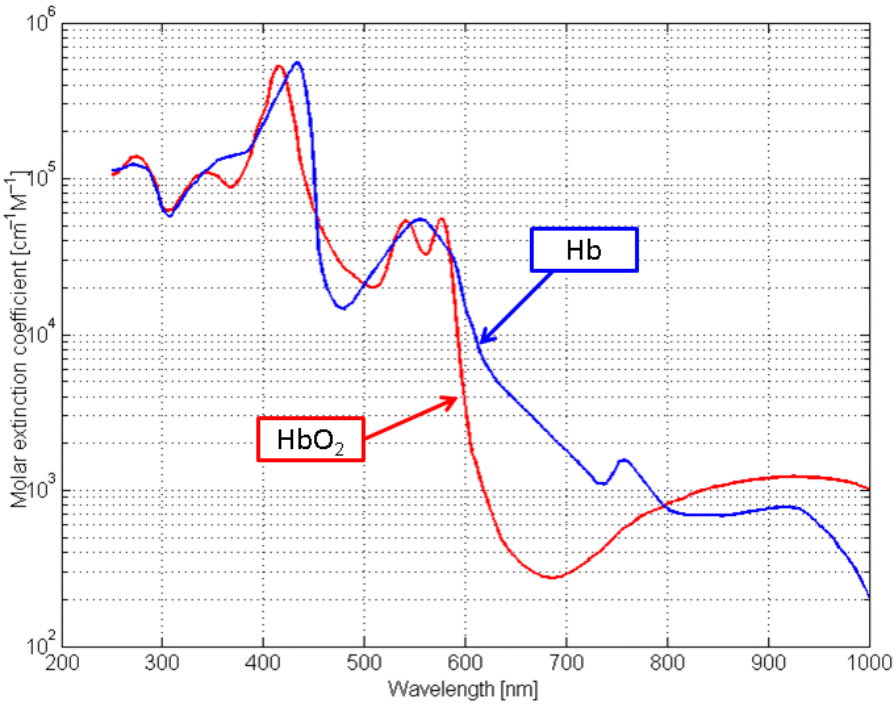

Figure 1.10: Extinction coefficients of oxygenated and deoxygenated haemoglobin [136].

For a wavelength longer than 600 nm, haemoglobin shows low absorption but it increases sharply with wavelength lower than 600 nm. Wavelengths at which oxygenated blood shows maximum absorbance are 416, 542 and 577 nm and minimum absorbance are 510 and 560 nm. However deoxygenated blood shows a minimum absorbance at 470 nm and maximum at 559 nm. Oxygen saturation of blood is estimated by variation of blood spectra with oxygen saturation.

The transmission of light in blood can be calculated by the Lambert-Beer law. According to the Lambert-Beer law, at any given wavelength the absorption is dependent on the extinction coefficient of the blood solution (ε), its concentration or haematocrit (c) and the path length (d) light has to travel through the solution.

$$I_T = I_0 * 10^{-(\varepsilon * c * d)} \qquad (1.1)$$

Where,

I_T = Intensity of light transmitted through solution

I_0 = Intensity of incident light

The optical density (OD) of a solution, which is also measure of its transmittance, can be defined as:

$$OD = -\log_{10} (I_T/I_0) = (\varepsilon * c * d) \qquad (1.2)$$

Where, I_T is intensity of transmitted light, I_0 is intensity of incident light, ε is extinction coefficient of solution, c is concentration and d is the path length. If the solution is blood, then the OD of blood will depend on extinction coefficient of haemoglobin, concentration (haematocrit) of the blood and the path length.

1.7. Principle of Spectrophotometric Retinal Oximetry

Spectrophotometric retinal oximetry is based on Lambert-Beer law. It requires images of retina at two or multiple wavelengths. The OD of retinal vessels is then calculated at chosen wavelengths. The OD of blood vessel is the ratio of measured light intensity at the centre of vessel (I_V) to the intensity just outside of the vessel (I_R).

$$OD = -\log_{10} (I_V/I_R) \qquad (1.3)$$

The OD of blood vessel measured at an isosbestic (insensitive to oxygen) wavelength does not depend on oxygen saturation, but does depend on other factors like vessel width, other pigmentation. OD calculated at a non-isosbestic (oxygen sensitive) wavelength depends on oxygen saturation as well as other factors similar to isosbestic wavelength. The ratio of optical densities (ODR) at isosbestic and non-isosbestic wavelength will cancel out effects from vessel diameter, other pigmentation and will only be sensitive to oxygen saturation.

$$ODR = OD_{\text{non-isosbestic}}/OD_{\text{isosbestic}} \qquad (1.4)$$

By calculating the ODR oxygen saturation of the blood vessel can be determined. Optical density ratio has a linear relationship with the oxygen saturation [137].

One of the widely used methods for retinal oximetry is calibration based two-wavelength retinal oximetry [137]. It uses two (one isobestic and one non-isobestic) wavelengths to the ODR. This technique then calibrates ODRs of arteries and veins assuming accepted blood oxygenation obtained from oxygen saturation measurements in healthy volunteers.

In brief, this technique uses the following equation to recover oxygen saturation:

$$OS = \frac{OD(\lambda_2)\varepsilon_{Hb}(\lambda_1) - OD(\lambda_1)\varepsilon_{Hb}(\lambda_2)}{OD(\lambda_1)\left(\varepsilon_{HbO_2}(\lambda_2) - \varepsilon_{Hb}(\lambda_2)\right) - OD(\lambda_2)\left(\varepsilon_{HbO_2}(\lambda_1) - \varepsilon_{Hb}(\lambda_1)\right)} \quad (1.5)$$

Where,

OS = Oxygen saturation

OD = Optical density at a given wavelength

ε_{Hb} = Extinction coefficient of deoxy-haemoglobin

ε_{HbO2} = Extinction coefficient of oxy-haemoglobin

Using one isobestic wavelength the equation (1.5) can be simplified into

$$OS = c_1 + c_2 \frac{OD(\lambda_A)}{OD(\lambda_B)} \quad (1.6)$$

Where,

λ_A = Oxygen sensitive wavelength

λ_B = Isobestic wavelength

C_1 and C_2 = Calibration coefficients

C_1 and C_2 are the calibration coefficients whose values can be calculated using data from non-pathological eyes and assuming standard values for venous and arterial oxygenations.

1.7.1. Hickam et al: Photographic Oximetry Method

Hickam et al [138] developed a photographic oximetry method for estimation of blood oxygen saturation by measuring the relative intensity at different wavelengths of light that has been reflected from or transmitted through blood. Filters were used to restrict light to achieve the desired wavelengths. Two wavelength imagers were set up to illuminate the fundus with two different wavelength combinations: centred at 640 (oxygen sensitive) & 800 nm (isobestic) and 640 & 505 nm. Images of an extended area of the retina were sequentially acquired and recorded on photographic films. The developed films were then used to generate absorption profiles with the help of a microdensitometer. The optic disc in the Hickam experiment acted as the reflective background. Optical density (OD) measurements were

performed for all the wavelengths and used to calculate the optical density ratios of the retinal vessels. The estimation of the oxygen saturation in retinal veins was defined using data from *in vivo* human experiments. This involved measuring the optical density ratios of retinal arteries in human subjects whose arterial oxygen saturation were altered by changing the inspired oxygen content with the use of various gas mixture of oxygen and nitrogen. The oxygen saturation of arterial blood was determined by the analysis of brachial artery blood samples at the time of imaging and was monitored during the imaging using an ear oximeter. In each subject, imaging during calibration involved using both wavelength combinations. The average retinal venous saturation was calculated at 58±10 % and 60±16 % for the (640, 505 nm) pair. *In vitro* validation experiments were performed by red-infrared images of heparinised venous blood samples from four normal subjects. The oxygenation of venous blood was changed by exposing the venous blood to air and mixing it with venous blood not exposed to air. The oxygen saturation of samples were determined by using a photometric method [139]. Venous blood samples with different oxygen saturation were inserted into glass capillaries of internal diameter of 250 and 500 μm placed in front of a white background. A linear relationship between red-infrared optical density ratios and the measured oxygen saturation of blood sample was confirmed. The standard deviation of the optical density ratios from the measured oxygen saturation was relatively small (6% and 9% oxygen saturation in 500 and 250 μm capillaries respectively). The two wavelength photography oximetry technique was limited by the influence of vessel diameter on oxygen saturation estimation.

1.7.2. Delori et al Method

Delori et al [140] developed a three-wavelength spectrophotometric technique for oximetry of blood in retinal vessels. Their technique was based on the three-wavelength method of Pittman and Duling [141] for transmission oximetry of whole blood with compensation for the effects of light scattering. They applied this method to retinal vessels and have developed a photo-electric system, the retinal vessel oximeter (RVO) that allows real-time measurements of oxygen saturation of discrete retinal vessels. A fundus camera comprising three interference filters was used with a photocathode and photomultiplier. A filter wheel was used to enable filtering of the light reflected from the fundus to be filtered into wavelengths centred at 558 nm, 569 nm and 586 nm. The estimation of light transmission through the vessels, using the average vessel and background fundus reflectance, enabled the calculation of optical density of the vessel at each wavelength. The algorithm used extinction

coefficient of oxygenated and deoxygenated haemoglobin and vessel transmission measurements at three wavelengths.

In vitro measurements were also performed on glass capillaries (internal diameters of 50 µm, 100 µm and 150 µm) containing flowing human blood and were used to calibrate the instrument with respect to a co-oximeter. The oxygen saturation of blood was changed using either a mixture of nitrogen and oxygen gas or by adding sodium dithionite. The three wavelength oximetry model was reported to be most accurate in the range of 50-100 % oxygen saturation but in the range between 0-50% there was a tendency towards overestimating the saturation.

In vivo studies of normal human subjects (n=22) included measurements of oxygen saturation in 85 retinal arteries and 102 retinal veins. The average oxygen saturation calculated in retinal arteries was 98±8% and 45±7% in retinal veins.

1.7.3. Schweitzer et al Method

Schweitzer et al developed a new method for the spatially resolved measurement of the oxygen saturation of retinal vessels [19]. They used imaging spectrometry for both measurements of transmission and reflectance spectra of whole blood in cuvettes as well as for fundus reflectance spectra. A model for the calculation of the oxygen saturation was developed, valid in the wavelength range between 510 nm and 586 nm. The opthalmospectrometer consisted of a modified fundus camera attached with spectrograph [142]. The instrument illuminated the retina with a small slit. A grating component within the spectrograph spectrally dispersed the reflected light from the fundus. To capture the reflectance spectrum an intensified charged coupled device was used. The reflectance spectrum was then used to perform oximetry measurements on retinal vessels.

In vitro experiments were performed using whole blood sample in quartz cuvettes of different thicknesses to determine the influence of various physiological conditions on the behaviour of light path in retina**.** It was reported that light transmission through blood decreases with increasing cuvette thickness and haematocrit within the wavelength range of 450 to 700 nm. At wavelength range of 500 to 600nm the internal reflectance was found to be independent of cuvette thickness. At wavelength range of 600 to 700 nm, the internal reflectance increased with increasing cuvette thickness.

Retinal vessel oximetry was performed in healthy human subjects (n=30) [143]. In each measurement, the oxygen saturation was simultaneously determined for 193 locations along a line of 1.5 mm at the fundus. The mean oxygen saturation in retinal arteries was (92.2±4.1) % and (57.9±9.9) % in retinal veins. The mean retinal arterio-venous difference of the oxygen saturation was (35.1±9.5) %.

1.7.4. Michelson et al Method

Michelson et al. developed an imaging ophthalmospectrometer to compare the oxygen saturation in retinal vessels of patients with primary open-angle glaucoma (POAG) and healthy subjects [144]. Oxygen saturation measurements were made at the supero-temporal retinal arteries and veins 1-3 mm from the disc margin. An oximetry model was used to calculate the OS which included corrections for light scattering by the blood cells and retinal tissues, retinal pigment epithelium and the choroid [145]. The technique used three isosbestic wavelengths (522 nm, 569 nm and 586 nm), and 560 nm as the non-isobestic wavelength to calculate the oxygen saturation. The use of additional wavelengths was to correct for the influence of light scattering and absorption by retinal pigment epithelium on the measured vessel reflectance.

Retinal oximetry was performed in 58 normal subjects, 49 patients with normal tension POAG and 45 patients with high tension POAG. The retinal arteriolar and venular oxygenations in the healthy subjects were 92.3 ± 3.4% and 55.7 ± 6.8% respectively. The retinal arteriolar oxygen saturation in eyes with normal tension POAG was reported to be significantly lower (89.7 ± 5.4%) than the healthy subjects. Whereas, no significant difference was not found between the retinal arteriolar oxygen saturation for high tension POAG group (91.4 ± 4.0%) and the healthy subjects. The retinal venular oxygen saturation in the normal tension POAG (56% ± 8.3%) and high tension POAG (58.3 ± 10.5%) groups were not significantly different to the retinal venous saturation in healthy individuals.

1.7.5. Beach et al Method

Beach et al. were first to report two-wavelength oximetry in retina using one isosbestic wavelength and other as oxygen sensitive [137]. They developed a two wavelength retinal imaging system which consisted of a modified fundus camera with an optical beam splitter which enabled simultaneous generation of two retinal images which were then filtered using

two interference filters, centred at 569 nm (isosbestic) and 600 nm (oxygen sensitive). The images were recorded using a digital camera. At each wavelength, optical densities were calculated for each of the retinal blood vessel. Optical densities at both wavelengths were used to calculate ODRs ($ODR = OD_{600} / OD_{569}$) along the retinal vessels. Oxygen saturation for each vessel was then calculated using ODR, which has linear relationship with the measured oxygenation [141]. They demonstrated a linear relationship between the ODR and oxygenation by performing retinal oximetry in healthy subjects during graded hypoxia.

Furthermore they also performed ODR measurements in 12 diabetic subjects without diabetic retinopathy during normal glucose level and high glucose level in blood [111]. The ODRs of the retinal arteries was reported to be the same during both levels of blood glucose. However, the ODRs of the retinal veins increased during acute hyperglycaemia, which indicates a decrease in venular oxygenation.

1.7.6. Denninghoff et al Method

Denninghoff et al. developed an instrument to measure retinal vessel oxygen saturation - 'Eye Oximeter' [146]. It consisted of four diode lasers which enabled to image retina at wavelengths of 629, 678, 821 and 899 nm. The wavelengths used in the oximeter was determined by careful theoretical calculations and analysis of the optimal wavelength combinations suitable for retinal vessel oximetry [147]. The eye oximeter had a horizontal polarizer positioned in front of the detector to get rid of the errors from specular reflection in the vessel wall which is believed to introduce errors in the oximetry calculation [148].

They used a model eye to validate and calibrate their oximeter [149]. Whole human blood at different oxygen saturation was used to test the oximeter, the oxygen saturation of the blood samples were changed by mixing with various combinations of nitrogen and oxygen gas providing a range of saturations between 6% - 87%. The oxygen saturation of blood samples were also verified by a CO-oximeter. The blood samples at varying oxygen saturation were injected into capillaries (internal diameters -110 – 268 μm) and then placed in a model eye with a 100% reflective *Spectralon* background. The extinction values of the blood samples in the model eye were calculated for all the four wavelengths (629, 678, 821 and 899 nm). The oximetry model to extract oxygen saturation was based on the Lambert-Beer law. The calculated oxygen saturation from oximeter was compared with the measured values of oxygen saturation of the blood samples.

They reported eye oximeter to be quite accurate at higher oxygen saturations (± 4% error) but the error increased with lower oxygen saturations. They also performed retinal oximetry measurements using the modified Eye Oximeter on one human subject. The mean oxygen saturation of the retinal arteries and veins on the optic disc were 102% 65% respectively. The mean oxygen saturation away from the optic disc were 98% and 63% and respectively for arteries and vein.

Recently, Denninghoff et al developed a new retinal oximeter which operates in blue-green spectra [150]. The oximeter is a modified confocal scanning laser ophthalmoscope that uses five monochromatic beams from a multi-wavelength argon-ion laser (457.9, 476.5, 488, 496.5, and 514.5 nm) to sequentially scan the retina.

They tested the oximeter on an enucleated swine eye vessel and a retinal vein in a human volunteer. The oxygen saturation for swine enucleated eye was reported as ∼1%, as expected. The human mean venous oxygen saturation was found to be 63-65% which is within the normal physiological range.

1.7.7. Stefansson et al Method

Stefansson et al. [151] developed a retinal oximeter which is based on two-wavelength oximetry technique described by Beach et al [137]. Their oximeter captured retinal images at four different wavelengths (542, 558, 586 and 605 nm), using a beam splitter with a commercial fundus camera (Topcon) captured by a CCD camera. Automated image processing algorithms were used for image registration and vessel detection. Only two images at 586 nm (isosbestic) and 605 nm (oxygen sensitive) wavelengths are used to calculate ODR and oxygen saturation. This technique involves calibration of ODRs of arteries and veins assuming accepted blood oxygenation obtained from oxygen saturation measurements on healthy volunteers [152].

Retinal oximetry was performed in 16 healthy subjects at normoxia and hyperoxia level [151]. The arterial oxygen saturation measured was 96% ± 9% (mean ± SD) during normoxia and 101% ± 8% during hyperoxia. The difference between normoxia and hyperoxia was reported to be statistically significant ($P = 0.0027$). Oxygen saturation values for venules were 55% ± 14% and 78% ± 15% for normoxia and hyperoxia respectively.

The oximeter developed by Stefansson et al is widely used in many clinical studies. A recent studies which used same oximeter, performed oximetry in 26 healthy individuals [153], and

they reported oxygen saturation values as 93.1% ± 2.3% in arterioles and 64.9% ± 3.3% in venules.

A retinal oxygen saturation value was measured with retinal oximetry in a multiethnic group of healthy subjects and to evaluate the association of retinal oxygen saturation with demographic and clinical parameters [154]. Retinal oximetry was performed in both eyes of 61 normal healthy subjects. Average arteriolar and venular oxygen saturation was 90.4 ± 4.3% and 55.3 ± 7.1% respectively. Demographic and clinical parameters did not seem to significantly influence retinal oximetry measurements, although arteriolar oxygen saturation was found to be higher in Asian population.

1.7.8. Hammer et al Method

Hammer et al. developed a dual wavelength retinal oximeter comprised of a fundus camera with an attached pass band filter with transmission wavelengths centred at 548 nm and 610 nm [18]. Retinal images were recorded onto a colour digital camera and an oximetry model, using the ODRs at the two wavelengths, was used to calculate the oxygen saturation. The oximetery model incorporated the correction for errors introduced by effects of vessel diameter and fundus pigmentation as described by Beach et al [137].

The oxygen saturation measurements reported in10 healthy subjects were demonstrated to be highly reproducible for retinal arterioles and venules. The arteriolar and venular oxygen saturation under normoxic conditions were 98% (± 10.1%) and 65% (± 11.7%) respectively. Hyperoxia (inhalation of 100% oxygen) increased the arteriolar and venular oxygen saturation by 2% and 7% respectively.

They also reported retinal oximetery in 41 diabetic patients with a range of retinopathy (from mild non-proliferative to proliferative diabetic retinopathy) and oximetry results compared to 12 healthy subjects [109]. They reported no significant difference in the arteriolar oxygen saturation between the controls and subjects with diabetic retinopathy of all severities. However increased venular oxygen saturation was reported with the increase in severity of diabetic retinopathy.

1.7.9. Harvey et al Method

Harvey et al developed a multispectral imaging system which imaged the retina at multiple wavelengths (420–720 nm) [155]. Their hyperspectral oximetry system consisted of a commercial fundus camera (Canon CF-60Z, Tokyo, Japan), integrated with a liquid crystal

tunable filter (LCTF) which enabled illumination of the retina using a number of user-selected wavelengths. A CCD was incorporated into the fundus camera which enabled the capture of retinal images. OD was calculated for all the vessels at wavelengths between 500 nm to 650 nm at 2 nm interval. Oxygen saturation was extracted by using an algorithm based on the Levenberg–Marquardt nonlinear fit to the complete set of ODs (λ).

They performed *in vitro* validation of the oximetry system, using a model eye with quartz capillaries (internal diameter 100 and 150 μm) filled with whole human blood of varying oxygen saturation [156]. The blood oxygen saturation measurement was also made by a CO-oximeter and was compared with the calculated oxygen saturation values obtained by the oximetry system.

They also performed oximetry in 14 healthy volunteers and one retinal vascular occlusion patient [155]. The retinal arteriolar and venular oxygen saturation in healthy subjects was reported as 104.3 ±16.7 and 34.8 ±17.8%. For RVO patient they reported lower than normal oxygen saturation in retinal arterioles, corresponding to the location of the vessel occlusion.

The reported value for retinal venous oxygen saturation by this method is lower than reported by others [151, 153, 157]. Their explanation for this lower reported values was use of multiple wavelengths as compared to two-wavelength oximetry method applied by others. They also reported, calculated oxygen saturation for some vessels in negative values and greater than 100% values as a limitation to their technique.

1.7.10. Gloster Fundus Oximetry Method

Gloster et al developed an apparatus to measure the oxygen saturation in choroid by measuring change in fundus reflectance at different oxygenation at different colours of light [158, 159]. They measured the light reflected from the fundus of the eye by a photomultiplier at few different colours using different filters and then they calculated change in reflectance or change in OD of the fundus.

In vitro validation was performed [158] by imaging optical cells filled with blood of different oxygen saturation. The oxygen saturation of sample was changed by bubbling nitrogen or oxygen through them. They were able to detect a change in reflection from the sample with varying oxygenation.

They also measured change in light reflectance from fundus with varying blood oxygenation in healthy human subjects. A breathing mixture of nitrogen and oxygen was used to alter the

blood oxygenation in the subject. They showed that the fundus reflection of red light changed significantly when the choroidal oxygenation was altered in subjects by nitrogen breathing or by apnea.

1.7.11. Laing et al: The Choroidal Eye Oximeter

Laing et al. developed an electro-optical instrument which can measure oxygen saturation of choroidal blood in human [160]. Their oximetry system was divided into two parts: an optical system and an electronic system. The optical system produced a monochromatic beam of light at chosen wavelength which illuminated the fundus. The light reflected back from the fundus was captured onto a photodetector of the electrical system. The Choroidal Eye Oximeter illuminated a region of fundus at two different wavelengths (805 nm and 650 nm) and recorded the amount of light reflected back from the fundus. By using the OD measurements at two wavelengths, one isosbestic (805 nm) and other oxygen sensitive (650 nm), they determined the oxygen saturation of the blood.

The evaluated the performance of the oximeter on healthy subjects' breathing room air, 100% oxygen and mixture of oxygen and nitrogen gas to induce hypoxia. For 9% inspired oxygen, the choroidal oximeter measured oxygen saturation of 60% in choroid, when the inspired oxygen was further reduced to 8%, that resulted in further decrease of choroidal oxygenation to 53%. The subjects were then switched to room air and the measured oxygen saturation was 96%. At 100% inspired oxygen, the measured choroidal oxygenation was almost 100%.

1.8. Aims of the Research

This thesis will evaluate use of IRIS snapshot multispectral fundus camera to perform retinal oximetry and development of a robust technique to evaluate retinal oxygenation in health and various conditions. This thesis also describes a new non-invasive technique to measure choroidal oxygenation using fundus reflection. The main aims of this thesis are:

1. To validate that IRIS snapshot hyperspectral fundus camera is sensitive to oxygen saturation of blood and discriminate between bloods with different oxygenation using a model eye (*in vitro*).
2. To test the sensitivity of IRIS snapshot hyperspectral fundus camera to measure a wide range of oxygen saturation in retinal vessels *in vivo* in animal (porcine) model.
3. To test the IRIS snapshot hyperspectral fundus camera and retinal oximetry algorithms on healthy human subjects.

4. To conduct a 'Human Hypoxia Trial' to assess the effect of acute mild hypoxia on retinal oxygenation of healthy individuals.
5. To utilise fundus reflection from the choroid to measure choroidal oxygen saturation non-invasively using the IRIS snapshot multispectral fundus camera.

Chapter 1 described the basic anatomy of the human eye, retina, and choroid, blood supply of the eye and common pathology of retinal diseases. The motivation and necessity behind retinal oximetry is also presented along with the methods and devices currently available for the retinal oximetry.

Chapter 2 introduces the IRIS snapshot multispectral fundus camera and its software control used in the research presented in this thesis.

Chapter 3 examines the ability of the IRIS snapshot multispectral fundus camera to detect the difference between bloods with different oxygen saturation *in vitro* in a model eye.

Chapter 4 presents retinal oximetry data over a wide range of oxygen saturation in an animal model. The use of animal model provided the opportunity to test and validate the oximetry system and algorithm over a wide range of oxygenation which cannot be performed in human subjects.

Chapter 5 describes the retinal oximetry performed in healthy human subjects. It explains in detail the imaging and image analysis protocol and the results. This chapter also discusses the limitations of retinal oximetry.

Chapter 6 investigates effect of acute mild hypoxia on retinal oxygenation and autoregulation in healthy human subjects. Retinal oximetry and vessel diameter measurements were performed in healthy individuals during normoxia and hypoxia and results were compared.

Chapter 7 presents a new method of measuring the choroidal blood oxygen saturation in human. A demonstration of the technique in human subject at different inspired oxygen level is presented.

Chapter 8 includes a general discussion and summary of retinal and choroidal oximetry. It also discusses potential clinical applications, limitations and future work of the project.

Chapter 2

IRIS Snapshot Multispectral Fundus Camera

2.1. Introduction

This chapter introduces the IRIS snapshot multispectral fundus camera used for retinal and choroidal oximetry work described in this thesis. The main components of the IRIS snapshot multispectral fundus camera are described in detail along with the graphical user interface (GUI) to control the system.

2.2. IRIS Snapshot Multispectral Fundus Camera

The IRIS snapshot multispectral fundus camera consists of a commercial fundus camera (Topcon TRC 50 IA, Tokyo, Japan) fitted with image replicating imaging spectrometer (IRIS) [161] which enables acquisition of images in a single snapshot at eight different wavelengths optimized for oximetry onto a single detector. This system was constructed within the Imaging Concepts Group (Prof. Andy Harvey, University of Glasgow, formerly at Heriot-Watt University, Edinburgh). The IRIS snapshot multispectral fundus camera is used in this thesis as an oximetric imaging system. The main components of the IRIS snapshot multispectral fundus camera are described in the later sections. The main purpose of this thesis was validation, development and demonstration of the device to perform oximetry in retinal and choroidal vessels. To that purpose, the validation experiments were performed in artificial eye, animal model and healthy humans. Furthermore a human hypoxia trial was also conducted by the author. Where it is applicable, credit is given in the text, the remainder of the work in this thesis is the author's own unless explicitly stated otherwise.

2.2.1. Fundus Camera

The IRIS snapshot multispectral fundus camera (Figure 2.1) consists of a commercial mydriatic fundus camera (Topcon TRC 50 IA, Tokyo, Japan) which was modified to integrate an image replicating imaging spectrometer (IRIS) into the optical path of the camera enabling the recording of eight wide-field narrowband spectral images of the retina onto a single detector in one snapshot.

The fundus camera consists of two sources of illumination. An inspection lamp with tungsten bulb provided the continuous light source to view and inspect the retina. A xenon flash as the secondary source was used to illuminate the retina to capture multispectral retinal images. The optical system of the fundus camera comprises an annular illumination which allows light through the pupil of the eye. The dilation of the pupil was required for best imaging as it was a mydriatic system. The light reflected from the fundus exits the pupil via centre of the illumination annulus. This design reduces corneal reflection from the illumination. It then passes through the optical components of the fundus camera forming a retinal image at the imaging plane.

After illuminating the retina using inspection lamp of fundus camera, a focusing knob was used to get the images with optimal focus. The fundus camera also had dioptre correction lenses, which could be used while imaging people with corrected vision.

The Topcon fundus camera had a field of view from 20° to 50°. For purposes of retinal imaging 50° field of view was used.

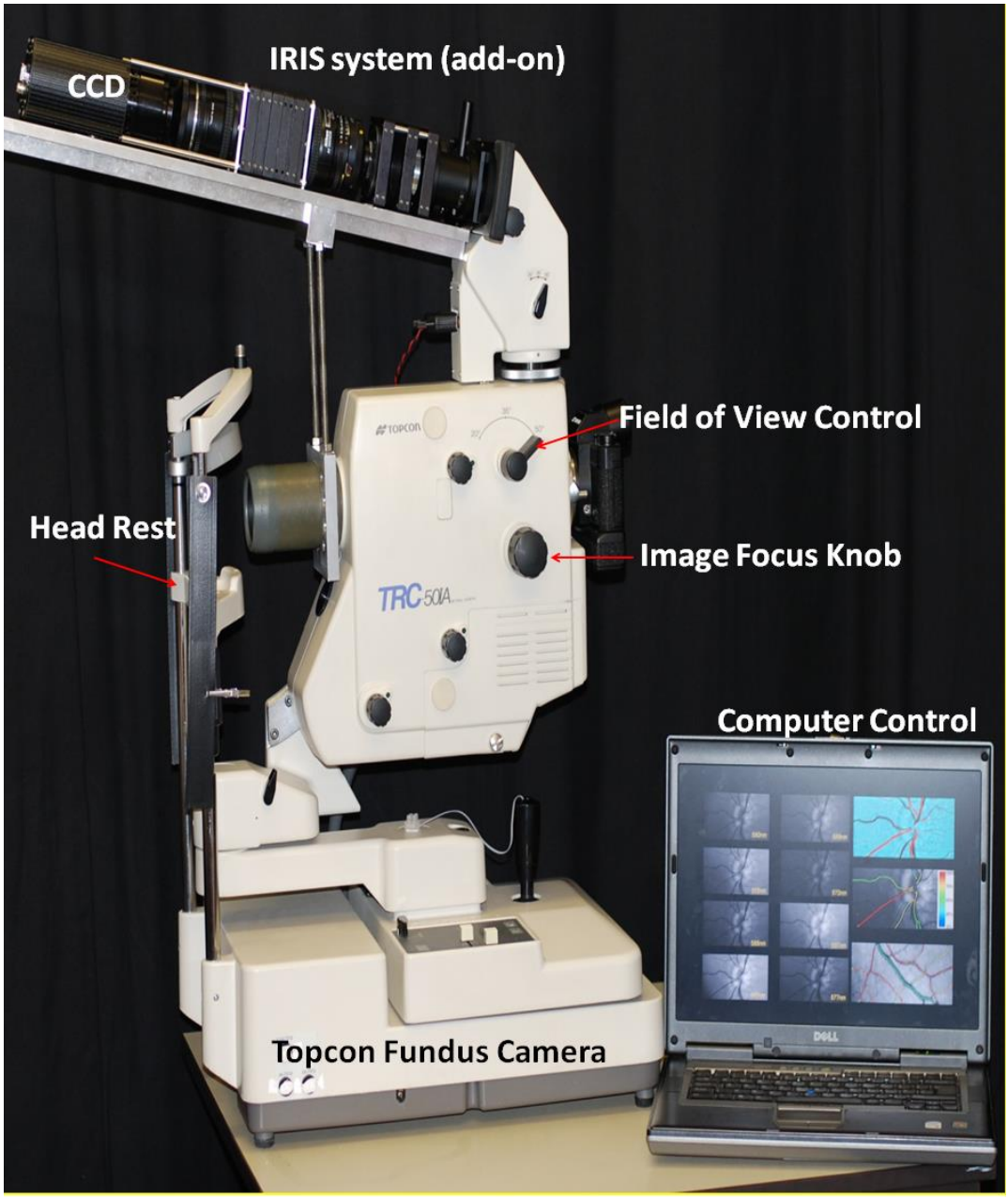

Figure 2.1: Photograph of the IRIS snapshot multispectral fundus camera. Main components are Topcon fundus camera, fitted with IRIS (image replicating imaging spectrometer) and a CCD (charged coupled device) to record the retinal image.

2.2.2. Image Replicating Imaging Spectrometer (IRIS)

IRIS is a birefringent spectral demultiplexer that allows capturing images of an object at multiple wavelengths onto single detector. IRIS is based on a set of retarders and Wollaston prism that spectrally demultiplexes the previously polarized incoming light. IRIS was invented by Andy Harvey and David Fletcher Holmes [162].

In a similar way to an interferometer, IRIS can reproduce the same intensity pattern all along the illumination spectral range. Each IRIS spectral band has an intensity pattern that is repeated along the illumination spectral range. IRIS employs a cascade of two-beam inferometers combined with Wollaston prism polarisers to simultaneously replicate and spectrally filter the image. The fundamental advantage of IRIS is that it provides almost 100% optical efficiency and snapshot spectral imaging. It provides safe and comfortable low intensity illumination at the retina and high signal to noise ratio whilst snapshot operation provides high quality oximetry.

The IRIS system used in this thesis was an 8-band IRIS and is shown in figure 2.2. The number of spectral bands generated by IRIS depends on number of Wollaston prisms and retarders used.

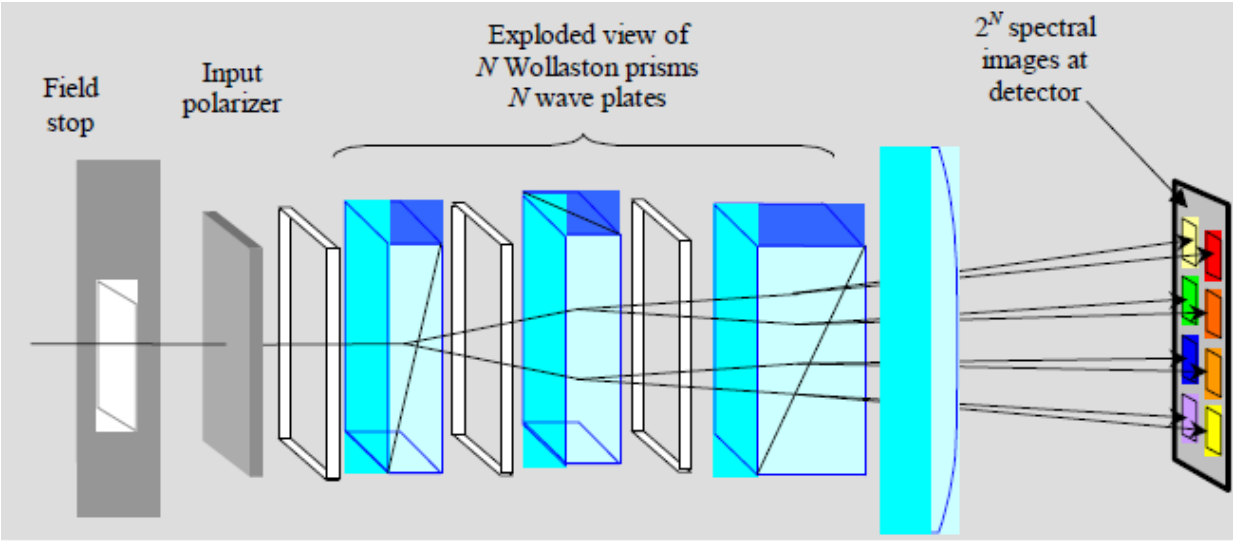

Figure 2.2: Diagram of an 8-band image replicating imaging spectrometer (IRIS) system [163].

If N is the number of retarders and prisms used then the total number of bands will be 2^N. 8-band IRIS combines 3 retarders and 3 Wollaston prisms to generate 8 replicated images. A detailed description of principle and working of IRIS can be found here [161].

The 8-band IRIS system used in IRIS snapshot multispectral fundus camera was designed to produce 8 sub-images of retina in the wavelength range of 560 nm to 600 nm. The spectral transmissions of 8-band IRIS system with the fundus camera are shown in figure 2.3.

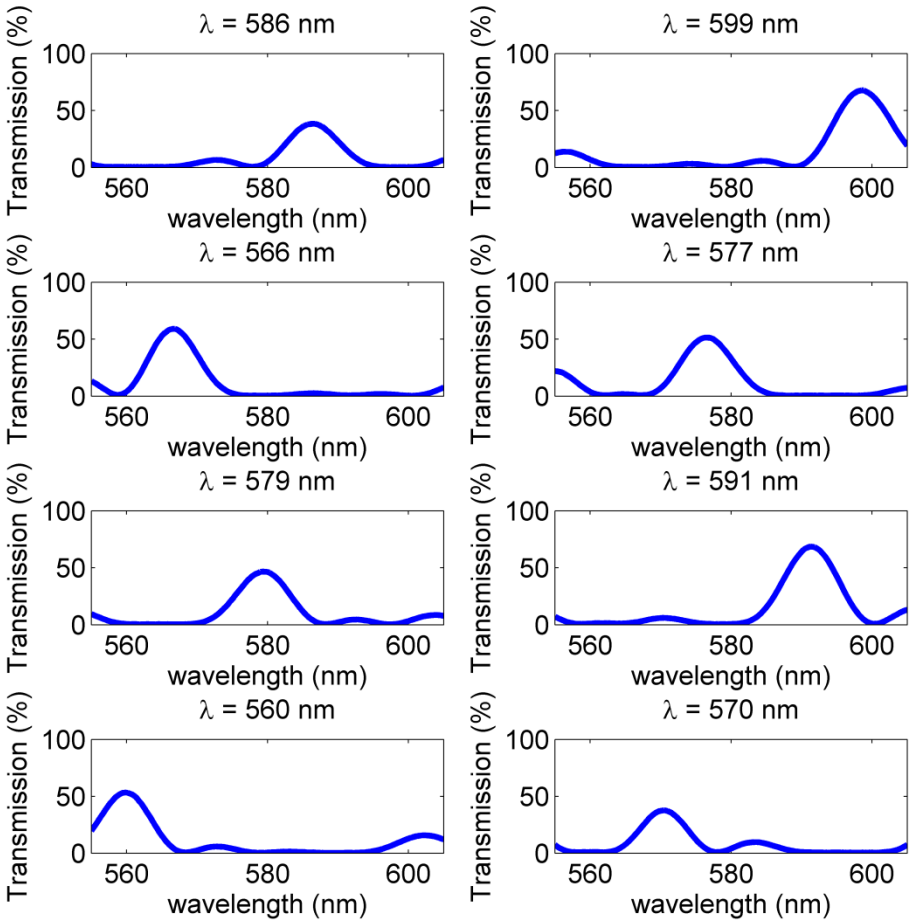

Figure 2.3: Transmission of an 8-band IRIS system fitted with snapshot fundus camera.

After integrating the IRIS with the fundus camera, 8 replicated images of the retina can be acquired in one snapshot onto a detector plane. An example of raw retinal image recorded by the system is shown in figure 2.4.

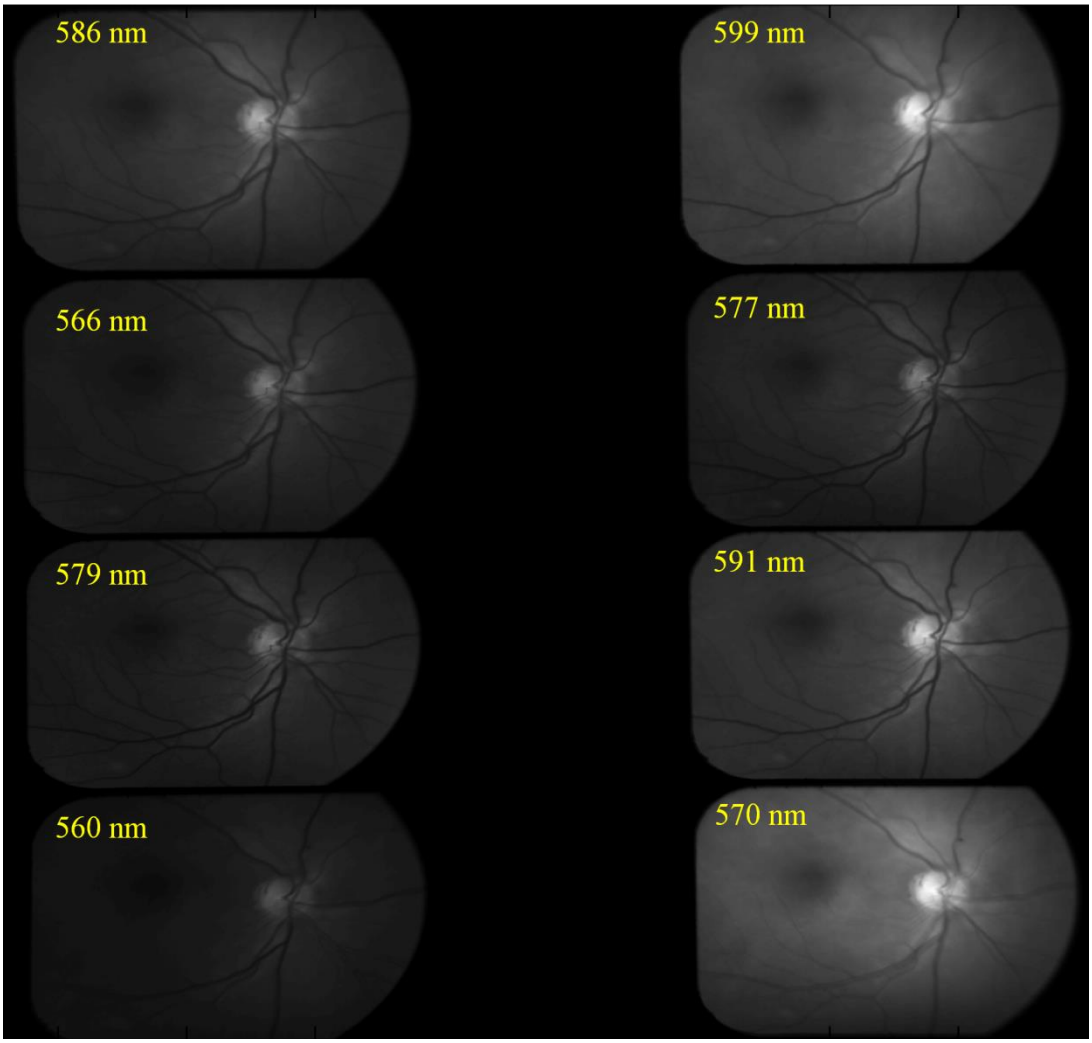

Figure 2.4: A raw retinal image recorded by IRIS snapshot multispectral fundus camera.

2.2.3. Charge-Coupled Device (CCD)

A low-noise charge-coupled device (CCD) camera (Retiga 4000R, QImaging, Canada) was incorporated into the fundus camera after the IRIS block to enable the capture of retinal images (Figure 2.1). The CCD camera has 4.19 million pixels with 12-bit digital output. The CCD detector size was 2048 x 2048 pixels providing a 50° field of view of retina.

2.2.4. Graphic User Interface (GUI) Control for the System

A GUI was developed in Matlab (MathWorks, Inc, MA, US) to control the IRIS snapshot multispectral fundus camera to acquire retinal images. The GUI was created by researchers at Imaging Concepts Group, Heriot-Watt University with the input from the author. The author's main contribution in the development of GUI was to test it, and make any necessary minor modifications in the algorithms.

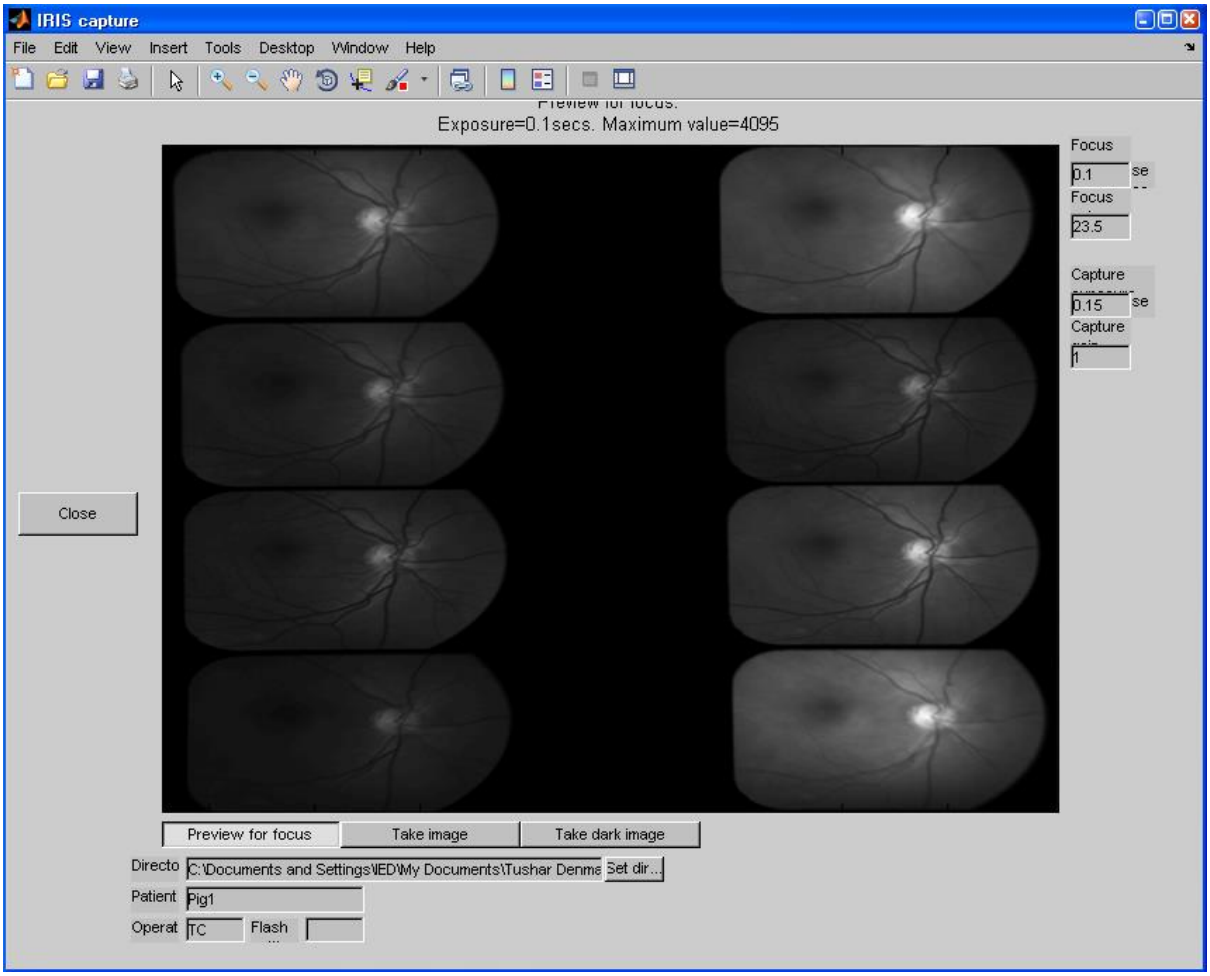

Figure 2.5: The graphical user interface (GUI) developed in Matlab to control the IRIS snapshot multispectral fundus camera for image acquisition.

The GUI controlled the fundus camera xenon flash and the CCD camera (Figure 2.5). The xenon flash was synchronised with the CCD camera for simultaneous capture of retinal images on CCD detector with flash. The GUI had a preview window to view live feed of retina, which helped in focus adjustments and ascertaining that the right region of retina was being imaged. The captured images were stored onto the hard drive in 12-bit matrix data format (.mat). GUI had an option to capture dark frame, which was used for dark calibration. The GUI also had the option to choose the exposure time, define the name of file and choose where to save it. The GUI also gave a warning if the images were overexposed or saturated, ensuring the quality control of the spectral image.

Chapter 3

In Vitro Validation of Oximetry in Model Eye

3.1. Introduction

In this chapter, we describe an *in vitro* validation of our spectral imaging system that performs retinal oximetry by using a model eye. The model eye provides a simulated environment that mimics the human eye to validate the oximetry technique. *In vitro* validation of many retinal oximetry systems using a model eye has been previously reported [19, 139, 140, 149, 156, 164-167].

The purpose of this study was to validate our imaging system and oximetry algorithms using animal blood with known oxygen saturation.

3.2. Methods

3.2.1. The Model Eye

The model eye (Figure 3.1) used in this study was previously constructed in the Imaging Concepts Group (Prof. Andy Harvey's Lab). The model eye simulated the optical property of the human eye and was used in this study to validate the IRIS snapshot multispectral fundus camera and oximetry algorithms. The model eye comprised of a front lens (+62.5 D doublet convex achromatic lens, Thorlabs ltd., Cambridgeshire, U.K.), a mid chamber, which can be filled with water, and a capillary holder resting against *Spectralon* (Labsphere Inc., New Hampshire, USA) background.

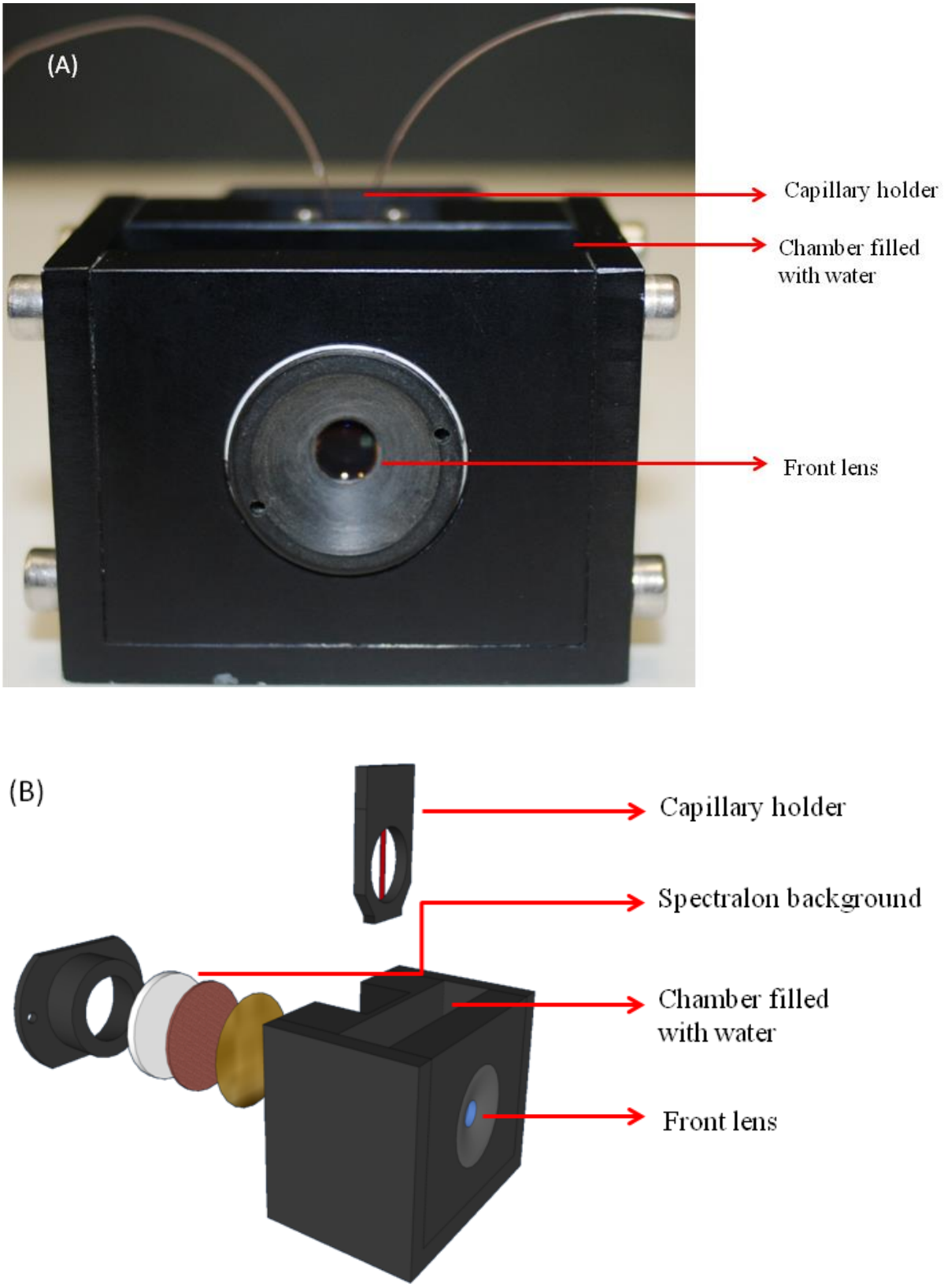

Figure 3.1: (A) The model eye front view, (B) Schematics of the model eye (by Al Gorman)

Spectralon, a polymer of carbon and fluorine, has the highest diffuse reflectance and provided an ideal background for the model eye. The capillary holder (Figure 3.2) held the blood-filled Fluorinated ethylene propylene (FEP) capillaries (Zeus Inc, Ireland), which represent the blood vessels of the retina. The chamber of the model eye was filled with saline water to mimic the vitreous humour of the eye and also resulted in the effective focal length of the front lens to be approximately 22 mm. The refractive index (n) of the FEP capillary used was 1.34 and the model eye chamber was filled with saline water (n = 1.33) creating a deliberate refractive index match to reduce specular reflection from the capillary walls.

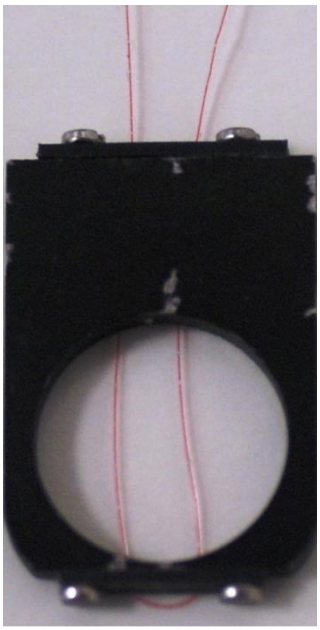

Figure 3.2: Capillary holder with blood filled FEP capillary.

3.2.2. The IRIS Snapshot Multispectral Fundus Camera

The IRIS snapshot multispectral fundus camera has been described in detail in Chapter 2. In summary, the system consists of a commercial fundus camera (Topcon TRC 50 IA, Japan), fitted with the IRIS snapshot device along with a CCD digital camera, enabling it to acquire images at 8 different wavelengths in a single snapshot.

3.2.3. Blood Sample Preparation

To validate the spectral imaging device and oximetry algorithms, defibrinated horse blood (E & O Laboratories ltd, Bonnybridge, U.K.) was used in the model eye. Two different levels of oxygen saturation blood sample were employed in the model eye. The first sample was fully oxygenated, which is found in normal healthy retinal arterioles and the second sample had approximately 60 % oxygenation, which is representative of the oxygen saturation found in

normal retinal venules. The horse blood straight from the bottle was usually fully oxygenated as they are supplied fully oxygenated by the manufacturer. To ensure that the sample was fully oxygenated and was the same as arterial level of blood oxygenation (95-100%), blood samples were exposed with atmospheric air for about 20 minutes in a 100 ml beaker. The sample was gently rolled/ shaken periodically to speed-up the re-oxygenation process.

3.2.3.1. De-oxygenation of Blood using Sodium Dithionite

Sodium dithionite ($Na_2O_4S_2$) was used to de-oxygenate the blood samples. Sodium dithionite induces dissociation of oxygen by reduction of the external oxygen without diffusing into the red blood cells, which does not affect structure and function of the cell membrane. The method used to deoxygenate the blood using sodium dithionite for this study was same as the method used by Saebvarnothing, and Bjvarnothingrnerud [168]. Many previous published studies have used sodium dithionite to deoxygenate blood [169-171] and to test their *in vitro* retinal oximetry models [140, 164]. In their study, Saebvarnothing and Jvarnothingrnerud [168] described the accuracy and repeatability of the method and found it to be highly reproducible and accurate. They also produced a table with amount of sodium dithionite to be added for a desired oxygen saturation value (see Table 3.1) and the change in oxygenation as a function of time after adding sodium dithionite (see Table 3.2).

Table 3.1: Comparison of the theoretical O_2 % values obtained and measured values[168]

Concentration (mg/g blood)	Theoretical O_2 %	Measured O_2 %
2.50	0	0
1.90	24.1	21.0
1.20	48.2	47.8
0.61	62.1	60.5
0.53	70.1	71.5

Table 3.2: Change in O_2 % as a function of time after adding sodium dithionite [168]

Concentration mg/g	O_2 % 1 min.	O_2 % 15 min.	O_2 % 30 min.	O_2 % 45 min.	O_2 % 60 min.
2.5	0	0	0	0	5.1
0.61	40.3	57.7	62.1	60.0	61.4
0.19	77.9	78.1	85.0	84.9	85.9

Based on the values given in Table 3.2, we used 0.61 mg of sodium dithionite (Fisher Scientific UK Ltd, Leicestershire, U.K.) per gram of blood to obtain a saturation level of approximately 62%. After adding the given value for sodium dithionite, the sample was mixed well and stored in a gastight glass syringe (Hamilton, Bonaduz, Schweiz). The gastight syringe prevented further contact with the air, which may have re-oxygenated the sample. The sample was then left to deoxygenate for 30 minutes, which gave a stable oxygenation value range between 60-62% for next 30 minutes. The blood sample from the glass syringe was then transferred to FEP capillaries using Nano Tight tubing sleeves and leur lock adapters (Idex, Upchurch Scientific, Germany). After adding the sodium dithionite to the sample, the blood deoxygenated very quickly, this change was visually apparent as well. Figure 3.3 shows oxygenated blood in a glass bottle (A) and after adding sodium dithionite (B). The blood with sodium dithionite appears darker than the oxygenated blood sample.

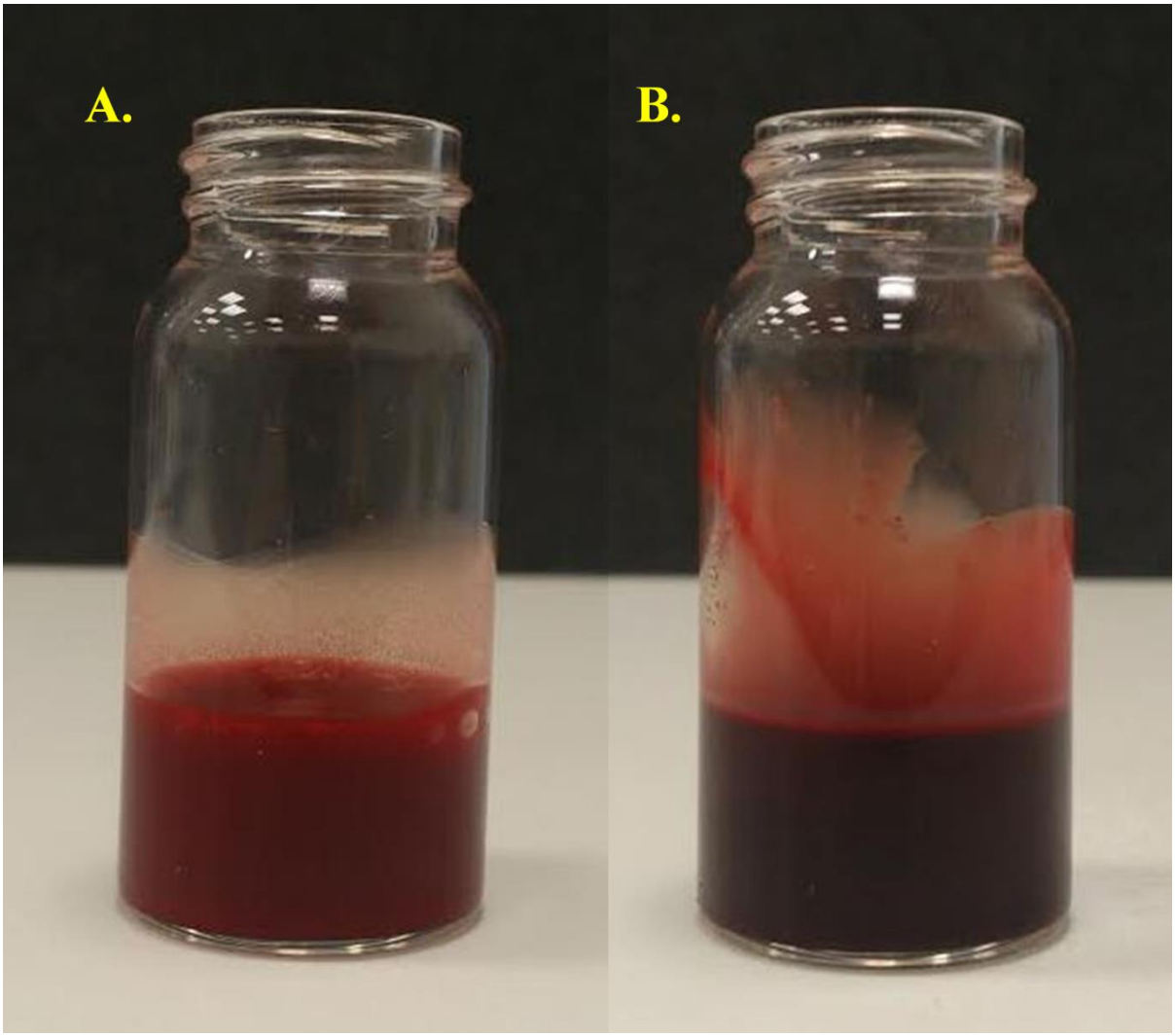

Figure 3.3: (A) Oxygenated blood sample and (B) deoxygenated blood sample using sodium dithionite. A colour difference can be visually observed between the two samples because of the oxygenation difference.

3.2.4. The Model Eye Experiment

The model eye was imaged by the IRIS snapshot multispectral fundus camera by positioning it in front of the camera objective. (Figure 3.4 (A))

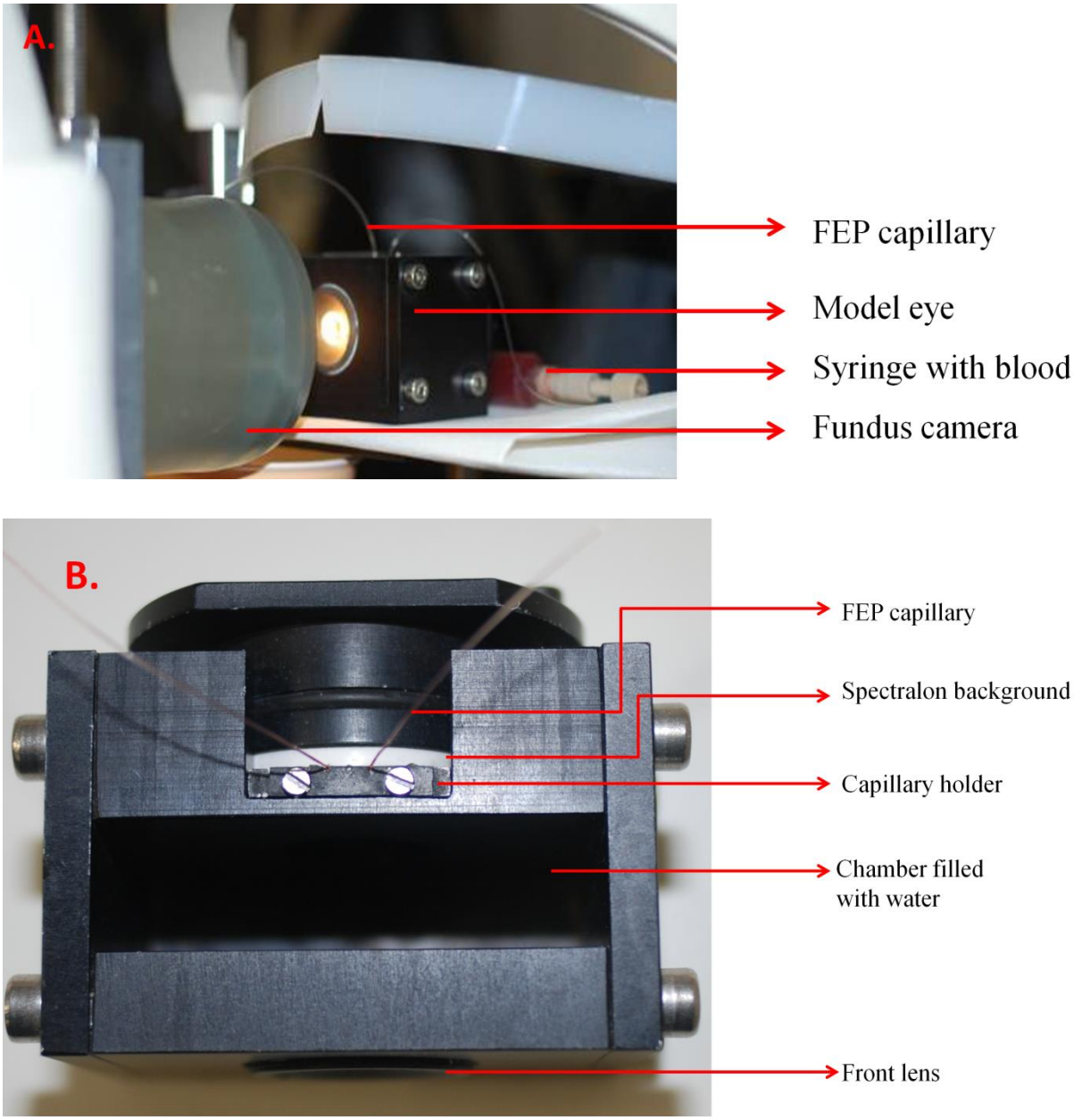

Figure 3.4: (A) The model eye in front of the fundus camera with blood filled FEP capillaries and (B) Model eye top view to show the arrangement of FEP capillaries and Spectralon background.

Two different blood oxygenations at 100% and 60 % which correspond to retinal arterioles and venules were imaged in model eye. Five samples at 100% and five samples at 60-62% were prepared as described in the method section of this chapter. The blood sample was then pumped into the FEP capillary using gastight syringe and Nano Tight sleeves and adapters and was placed in the model eye using the capillary holder (Figure 3.2). The mid chamber of model eye was filled with saline water for refractive index matching and the model eye was then placed in front of the fundus camera (Figure 3.4). Three sets of spectral images were

then taken for each blood oxygenation for every sample. Images were then analysed for oximetry.

3.2.5. Image Processing and Oximetry Analysis

The IRIS snapshot multispectral fundus camera captured images at 8 different wavelengths in single snapshot. An example of the raw image captured by the fundus camera is shown in Figure 3.5. All processing and analysis of raw spectral images for oximetry calculations were performed using Matlab (MathWorks, MA, U.S.).

The first step in image processing was to register all eight sub-images at different wavelengths into a common coordinate system. After image registration, a vessel tracking algorithm was implemented to track the vessels. To track a section of vessel, a start and end point was selected by the user and the algorithm searched for pixels between two points with the lowest intensities and finds its shortest path. As the background intensity was higher than that of vessel, the algorithm searched for pixel intensity and then classified pixels as vessel or background based on the pixel intensity. As for the model eye, which contained only two artificial vessels (FEP Capillary), the tracking was fairly simple. The same tracking algorithms were used for human retinal vessels as well and are described in detail in Chapter 5.

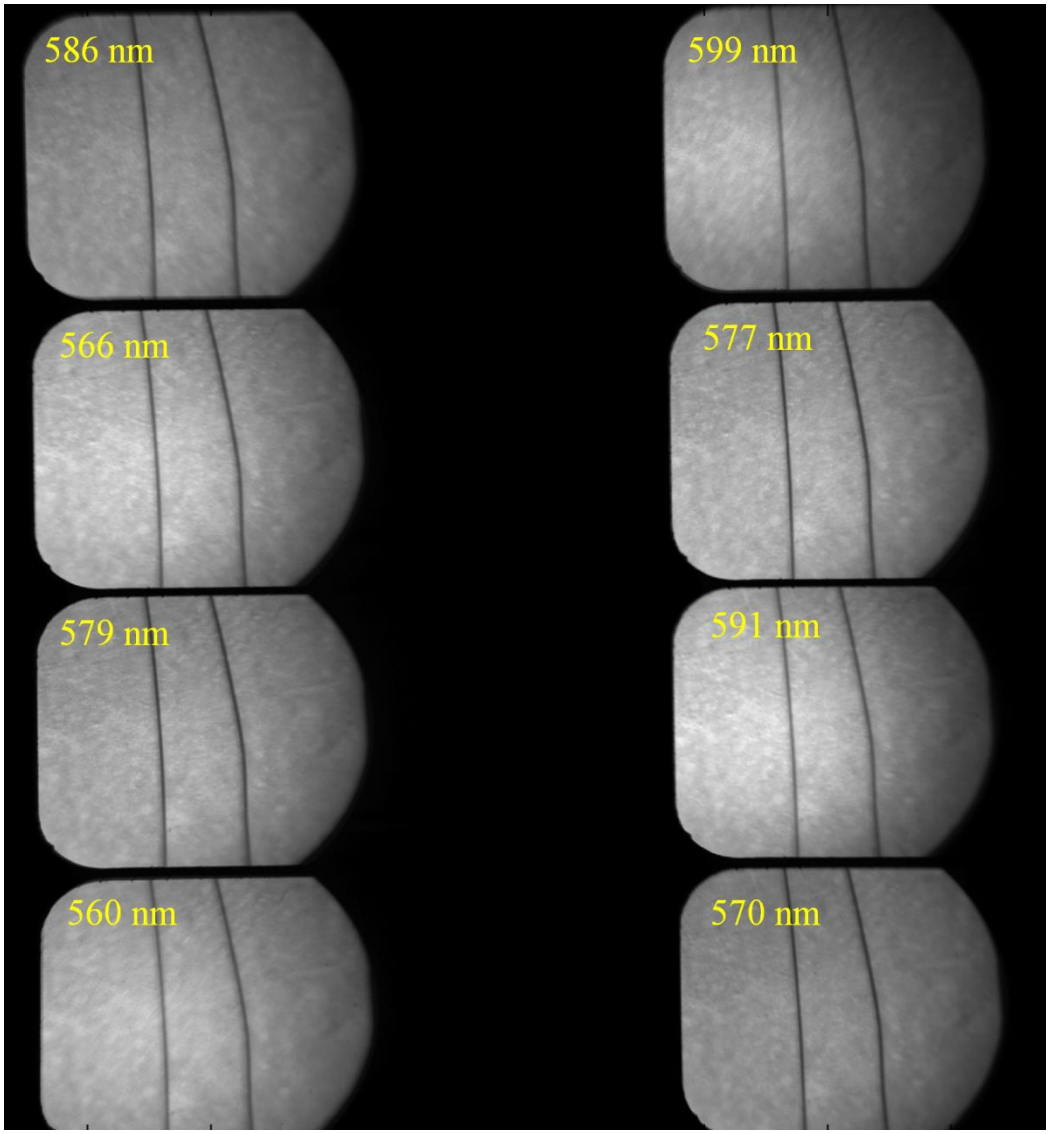

Figure 3.5: Raw image of model eye captured by IRIS snapshot device, fitted with fundus camera, each image contains eight sub images at different wavelengths optimised for oximetry.

Once the vessels were tracked, the centreline coordinates along each vessel was utilised to calculate the intensity values inside and outside of the blood vessels (FEP capillary). The algorithm identified each pixel and then classified them as vessel or background. The values of I_V and I_F can be extracted from line profile across a blood vessel (Figure 3.6).

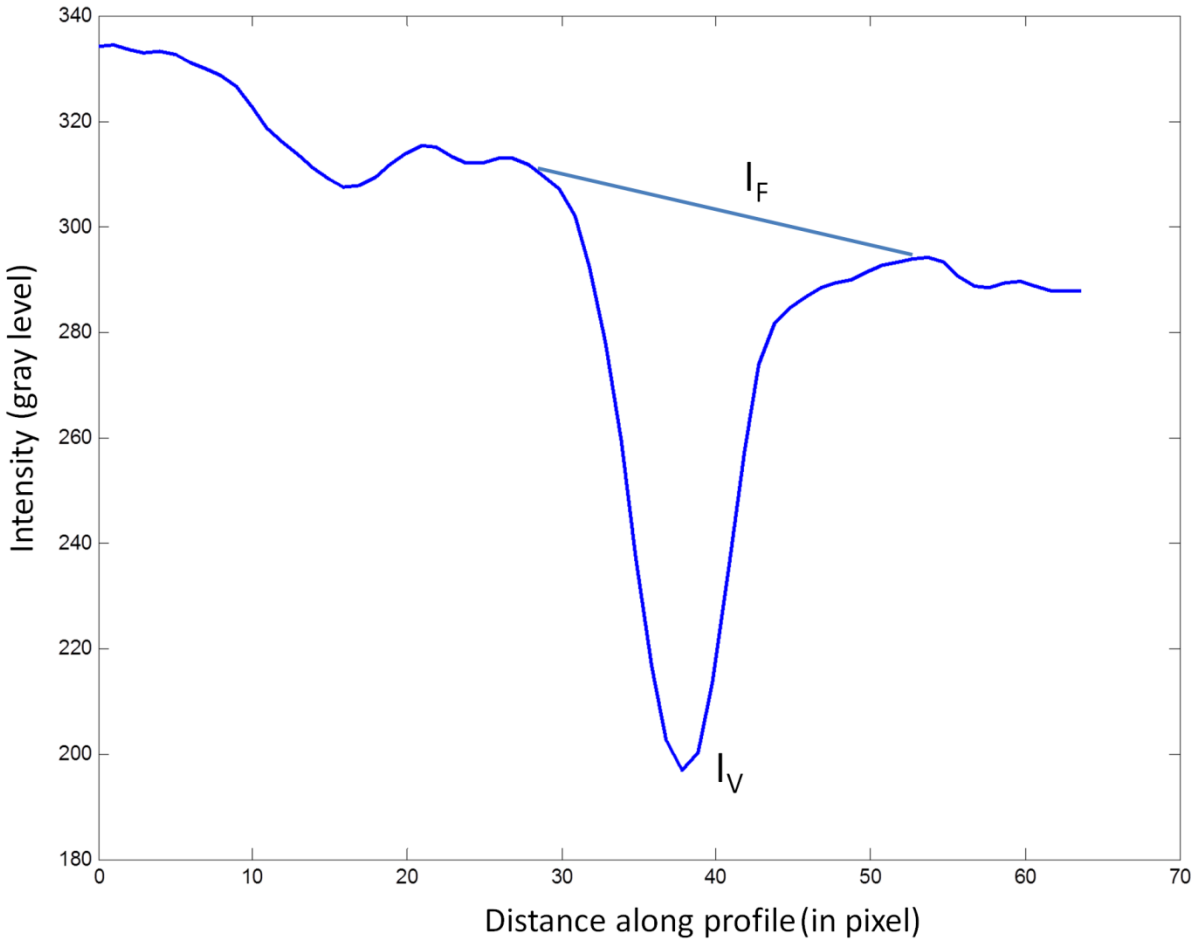

Figure 3.6 Line profile across blood filled FEP capillary. I_V is the light intensity at the centre of the capillary and I_F is the intensity outside of the capillary.

Using light intensities values inside and outside of the vessel, light transmission and optical density of the vessel was subsequently calculated.

Light transmission of the blood vessel (FEP capillary) can be calculated by following equation:

$$T = I_V/I_F \qquad (3\text{-}1)$$

Where,

T = Transmission of vessel

I_V = Intensity inside the vessel

I_F = Intensity outside the vessel

The optical density (OD) is the ratio of the measured light intensity at the centre of the vessel to the intensity just outside of the vessel.

$$OD = -\log_{10} (I_V/I_F) \quad (3\text{-}2)$$

Where I_V and I_F are the intensities of light reflected from the vessel and adjacent to the vessel, respectively.

As we know from (3-1), (I_V/I_F) is also the transmission of the vessel, so OD can also be represented as following:

$$OD = -\log_{10} (T) \quad (3\text{-}3)$$

After calculating the values for light transmissions for each pixel of vessels, OD was calculated for every point along the vessel section for all the wavelengths.

3.2.6. Oxygen Saturation Calculation

To recover oxygen saturation values from optical density values, the two-wavelength oximetry technique was used. In this method, the two wavelengths used were; one isobestic and another sensitive to oxygen saturation. This technique is described in detail in Chapter 1. In brief, this technique uses the following equation to recover oxygen saturation:

$$OS = \frac{OD(\lambda_2)\varepsilon_{Hb}(\lambda_1) - OD(\lambda_1)\varepsilon_{Hb}(\lambda_2)}{OD(\lambda_1)\left(\varepsilon_{HbO_2}(\lambda_2) - \varepsilon_{Hb}(\lambda_2)\right) - OD(\lambda_2)\left(\varepsilon_{HbO_2}(\lambda_1) - \varepsilon_{Hb}(\lambda_1)\right)} \quad (3\text{-}4)$$

Where,

OS = Oxygen saturation

OD = Optical density at a given wavelength

ε_{Hb} = Extinction coefficient of deoxy-haemoglobin

ε_{HbO2} = Extinction coefficient of oxy-haemoglobin

Using one isobestic wavelength the equation (5-4) can be simplified into

$$OS = c_1 + c_2 \frac{OD(\lambda_A)}{OD(\lambda_B)} \quad (3\text{-}5)$$

Where,

λ_A = Oxygen sensitive wavelength

λ_B = Isosbestic wavelength

C_1 and C_2 = Calibration coefficients

The two-wavelength technique [137] is an established and widely used calibration based method for oximetry. In equation (3-5), C_1 and C_2 are the calibration coefficients whose values can be calculated using data from non-pathological eyes and assuming standard values for venous and arterial oxygenations.

3.3. Results

3.3.1. Oxygen Saturation Calculation of Blood in FEP Capillaries

Oxygen saturation was measured for two oxygenation levels in five samples each. Three repeated measurements were made for each sample. The calculated oxygen saturations were 97.6 ± 1.1 (mean ± SD) for the samples at 100% oxygenation and 61.8 ± 4.2 (mean ± SD) for the samples at 60-62% oxygenation. A significant and strong correlation (r = 0.88, $P < 0.0001$, Spearman's rank correlation test) was found between known and calculated oxygen saturation in all the samples.

Figure 3.7 shows the calculated oxygen saturation values for both oxygenations, the error bar represents the standard deviation for 5 samples of same oxygenation. Table 3.3 shows the mean oxygen saturation calculated for every individual samples.

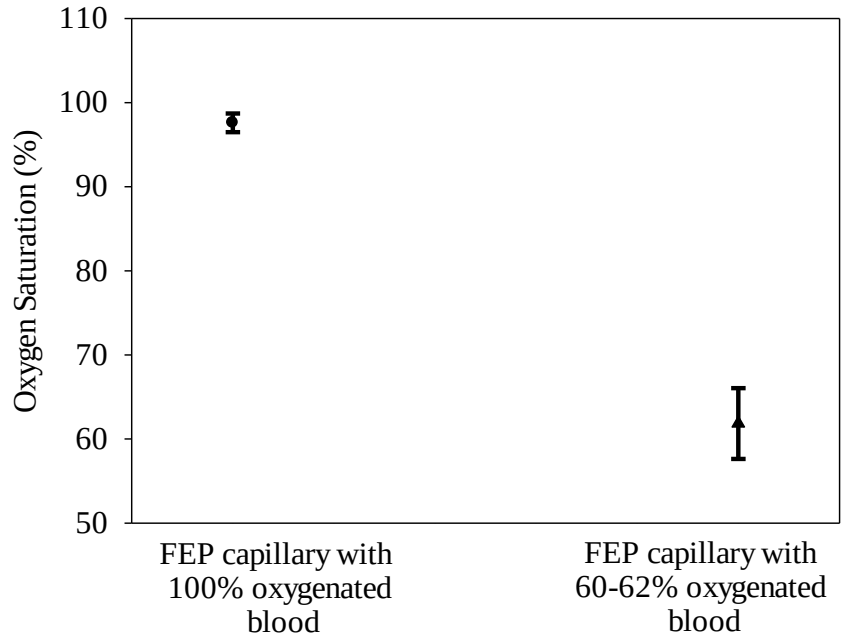

Figure 3.7: Mean oxygen saturation calculated in five blood samples at 100% and five blood samples at 60-62%. The error bar represents the standard deviation in the calculation.

Figure 3.8 and 3.9 shows the pseudocolour oximetry map of model eye containing FEP capillaries with blood at 100% oxygen and 60-62% oxygen respectively.

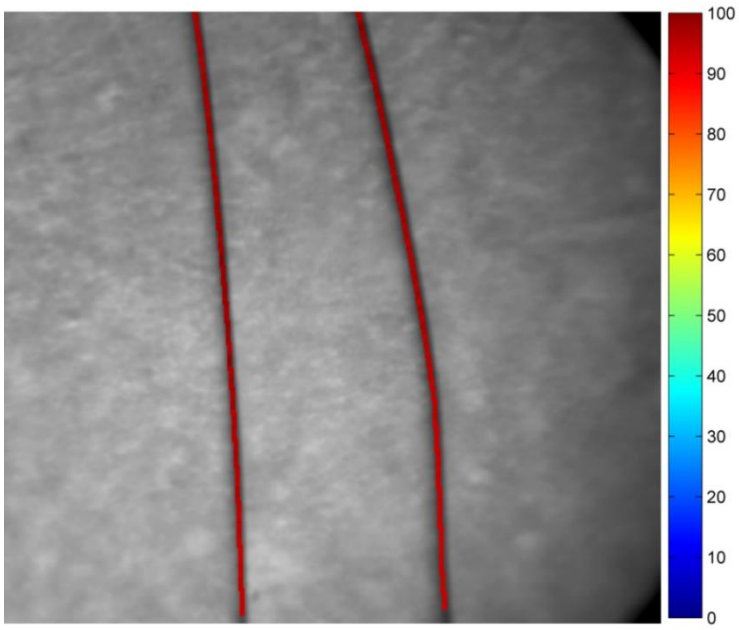

Figure 3.8: Pseudocolour oximetry map for 100 % oxygenated blood filled in FEP capillary against Spectralon background in model eye.

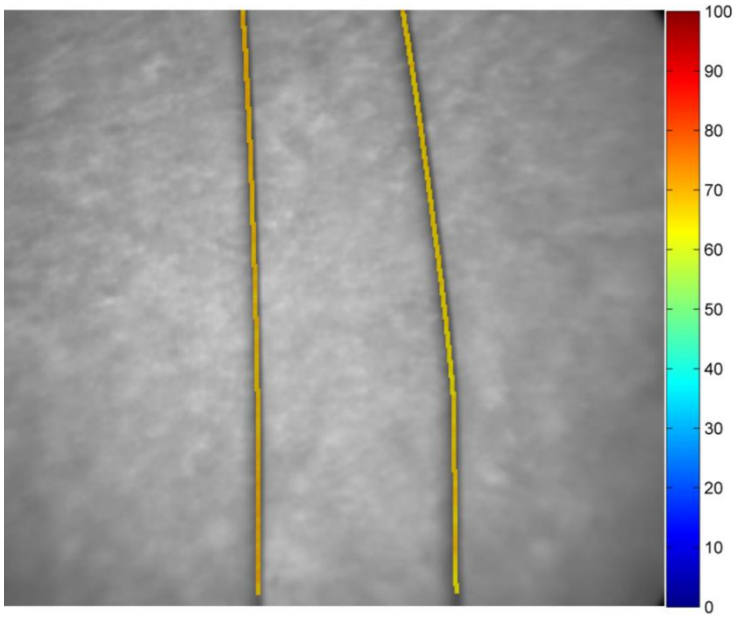

Figure 3.9: Pseudocolour oximetry map for 60-62% oxygenated blood filled in FEP capillary against Spectralon background in model eye.

Table 3.3: Mean calculated oxygenation saturation values for all five blood samples at known blood oxygenation at 100% and 60-62%

Sample number	Oxygenation (%) (100% known value)	Oxygenation (%) (60-62% known value)
1.	98.2	65.3
2.	96.3	58.9
3.	97.6	62.5
4.	99.1	66.2
5.	96.8	56.3
Average Oxygen Saturation	97.6	61.8
Standard Deviation	1.11	4.20

3.3.2. Repeatability of Calculated Oxygen Saturation Values

For every blood sample, 3 repeated measurements were taken. We assessed the repeatability of our system by calculating mean oxygen saturation values and standard deviation for three repeated measurements in the five samples of each oxygenation. The intra-sample standard deviation for three repeated oximetry calculations at 100% blood oxygenation varies between 0.3% to 1.1%. For 60-62%, blood oxygenation varies between 0.4% to 1.2%. Table 3.4 shows the calculated oxygenation (mean ± SD) values for five samples at 100% known oxygenation and Table 3.5 is the same for known oxygenation of 60-62%.

Table 3.4: Calculated oxygen saturation values (mean ± SD) for three images for the same sample of known oxygenation of 100%

Sample number	Known oxygenation (%)	Calculated mean oxygenation (in 3 images, %)	Standard deviation (%)
1.	100%	98.6	0.4
2.	100%	96.2	1.1
3.	100%	97.4	0.3
4.	100%	99.1	0.6
5.	100%	96.4	1.1

Table 3.5: Calculated oxygen saturation values (mean ± SD) for three images for the same sample of known oxygenation of 60-62%

Sample number	Known oxygenation (%)	Calculated mean oxygenation (in 3 images, %)	Standard deviation (%)
1.	60-62 %	64.4	1.1
2.	60-62 %	58.8	0.7
3.	60-62 %	61.5	1.2
4.	60-62 %	66.3	0.4
5.	60-62 %	56.5	0.7

3.4. Discussion

This validation study demonstrates that the multispectral imaging device and the oximetry algorithms used in this study are capable of measuring oxygen saturation and can distinguish difference between arterial and venular oxygen saturation. The oximetry algorithms can clearly distinguish and calculate oxygen saturation for blood samples with different oxygen saturation using a model eye. The statistical test performed on the data showed a strong and significant correlation between known and calculated oxygen saturations ($r = 0.88$, $P < 0.0001$, Spearman's rank correlation test).

The calculated oxygen saturation for five samples at 100% oxygenation was 97.6 ± 1.1 (mean ± SD). The standard deviation in this case, for five samples of the same oxygenation, was found to be 1.1% which proved that our system is quite reproducible. We also calculated intra-sample repeatability for each of those five samples using three repeated measurements (Table 3.4), and found it to be highly repeatable (SD range = 0.3% to 1.1%).

The calculated oxygen saturation for five samples at 60-62% oxygenation was 61.8 % with a standard deviation of 4.2%. The standard deviation in this case was four times higher than the previous oxygenation, but still within an acceptable range. When we calculated intra-sample standard deviation for these five samples using three repeated measurements (Table 3.5), it was found to be in the range of 0.4% to 1.2%. The reason why we get low intra-sample standard deviation than inter-sample standard deviation in case of deoxygenated blood can be explained by the method used for deoxygenation of blood. We used sodium dithionite to

deoxygenate the blood sample. It is an accurate and a widely used method for blood deoxygenation. All five blood samples were deoxygenated using the same concentration of sodium dithionite to provide an expected saturation of 60-62% in 30 minutes after mixing with blood. However, the oxygen saturation level is quite stable and will remain at the same saturation for a further 30 minutes, although we did not confirm this experimentally using blood gas analysis. For each deoxygenated blood sample, the standard deviation between the three repeated measurements is very low (0.4% - 1.1%). This shows that our oximetry algorithms are capable of calculating oxygen saturation.

The model eye provided a useful apparatus to acquire multispectral images of blood samples with different oxygen saturation. The model eye has a very simple optical design and it proved to be a useful tool as the first step for the demonstration and validation that we can distinguish and quantify the oxygenation of an artery and vein with the multispectral fundus camera and oximetry algorithms. The anatomy, physiology and optical design of human eye, is far more complex than the model eye. The retinal blood vessels lie in fundus and there are neural tissues anterior to the blood vessels. The blood vessels network is more dense than model eye and smaller vessels crossover each other as well. Figure 3.10 shows the whole mount of human retina with blood vessels, glial cells and astrocytes. In this figure, blood vessels appear in green, and it indicates one of the many complexities of real human eye versus a model eye. Nonetheless, the model eye was an informative first step towards validation of the IRIS snapshot multispectral fundus camera. In the next chapter, we will describe the *in vitro* validation in an animal model, with comparison of the oximetry results with blood gas analysis (gold standard) at a wide range of oxygenations.

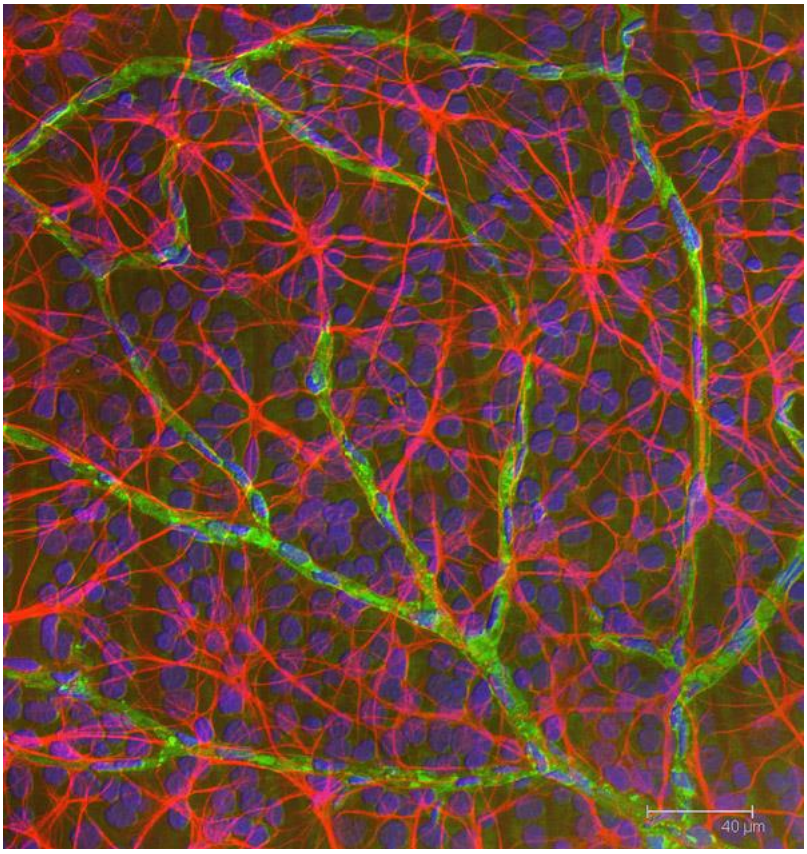

Figure 3.10: Whole mount of human retina showing astrocytes, one of the glial cells of the retina and blood vessels. Astrocytes (in red), blood vessels (in green) and the ganglion cell nuclei (in blue) [172].

The retinal arterioles and venules are 110 µm and 190 µm respectively in diameter [173]. We used FEP capillaries of 150 µm diameter as proxy retinal blood vessel. The reason for this chosen diameter is that this is within the normal average range of retinal arterial and venular blood vessel diameter.

We used defibrinated horse blood to validate our retinal oximetry system. The size and properties of horse red blood cells are comparable to human red blood cells [174, 175]. The Average diameter of a human red blood cell is between 5-7 µm and of a horse's is between 4-5 µm. The haematocrit value and haemoglobin dissociation curve (see figure 3.11) of human and horse are very similar [176]. So the horse blood provided a good way to validate the sensitivity of our oximetry system at varying oxygenations.

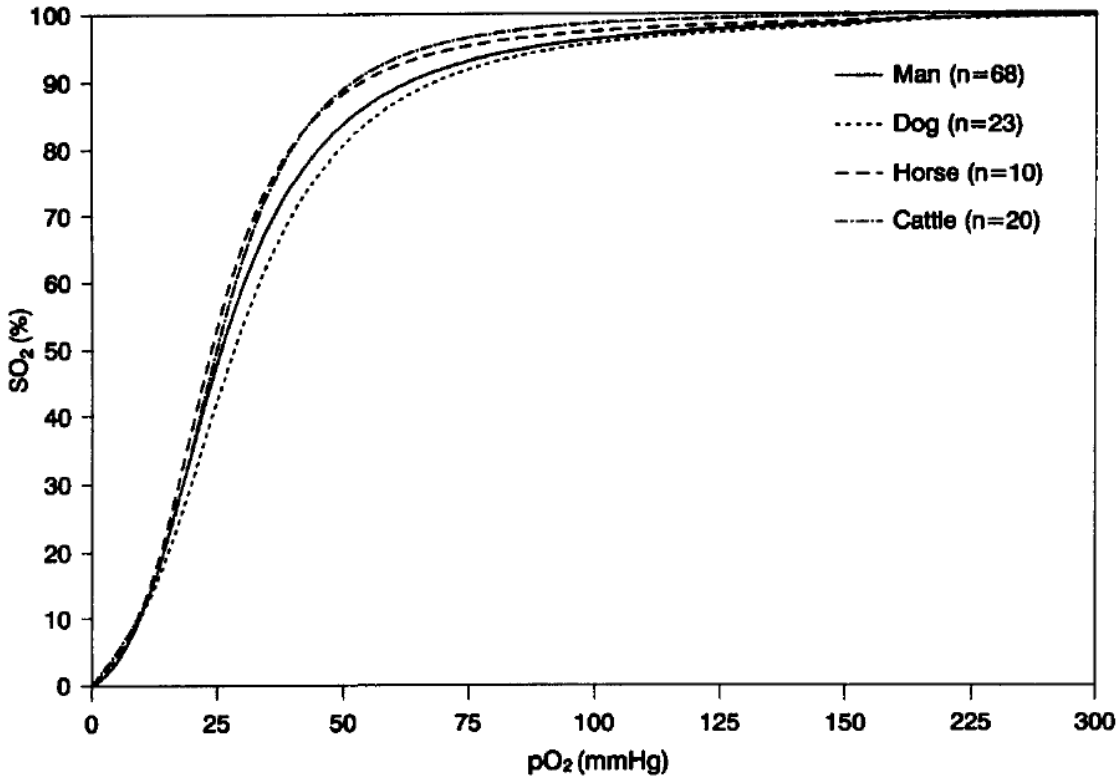

Figure 3.11: Oxyhaemoglobin dissociation curve for human, dog, horse and cattle [176].

3.4.1. Conclusion

In this study, we have demonstrated using model eye that our multispectral fundus camera is capable of imaging and performing oximetry, and can differentiate and quantify arterial and venular oxygenation. This *in vitro* validation also shows that our oximetry system is repeatable. In the next chapter, *in vivo* validation of our oximetry system in animal model will be described.

Chapter 4

In Vivo Validation of Oximetry in Animal (Porcine) Model

4.1. Introduction

In the previous chapter, we have demonstrated *in vitro* validation of our multispectral retinal oximetry system.

This chapter describes the validation experiment performed to assess the IRIS snapshot multispectral fundus camera and the oximetry algorithms. Retinal oximetry was performed in animal model at different levels of inspired oxygen

The purpose of this chapter was to assess the validity of our retinal oximetry system, by comparison to blood gas analysis in an animal (porcine) model, breathing different levels of inspired gas mixture.

4.2. Methods

This study was conducted at the Panum Institute, University of Copenhagen, Copenhagen. The study was approved by the Danish Animal Experiments Inspectorate and permission was granted for the use of animals (permission no. 2007/561-1386). Handling and preparation of the animals were performed by experienced animal technicians of the institute.

4.2.1. Pig as a Suitable Animal Model

The pig's eye is very similar to human eye and is widely used to understand human ocular pathophysiology [177-179]. The size and structure of the pigs eye is quite similar and is comparable to human eye [180]. The retinal vasculature of porcine eye is also similar to that of human. The retinal vasculature of pig has several arteries and veins and an optic disk, but it lacks a macula. It has a lateral foveal streak with increased cone photoreceptor concentration [181-184]. There are important differences between the human and pig retina. There is no central artery or vein; the pig eye is supplied by a branch of the external carotid, as opposed to internal carotid in humans [181].

The fundus of the pig looks off-white in colour with a greenish tint (Figure 4.1) as compared to the human fundus, which is orange in colour.

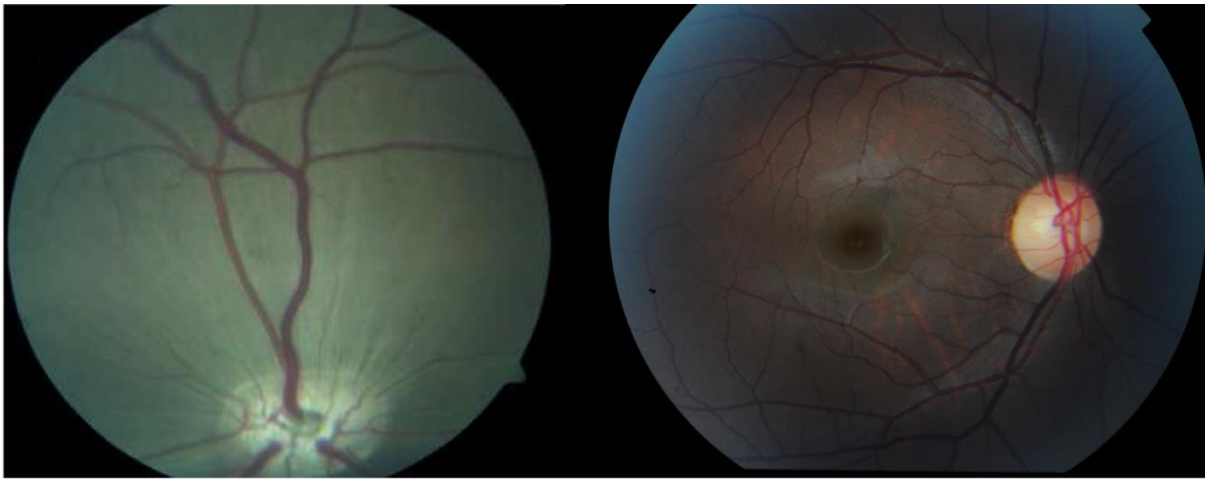

Figure 4.1: A porcine fundus (left) and human fundus (right). A difference in fundus colour is observable. The retinal vessels in the porcine fundus are also greater in diameter than in the human fundus. A distinct fovea can be seen in human but not in porcine fundus.

4.2.2. Preparation of Animal and Experimental Procedure

Four pigs aged 3-4 months, weighing 25-30 kg were used for the study. All pigs used in the experiment were female domestic pigs of the Danish Landrace (Duroc/Hampshire/Yorkshire) breed. The pigs were anesthetized before the experiment. Anaesthesia was induced by intramuscular administration of midazolam, titemine, zolazepam, ketamine, xylazine and methadone. Continuous infusion of 15 mg/kg/h propofol (B. Braun AG, Germany) was used to maintain the anaesthesia.

The animals were tracheally intubated to control the oxygen fraction in inspired air. A mixture of room air, pure oxygen and pure nitrogen was provided by the respirator resulting in the oxygen fraction ranging from 5 % to 100 %. Heart rate and peripheral oxygen saturation were continuously monitored by a pulse oximeter. All animals were subjected to three different levels of oxygen in the inspired air (100% oxygen, 21% oxygen and 10% oxygen).

Catheters were placed in the left femoral artery for extraction of blood for gas analysis. At each level of inspired oxygen, femoral arterial blood gas analysis and retinal oximetry was performed.

4.2.3. Retinal Image Acquisition

The retinal images of each animal were acquired using the multispectral IRIS snapshot fundus camera, described in detail in Chapter 2. Retinal images were taken at three (100%, 21% and 10%) inspired levels of oxygen.

4.2.4. Image Processing: Registration and Vessel Tracking

Retinal images were processed and analysed for oximetry using Matlab (MathWorks, MA, U.S.) program. The IRIS snapshot system acquires images at 8 different wavelengths in a single snapshot. An example of porcine retinal image acquired by the system is shown in figure 4.2.

The first step in image processing is to co-register all the eight sub-images at different wavelengths into a common coordinate system. This was achieved using an image registration algorithm. The registration of retinal IRIS sub-images is a two-step process. In the first step, the sub-images are cropped from the full frame and then a transformation is applied to each sub-image to bring the entire image set into a common coordinate system. In the next step, a reference image was chosen from these sub-images, and the remaining images were registered to the coordinates of the reference image. The registration process employs a cross-correlation technique, which measures the degree of similarity between two images. The maximum of cross correlation of each sub-image is decided by rotating and translating the images in comparison to the reference image.

Once the registration was complete, the images were inspected by viewing them using Matlab to detect any mis-registration. Images which were not registered properly were registered again.

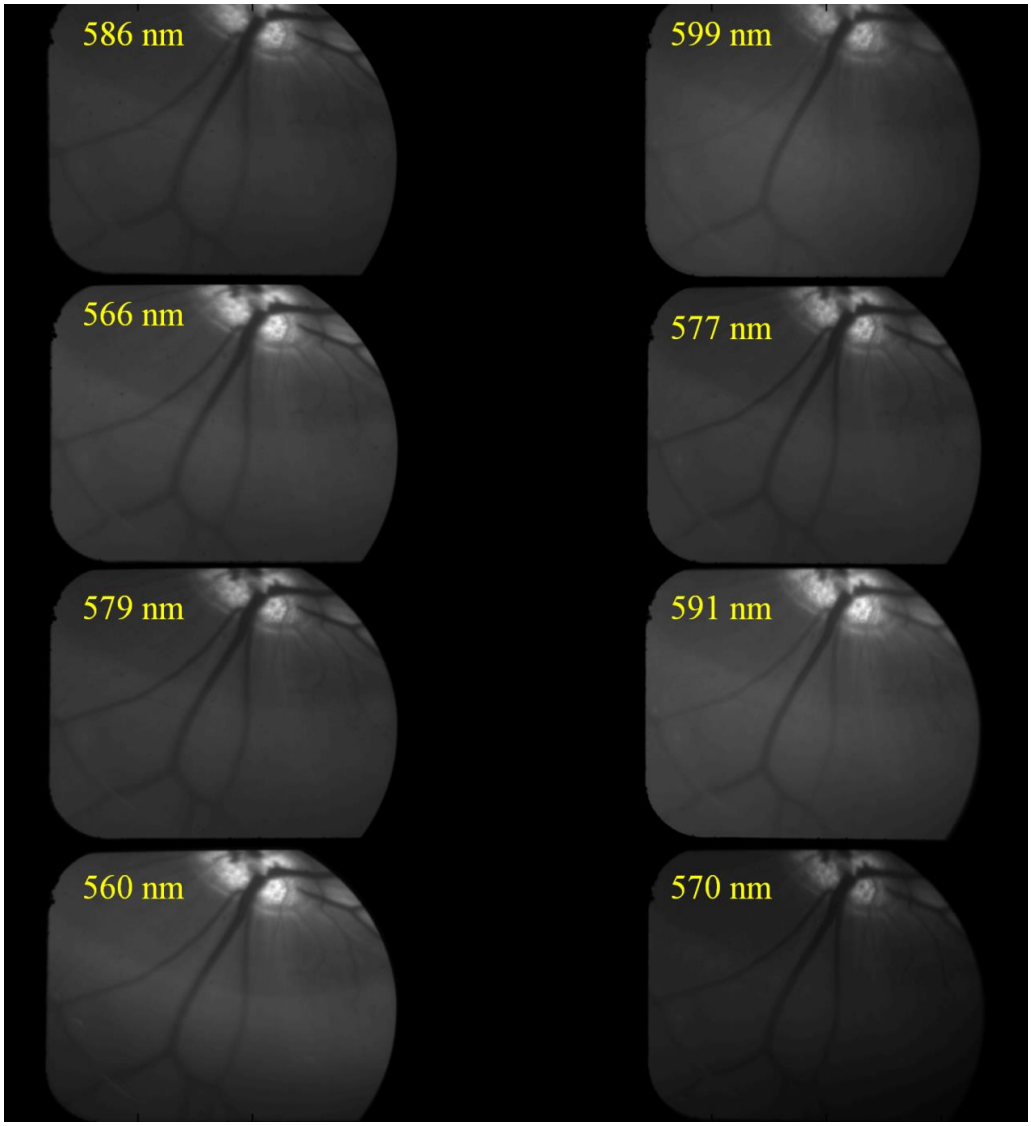

Figure 4.2: Retinal image captured by IRIS system, each image has eight sub-images at different wavelengths in 560 nm - 600 nm range, which are suitable for oximetry.

After the registration, a vessel detection algorithm was applied to detect and track vessels. A semi-automated tracking algorithm was used. The user selects the start and end points of a given vessel, and the algorithm searched for pixels between two points with the lowest intensities and finds its shortest path. Once the vessels are tracked, the centreline coordinates along each vessel were utilised to calculate the intensity values inside and outside of the blood vessels. The algorithm identified each pixels and then classified them as vessel or background. The intensity values calculated were used for optical density calculations for oximetry.

4.2.5. Vessel Profile Extraction and Calculation of Light Transmission of Retinal Vessels

The light transmission through a blood vessel can be expressed as the ratio of the measured light intensity at the centre of the vessel (I_V) to the intensity just outside of the vessel (I_F):

$$T = I_V/I_F \quad (4\text{-}1)$$

Where,

T = Transmission of vessel

I_V = Intensity inside the vessel

I_F = Intensity outside the vessel (fundus)

The values of I_V and I_F can be extracted from line profile along a blood vessel (Figure 4.3). Once the vessels are tracked, their centreline coordinates were utilised to calculate the intensity values inside and outside of the blood vessels. The algorithm identified each pixel and then classified them as vessel or background. This was achieved by calculating the perpendicular of the gradient between two consecutive points along the centre of the blood vessel. Using these intensities values transmission for all the vessel segments were calculated for all the wavelengths.

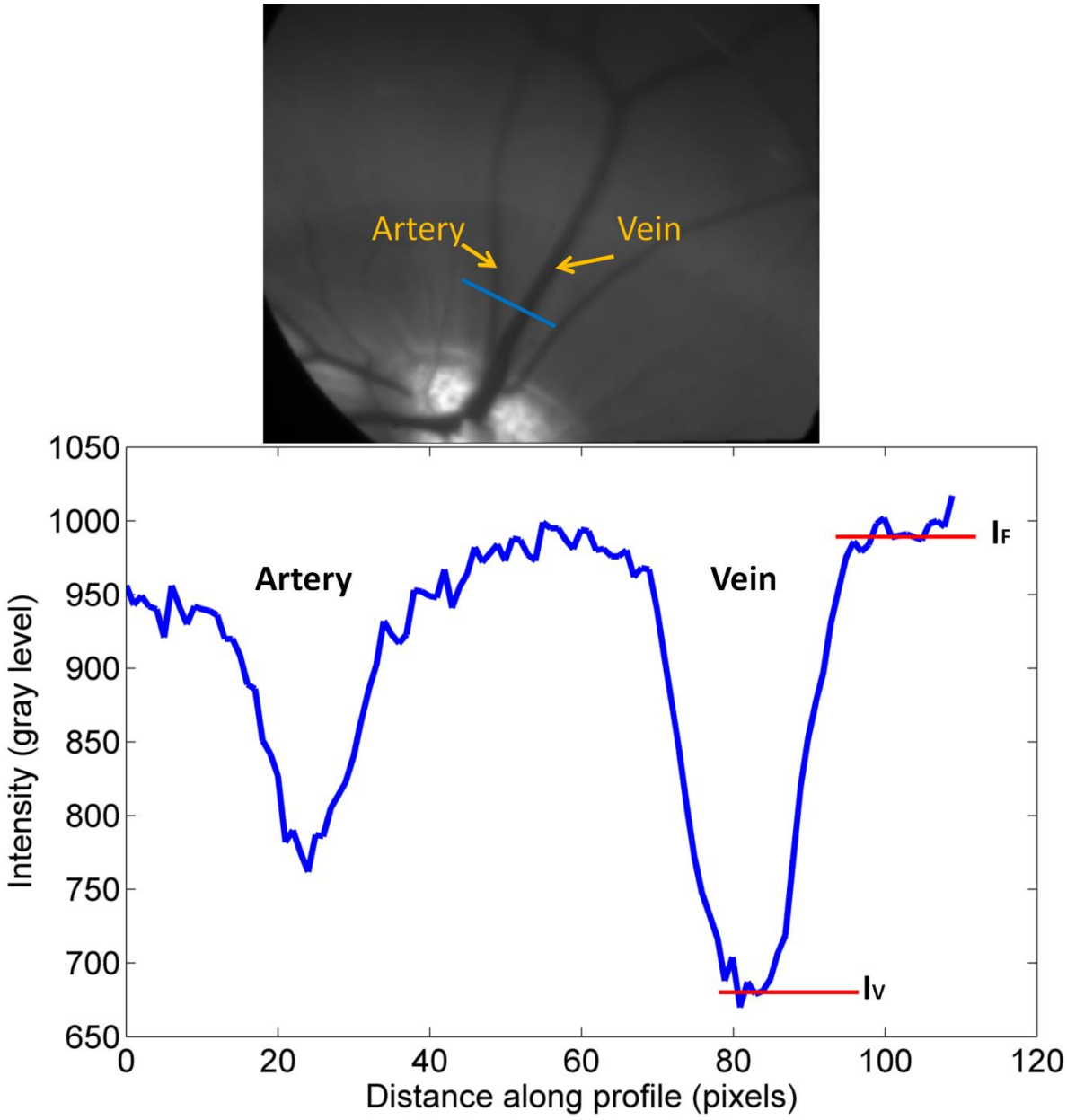

Figure 4.3: Line profile across artery and vein (shown in the retinal image above). I_V is the light intensity at the centre of the blood vessel and I_F is the intensity outside of the blood vessel.

4.2.6. Optical Density Calculation

The optical density (OD) is the logarithm of the ratio of the measured light intensity at the centre of the vessel to the intensity just outside of the vessel.

$$OD = -\log_{10} (I_V/I_F) = -\log(T) \qquad (4\text{-}2)$$

Where, I_V and I_F are the intensities of light reflected from the vessel and adjacent to the vessel, respectively.

As we know from (4-1), (I_V/I_F) is also the transmission of the vessel, so OD can also be represented as following:

$$OD = -\log_{10}(T) \tag{4-3}$$

After calculating the values for light transmission of each blood vessels as described in 4.2.5, the OD was calculated for every point along the vessel section for all the wavelengths.

4.2.7. Vessel Diameter Calculation

The diameter of the vessels was measured utilising an algorithm based on the methods reported by Fischer et al [185]. The algorithm utilises the full-width half maximum (FWHM) to estimate the diameter of the vessel. As in the process to calculate the transmission, the vessel profile was already extracted for each vessel section, the same was used to determine the vessel diameter, giving us vessel diameter values for the same vessels for which oximetry had been performed.

As the magnification of the imaging system was unknown as well as focal length of the eye, vessel diameter values were only given in terms of camera pixels.

4.2.8. Oxygen Saturation Calculation

To recover oxygen saturation values from ODs two-wavelength oximetry technique was used. In this method, the two wavelengths used were one isobestic and another sensitive to oxygen saturation. This technique is described in detail in Chapter 1. In brief, this technique uses the following equation to recover oxygen saturation:

$$OS = \frac{OD(\lambda_2)\varepsilon_{Hb}(\lambda_1) - OD(\lambda_1)\varepsilon_{Hb}(\lambda_2)}{OD(\lambda_1)\left(\varepsilon_{HbO_2}(\lambda_2) - \varepsilon_{Hb}(\lambda_2)\right) - OD(\lambda_2)\left(\varepsilon_{HbO_2}(\lambda_1) - \varepsilon_{Hb}(\lambda_1)\right)} \tag{4-4}$$

Where,

OS = Oxygen saturation

OD = Optical density at a given wavelength

ε_{Hb} = Extinction coefficient of deoxy-haemoglobin

ε_{HbO2} = Extinction coefficient of oxy-haemoglobin

Using one isobestic wavelength the equation (4-4) can be simplified into

$$OS = c_1 + c_2 \frac{OD(\lambda_A)}{OD(\lambda_B)} \quad (4\text{-}5)$$

Where,

λ_A = Oxygen sensitive wavelength

λ_B = Isobestic wavelength

C_1 and C_2 = Calibration coefficients

The two-wavelength technique [137] is a established and widely used calibration-based method for oximetry. In equation (5-5), C_1 and C_2 are the calibration coefficients whose values can be calculated using data from non-pathological eyes and assuming standard values for venous and arterial oxygenations.

4.3. Results

One pig died during data accumulation stage, so the results are based on data from three pigs. At each level of inspired oxygen femoral arterial blood gas analysis was performed and then retinal images were acquired. Each retinal image was analysed for retinal oximetry, arteriovenous oxygen saturation difference and vessel diameter.

4.3.1. Oxygen Saturation in Retinal Arterioles and Venules at 10% Inspired Oxygen

At 10% inspired oxygen, the average oxygen saturation value (± SD) for retinal arterioles and venules were 44.1 % ± 11.9 % and 20.4 % ± 10.1 %, respectively. The arteriovenous oxygen saturation difference was calculated to be 27.6 % ± 2.6 %. The femoral-artery oxygen saturation measured by blood gas analysis was 43.7 ± 11.9 %. The retinal vessel diameter (in pixels) was measured as 27.4 ± 2.6 for arterioles and 39.1 ± 4.2 for venules.

Table 4.1 shows the measured and calculated values for oxygen saturation, arteriovenous oxygen saturation difference and vessel diameters for all three inspired oxygen level.

4.3.2. Oxygen Saturation in Retinal Arterioles and Venules at 21% Inspired Oxygen

The femoral artery oxygen saturation measured by blood gas analysis at 21% inspired oxygen was 92.2% ± 1.5. The average oxygen saturation value (± SD) for retinal arterioles and

venules were 91.2% ± 1.1 % and 56.4 % ± 2.0 %, respectively. The arteriovenous oxygen saturation difference was calculated to be 34.8 % ± 2.5 %. The retinal arteriolar diameter (in pixels) was 21.3 ± 6.3 and venular diameter was found to be 31.1 ± 3.7.

4.3.3. Oxygen Saturation in Retinal Arterioles and Venules at 100% Inspired Oxygen

At 100% inspired oxygen, the average oxygen saturation value (± SD) for retinal arterioles and venules were 97.3 % ± 0.8 % and 62.5 % ± 1.7 %, respectively. The arteriovenous oxygen saturation difference was calculated to be 35.1 % ± 1.5 %. The femoral artery oxygen saturation measured by blood gas analysis was 99.6 ± 0.4 %. The retinal vessel diameter (in pixels) was measured as 19.1 ± 3.5 for arterioles and 27.1 ± 2.8 for venules.

4.4.4. Comparison of Femoral Arterial Oxygen Saturation with Measured Retinal Arterial Oxygen Saturation

At all three inspired oxygen levels (100%, 21%, 10%), femoral arterial oxygen saturation was measured by blood gas analysis before taking the retinal images. The comparison of femoral arterial oxygen saturation versus calculated retinal arterial saturation is presented in a graph in figure 4.4. The retinal arterial oxygen saturation measured by our oximetry system significantly correlated with the blood gas analysis values for femoral arterial oxygen saturation ($r = 0.90$, $P < 0.0001$, Spearman's rank correlation test).

Table 4.1: Mean oxygen saturation and vessel diameter values at 10%, 21% and 100% inspired oxygen (mean ± SD, n=3)

	Inspired Oxygen (%)		
	10%	21%	100%
Femoral artery saturation (%)	43.7 ± 11.9	92.2 ± 1.5	99.6 ± 0.4
Retinal arteriolar saturation (%)	44.1 ± 14.9	91.2 ± 1.1	97.3 ± 0.8
Retinal venular saturation (%)	20.4 ± 10.1	56.4 ± 2.0	62.5 ± 1.7
Retinal arteriovenous difference (%)	23.7 ± 6.1	34.8 ± 2.5	35.1 ± 1.5
Retinal arteriolar diameter (pixels)	27.4 ± 2.6	21.3 ± 6.3	19.1 ± 3.5
Retinal venular diameter (pixels)	39.1 ± 4.2	31.1 ± 3.7	27.1 ± 2.8

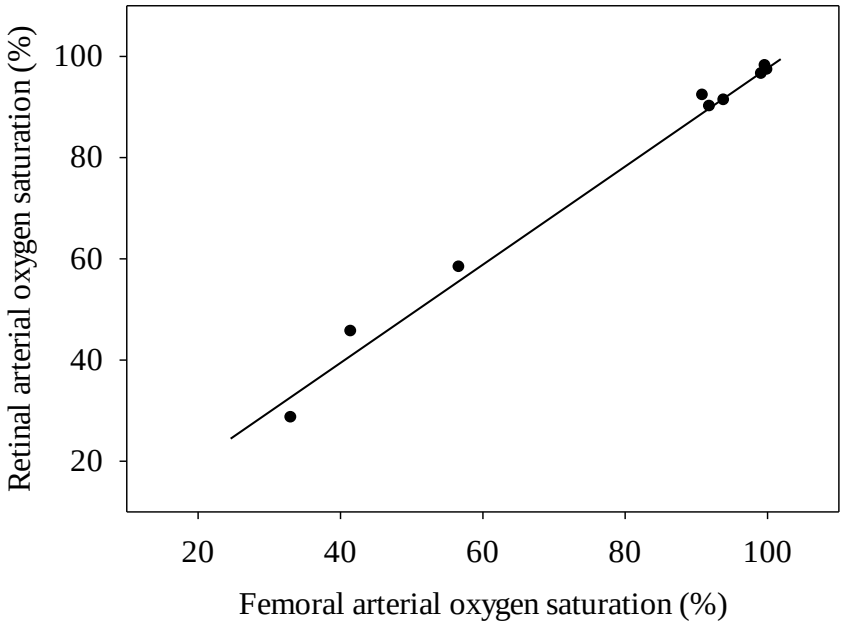

Figure 4.4: Comparison of femoral artery oxygen saturation with measured retinal artery oxygen saturation.

4.4.5. Pseudocolour Oximetric Maps of Retinal Vasculature at Different Inspired Oxygen Level

Figure 4.5 to 4.13 shows the pseudocolour images of the calculated oxygen saturations along the retinal arterioles and venules in the porcine subjects at different inspired oxygen levels.

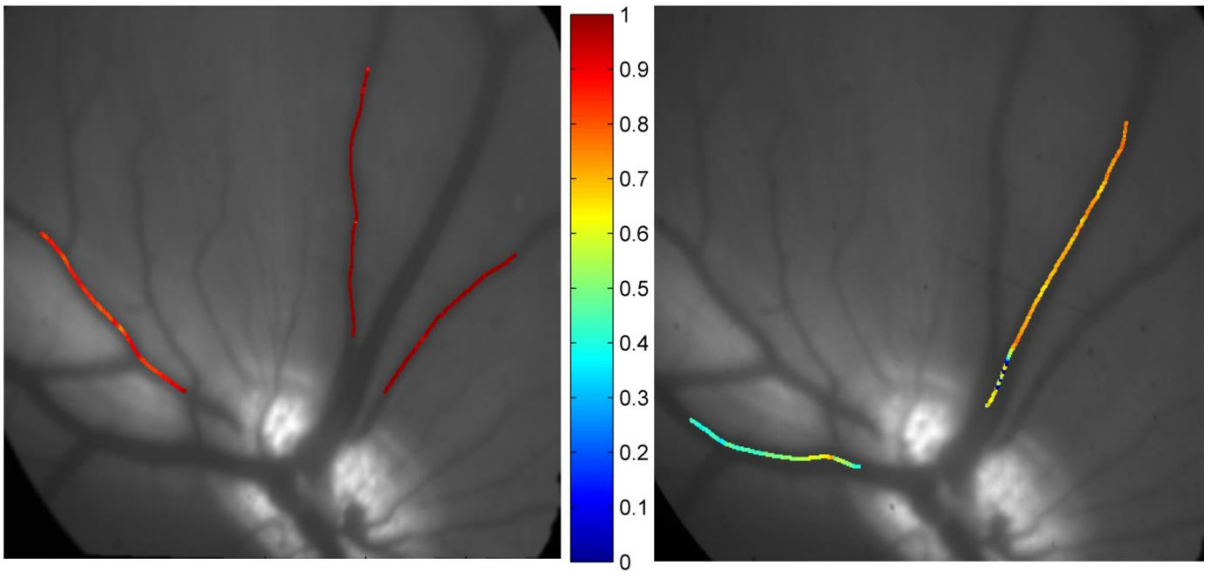

Figure 4.5: Pseudocolour oximetry map of retinal arterioles (left) and venules (right) at 100% inspired oxygen. Retinal arterioles oxygen saturation was 97.3 % and femoral artery oxygen saturation was 100%.

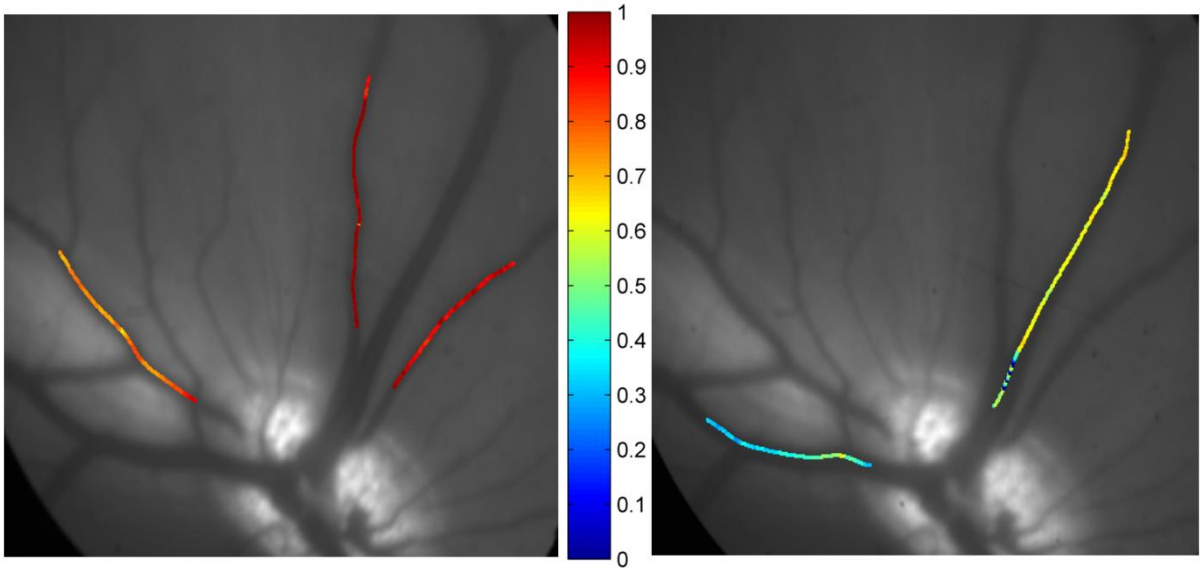

Figure 4.6: Pseudocolour oximetry map of retinal arterioles (left) and venules (right) at 21% inspired oxygen. Retinal arterioles oxygen saturation was 92.3 % and femoral artery oxygen saturation was 90.9%.

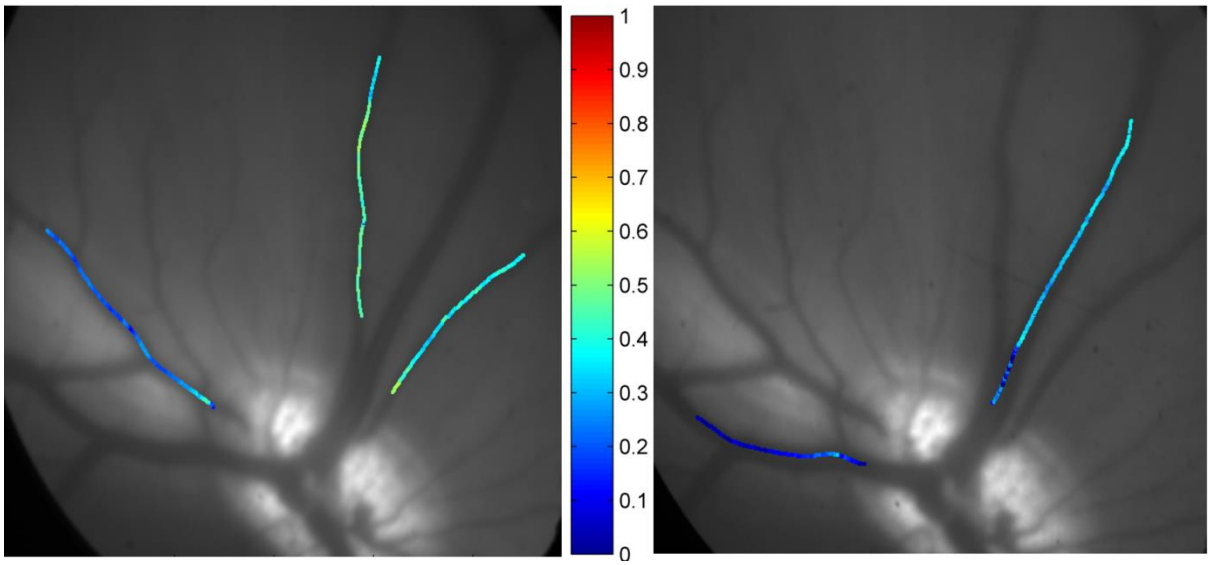

Figure 4.7: Pseudocolour oximetry map of retinal arterioles (left) and venules (right) at 10% inspired oxygen. Retinal arterioles oxygen saturation was 45.6 % and femoral artery oxygen saturation was 41.5%.

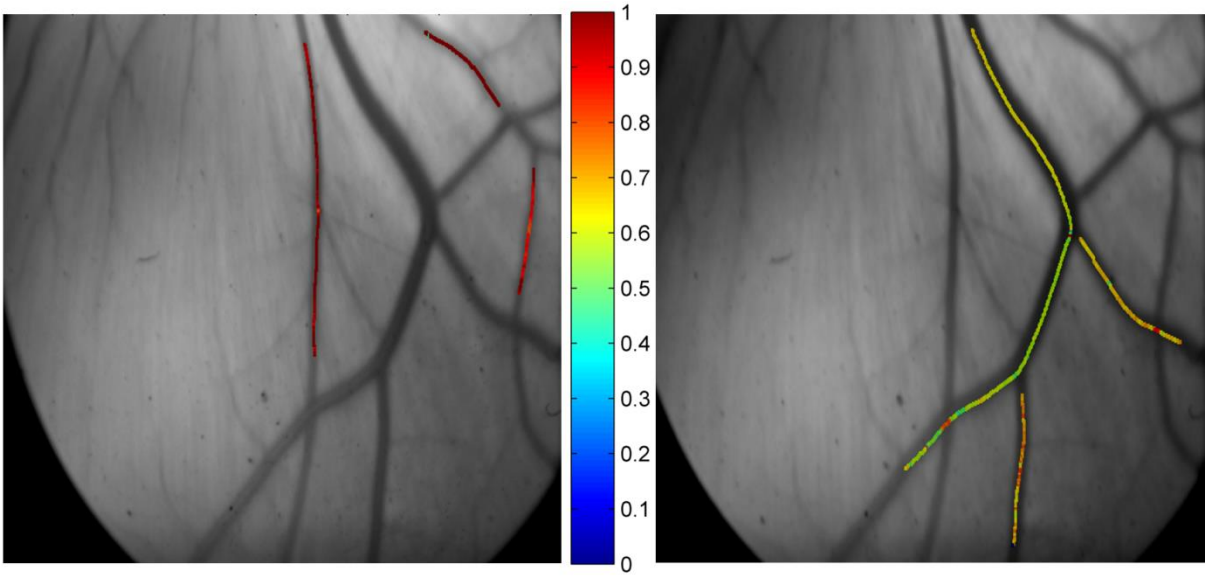

Figure 4.8: Pseudocolour oximetry map of retinal arterioles (left) and venules (right) at 100% inspired oxygen. Retinal arterioles oxygen saturation was 98.1 % and femoral artery oxygen saturation was 99.7%.

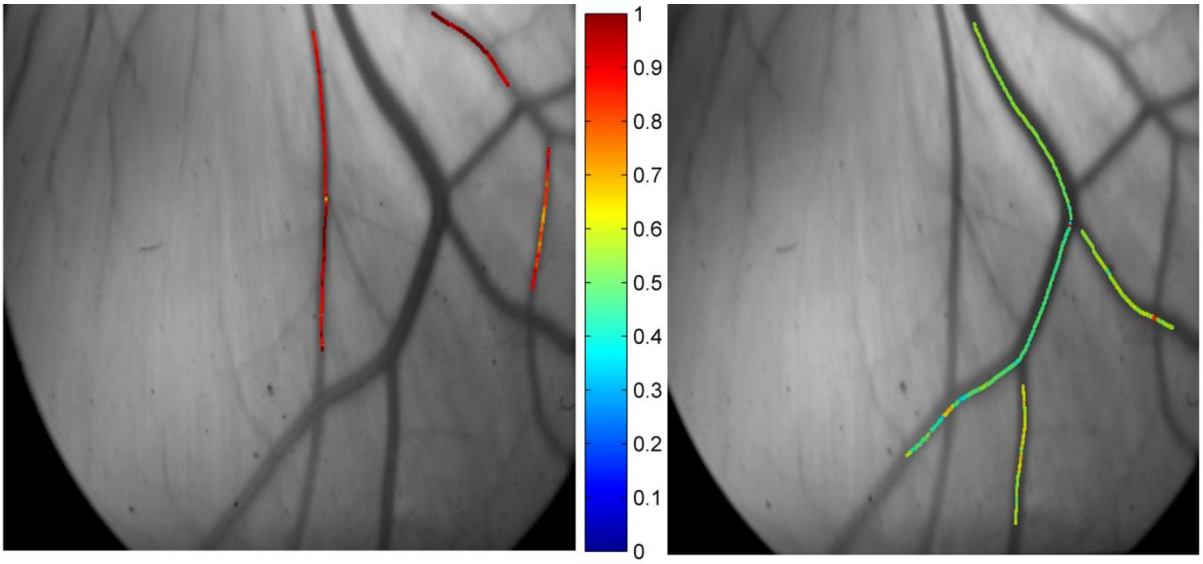

Figure 4.9: Pseudocolour oximetry map of retinal arterioles (left) and venules (right) at 21% inspired oxygen. Retinal arterioles oxygen saturation was 90.1 % and femoral artery oxygen saturation was 91.9%.

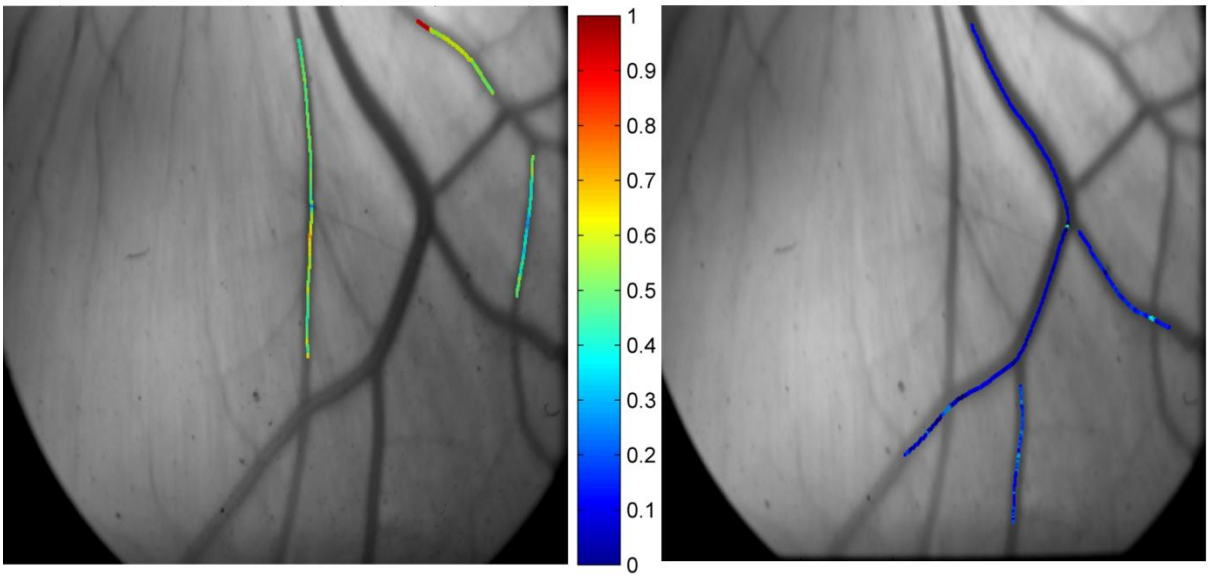

Figure 4.10: Pseudocolour oximetry map of retinal arterioles (left) and venules (right) at 10% inspired oxygen. Retinal arterioles oxygen saturation was 58.3 % and femoral artery oxygen saturation was 56.7%.

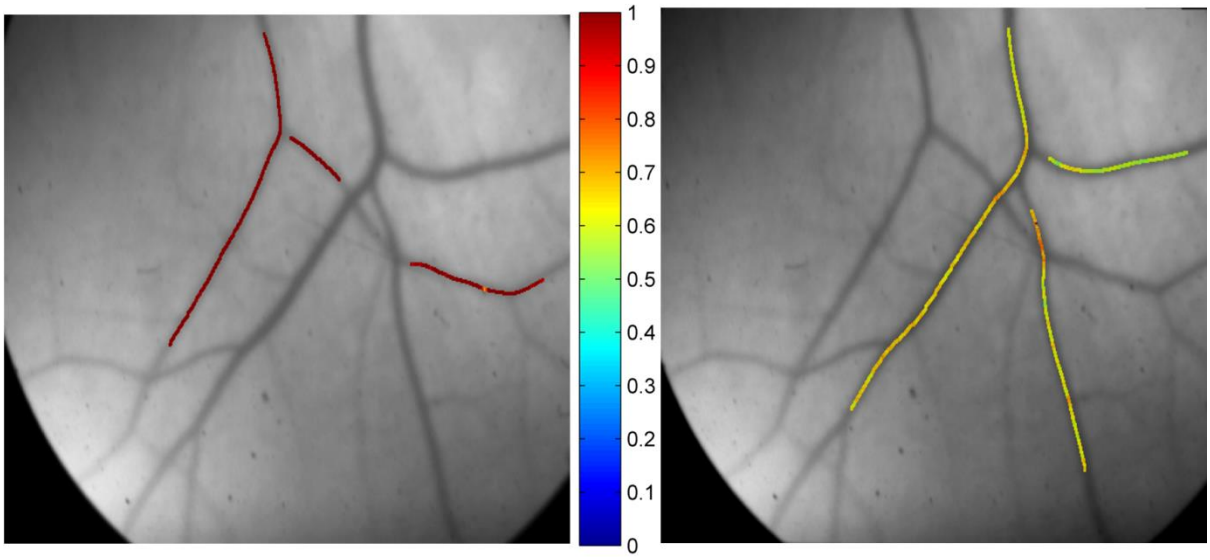

Figure 4.11: Pseudocolour oximetry map of retinal arterioles (left) and venules (right) at 100% inspired oxygen. Retinal arterioles oxygen saturation was 96.5 % and femoral artery oxygen saturation was 99.2%.

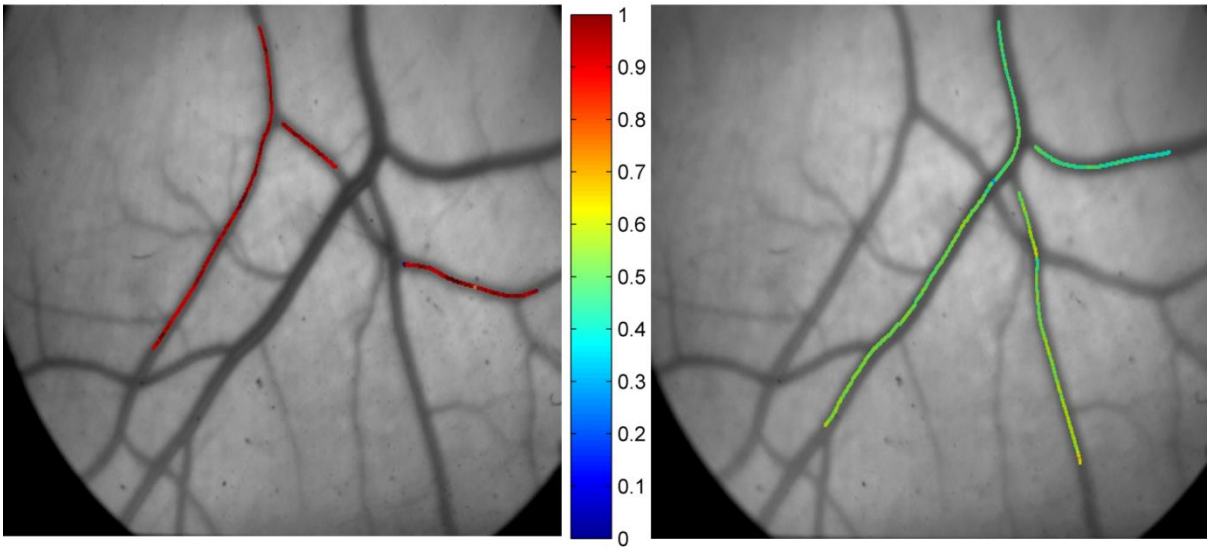

Figure 4.12: Pseudocolour oximetry map of retinal arterioles (left) and venules (right) at 21% inspired oxygen. Retinal arterioles oxygen saturation was 91.3 % and femoral artery oxygen saturation was 93.9%.

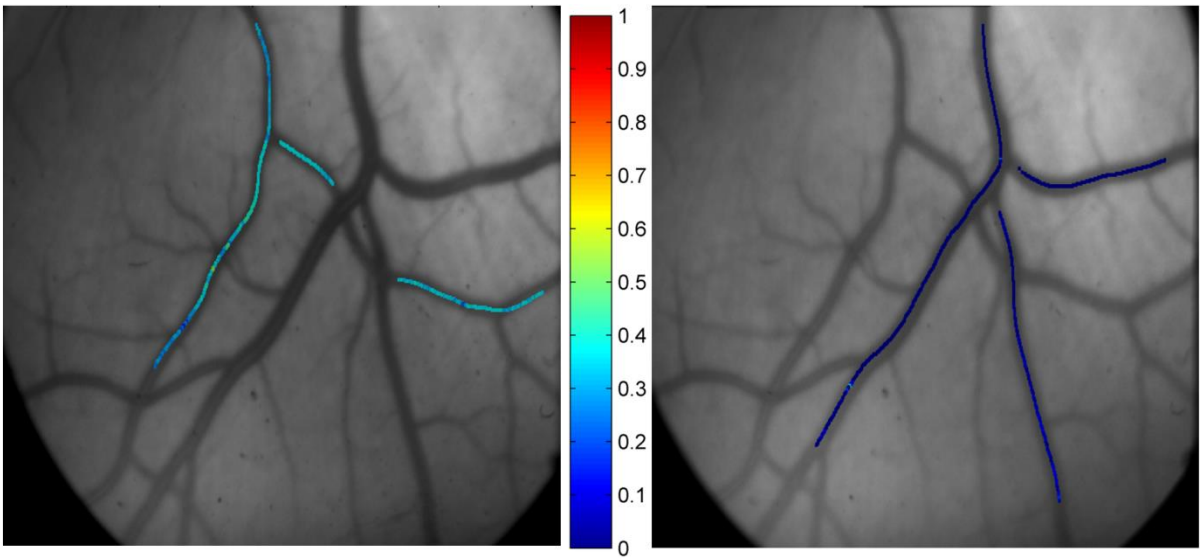

Figure 4.13: Pseudocolour oximetry map of retinal arterioles (left) and venules (right) at 10% inspired oxygen. Retinal arterioles oxygen saturation was 28.6 % and femoral artery oxygen saturation was 33.1%.

4.5. Discussion

The oxygen saturation values measured by our oximetry system correlated significantly with the femoral arterial blood gas analysis, which is considered as the gold standard in the field. In the previous chapter, we have demonstrated that our system is capable of measuring difference in oxygen saturation *in vitro* in model eye. Although *in vitro* validation of the system was a good starting point, but *in vivo* validation in animal model, where we controlled the inspired air oxygen and compared our oximetry values with an established method like blood gas analysis proved to be a reasonable method to calibrate and validate our oximetry system. Using the animal model also provided the opportunity to test oximetry for a broader range of systemic oxygen saturation, than possible in humans.

In this study, we successfully demonstrated that our device is sensitive to oxygen saturation at different inspired oxygen levels as well as oxygen saturation differences in retinal arterioles and venules at the same inspired oxygenation. Figure 4.3 in the method section, shows a line profile across an arteriole and a venule of pig retina. As we know that the more oxygenated the blood is in the vessel, the more transmissive (less optically dense) it will be for light, and vice versa. And it is clear from the Figure 4.3, the arteriole is more transmissive that the respective vein.

For the same level of inspired oxygen, we get different levels of femoral arterial oxygen saturation in pigs. At 100% and 21%, all the pigs have almost similar femoral arterial oxygen saturation, but at 10% of inspired oxygen the standard deviation in measured femoral arterial saturation in the pigs were 12% (Table 4.1) and standard deviation in the calculated retinal oxygen saturation was around 15%. The femoral arterial oxygen saturation values at 10% inspired oxygen was 43% which is considerably lower than in reported in human [34, 186], but pigs have shown to be have lower oxygenation in normal state than human [187]. A recently published study [188] on pigs, which also compared retinal oximetry and femoral artery oxygenation at different inspired oxygen levels also reported lower arterial saturation at 10% inspired oxygen. Results from that study are comparable with this study.

We did not perform blood gas analysis of venous blood to compare it with the calculated retinal venular oxygen saturation. The retinal venular oxygen saturation for 100%, 21% and 10% inspired oxygen was calculated to be 62.5% ± 1.7%, 56.4% ± 2.0% and 20.4% ± 10.1 respectively with an arteriovenous oxygen saturation difference of 35.1% ± 1.5%, 34.8% ± 2.5% and 23.7% ± 6.1%. The arteriovenous oxygen saturation difference remained the same for 100% and 21% inspired oxygen but reduced for 10% inspired oxygen.

The retinal vessels diameter values increased as we changed the inspired oxygen level from 100% to 10% (see Table 4.1 for values). The increment in retinal vessel diameter from 100% to 21% inspired oxygen is small, but a considerable increment was seen at inspired oxygen level of 10%. Figure 4.14 shows the retinal image of same pig at inspired oxygen level of 100% (left) and 10% (right). An increase in retinal arteriolar and venular diameter can be observed in the image visually.

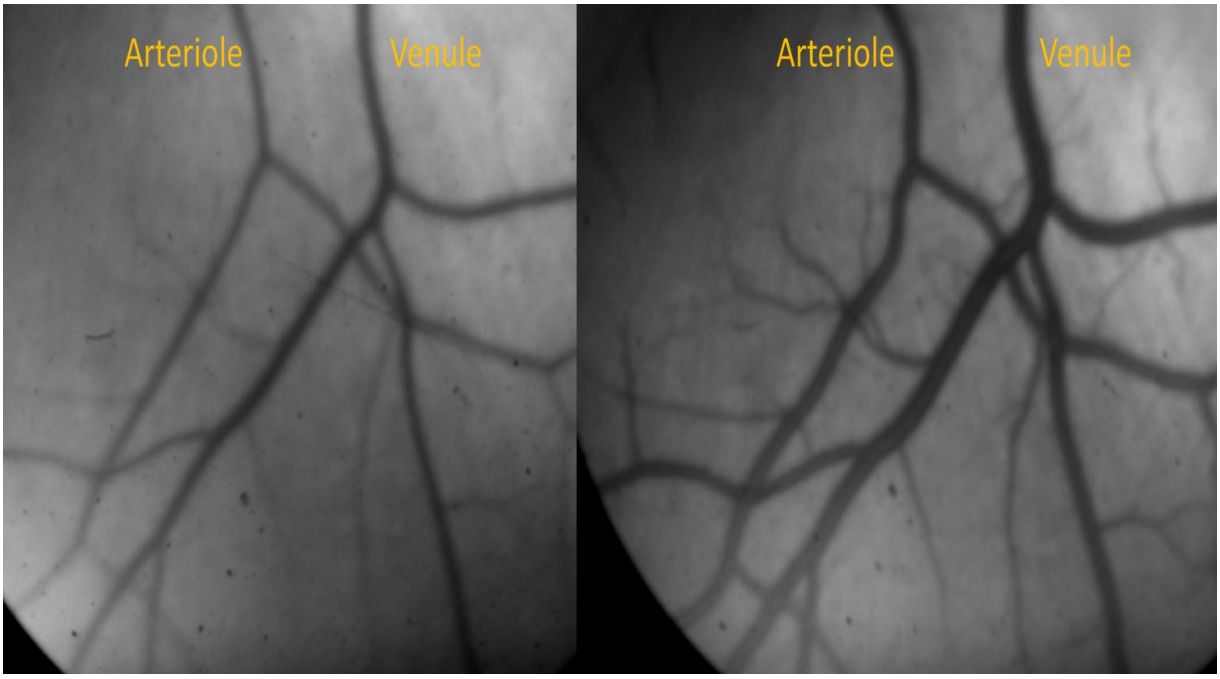

Figure 4.14: Retinal image of same pig at 100% inspired oxygen (left) and 10% inspired oxygen (right). Retinal vessel diameter increment can be observed visually.

Hypoxia is known to induce vasodilation of the retinal vessels which results in increased retinal blood flow.[28-34] The other phenomenon which can be observed in the image above is how the blood vessels (both arterioles and venules) became much darker in appearance at lower inspired oxygen. This can be attributed to the fact that blood vessels with lower oxygen saturations are less transmissive to light and appear darker. Due to the same effect smaller blood vessels can be seen in the retinal image (right) at 10% inspired oxygen.

The pig is a suitable animal model to validate the oximetry algorithms over a range of inspired oxygen. Although quite similar, there are a few basic differences between the pig and human retina. The pigs retinal vessel [189] are slightly larger in diameter than human and has less dense vasculature. Human retinal vessel lie embedded in nerve fibre layer whereas porcine retinal vessels lie superficially in the inner retina [182].

One of the issues in imaging was corneal dryness in the animals. As the pigs were anesthetised, a clip was used to keep the eye opened for fundus imaging. This could have resulted in corneal dryness and degradation of cornea resulting in poor image quality. To avoid that, the eyes were opened only to acquire the images and then it was shut properly. Also the eye was constantly irrigated with saline water before and after imaging to keep it from drying.

One other possibility which could alter normal physiology in animals is the anaesthesia. Propofol has been shown to lower the systemic blood pressure, heart rate and cardiac output via peripheral vasodilation [190-192]. Although, there may be effect of anaesthesia on vital signs of the animals, but they were stable during each of the inspired oxygen level before femoral artery blood gas analysis and retinal imaging were done.

In conclusion, we have demonstrated in animal model, that our retinal oximetry system is capable of measuring oxygen saturation over a broad range of oxygenation values.

Chapter 5

Human Retinal Imaging and Oximetry

5.1. Introduction

The main aim of this chapter is to demonstrate the use of the IRIS snapshot multispectral fundus camera to perform oximetry in human retinal vessels.

This chapter will describe the use of the IRIS snapshot multispectral fundus camera to image the human retina and image processing methods used to perform oximetry in retinal vessels. Furthermore, it will also describe a protocol for oximetry in retinal arteries and veins.

5.2. Methods

This study was approved by Heriot-Watt University Ethics Committee. All procedures were performed according to the Tenets of the declaration of Helsinki.

5.2.1. Recruitment of Subjects

Eighteen healthy subjects were recruited for the study (age 28 ± 6 years; twelve males and six females). Subjects included staff and student members within the research group and school, who volunteered to participate in the study. All subjects provided written informed consent before participation in the study.

On the day of study, participants were briefed about the study protocol and the risks, if any. They were provided with an information sheet. All participant queries related to the experiment were answered to their satisfaction. Subjects were asked to refrain from consuming alcohol or caffeinated drinks prior to the experiment. Participant age, sex, weight and height were recorded.

Pupils were dilated before retinal imaging with 1% tropicamide (Bausch & Laumb, Chauvin Pharmaceuticals, Ltd., U.K.). In about ten to fifteen minutes maximum dilation of the pupil was achieved, and the subjects were ready to be imaged. Fingertip pulse oximetry (AUTOCORR; Smiths Medical ASD, Inc., Rockland, MA) was employed to continuously monitor the peripheral arterial oxygenation throughout the experiment.

5.2.2. Retinal Spectral Image Acquisition

The IRIS snapshot multispectral fundus camera has been previously described in detail in Chapter 2. The IRIS snapshot method enabled us to acquire images in a single snapshot at eight different wavelengths that were optimised for oximetry. The snapshot technique is easy to acquire with minimum discomfort to the subject. The subjects were seated in front of the camera, with their head on the head mount and their forehead firmly positioned against the forehead strap. The subjects were instructed to minimise the head or eye movement, until the retinal images were acquired. The retina was then visualised using the inspection lamp of the camera through the eyepiece. The camera focus was adjusted until the edges of retinal blood vessels appeared sharp. The optic disk and macula were captured in all images, ensuring that similar retinal vasculature was imaged for all subjects.

Head and eye movement and random eye blinks caused changes in the focus of the images, decreasing image quality and increased error in oximetry measurements. After capturing each image set, the quality of the images was determined by the operator and a new image was acquired if needed. The image was rejected if it was not in perfect focus and/or the image region did not include the optic disc and macula. At least five good quality images were captured for each subject. This imaging protocol ensured that retinal images captured were of the optimum quality: very few images were excluded from the study.

5.2.3. Retinal Spectral Image Selection and Processing

Raw images were scrutinised before they were selected for further processing using Matlab (MathWorks, MA, U.S.). Images were visually assessed to be optimal focused, which contained the optic disc and macula and were free from artefact were selected for oximetry. An example of a raw retinal image captured by IRIS is shown in Figure 5.1.

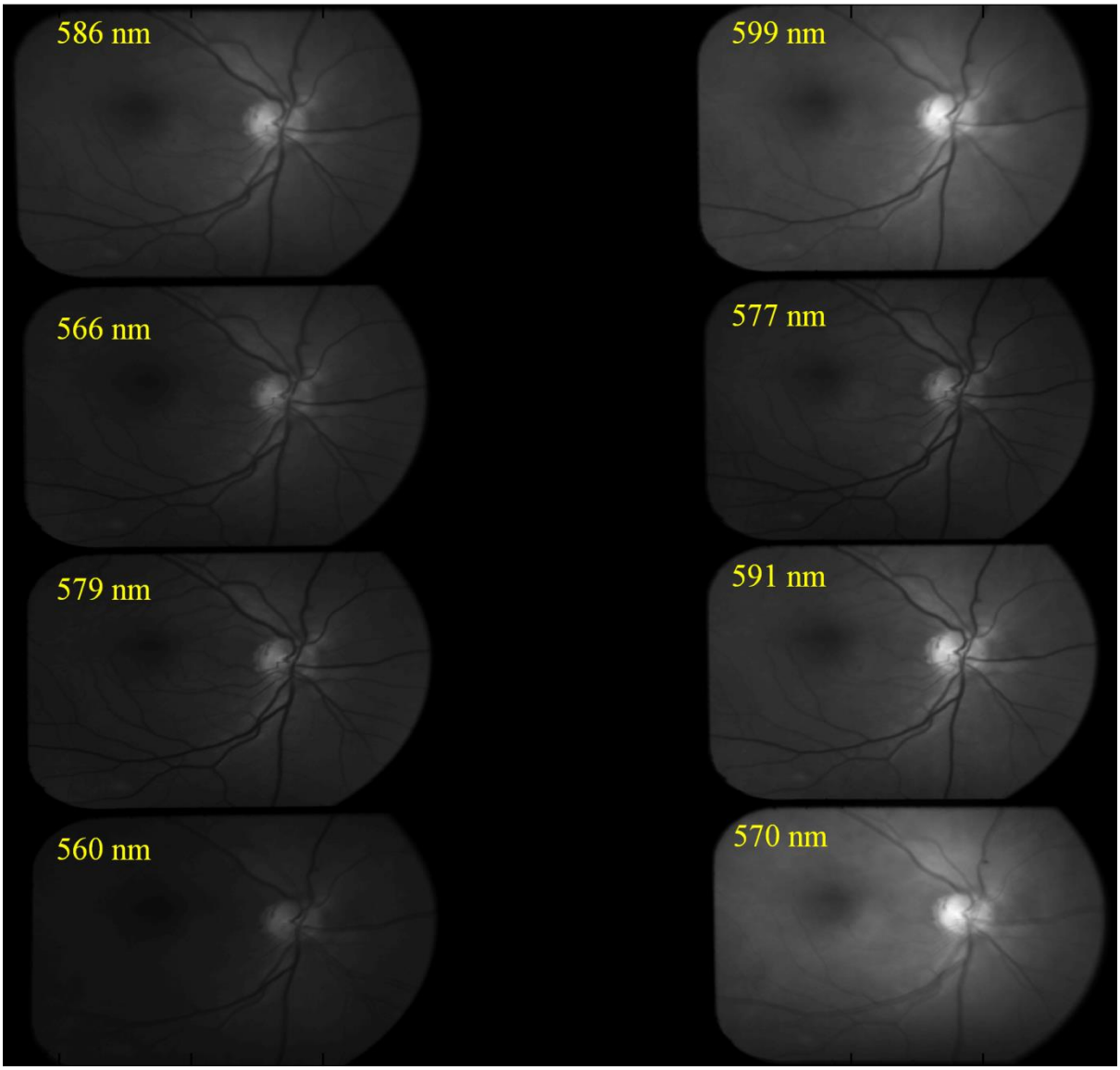

Figure 5.1: Raw image captured by IRIS snapshot device attached to fundus camera. Each image contains eight sub images at different wavelengths optimised for oximetry.

The image processing algorithm used in the human retinal images was similar to that used for the model eye and porcine eye oximetry described in Chapter 3 and 4 respectively. The image processing steps are described in the following sections.

5.2.3.1. Image Registration

Image registration is the process of aligning images of the same scene to the same coordinate system. The IRIS system captured eight sub-images at different wavelengths in one snapshot (Figure 5.1). Due to different beam paths through the imaging lens, each sub-image of IRIS is subject to a different non-rectilinear geometric distortion. The registration of retinal images is a very crucial step in order to perform oximetry accurately at a given vessel point.

The registration of retinal IRIS sub-images is a two-step process. In the first step, the sub-images are cropped (Figure 5.2) from the full frame (Figure 5.1) and then a transformation is applied to each sub-image to bring the entire image set into a common coordinate system.

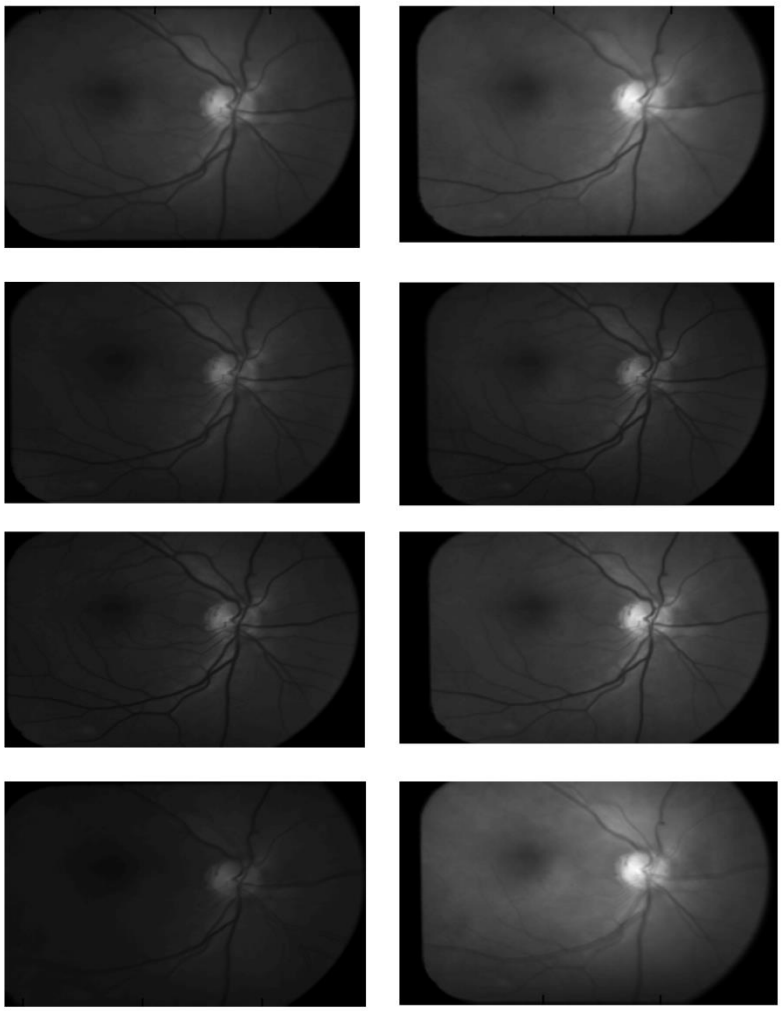

Figure 5.2: IRIS sub-images; cropped and approximately registered.

In the next step, a reference image was chosen from those sub-images, and the remaining images were registered to the coordinates of the reference image. The registration process employs a cross-correlation technique that measures the degree of similarity between two images. The maximum cross-correlation of each sub-image was decided by rotating and translating the image in comparison to the reference image. The cross-correlation technique utilised unique features within each retinal image, which are similar in appearance, but independent of the wavelength. Some unique features that can be utilised are the location of the optic disc, and retinal vessels. The distortion caused by the imaging lens can be assumed to be constant with time. Once the first image has been registered, the same transformation

can be applied to all subsequent images of the same retinal data set. An example of a registered image is shown below in Figure 5.3.

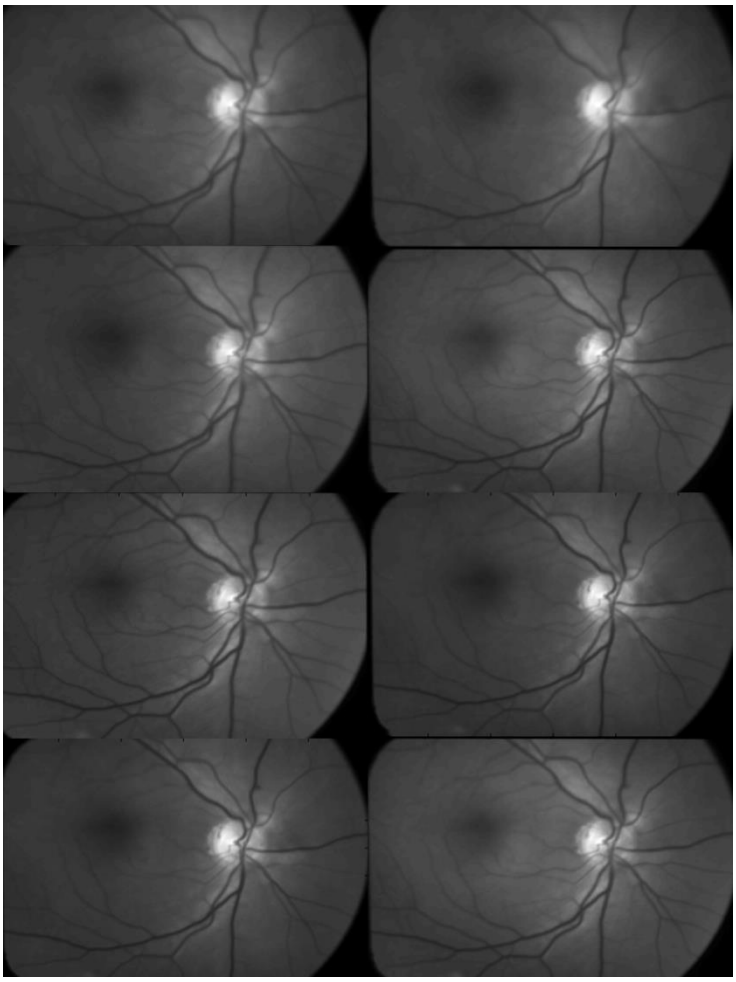

Figure 5.3 Eight registered IRIS images of the same eye at different wavelengths.

After the registration process was completed, the registered images were visually verified as registered correctly. Occasionally, some images were found to be mis-registered, and were either registered again correctly or removed from the analysis.

5.2.3.2. Vessel Detection and Tracking

After registering the IRIS images, the retinal vessels were tracked (Figure 5.4) using a semi-automated vessel-tracking algorithm. As all eight sub-images were co-registered, vessel tracking was performed on one reference image (579 nm) where retinal vasculature was easily distinguished and then applied to all other sub-images. The option of tracking the vessels at any other wavelength image could also be done, if needed.

Vessel segments were tracked in a standardised manner, based on vessel width, length, start and end points (Table 5.1). Vessel segments with a width of 12 pixels or wider and length of 100 - 200 pixels were selected. Furthermore parts of vessels close to the optic disc or bright area surrounding it were avoided. Vessel segments with strong background variations in reflectivities were also excluded as they are known to exhibit higher levels of artifactual errors in oximetry. To track a section of vessel a start and end point was selected by the user and the algorithm searched for pixels between two points with the lowest intensities and finds its shortest path.

Once all the retinal vessels were tracked, the algorithm saved the vessel coordinates for all the tracked vessels for calculation of transmission and further analysis.

Table 5.1: Selection criteria of retinal vessel for oxygen saturation measurements

Retinal Vessel Selection	**Criteria**
Retinal vessel width	12 pixels or wider
Retinal vessel length	100 to 250 pixels (preferably as close to 250 pixels as possible)
Start point of vessel	Close to optic disc but always exclude pixels with optic disc or bright area surrounding it
End point of vessel	After length of 250 pixels, excludes pixels at edge of the image
Exclude segments of vessel if	• Vessel with strong background reflection • Vessel segments affected by strong brightness

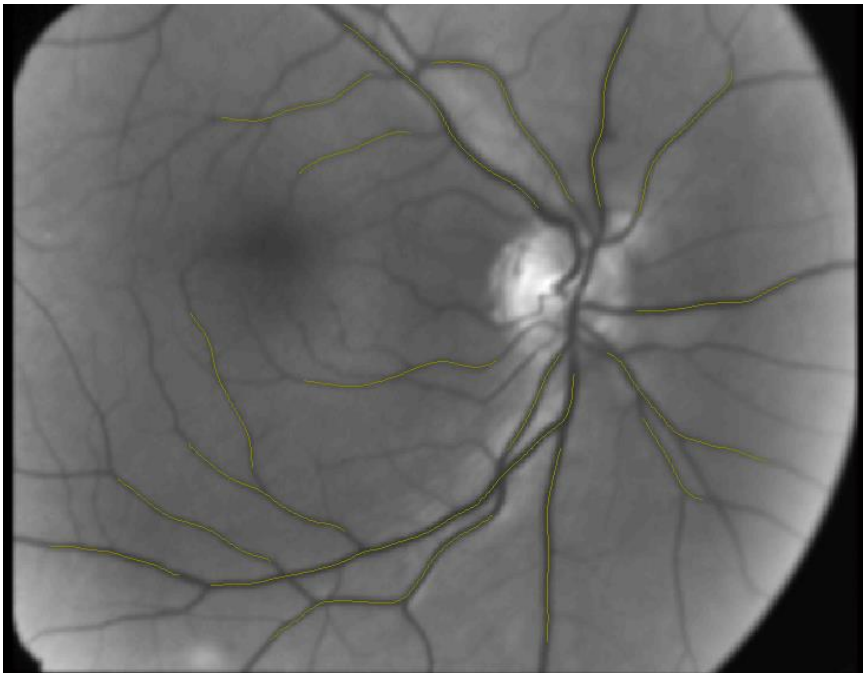

Figure 5.4: Retinal image showing tracked vessel using vessel tracking algorithm.

The vessel tracking algorithm GUI (see figure 5.5) also had some useful options like 'Change layer' (which switches between different sub-images at different wavelength, giving option to the user for better recognition of vessels), 'Undo last vessel' (the user can undo the last tracked section without losing any work), 'Magnifier' (which zooms a particular region, enabling better visibility of vessels) and 'Track manually' (option which you can use to track some vessels which cannot be tracked otherwise).

Figure 5.5: Graphical user interface for vessel tracking algorithm. You can see various useful options like 'Undo last vessel', 'Magnifier', 'Change layer' etc.

The semi-automated nature of the vessel tracking algorithm made it less prone to errors, as the user decides the start and end point of the section of vessels to be tracked. But in certain cases for example, if two vessels are very close to each other or crossing over each other, the algorithm was unable to track it or tracked a wrong section. To overcome this issue such vessels were tracked in smaller segments. One of the vessels was tracked along the full length and other was tracked in two sections. In figure 5.6, two retinal vessels A and B are crossing over each other and cannot be tracked automatically. To ensure proper tracking, vessel A was tracked in two segments and vessel B in one.

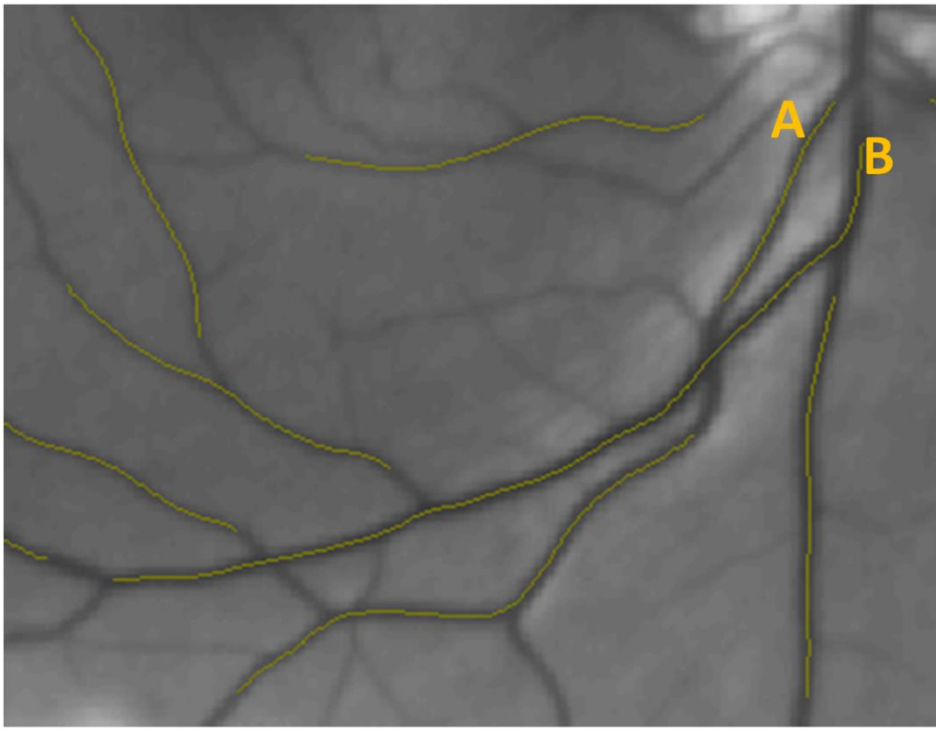

Figure 5.6: Vessel A and B are crossing each other in this image, to ensure proper tracking vessel A was tracked in two segments and vessel B in one continuous segment.

The graphical user interface and algorithm to track the vessels provided the flexibility and options to override and redo any step of the process, if needed. This manual control of the process ensured quality and error check.

5.2.3.3. Vessel Profile Extraction and Calculation of Light Transmission of Retinal Vessels

The method used for vessel profile extraction and calculation of the light transmission is the same as described in Chapter 4, section 4.2.5.

5.2.3.4. Optical Density Calculation

The method used for optical density calculation is the same as described in Chapter 4, section 4.2.6.

5.2.3.5. Vessel Diameter Calculation

The method used for vessel diameter calculation is the same as described in Chapter 4, section 4.2.7.

5.2.3.6. Oxygen Saturation Calculation

The method used for Oxygen saturation calculation is the same as described in Chapter 4, section 4.2.8.

5.2.3.7. Wavelength Selection for Two-Wavelength Oximetry

The IRIS snapshot technique takes retinal images at eight different wavelengths optimised for oximetry. Algorithms exploiting optical absorption measurements in all eight spectral bands are under development and offer the future prospect of robust, calibration-free oximetry. In this thesis, two-wavelength oximetry technique was used throughout all the experiments. Having eight spectral band images would give a choice of using any two optimum wavelengths for oximetry. Out of those eight wavelengths, five are oxygen sensitive and three are isobestic. Different authors have used different wavelengths for two-wavelength oximetry (Table 5.2); a review of the topic is presented in Chapter 1.

Table 5.2: Retinal vessel oxygen saturation values reported in normal subjects and wavelength combination used by different authors.

Authors	Oxygen Saturation (± SD)		Wavelengths
	Arterioles	Venules	
Hickam et al.[138]		58% (± 10)	640 nm, 800 nm
		60% (± 16)	640 nm, 505 nm
Delori et al.[140]	98% (± 8%)	45 % (± 7)	558 nm, 569 nm, 586 nm
Schweitzer et al.[19]	92.2 % (± 4.1)	57.9 % (± 6.8)	510-586 nm
Denninghoff et al.[149]	101 %	65 %	629 nm, 628 nm,
	98 %	63 %	821 nm, 899 nm
Beach et al.[137]		55% (± 3.8)	569 nm, 600 nm
Stefansson et al.[151, 157]	96 % (± 9)	55 % (± 14)	586 nm, 605 nm
	92.2 % (± 3.7)	55.6 % (± 6.3)	570 nm, 600 nm
Hammer et al.[18]	98 % (± 10)	65 % (± 11)	548 ± 10 nm (FWHM)
			610 ± 10 nm (FWHM)

* FWHM - full width half maximum

To decide which two wavelengths to use for oxygen saturation calculation we used an automated algorithm, which recovers oxygen saturation for different combinations of two wavelengths out of eight images captured by IRIS. We then decided which combination of wavelength was optimum for performing oximetry based on the oxygen saturation values yielded by them for arteries and veins.

Out of 28 possible wavelength combinations, only 15 consisted of one isobestic and one oxygen sensitive wavelength that were suitable for two-wavelength oximetry.

Using two-wavelength oximetry, for these 15 possible combinations of wavelengths, oxygen saturation was calculated for one arteriole and venule of 5 normal subjects. The values are given in table 5.3.

Of all these wavelength combinations, 566 nm and 599 nm produced the value of oxygen saturation for arteriole and venule within the acceptable physiological range as 96.3 % and 67.2 % respectively. The standard deviation for this combination was 2.1 % and 4.2 % for arteriole and venule respectively. There are a few other wavelength combinations, which give oxygen saturation values for arteriole and venule in the correct range, but the standard deviation for them is comparatively higher. Other combinations either provided right arteriolar oxygen saturation value but wrong venular oxygen saturation values or vice versa.

Based on this experiment, we decided to use the combination of 566 nm and 599 nm as two wavelengths for the oximetry technique. Similar range of the wavelengths are used by Stefansson et al [157] and Beach et al [137], both of which are established and highly published methods.

Table 5.3: Oxygen saturation values for arteriole and venule at different wavelength combinations of IRIS wavelength. 566 nm and 599 nm combination (highlighted) yielded the optimum oxygen saturation values for arteriole and venule.

Wavelength Combinations	**Oxygen Saturation (%)**		**Standard Deviation (%)**	
	Arteriole	**Venule**	**Arteriole**	**Venule**
586 nm & 579 nm	77.7	71.2	8.5	7.7
586 nm & 560 nm	64.4	97.1	5.8	7.1
586 nm & 599 nm	99.7	71.4	7.5	7.6
586 nm & 577 nm	79.4	75.1	4.6	6.2
586 nm & 591 nm	89.5	67.4	5.5	8.5
566 nm & 579 nm	81.6	79.0	9.3	4.3
566 nm & 560 nm	66.1	98.6	15.2	7.2
566 nm & 599 nm	**96.3**	**67.2**	**2.1**	**4.2**
566 nm & 577 nm	79.4	72.1	3.4	12.3
566 nm & 591 nm	86.2	60.0	13.4	9.5
579 nm & 570 nm	104	73.2	7.8	7.6
560 nm & 570 nm	82.1	88.7	9.9	3.2
599 nm & 570 nm	90.2	62.5	10.2	12.1
577 nm & 570 nm	86.3	97.0	6.9	3.2
591 nm & 570 nm	92.1	93.9	11.2	4.8

5.2.3.8. Analysis of Oxygen Saturation Data

All the retinal images were processed for oxygen saturation calculations, arterio-venous difference in oxygen saturation and vessel diameters. Pseudo-colour maps corresponding to values of oximetry for retinal vessels were also generated for retinal images and are presented in the results section.

5.3. Results

5.3.1. Oxygen Saturation in Retinal Arterioles and Venules

The average oxygen saturation value (± SD) for retinal arterioles and venules were 96.08 % ± 1.9 % and 68.04 % ± 2.1 %, respectively. The retinal arterioles oxygen saturation significantly correlated with the pulse oximetry values (r = 0.95, $P < 0.001$, Spearman's rank correlation test). The arteriovenous oxygen saturation difference was calculated to be 28.04 % ± 1.8 % (see table 5.4 for values). A comparison of oxygen saturation values between arterioles and venules is shown in Figure 5.7.

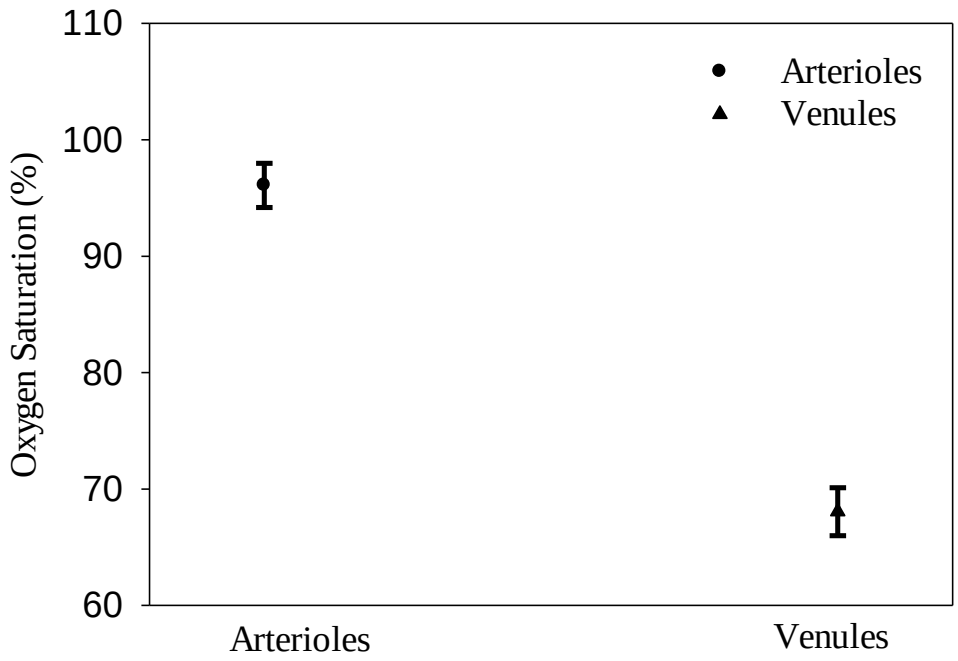

Figure 5.7: Average oxygen saturation in arterioles and venules in 18 healthy volunteers. The circle and triangle represents the mean value of oxygen saturation (for arterioles and venules respectively) whilst the error bars indicate the standard deviation.

Table 5.4: Oxygen saturation and vessel diameter values for subjects

Demographics and O_2 Saturation Values for Subjects	**Normoxia**
Retinal arteriole O_2 Saturation in % (mean ± SD)	96.08 ± 1.9
Retinal venule O_2 Saturation in % (mean ± SD)	68.04 ± 2.1
Retinal arteriovenous saturation difference in % (mean ± SD)	28.04 ± 1.8
Fingertip pulse O_2 saturation in % (mean ± SD)	97.6 ± 1.5
Vessel diameter arteriole (pixel)	14.0 ± 0.8
Vessel diameter venule (pixel)	18.8 ± 0.6
Age, X (mean[total range])	28 [22-51]
Sex distribution (Male/Female)	12/6

5.3.2. Retinal Arterioles and Venules Vessel Diameter

The average vessel diameters (in pixels) for retinal arterioles and venules were 14.0 ± 0.8 and 18.8 ± 0.6 respectively. See figure 5.8 and table 5.4 for vessel diameter comparison for arterioles and venules.

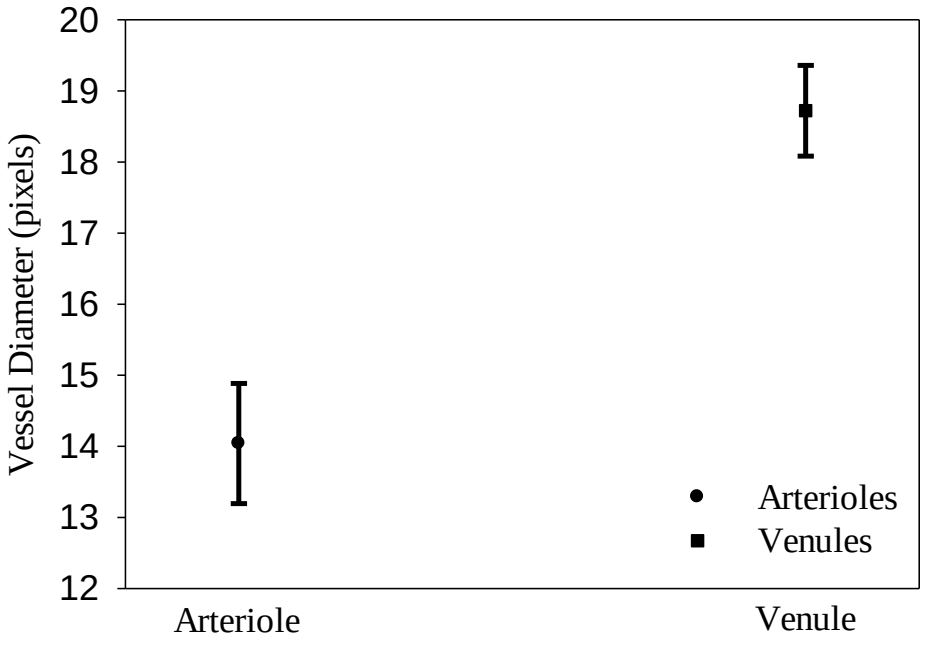

Figure 5.8: Average vessel diameter (in pixels) for arterioles and venules in 18 healthy volunteers. The circle and square represents mean (for arterioles and venules respectively) whilst the error bars indicate the standard deviation.

5.3.3. Oximetric Maps of Retinal Vasculature in Normal Subjects

Figure 5.9 (A) shows the pseudocolour images of the calculated oxygen saturations along the retinal arterioles and venules in representative ten subjects. 5.9 (B) shows average oxygen saturation in arterioles and venules of the individual subjects and 5.9 (C) shows the arterioles and venules average vessel diameter in pixels.

Subject 1.

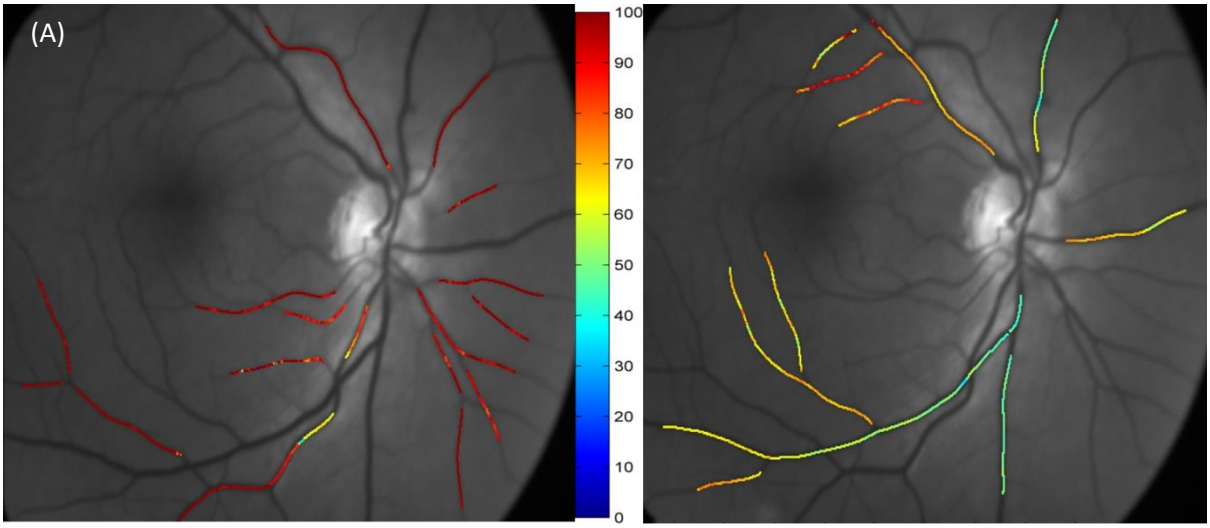

(B) Average Oxygen Saturation

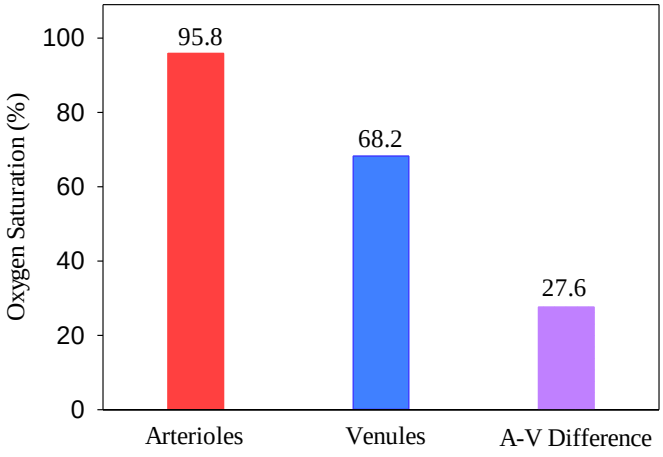

(C) Vessel Diameter

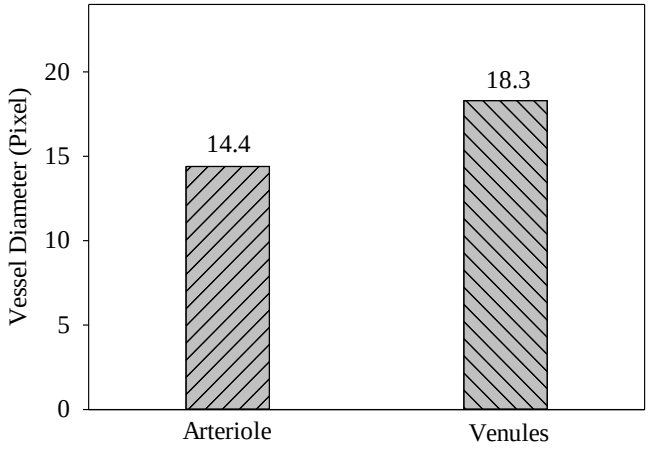

Subject 2.

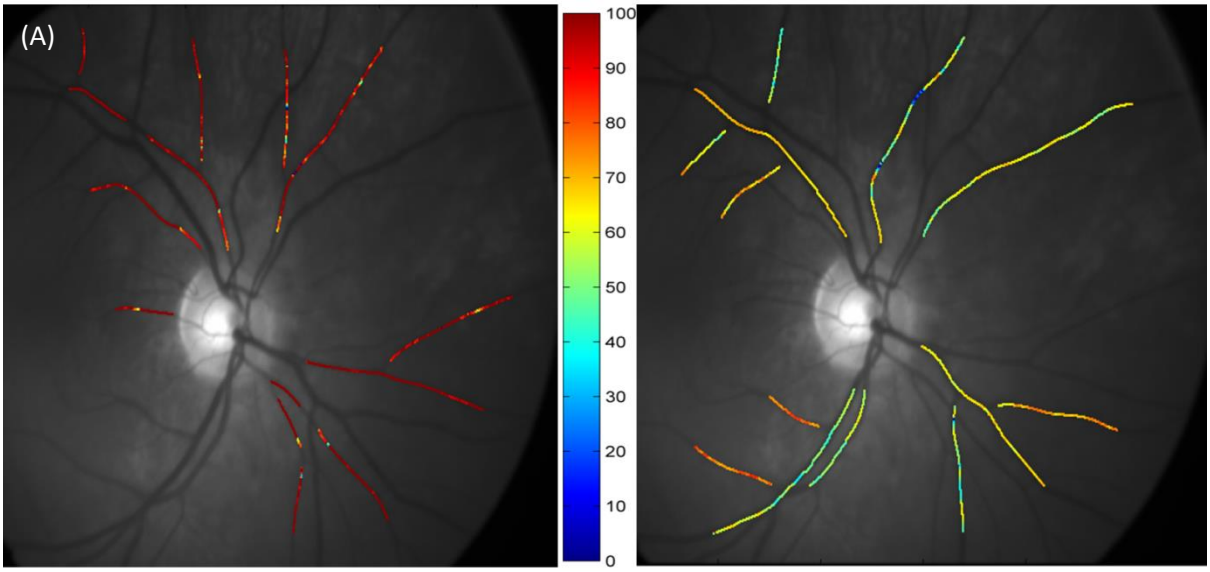

(B) Average Oxygen Saturation

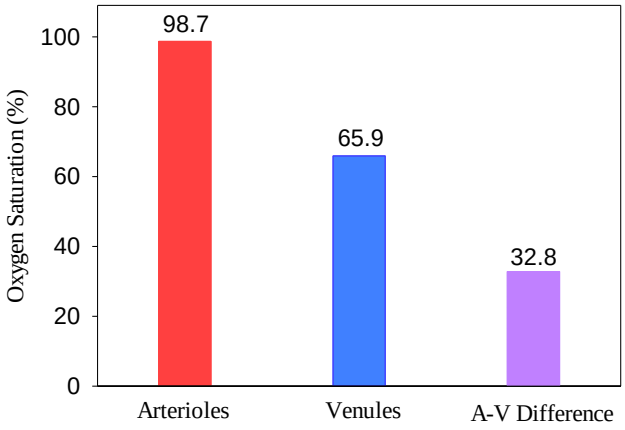

(C) Vessel Diameter

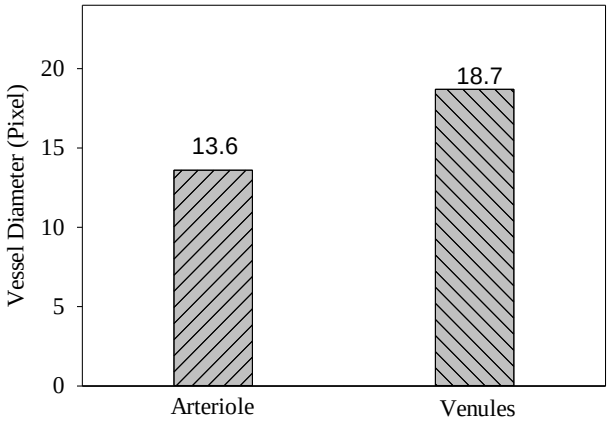

Subject 3.

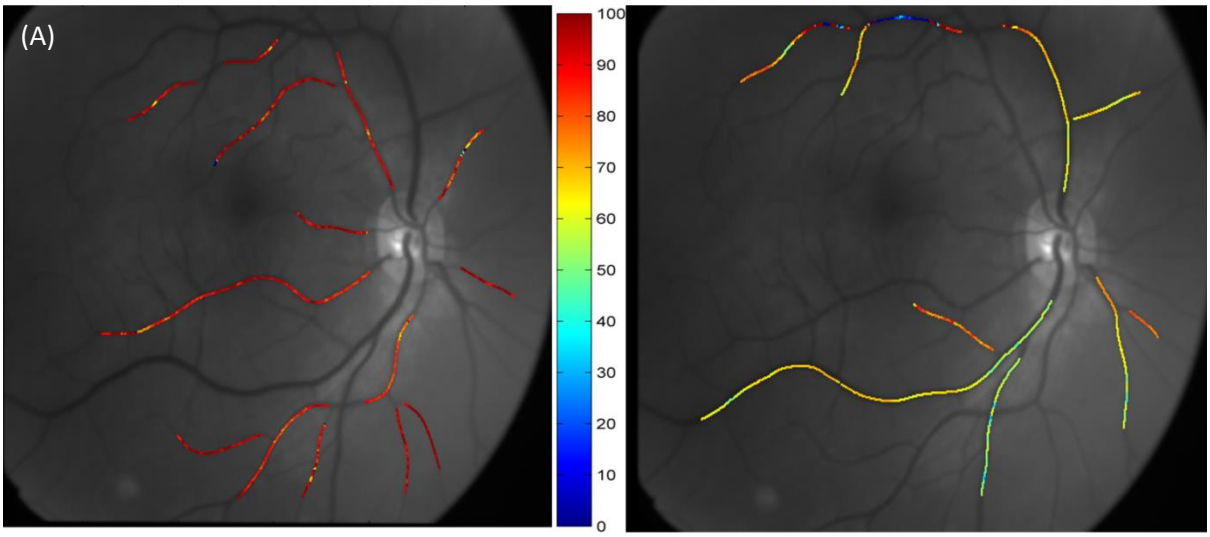

(B) Average Oxygen Saturation

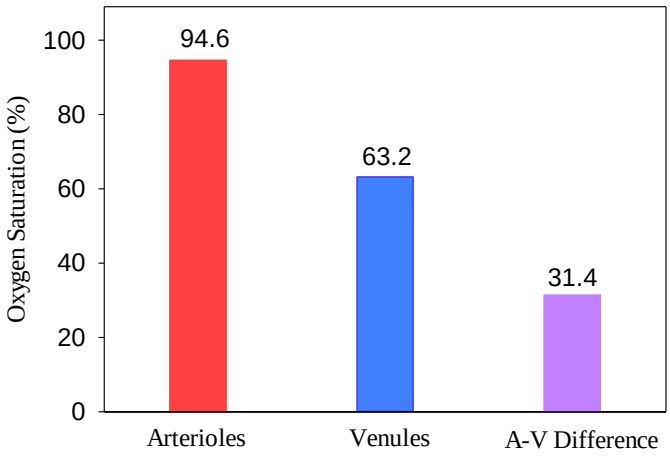

(C) Vessel Diameter

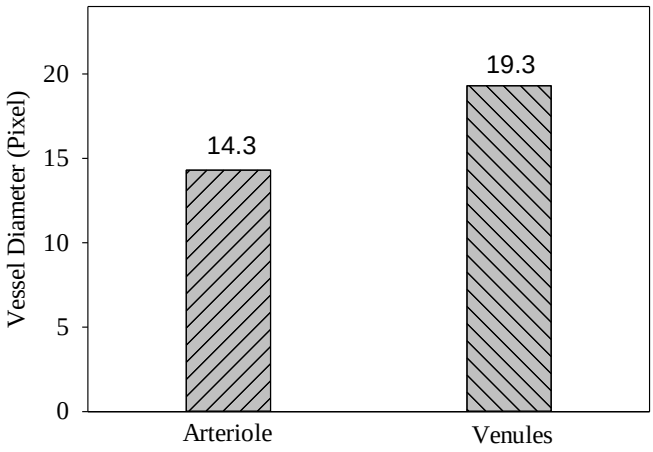

Subject 4.

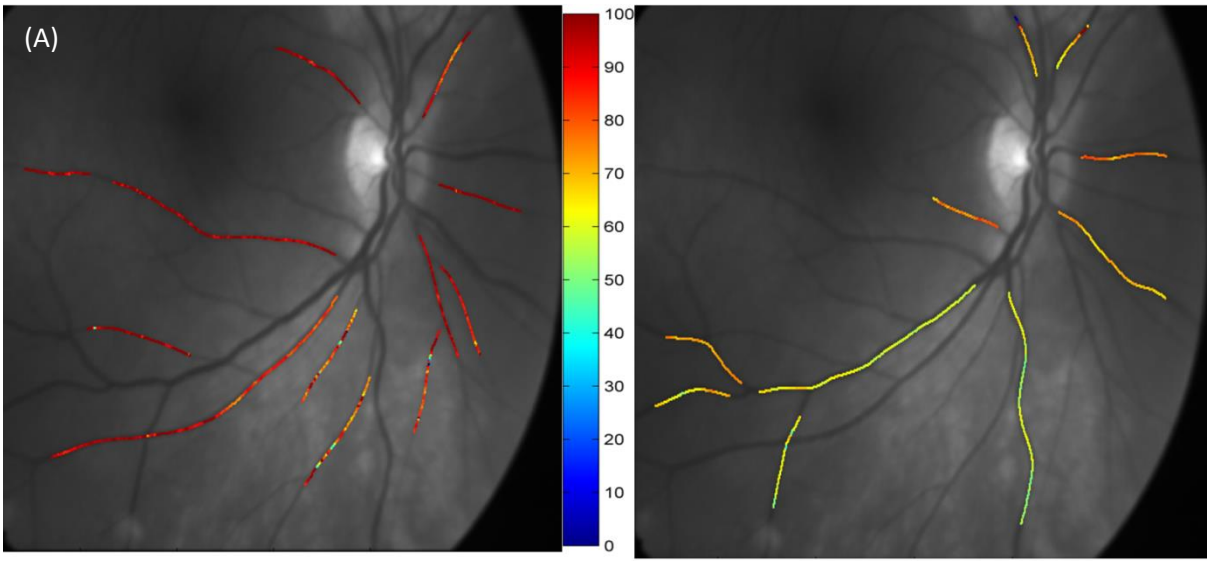

(B) Average Oxygen Saturation

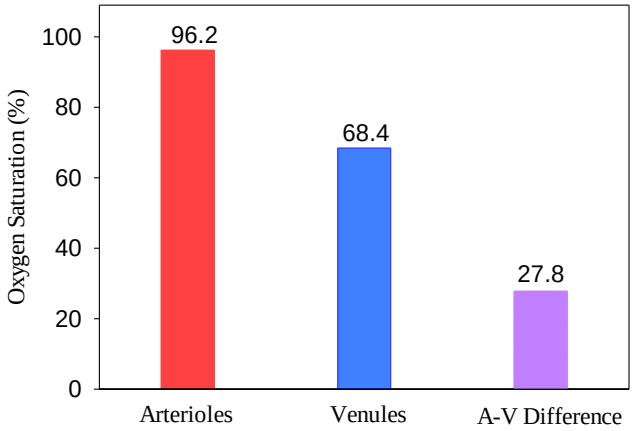

(C) Vessel Diameter

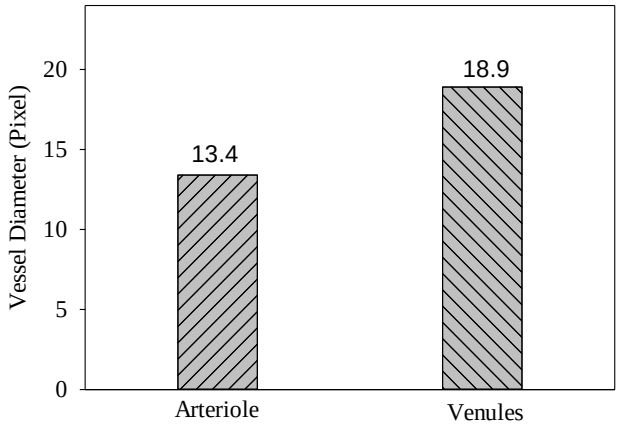

Subject 5.

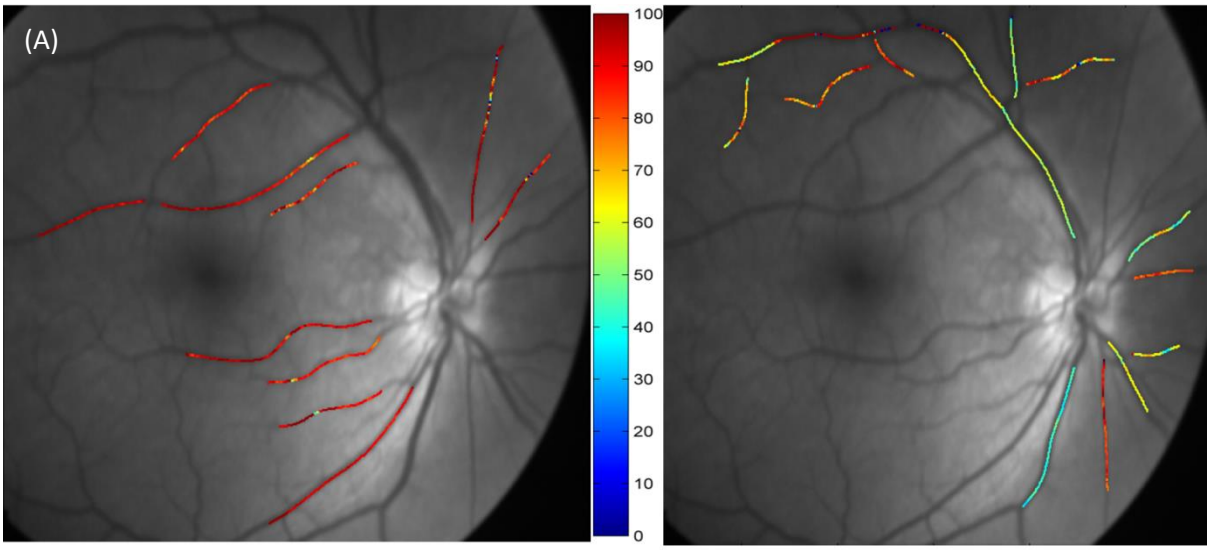

(B) Average Oxygen Saturation

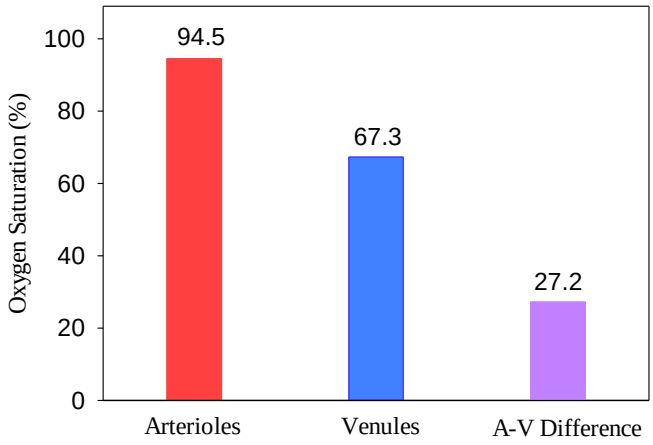

(C) Vessel Diameter

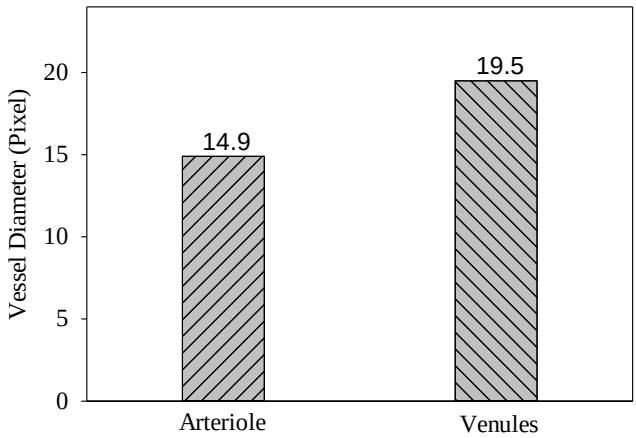

Subject 6.

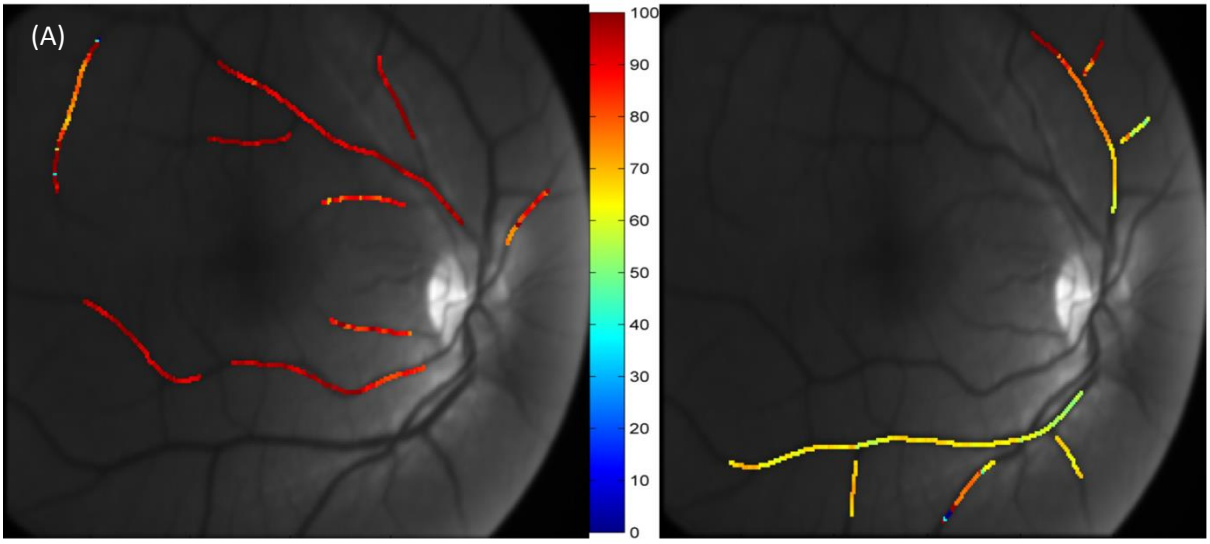

(B) Average Oxygen Saturation

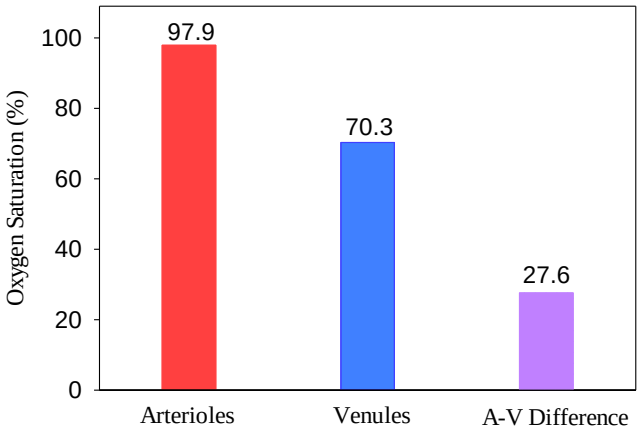

(C) Vessel Diameter

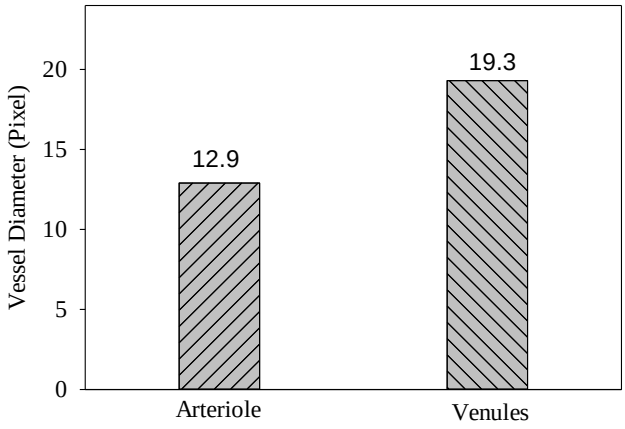

Subject 7.

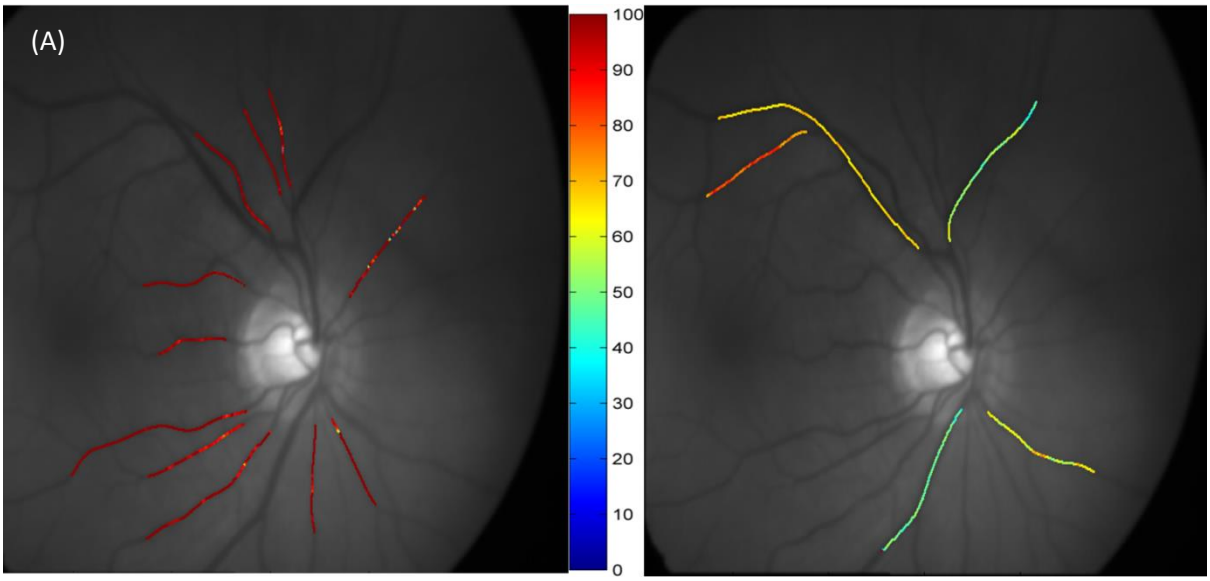

(B) Average Oxygen Saturation

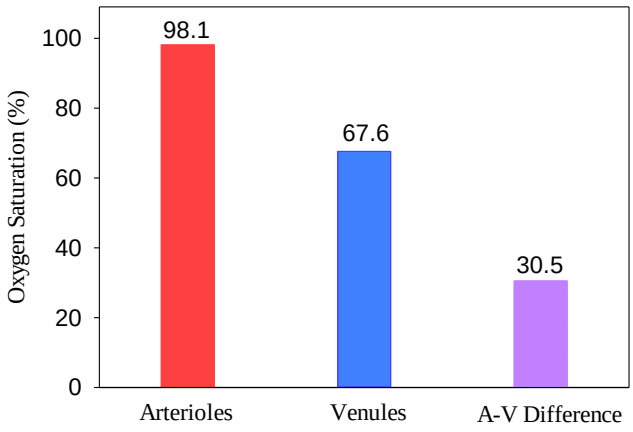

(C) Vessel Diameter

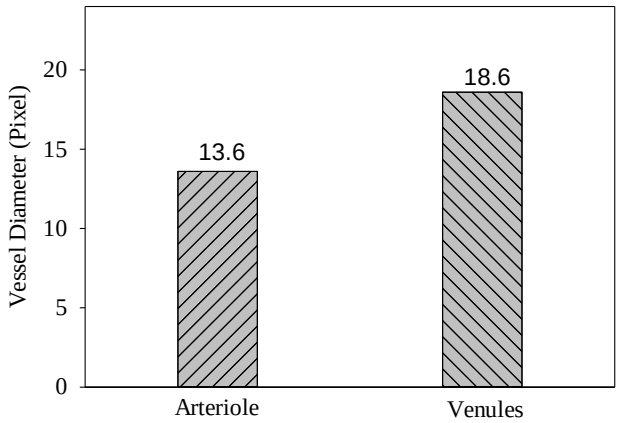

Subject 8.

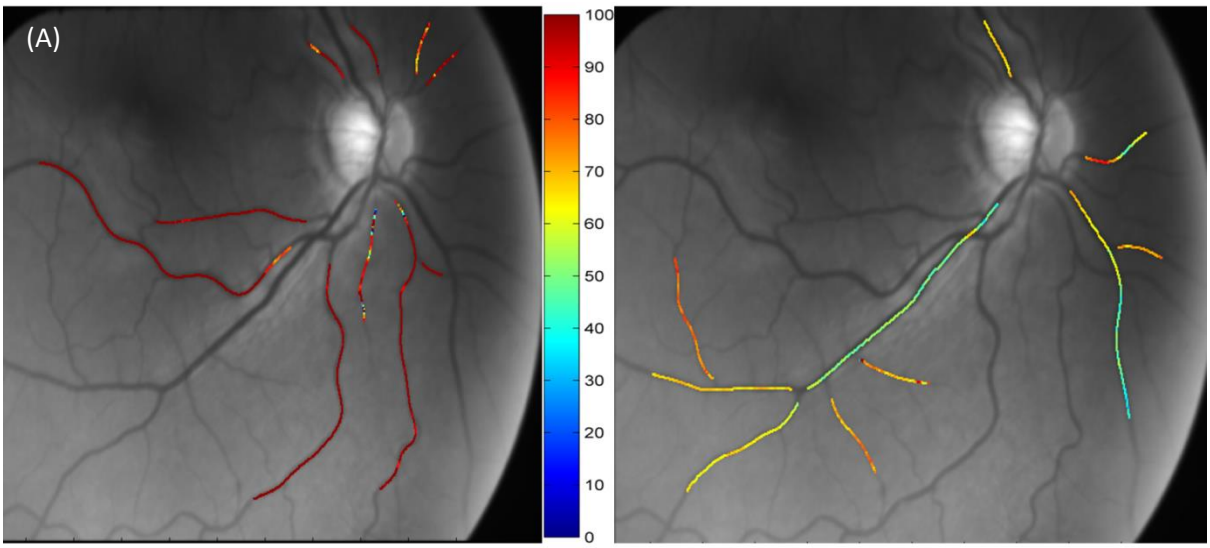

(B) Average Oxygen Saturation

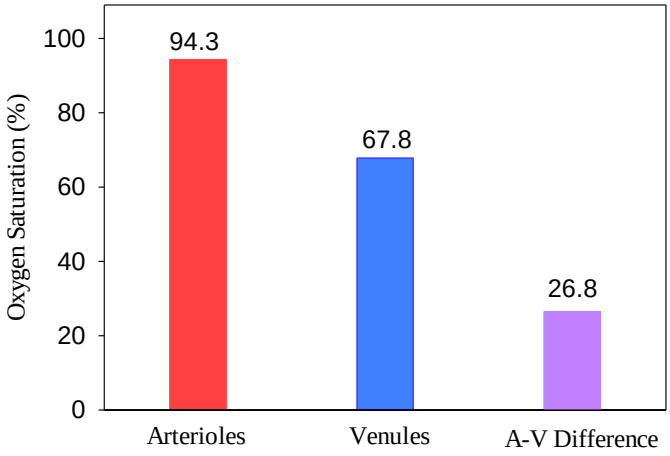

(C) Vessel Diameter

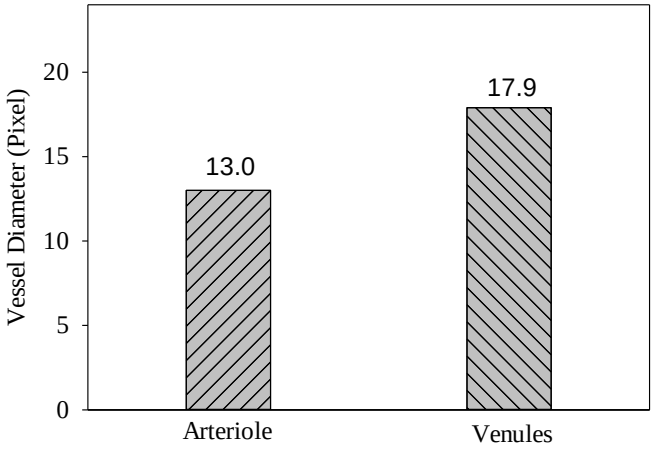

Subject 9.

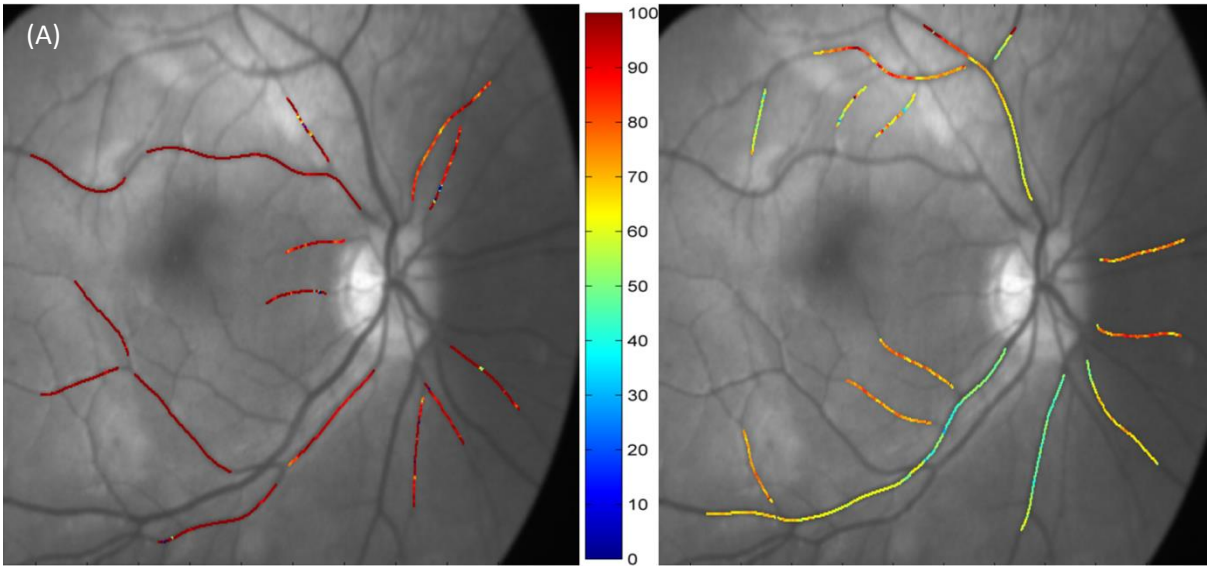

(B) Average Oxygen Saturation

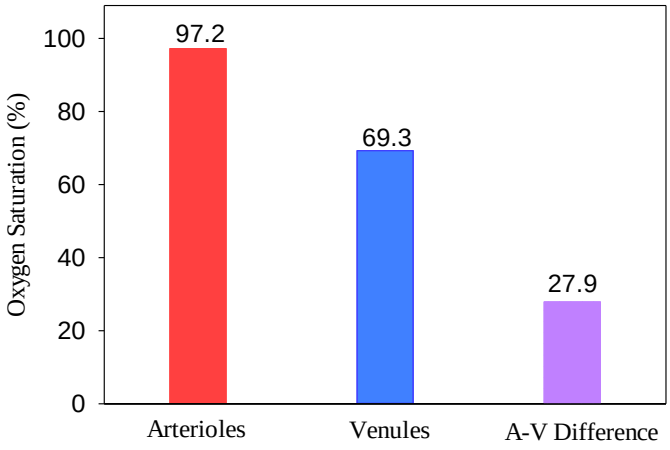

(C) Vessel Diameter

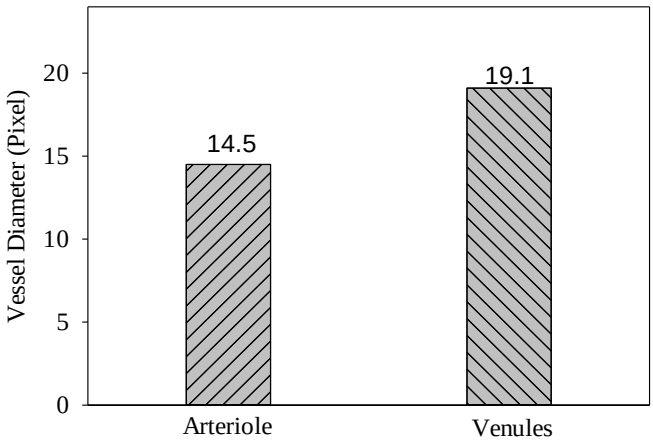

Subject 10.

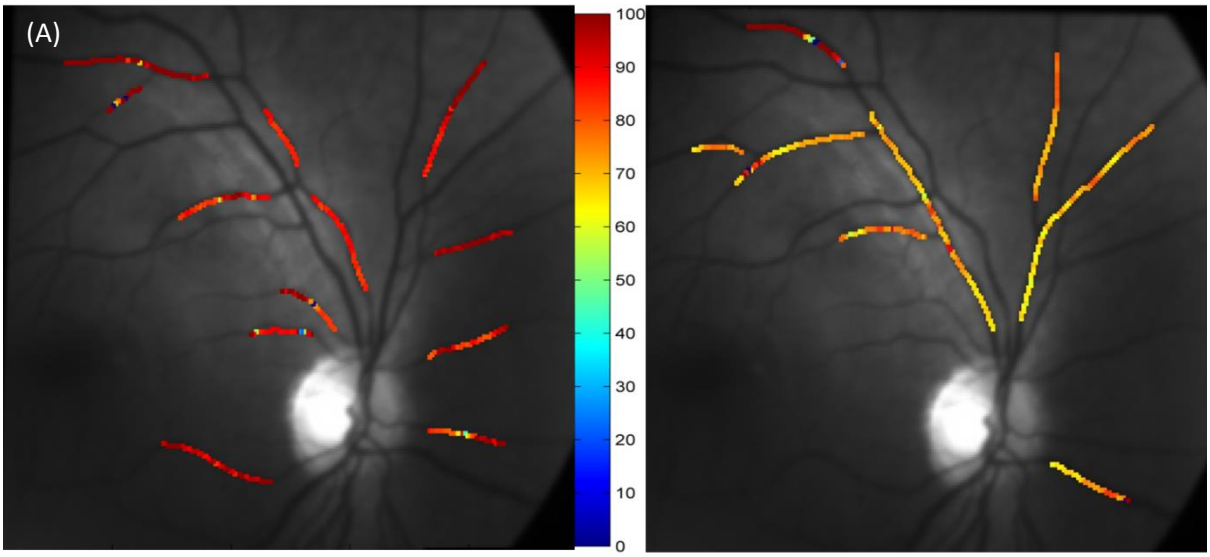

(B) Average Oxygen Saturation

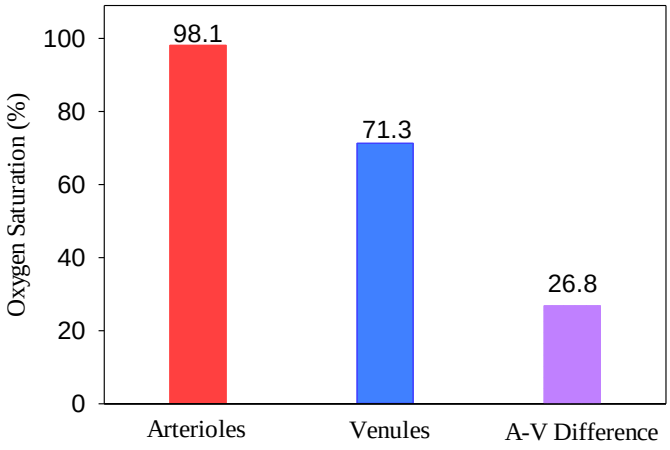

(C) Vessel Diameter

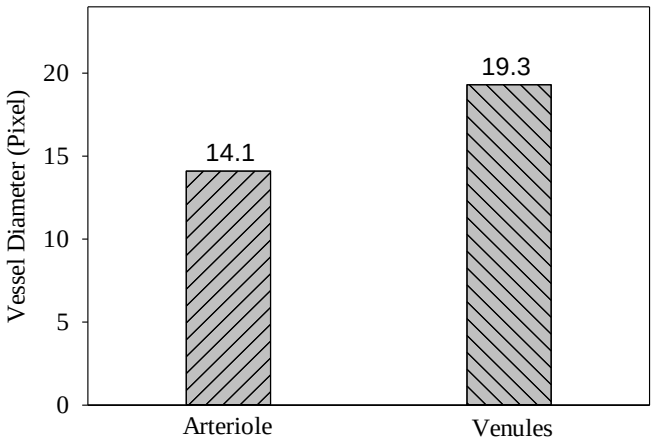

5.4. Discussion

5.4.1. Oxygen Saturation in Retina: Qualitative features

Spectral images of retina at four different wavelengths are shown in Figure 5.10. Some qualitative features can be directly observed in these images as wavelengths change. Figure 5.10 (A) and (B) are retinal images at isobestic wavelength of 566 nm and 586 nm and (C) and (D) are at oxygen sensitive wavelengths of 591 nm and 599 nm respectively. At isobestic wavelengths (A and B), both arterioles and venules look similar to each other, but on oxygen sensitive wavelengths (C and D), they can be easily distinguished. The arterioles (marked by red arrows) looks less optically dense than the venules (marked by blue arrow). Progressing from isobestic wavelength (A or B) to oxygen sensitive wavelength (C) to even more sensitive (D) the arterioles almost disappears. This effect can be explained as retinal arterioles have higher oxygen saturation than retinal venules, and oxygenated blood is more transmissive than deoxygenated blood. This visual difference confirms that our imaging setup is capable of sensing oxygen saturation in retinal images. Also this feature was used to differentiate between arterioles and venules whilst tracking retinal vessels.

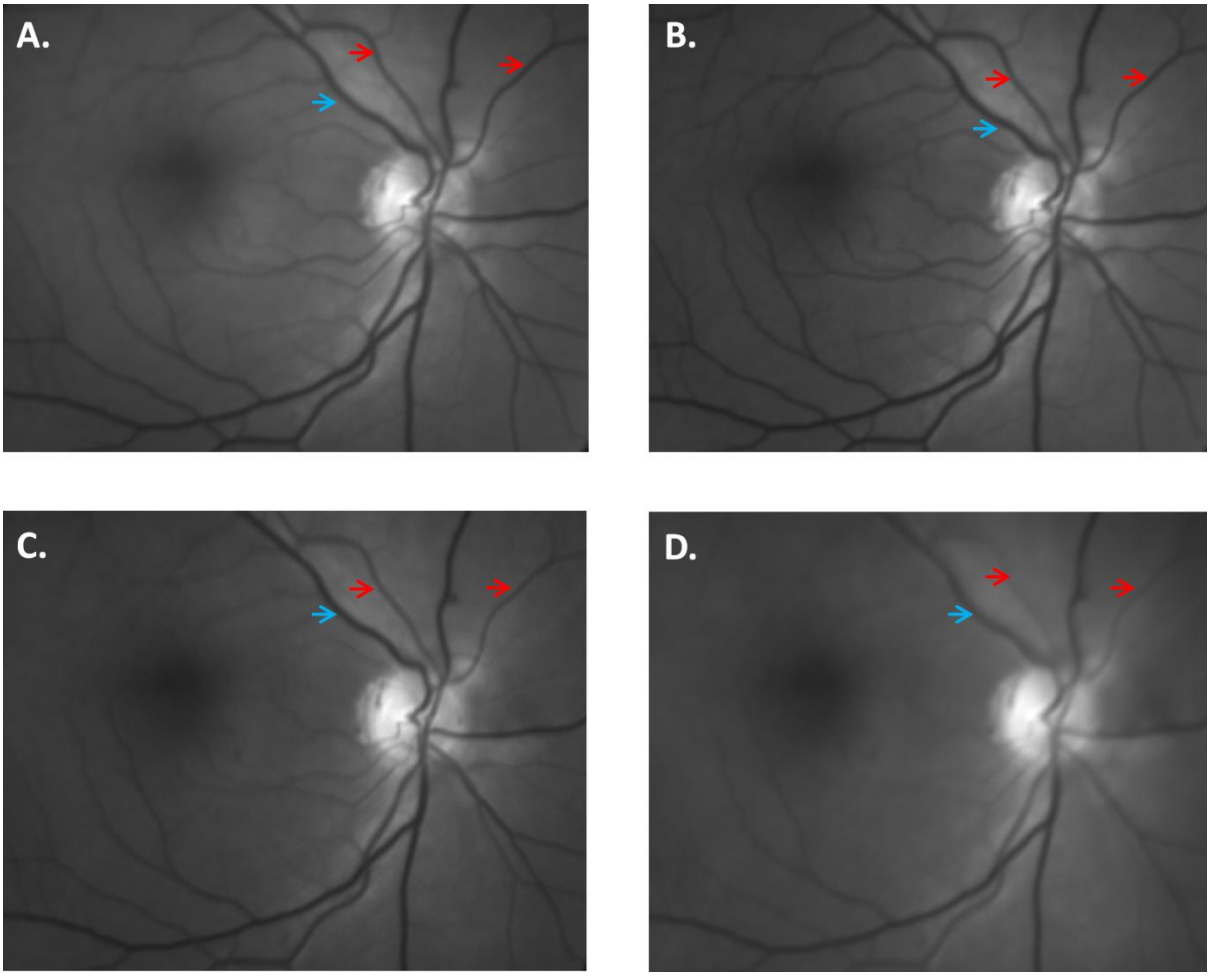

Figure 5.10: Image of retina at different wavelengths, (A) at 566 nm, (B) at 586 nm, (C) at 591 nm and (D) at 599 nm. Image (A) and (B) are at isobestic wavelengths and (C) and (D) are at oxygen sensitive wavelengths. The red arrows are pointing at arterioles and blue arrow at venules. Arterioles carrying more oxygenated blood than venules looks more transparent, as oxygenated blood is more transmissive or less optically dense to light.

5.4.2. Oxygen Saturation in Retina: Quantitative features

Oxygen saturation in retinal arterioles (96.08 % ± 1.9 %) and retinal venules (68.04 % ± 2.1 %) of healthy subjects were measured. The IRIS snapshot multispectral fundus camera used has been shown to be sensitive to oxygen saturation in retinal arterioles and venules. We found a significant correlation of pulse oximeter oxygen saturation values with measured retinal arterioles oxygen saturation. Our reported oxygen saturation values for retinal arterioles and venules were within the normal physiological range and similar to the values reported by many groups [18, 137, 151, 154, 157]. The calculated retinal arteriovenous oxygen saturation difference was 28.04 % ± 1.8 %.

The pseudocolour retinal oximetry image is shown in Figure 5.11. The oxygen saturation of the retinal arterioles are generally greater than 90%. At certain points in retinal arterioles, lower than expected oxygen saturation values can be found. This error can be caused if one vessel is in close proximity to another, or if a vessel crosses over another vessel, causing errors in vessel profile analysis. This can be prevented by careful selection of the vessel sections during the vessel tracking. Many times this cannot be avoided and that is why averaging over a large vessel section for calculating oxygen saturation values is better. Similar effects are observed in venules. In most venules, the oxygen saturation is between 50 % to 70%, within the normal reported range (see table 5.1). But unexpected variations in pseudocolour maps can be seen at times. These variations in oxygen-saturation values can be attributed to a number of factors such as variation in fundus background due to pigmentation, uneven illumination of retina, another vessel in close proximity or crossing over. It can also be explained by physiological variability in the function of retina. Different quadrants of retina can have different blood flow [193] and oxygen consumption, which depends on metabolic activity of the surrounding tissues.

5.4.3. Wavelength Selection for Retinal Oximetry

The IRIS multispectral snapshot instrument gives us eight spectral images of retina in a single image. Within the wavelength range of 560 nm to 600 nm there are two isobestic points which can be used along with other oxygen sensitive wavelength for two wavelength oximetry. As described in section 5.2.3.7. of this chapter we decided to use 566 nm and 599 nm for oxygen saturation calculations. There is about four-fold difference in extinction coefficient of both oxygenated and deoxygenated haemoglobin between these two wavelengths (see Figure 5.11, selected wavelength marked by dashed line). This great difference in extinction coefficient between selected pair of wavelength makes it more sensitive and suited for oximetry.

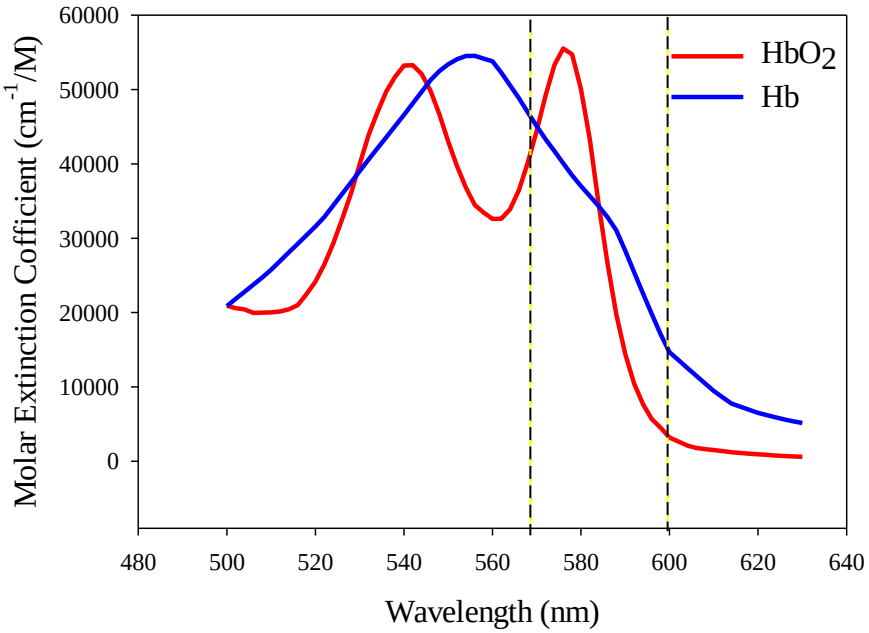

Figure 5.11: Extinction coefficients of oxygenated (red line) and deoxygenated (blue line) haemoglobin at different wavelengths.

The chosen wavelength combination 566 nm and 599 nm yield the optimum value of oxygen saturation for retinal arterioles and venules with the least standard deviation in oximetry. Similar wavelength combination are also used by Beach et al [137] and Stefansson et al [151].

5.4.4. A Standardised Protocol for Retinal Oximetry

The application of multispectral imaging to perform oximetry in retinal vasculature in normal healthy individuals has been presented in this study. Based on our experience from this study, we standardised a protocol for imaging and oximetry in retina. Devising this protocol proved to be very helpful for experimental studies of hypoxia (Chapter 6, Human Hypoxia Trial).

5.4.5. Limitations of the Study

The present study has a number of limitations. One of the main limitations of this study is that it is based on calibration based, two wavelength retinal oximetry. Two-wavelength oximetry uses an established calibration technique that employs assumed values of oxygenation of arteries and veins in healthy eyes based on normal physiology. Using this technique, absolute oximetry is not possible. However, many groups have reported that it gives repeatable measurements and is sensitive to changes in oxygen saturation, but one

should keep this limitation in mind. One example of calibration-based bias can be seen in different reported values for mean venous oxygenation by different groups. In this study, we report a mean venous saturation of 68%, whereas, Hammer et al [18] found 65% and Hardarson et al [151] found 52%. In fact, two studies published by same group, within a year, reports a mean venous saturation of 55% [157] and 65% [153]. Still, two wavelength oximetry can easily distinguish and is sensitive to oxygen saturation of retinal arteries and veins (presented in this study) and can be used to compare oxygen saturation between groups.

One of the other limitations is the small sample size of subjects recruited for the study. After validation of our system *in vitro* in model eye and *in vivo* in an animal model (described in Chapter 3 and 4), we designed an experiment to test in human subjects. Considerable amount of time was employed to design and improve algorithms essential to do image analysis and oximetry and standardising a protocol for oximetry analysis. It takes approximately ten hours for data acquisition and processing, of one retinal image.

A further limitation of this study was that no in-depth analysis of repeatability of the oximetry has been performed. This will be addressed in future studies. Although *in-vivo* validation of our imaging system (in Chapter 4) in animal model breathing different inspired oxygen affirms the ability of our oximetry system to detect changes in the oxygen saturation of the retinal vasculature.

Although great care was taken during analysis of spectral images, they can cause error in oximetry. For example, co-registration of spectral images is one of the important steps. The registration process is automated, but sometimes, mis-registration of sub-images was found to be cause of unexpected error in optical density and oxygenation values. To overcome this error, every image after being registered, was visually inspected and verified. Another crucial step in image analysis is detection and tracking of the retinal vessels. The vessel tracking process was semi-automated and eliminated most of the error. Vessel segments very near to the optic disc or bright area surrounding it, or vessel segments with high background variations in reflectivities, are known to introduce errors in oximetry calculations. Therefore, a detailed selection criteria was implemented (see table 5.1) for vessel tracking.

5.4.6. Conclusion

This present study has described the techniques used to image the retina and perform oximetry in retinal vessels. Oxygen saturation in retinal arterioles (96.08 % ± 1.9 %) and

retinal venules (68.04 % ± 2.1 %) of healthy subjects were measured, and were found to be significantly correlated to the pulse oximetry values. Retinal arteriolar and venular oxygen saturation values are consistent with previous studies. Additionally, based on this study, we devised a protocol to image the retina and process the images to perform oximetry in a standardised manner.

Chapter 6

Human Hypoxia Trial

6.1. Introduction

In Chapter 5, the methods for calculating oxygen saturation of retinal vessels in healthy subjects were described in detail, including imaging and processing techniques leading to oximetry.

One of the applications of retinal oximetry is the assessment of retinal oxygenation, circulation and physiology. Hypoxia is confirmed to be an underlying condition of many retinal disorders. A detailed overview of hypoxia and retinal diseases is presented in Chapter 1.

The purpose of this chapter is to study the effect of acute mild hypoxia on retinal vessel oxygenation in healthy individuals by using retinal oximetry, arteriovenous oxygen saturation difference and vessel diameter.

This is the first study to report the effect of acute mild hypoxia on retinal oxygenation in healthy humans. A version of this chapter has been published in Investigative Ophthalmology and Visual Sciences journal [194].

6.2. Methods

This study was approved by Heriot-Watt University Ethics Committee. All procedures were performed according to the Tenets of declaration of Helsinki.

6.2.1. Recruitment of Subjects

Ten healthy subjects were recruited for the study (age 25 ± 5 years), comprising six males and four females. The study protocol was explained to the subjects and they were informed about the associated risks. Subject's queries, if any, were answered and when they were satisfied, a written informed consent was obtained and they were assigned a time slot for participation in the experiment. They were also asked to refrain from consuming any caffeinated beverages or alcohol on the day of study and any consumption of alcohol prior to

the day of study. All the subjects recruited were healthy, non-smokers, without history of any respiratory disorder and were taking no medication.

On the day of study, they were once again briefed about the experimental protocol. Age, sex, weight were recorded. Tropicamide (1%, Bausch & Laumb, Chauvin Pharmaceuticals, Ltd., U.K.) was used to dilate the pupil. Ten to fifteen minutes after application of the Tropicamide by means of an eye drop, maximum dilation of pupil was achieved, and the subjects were ready to be imaged.

6.2.2. Retinal Spectral Image Acquisition

Multispectral retinal images were acquired under both normoxia (21% inspired oxygen) and hypoxia (15% inspired oxygen) conditions using our IRIS snapshot multispectral fundus camera, described in Chapter 2. Hypoxia is induced by a hypoxia generator (Everest Summit II Hypoxic Generator; Hypoxico, Inc., New York, U.S.) which is described in the following section. Fingertip pulse oximetry (AUTOCORR; Smiths Medical ASD, Inc., Rockland, MA) was employed to continuously monitor the peripheral arterial oxygenation throughout the experiment. The order of image acquisition at normoxia and hypoxia was randomised between the subjects to remove order effect. At both normoxia and hypoxia conditions, retinal images were visually inspected to be in proper focus and for presence of macula and optic disc. If images were out of focus or unsatisfactory, a new set of image were acquired.

6.2.3. Hypoxia Generator

To induce hypoxia in the subjects a hypoxia generator (Everest Summit II Hypoxic Generator; Hypoxico, Inc., New York, U.S.) was used. The hypoxia generator (see Figure 6.1) induced hypoxia by reducing fraction of inspired oxygen of the inhaled air. The hypoxic air comes through the generator via a delivery hose, which is then purified by a HEPA filter and supplied via a non-rebreather face mask. The face mask can be comfortably placed on the face covering both mouth and the nose. The hypoxia generator was calibrated prior to use, using a Servomex gas analyser that measured the percentage oxygen output of the system to ± 0.1%.

Figure 6.1: Hypoxia generator (Everest Summit II Hypoxic Generator; Hypoxico, Inc., New York, U.S. used in the study to induce hypoxia in subjects.

The hypoxia generator comes with 23 different settings which supplied different percentages of oxygen ranging from 21% to 11%, depending on which settings are used. For this study we used the setting which gives 15% of fraction of inspired oxygen.

6.2.4. Repeatability Study

To assess the significance of any hypoxia-induced intra-subject variations in oximetry and vessel diameter, it is important to assess whether the variation between nominally identical measurements is sufficiently small compared to the magnitude of the observed changes with hypoxia. This was assessed using five repeated measurements on five subjects using identical procedures to those used throughout this study. The retinal images were recorded at one minute intervals, with the camera realigned and refocused as necessary. Vessel oximetries and vessel diameters were calculated for one arteriole and one venule in each eye for each of five individuals. Results from the repeatability experiment are included in the result section.

6.2.5. Retinal Image Processing and Oximetry Analysis

The retinal image processing and oxygen saturation calculation method used in this study is the same as that described in Chapter 5.

Briefly, the best quality images at each inspired oxygen (normoxia and hypoxia) level were selected and then were co-registered. Retinal images were then processed to track vessels, calculate the *OD* and *ODR*, and hence calculate oxygen saturation at each pixel along the

centre-line of the selected vessels. For each subject, arterial and venous oxygen saturation was then calculated for each point along a vessel for each level of inspired oxygen. Vessel segments were selected in a standardized manner, based on vessel width (12 pixels or wider) and vessel length (100 to 200 pixels). Furthermore, parts of the vessels close to the optic disk were avoided. Care was also taken to exclude vessels with strong background variations in reflectivities, known to exhibit higher levels of artifactual errors in oximetry. Oximetry was averaged along major vessel segments (between branches) yielding a measure of mean and standard deviation of the oximetry by vessel segment for each image.

The same arterioles and venules were selected under normoxic and hypoxic conditions and comparison of oximetry between normoxic and hypoxic conditions was performed between the same vessel segments.

6.2.6. Statistical Analysis

Paired-sample t-test with significance accepted at $P < 0.05$ was used to compare oxygen saturation values during normoxic and hypoxic levels. Spearman's rank correlation test was used to compare the measured retinal arteriole oxygen saturation with pulse oximeter values. Statistical analysis was performed using commercial software (Sigma Plot, ver. 12.0, Systat Software Inc.).

6.3. Results

6.3.1. Repeatability of Oximetry System and Vessel Diameter Calculation

Table 6.1 shows the oxygen saturation and vessel diameter as the mean ± SD of repeated measurements in five subjects. The intra-subject standard deviation for five repeated oximetry calculations for arterioles and venules of five subjects varied between 0.4 - 1.0 %. The intra-subject standard deviation for repeated vessel diameter calculation was between 0.2 - 0.3 pixels for arterioles and 0.3 - 0.4 pixels for venules.

Table 6.1: Oximetry values in (%) and vessel diameter in pixels of five images within the same subject. In each subject, one arteriole and one venule was measured to assess repeatability of measurements.

Subject No.	Arterioles		Venules	
	O_2 Saturation (%) (Mean ± SD)	**Arteriole Diameter(pixel) (Mean ± SD)**	**O_2 Saturation (%) (Mean ± SD)**	**Venule Diameter(pixel) (Mean ± SD)**
1.	98.6 ± 1.0	14.4 ± 0.3	71.3 ± 0.7	18.5 ± 0.4
2.	98.3 ± 0.7	15.2 ± 0.3	72.2 ± 0.4	18.5 ± 0.3
3.	97.0 ± 0.5	13.6 ± 0.3	69.2 ± 1.0	18.9 ± 0.2
4.	99.4 ± 0.4	14.6 ± 0.2	71.9 ± 0.5	18.4 ± 0.4
5.	98.1 ± 0.5	14.5 ± 0.3	65.7 ± 0.6	18.9 ± 0.2
CV	1%	4.1%	3.5%	2.1%

$$CV = \left(\frac{Standard\ Deviation}{Mean} \times 100\right)$$

6.3.2. Normoxia

Under normoxia, the pulse oximetry was found to be 98.6 ± 0.7 %. The retinal arterial O_2 saturation was in close agreement with this value (98.5 ± 1.6 %). The retinal venous O_2 saturation was 70.7 ± 2.7 %. The arteriovenous difference was calculated to be 27.8 ± 2.9 % (mean ± SD) under the normoxic condition (see Table 6.2 for values). A comparison of oxygen saturation in the arterioles and venules in subjects at normoxia is shown in Figure 6.2.

6.3.3. Comparison of Oxygen Saturation in Normoxia and Hypoxia

A reduction in the fraction of inspired oxygen resulted in a decline ($P<0.001$) in the pulse oximetry value to 89.6 ± 0.5%. The retinal arterial and venous oxygen saturations reflected this decrease and were found to be 90.3 ± 2.0 % and 62.4 ± 2.2 % respectively, with an arteriovenous difference of (27.9 ± 2.1 %). A comparison of oxygen saturation in the arterioles and venules in subjects at normoxia and hypoxia is shown in Figure 6.2.

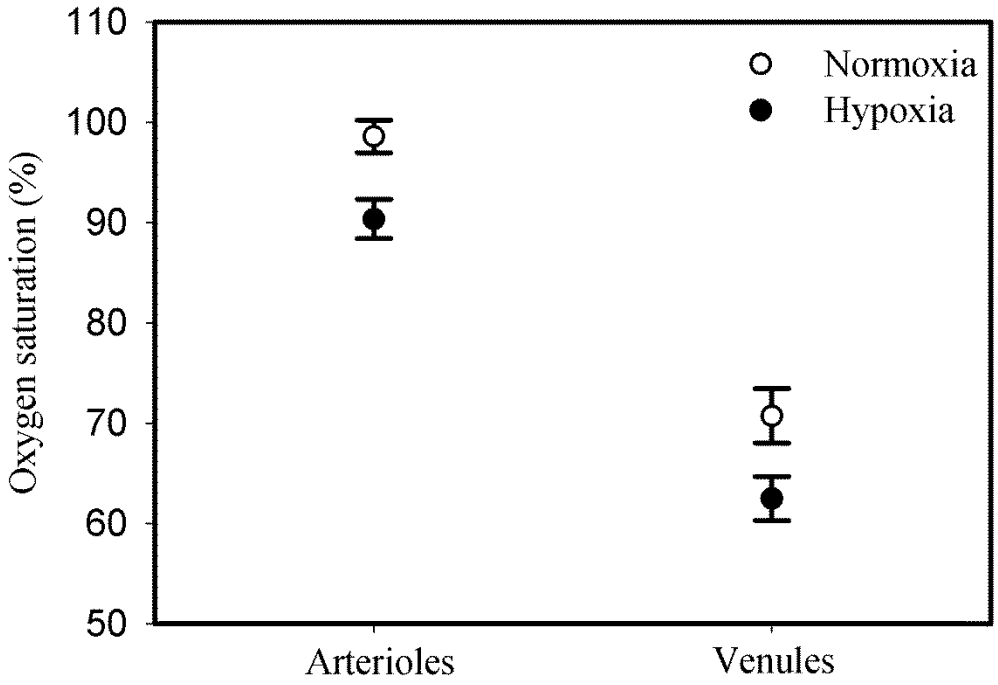

Figure 6.2: The effect of hypoxic exposure on oxygen saturation in normoxia (open circle) and hypoxia (closed circle). The open and closed circle represents the mean whilst the errors bars indicate the standard deviations.

Table 6.2: Oxygen Saturation and vessel diameter values for subjects under normoxia and hypoxia conditions

Demographics and O_2 Saturation Values for Subjects	**Normoxia**	**Hypoxia**	***P****
Retinal arteriole O_2 Saturation in % (mean ± SD)	98.5 ± 1.6	90.3 ± 2.0	<0.001
Retinal venule O_2 Saturation in % (mean ± SD)	70.7 ± 2.7	62.4 ± 2.2	<0.001
Retinal arteriovenous saturation difference in % (mean ± SD)	27.8 ± 2.9	27.9 ± 2.1	0.31
Fingertip pulse O_2 saturation in % (mean ± SD)	98.6 ± 0.7	89.6 ± 0.5	<0.002
Vessel diameter arteriole (pixel)	14.4 ± 1.2	15.0 ± 1.1	<0.001
Vessel diameter venule (pixel)	18.7 ± 1.0	19.3 ± 1.1	<0.001
Age, X (mean[total range])	25 [22-51]	25 [22-51]	--
Sex distribution	6/4	6/4	--

* Paired t-test

6.3.4. Retinal Vessel Diameter in Normoxia and Hypoxia

Figure 6.3 shows the effect of hypoxic exposure on retinal vessel diameter. Retinal vessel (arterioles and venules) diameter (in pixels) was measured from the retinal images of subjects under both normoxic and hypoxic conditions. During normoxia retinal arteriole and venule diameter was 14.4±1.2 and 18.7±1.0 pixels, respectively. There was a small but significant increase ($P<0.001$, paired t-test) in retinal vessel diameter under hypoxic conditions (arteriole, 15.0±1.1 and venule 19.3±1.1). The paired t-test is between the same vessel sections in the same eyes.

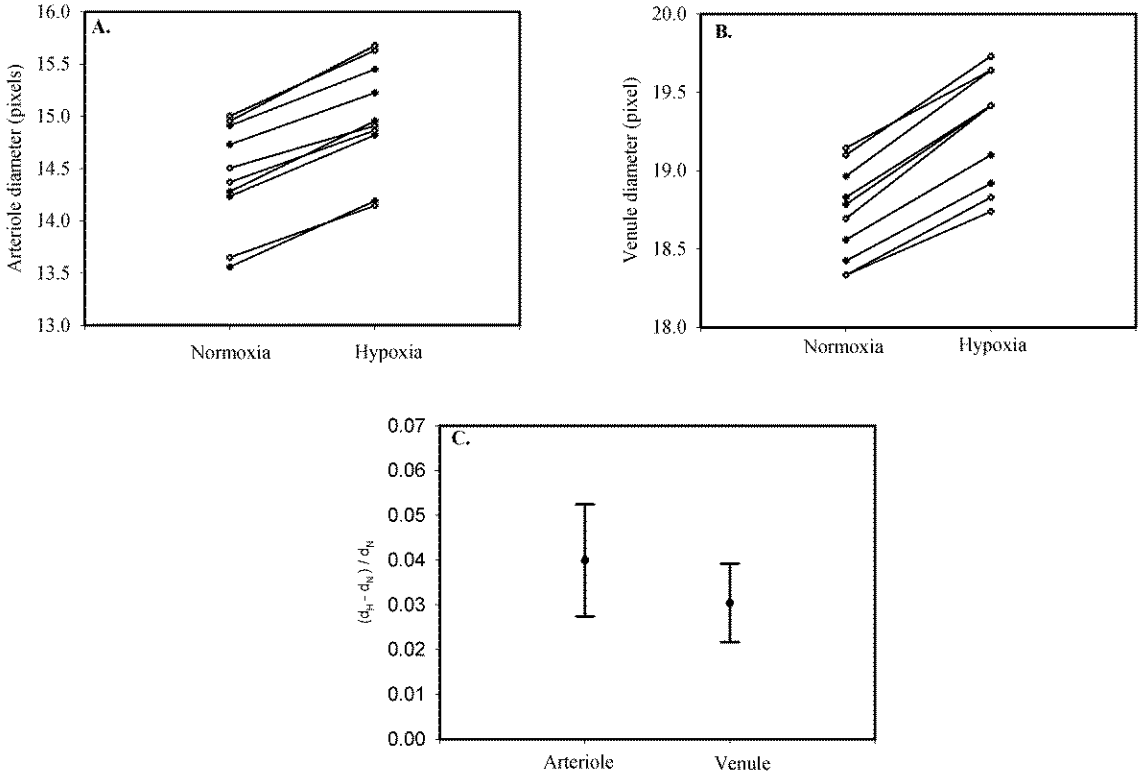

Figure 6.3: The effect of hypoxic exposure on vessel diameter (in pixels) in (A) arterioles and(B) venules compared with normoxia. (C) shows fractional increase, $(d_H-d_N)/d_N$in diameter, where d_H and d_N are vessel diameter in pixels during hypoxia and normoxia respectively.

6.3.5. Oximetric Maps of Subjects Retinal Vasculature during Hypoxia and Normoxia

Figure 6.4: shows the pseudocolour images of the calculated oxygen saturations along the retinal arterioles in ten subjects during normoxia (A), hypoxia (B) and retinal venules during normoxia (C) and hypoxia (D).

Subject 1.

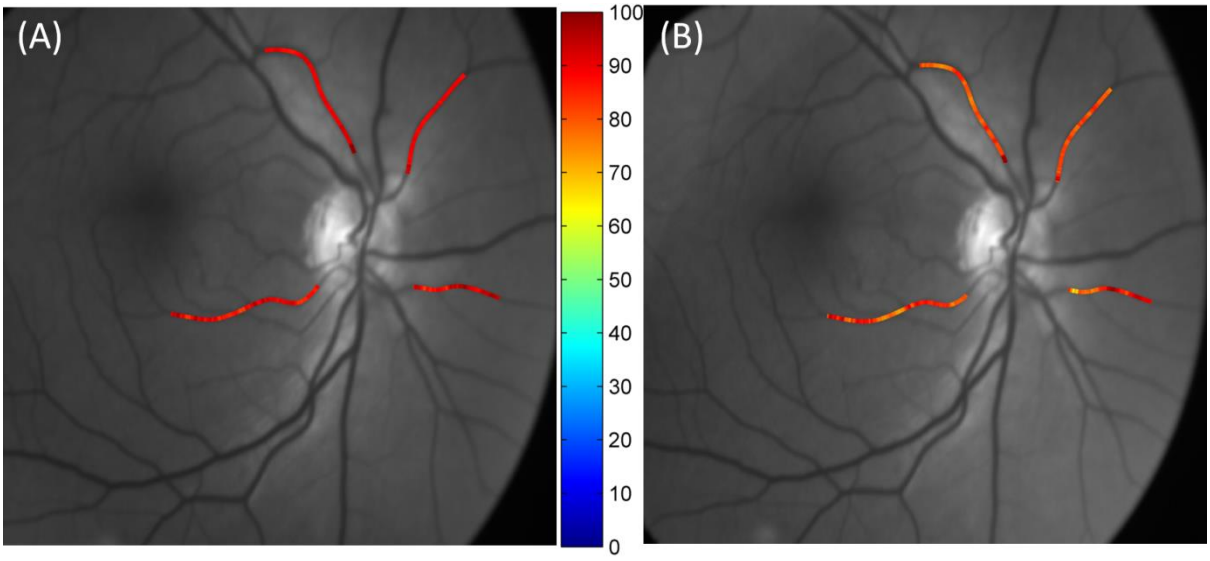

(A) Arterioles in Normoxia, (B) Arterioles in Hypoxia

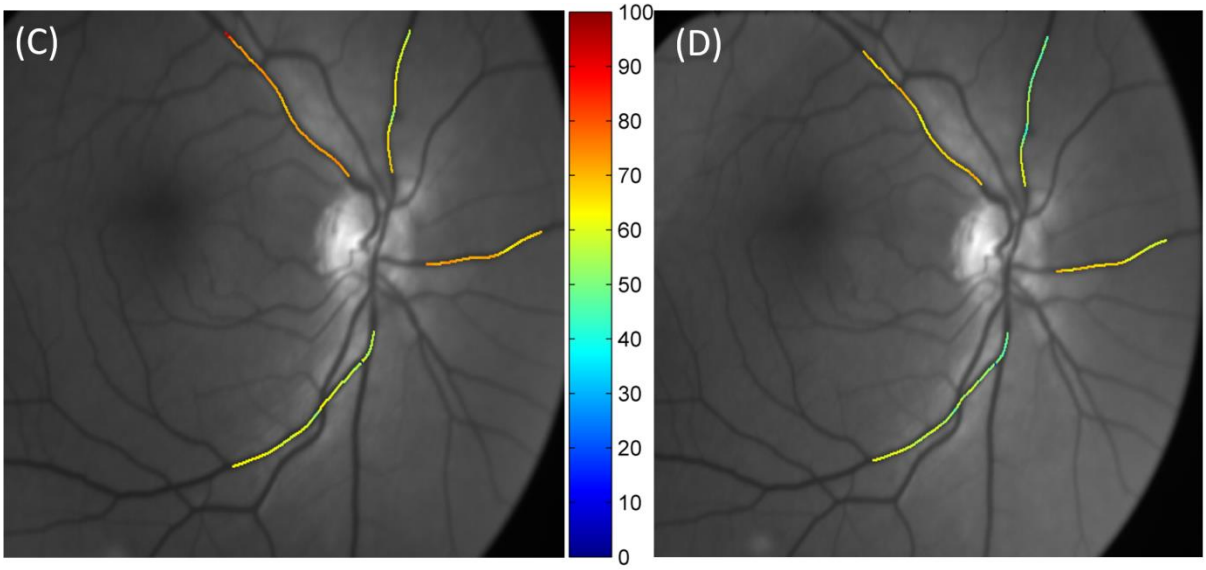

(C) Venules in Normoxia, (D) Venules in Hypoxia

Subject 2.

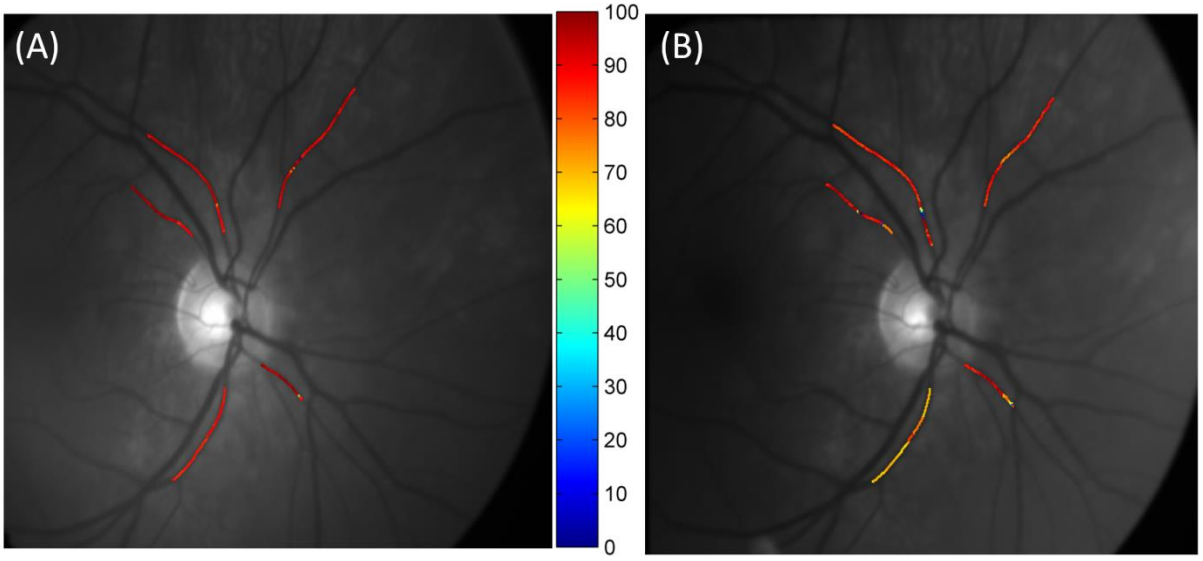

(A) Arterioles in Normoxia, (B) Arterioles in Hypoxia

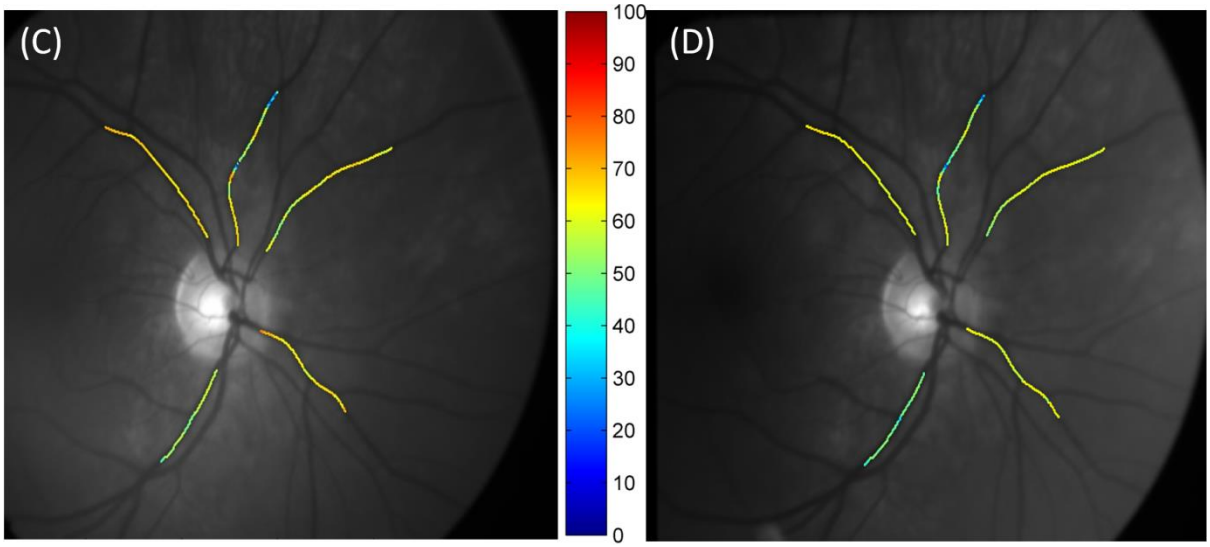

(C) Venules in Normoxia, (D) Venules in Hypoxia

Subject 3.

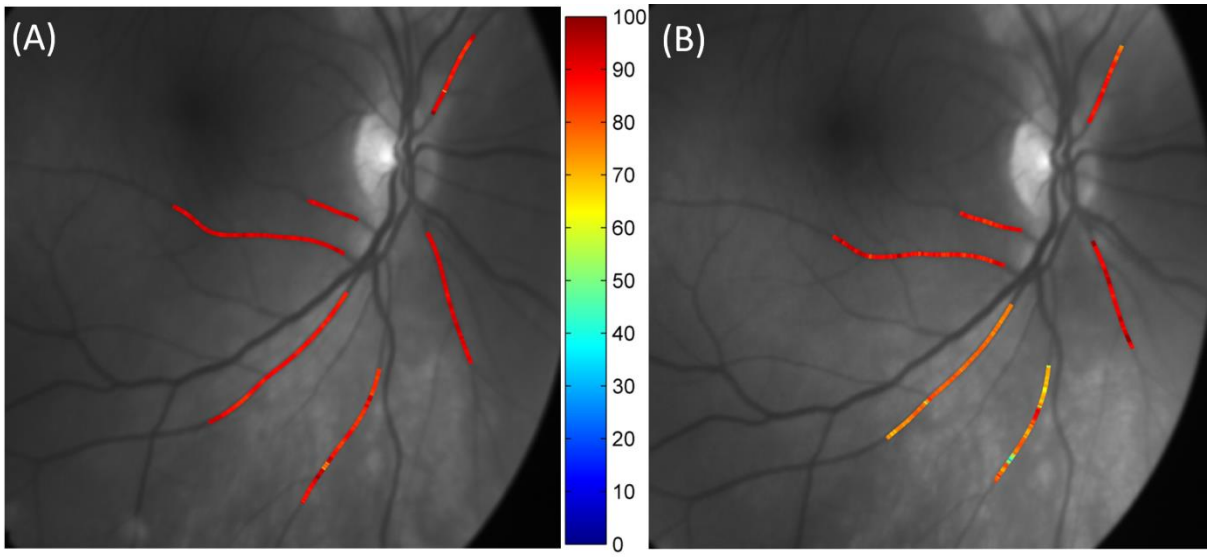

(A) Arterioles in Normoxia, (B) Arterioles in Hypoxia

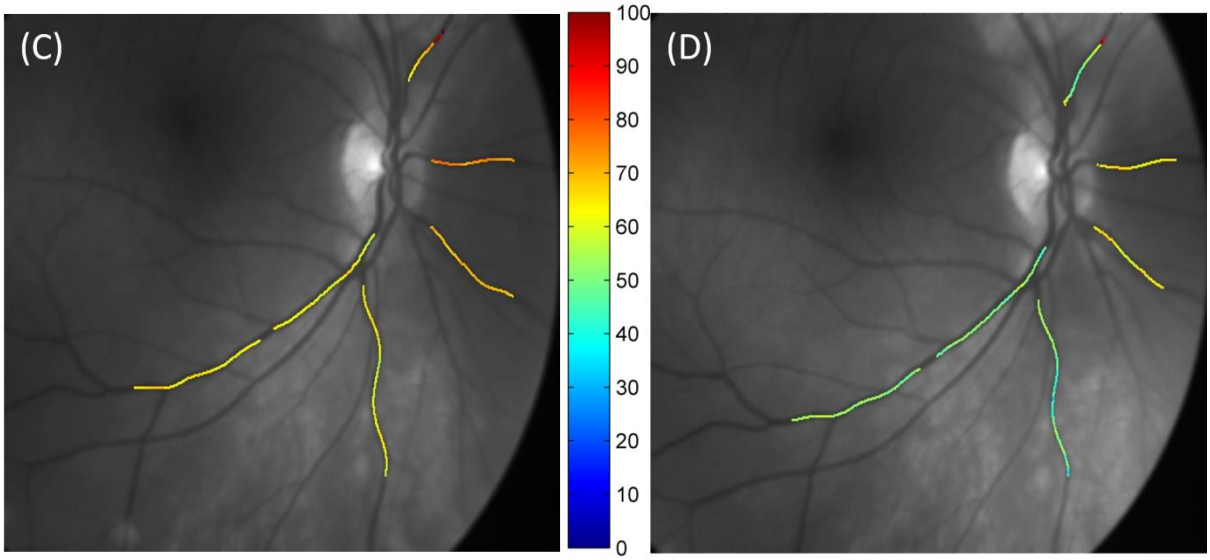

(C) Venules in Normoxia, (D) Venules in Hypoxia

Subject 4.

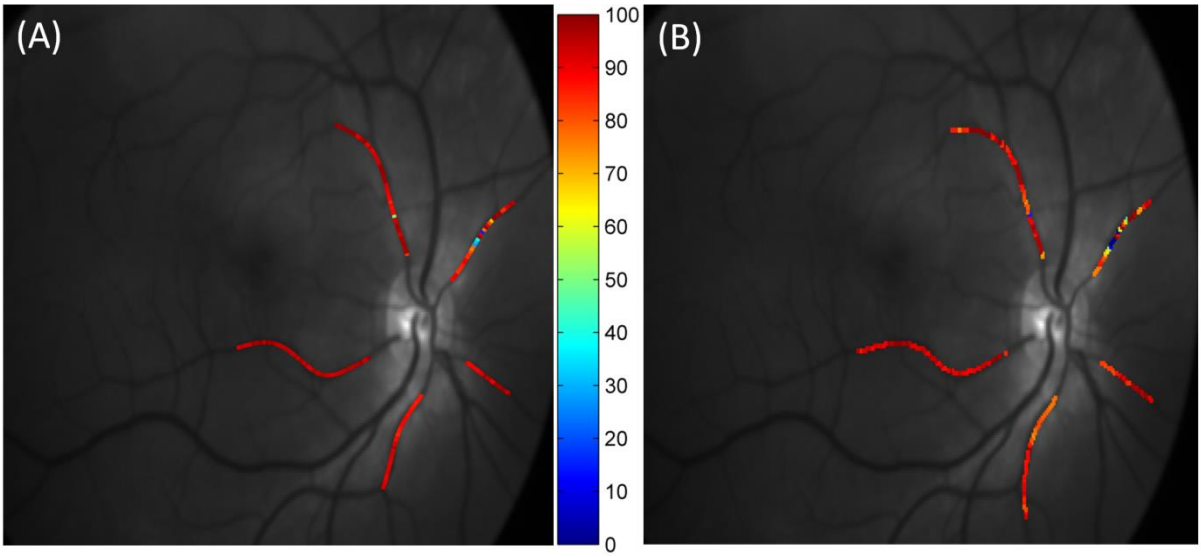

(A) Arterioles in Normoxia, (B) Arterioles in Hypoxia

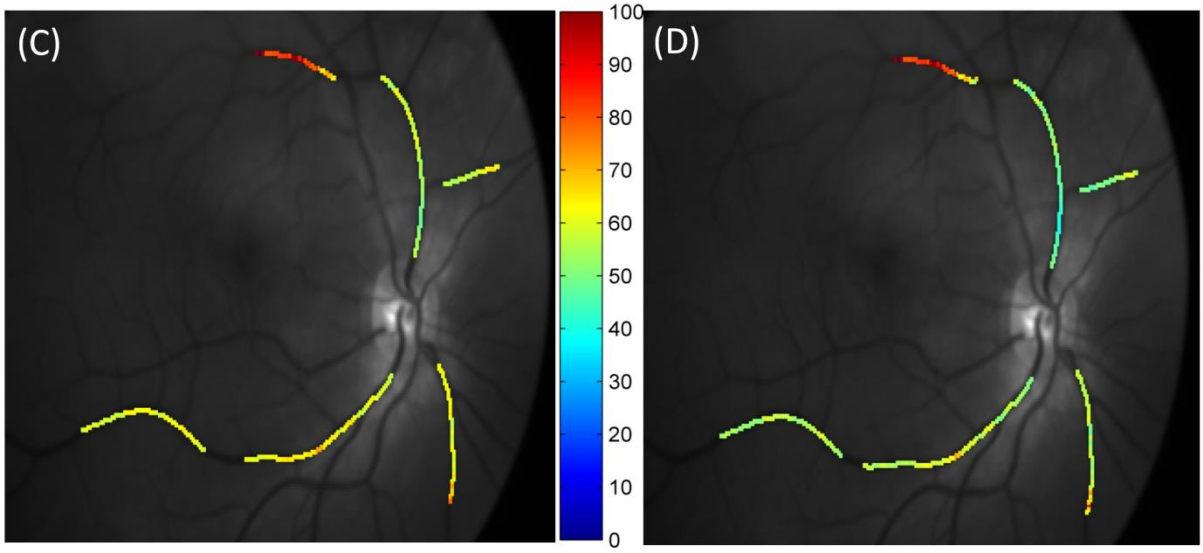

(C) Venules in Normoxia, (D) Venules in Hypoxia

Subject 5.

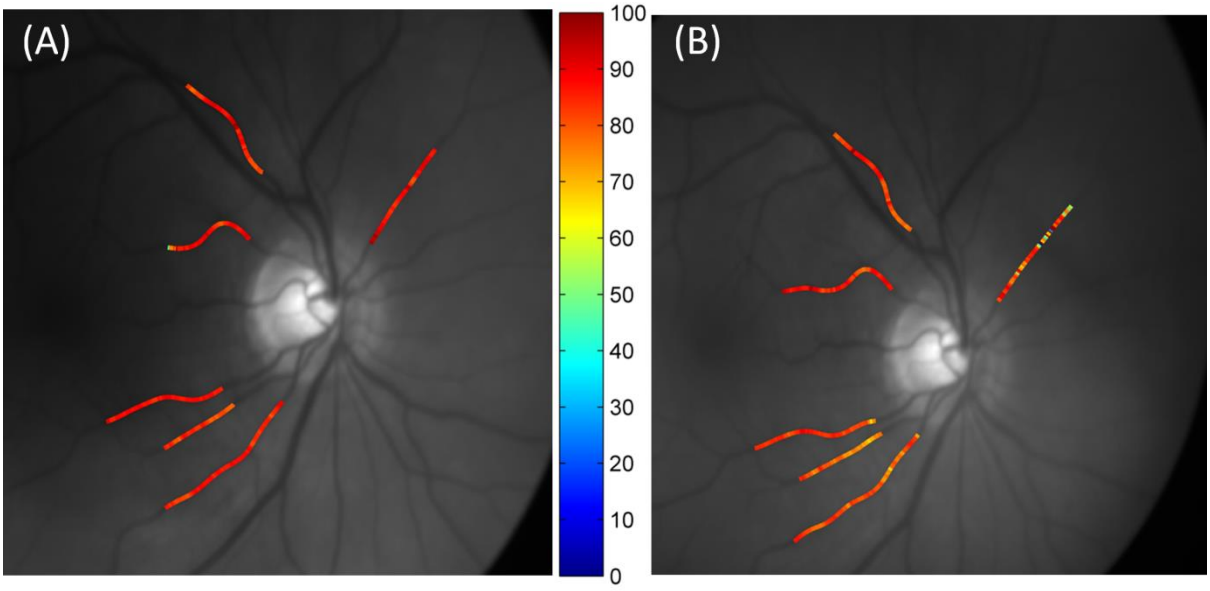

(A) Arterioles in Normoxia, (B) Arterioles in Hypoxia

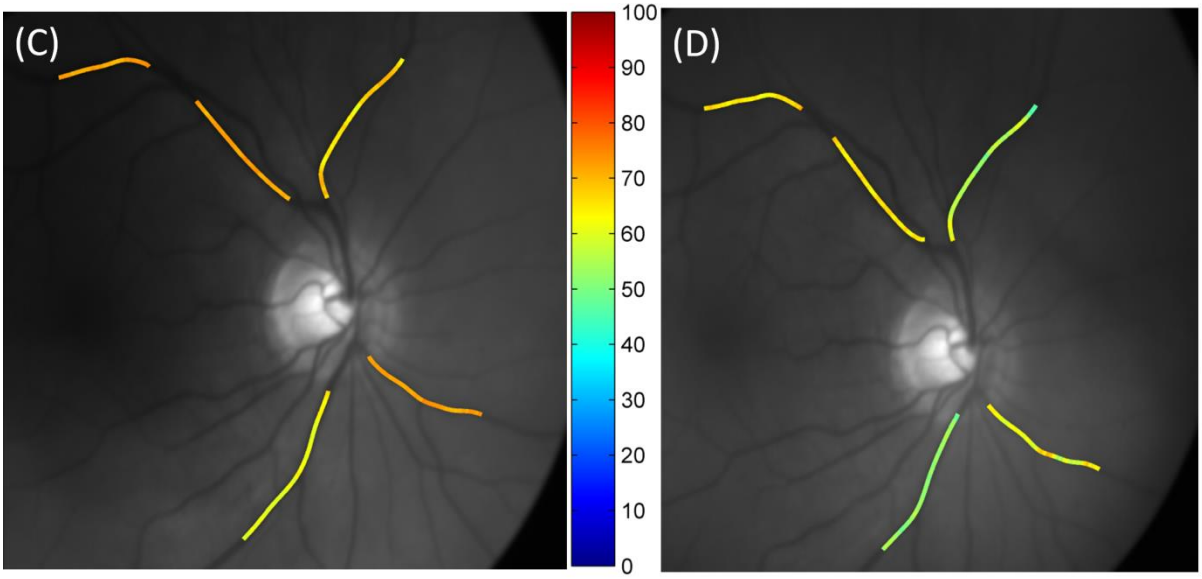

(C) Venules in Normoxia, (D) Venules in Hypoxia

Subject 6.

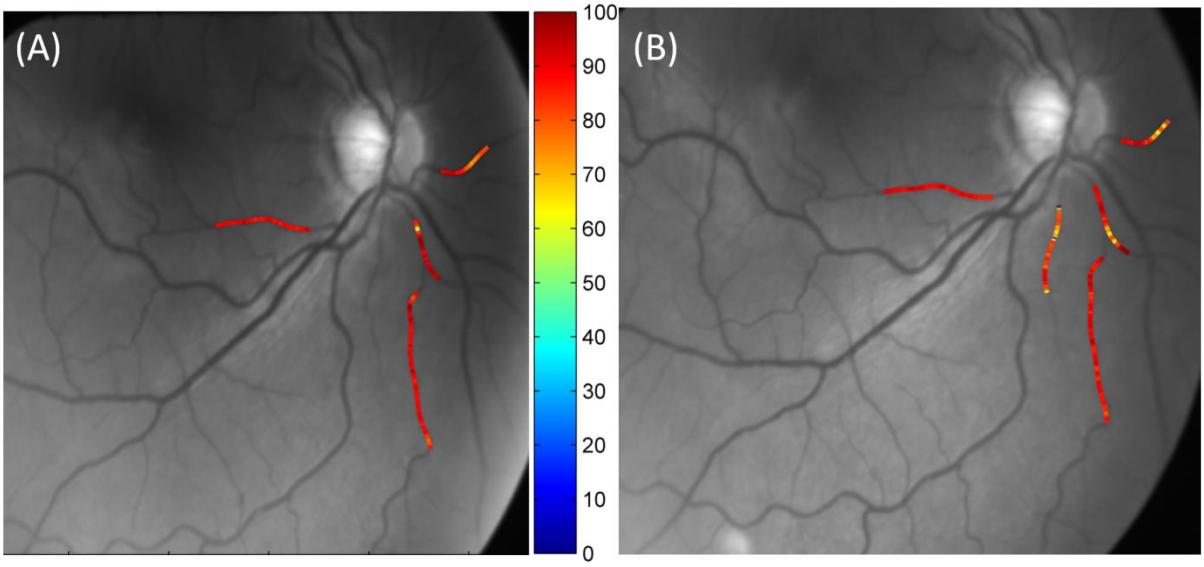

(A) Arterioles in Normoxia, (B) Arterioles in Hypoxia

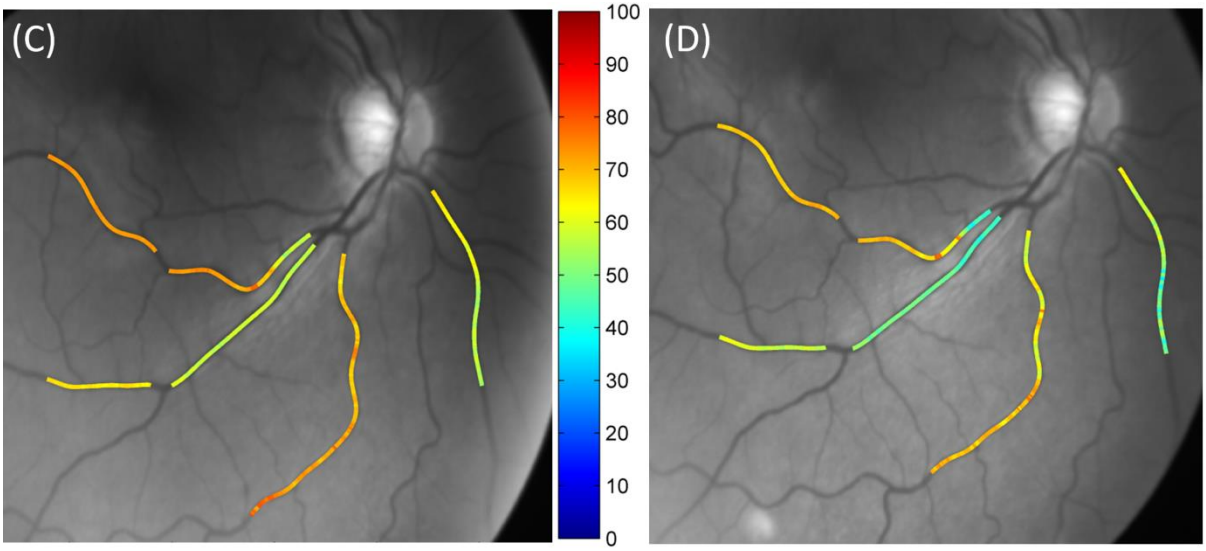

(C) Venules in Normoxia, (D) Venules in Hypoxia

Subject 7.

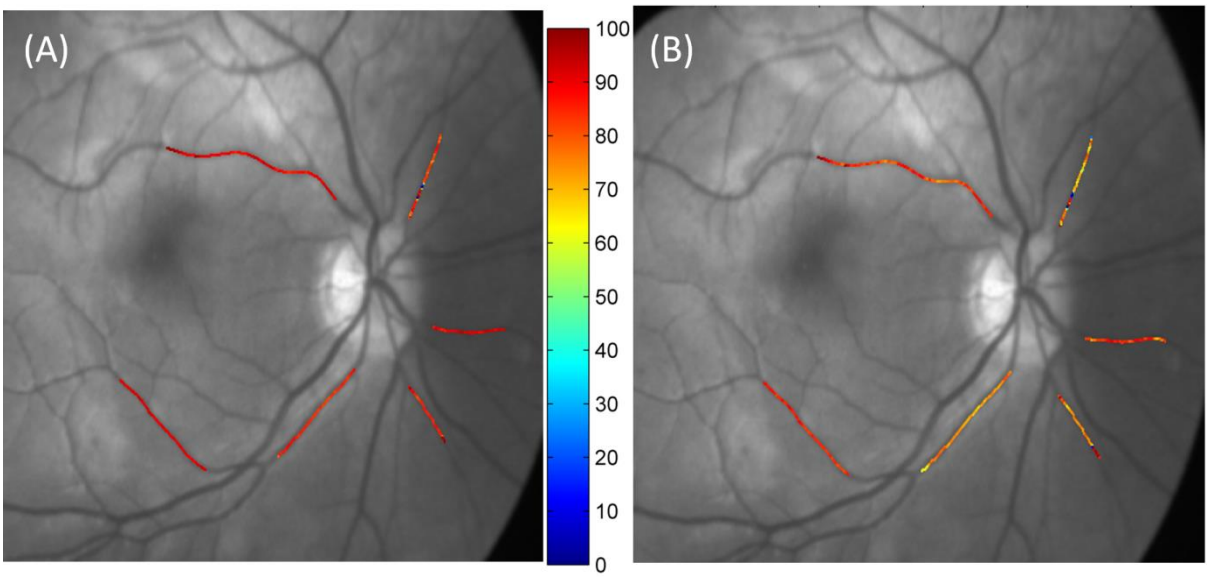

(A) Arterioles in Normoxia, (B) Arterioles in Hypoxia

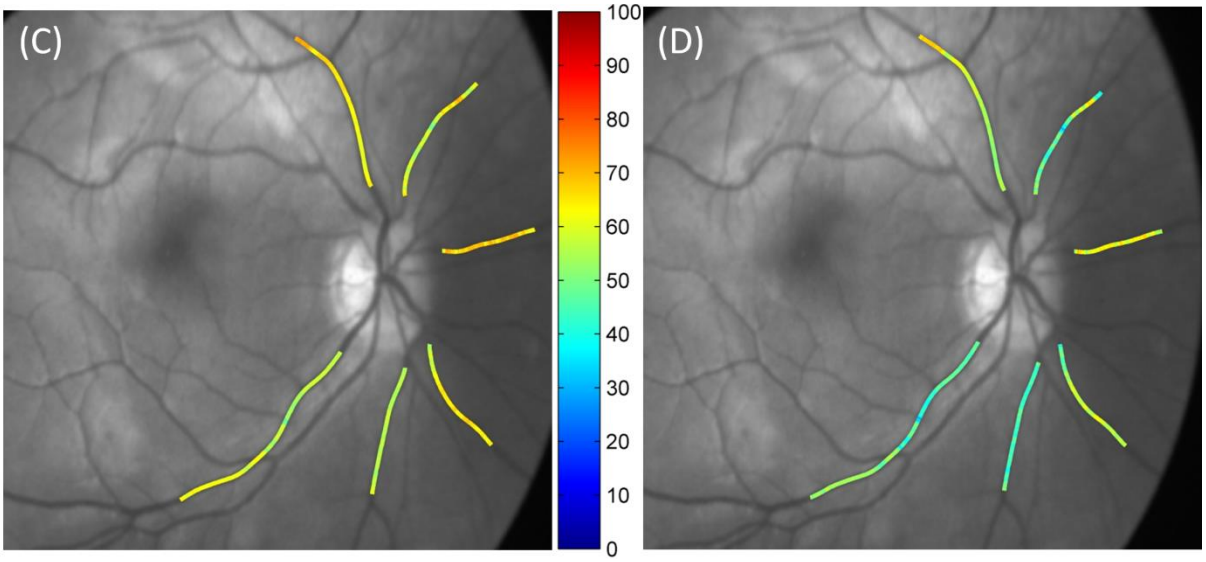

(C) Venules in Normoxia, (D) Venules in Hypoxia

Subject 8.

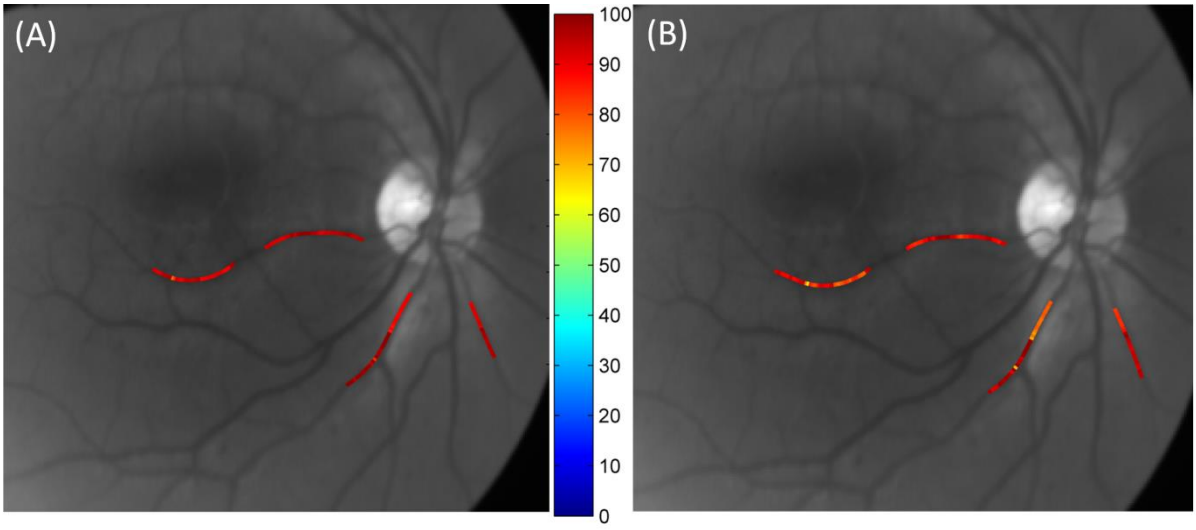

(A) Arterioles in Normoxia, (B) Arterioles in Hypoxia

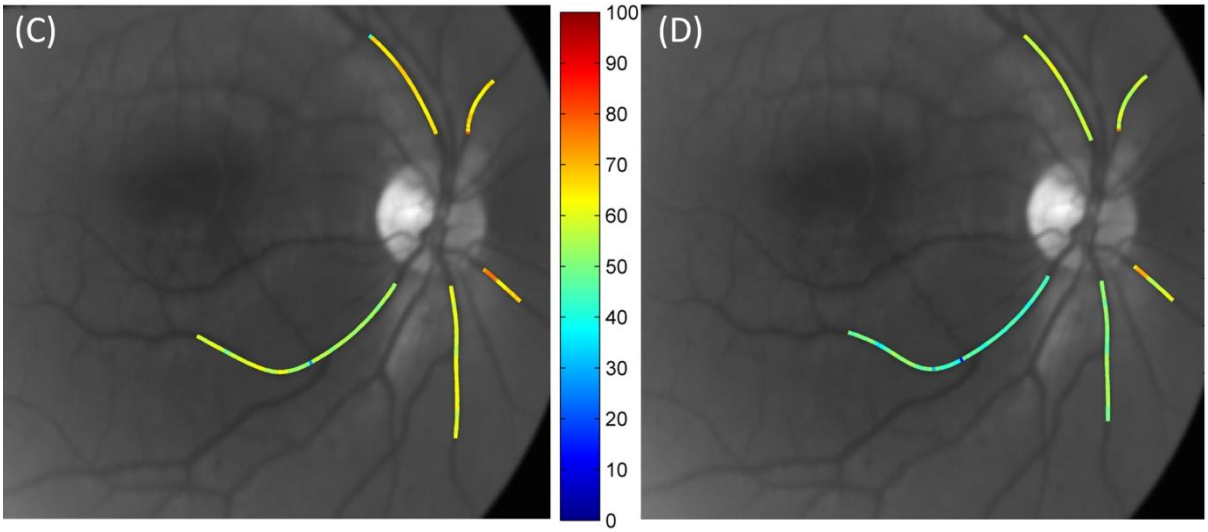

(C) Venules in Normoxia, (D) Venules in Hypoxia

Subject 9.

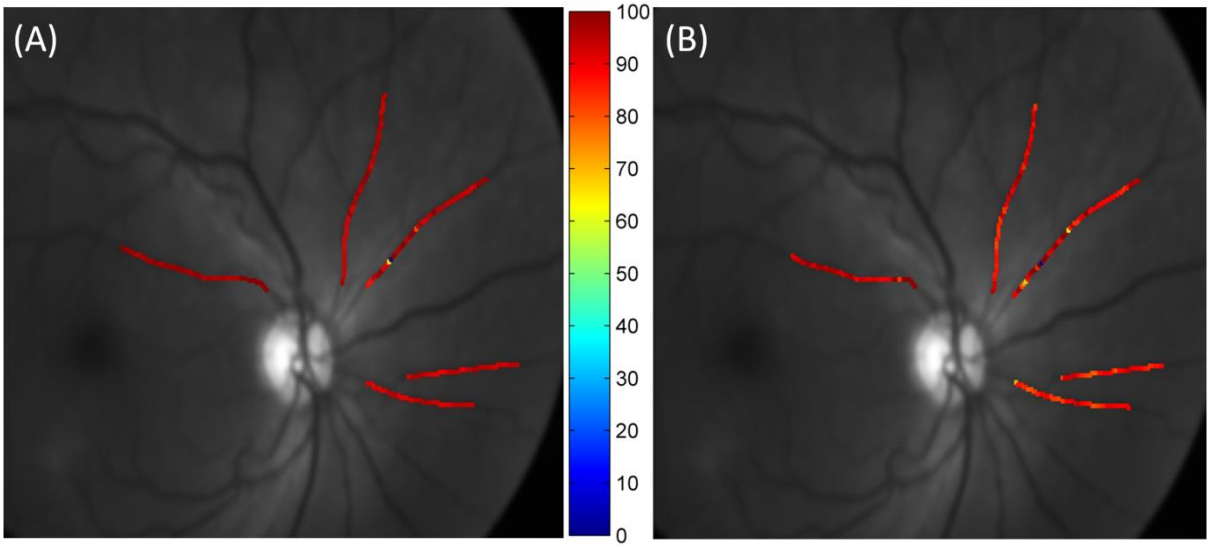

(A) Arterioles in Normoxia, (B) Arterioles in Hypoxia

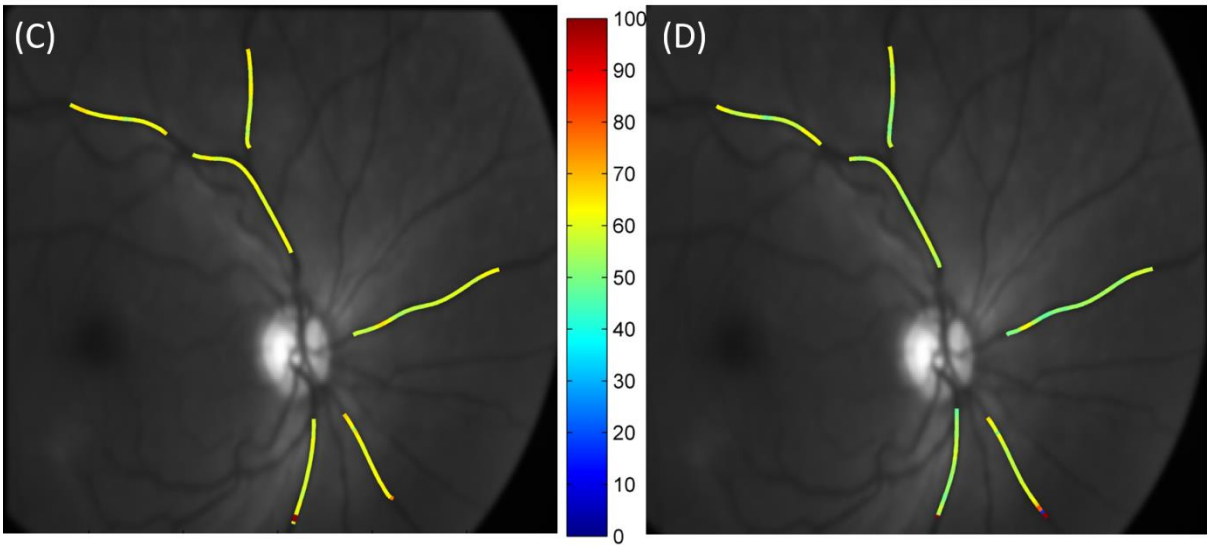

(C) Venules in Normoxia, (D) Venules in Hypoxia

Subject 10.

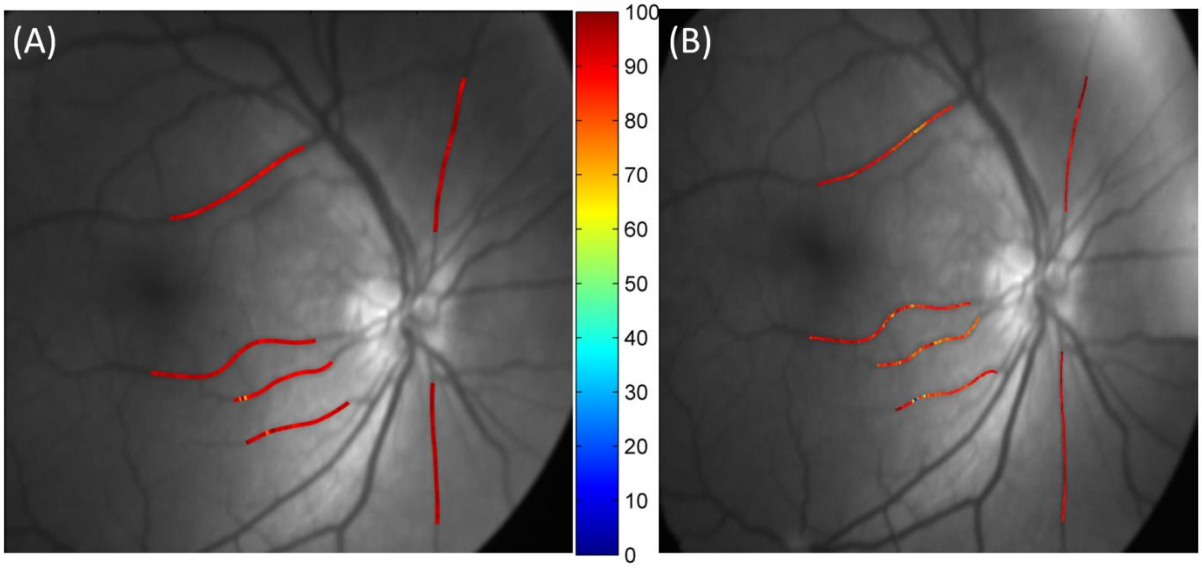

(A) Arterioles in Normoxia, (B) Arterioles in Hypoxia

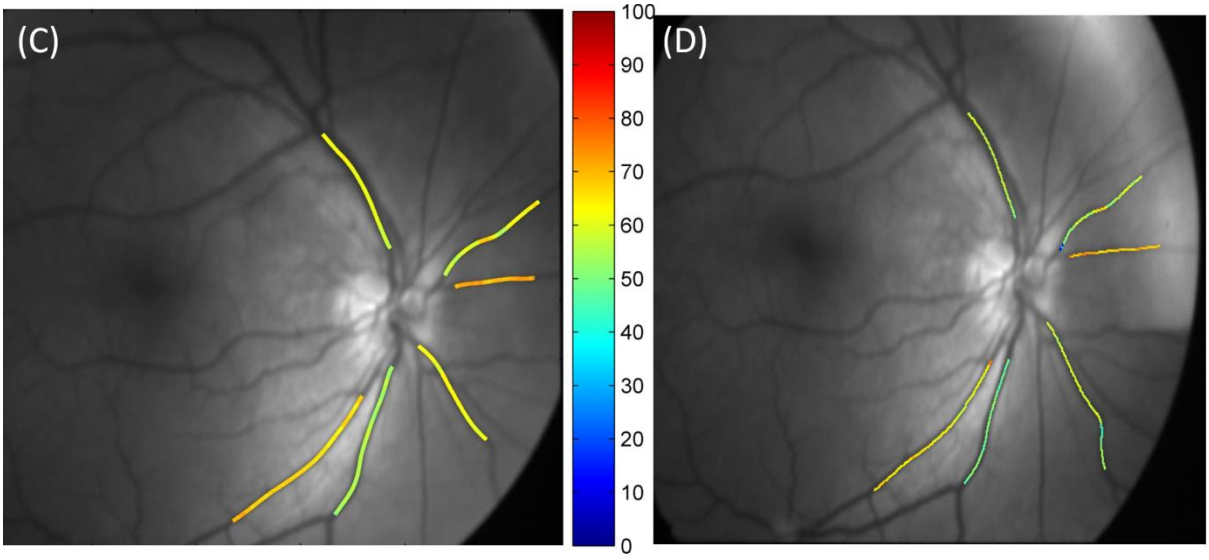

(C) Venules in Normoxia, (D) Venules in Hypoxia

6.4. Discussion

6.4.1. Repeatability of Retinal Oxygen Saturation Measurements and Vessel Diameter Calculation

As presented in the result section of this chapter, oxygen saturation and vessel diameter measured by our system is reliable and repeatable over time. In this study, we assessed the effect of acute mild hypoxia on retinal oxygen saturation by comparing oximetry, arterio-venous oxygen saturation difference and vessel diameter between retinal images acquired at normoxia and hypoxia. To rely on the results produced by this method, it was of crucial importance to ascertain what the variations between nominally identical measurements were and see if the results are repeatable or not. The repeatability experiment affirmed that the changes in oxygen saturation and vessel diameter we see is due to hypoxic exposure and is not due to chance or any random variations.

Furthermore, the repeatability results also strengthened the idea of using our retinal oximetry device to assess retinal circulation in health and diseases.

6.4.2. Retinal Oxygen Saturation Measurements in Normoxia and Hypoxia

Retinal oxygen saturation measured in arterioles at normoxia level (98.5 ± 1.6) and hypoxia (90.3 ± 2.0) and venules (70.7 ± 2.7) for normoxia and (62.4 ± 2.2) for hypoxia. We compared arteriolar oxygen saturation values measured by our oximetry device with pulse oximeter and found significantly correlated values ($r=0.96$, $p < 0.0001$, Spearman's rank correlation test). Our oximetry system is sensitive to changes in oxygen saturation in retinal arterioles and venules with changes in inspired oxygen.

6.4.3. Effect of Acute Mild Hypoxia on Retinal Oxygenation and Retinal Circulation

In this study, we examined the effect of acute mild hypoxia on retinal oxygenation by measuring oxygen saturation, arterio-venous oxygen saturation difference and vessel diameter. We can draw the following conclusions from the results:

- A reduction in the fraction of inspired oxygen (from 21% to 15%) resulted in a decline ($P<0.001$) in retinal arterial and venous oxygen saturation.

- Despite the decrease in arterial and venous oxygen saturation, we calculated that the arteriovenous oxygen saturation difference remained unchanged during hypoxia when compared with normoxia.
- During acute mild hypoxic exposure, the diameters of the retinal arterial and venous vessels were observed to increase by a small but highly significant ($P<0.001$) increment of 4% and 3%, respectively. This increase in retinal vessel diameter is compatible with an autoregulatory response to meet the metabolic demand under conditions of hypoxia.

Mild hypoxia was induced by reducing the FiO_2 to 15%. This resulted in decreased oxygen saturation in both the retinal arterioles and venules, while the arteriovenous oxygen-saturation difference remained unchanged. The pulse oximeter reading during the hypoxia phase of the experiment agreed with the observed decrease in retinal arterial O_2 saturation. Blood flow was not measured directly, but there should be an increase in blood flow since a significant increase in retinal-vessel diameter was observed. An increase in retinal-vessel diameter and blood flow has also previously been reported to accompany hypoxia [28-34] and measurement of the changes in retinal-vessel diameter and arteriovenous oxygen difference have previously been employed to estimate the relative change in retinal blood flow [186]. Assuming, as stated by Poiseuille's law [195], that blood flow increases with the fourth power of the calibre, then the 3.5% average increase in vessel diameter that was measured corresponds to an increase in blood flow of 16%. The rate of oxygen delivery is equal to the product of the arteriovenous oxygen difference and blood flow suggesting therefore that the absolute magnitude of oxygen delivery by the retinal vessels increased during hypoxia. This increase may compensate for a reduced contribution from the choroidal circulation, which is reported to be insensitive to changes in oxygen saturation [26, 27].

This is one of the first studies to assess the effect of acute mild hypoxia (10-minute exposure) on retinal circulation. Previous studies on retinal circulation have examined the effect of severe and chronic hypoxia over a longer period of time (from hours to days). Collectively these studies imply that hypoxia induces vasodilation of the retinal vessels and increases retinal blood flow [28-34]. In a study conducted at an altitude of 5,300m (partial pressure of oxygen is equivalent to 10% inspired oxygen at sea level), it was reported that the retinal arterial and venous diameter increased by 18% and 21% respectively, within two hours of exposure to altitude [34]. In another study [28], a moderate but significant increase in retinal vessel diameter was observed in monkeys during mild hypoxia (PaO_2 = 59 mmHg, which

approximates FiO_2 of 15%). This is consistent with our measurements on humans. At a severe level of hypoxia (PaO_2 = 35 mmHg, approximates FiO_2 of 11%) vasodilation was more pronounced.

In many retinal diseases including diabetic retinopathy, glaucoma and age-related macular degeneration, retinal circulation and functions are impaired. In these diseases, retinal circulation does not properly respond to hypoxia, flicker stimulation or dark adaptation [13, 23, 25]. Improved understanding of the effects of hypoxic stress on retinal oxygenation and functions in normal healthy individuals such as we describe here therefore provides a route to developing an understanding of these disease mechanisms and potentially for clinical diagnosis.

The retina and brain share a similar vascular blood supply and similar vascular regulatory processes [196, 197]. The retinal artery stems from the ophthalmic artery, which is a branch of the internal carotid artery and is considered part of the cerebral vasculature [31]. Autoregulatory control mechanisms are present in both the cerebral and retinal circulations. These structural and functional similarities suggest the use of retinal vasculature changes, including vascular calibre, and intravascular oxygen saturation as plausible surrogate measures for cerebral vascular changes [31, 198].

The autoregulatory mechanism centres on maintenance of blood-flow provision in the presence of changes in perfusion pressure [199]. Cerebral autoregulatory responses were first reported by Fog [200, 201] using a feline model, with the conclusion that autoregulatory responses were independent of neurogenic stimuli. In humans, the manipulation of mean arterial pressure, either by whole body tilting or by occlusion and reperfusion of the circulation to the lower limbs, have shown that cerebral blood flow (CBF) is maintained during pressure perturbation thus demonstrating autoregulation [199]. In the 1980s measurement of cerebral blood flow from vessel diameter and peak blood-velocity using transcranial ultrasound of the middle cerebral artery provided a more complex assessment of CBF[202]. Using body tilting to reduce mean arterial pressure from 91 mmHg to 68 mmHg, Tachibana et al [31] reported a small (6%) increase in retinal-arterial diameter during the exposure to lower mean arterial pressure. This finding suggests that the retinal vessel response to a decrease in perfusion pressure is in the same direction and magnitude as the cerebral circulation.

The effects of inhalation of gas with a reduced oxygen content (hypoxia) or elevated carbon dioxide content (hypercapnia) on cerebral autoregulation have also been investigated [203, 204]. Acute hypercapnia results in vasodilatation of the cerebral circulation but vasoconstriction of the peripheral circulation, whereas acute hypoxia results in vasodilatation of both the cerebral and peripheral circulation. The degree of hypoxia is also important, since Iwasaki et al [204] observed no effect on the cerebral circulation of inhaling gas with an oxygen content above 16%, however, at the lower level of 15% oxygen content there was an increase in cerebral blood flow suggesting a threshold level for increases in cerebral blood flow velocity.

One might also consider the potential to use imaging of retinal circulation as a convenient indicator of cerebral circulatory processes. However, despite the many similarities between the cerebral and retinal circulation [196, 198] it should also be recognised that differences also exist: for example the intra-ocular pressure is higher than in the brain and the retinal vasculature is more sparse leading to a higher arterio-venuous oxygen difference. To discuss the similarities and differences between them is neither the aim nor within the scope of this chapter. This issue is highlighted here as an indication of the merit for further studies to establish the value of this potential.

6.4.4. Limitations of the Study

Limitations of the oximetry technique used in this study have been described in Chapter 5, which additionally applies to this study. An application of two-wavelength oximetry is described here using an established calibration technique that employs assumed values of oxygenation of veins and arteries in healthy eyes based on normal physiology. One of the limitations of this study is that it is based on calibration-based two-wavelength retinal oximetry. With this technique absolute oximetry is not possible. The calculated venous oximetry value of 70% is higher but comparable to values reported by Hammer et al [18], however, in this study, the conclusions are based on changes in measured blood oxygenation and these conclusions are unaffected by a scaling or offset of oximetry with respect to absolute values. We report here a significant increase in vessel calibre during hypoxia, which corresponds to an increase in blood flow, although we did not measure blood flow directly to affirm this conclusion.

6.4.5. Conclusion

The retinal-arterial oxygen saturation recorded using a novel snapshot spectral retinal camera under normoxia significantly correlated with the pulse oximetry values ($r=0.96$, $p < 0.0001$, Spearman's rank correlation test). The acute inhalation of a hypoxic gas mixture resulted in a decline in both retinal arterial and venous saturation, as well as a significant increase in retinal vessel calibre, suggesting an autoregulatory response. Our study, on a small group of normal volunteers, suggests that this retinal-oximetry method using spectral imaging is reliable and sensitive to small changes in oxygen saturation and retinal-vessel calibre. The ability to perform non-invasive oximetry in retinal vessels *in vivo* allows assessments of retinal circulation in health and disease.

Chapter 7

Red-Eye Reflectivity (Choroidal) Oximetry

7.1. Introduction

In this chapter, a new spectral imaging technique that non-invasively measures the oxygen saturation of choroidal blood in the back of the human eye, using red-eye reflections is presented. This chapter describes a very simple imaging setup, using the fundus camera, which is capable of simultaneously imaging both eyes, at infrared wavelengths and methods used to calculate the intensity ratio. This chapter also demonstrates the sensitivity of this technique with a change in oxygenation, by reducing the inspired oxygen in healthy human subjects.

7.1.1. Red-Eye Reflection

The red-eye effect which is seen in colour photographs (Figure 7.1) is due to the reflection produced from blood in the choroid. Figure 7.2 shows a cross section view of the human eye and the path followed by a ray of light. When a ray of light with intensity I_0, enters the eye through the cornea, it hits the fundus (back of eye), and passes through different ocular layers and comes back out of the eye with intensity I_T. This reflected light appears as 'Red-Eye' in colour photographs. Most components of the eye (i.e. cornea, lens, aqueous and vitreous humour), before the light hits the retina, are transparent in visible and near infrared region.

Figure 7.1: The red-eye effect seen in a colour photograph

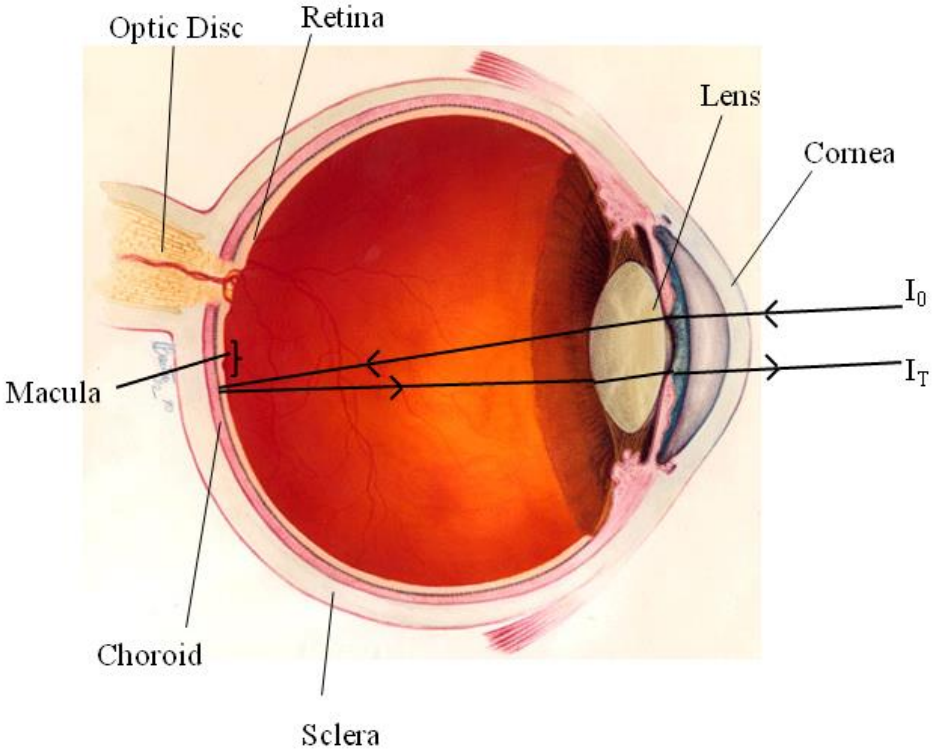

Figure 7.2: Cross section of human eye

When the light (I_0) is incident upon the fundus it passes through the different layers as shown in Figure 7.3. Light goes through the retina, pigment epithelium layer and then passes through the choroid, hits the sclera and then is reflected back (I_T).

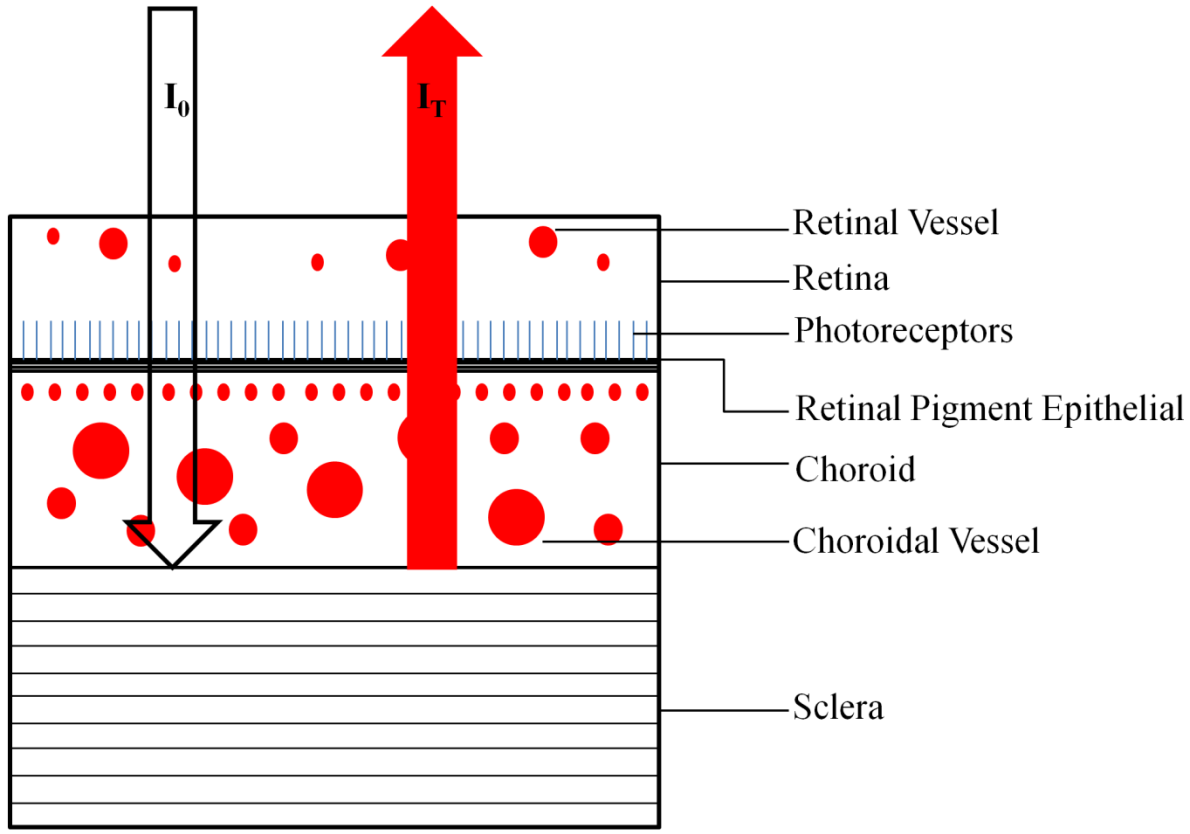

Figure 7.3: Human fundus and the light path

The blood vessels in retina and the choroid are the major components that affect the reflected light. The photoreceptor layer and nerve fibre layers in retina shows very less sensitivity to near infrared light. The other layer which absorbs light is the retinal pigment epithelium (RPE) layer and the amount of light absorption depends on both eye and skin pigmentation. As we know that in comparison to the retinal circulation the choroid has an extremely dense vascular structure and high blood flow rate so we can say that the major contributing factor for red-eye effect is the blood in the choroid.

Choroidal vessels (arteries and venules) have a very high oxygen tension and a very low arteriovenous oxygen saturation difference of just about 3%.[20] So if we consider choroidal arteries and arterioles with oxygen saturation at about 100%, choroidal veins and venules will have oxygen saturation of about 97%. The red-eye reflection which we get from choroidal vasculature is due to blood with oxygen saturation of about 97-100%.

7.1.2. Motivation for Using Red-Eye Reflection for Choroidal Oximetry

The choroidal blood supply comes from ophthalmic artery which is a branch of the internal carotid artery and is considered as a part of the cerebral vasculature [31]. Red-eye reflection choroidal oximetry may provide us with an opportunity to monitor the cerebral circulation in an easy and efficient way. The reflection from the choroid varies with the change in oxygen saturation of blood. This is due to difference in absorption coefficient of oxygenated and deoxygenated haemoglobins. Using the same principle upon which retinal oximetry is based; red-eye reflection choroidal oximetry utilises the difference in the absorbance coefficients of deoxyhaemoglobin and oxyhaemoglobin at different wavelengths. Similar to two-wavelength retinal oximetry, using two wavelengths (one isosbestic and other oxygen sensitive) to record red-eye reflection, the oxygen saturation of choroidal blood can be determined.

There are some unique advantages to using red-eye reflection choroidal oximetry over retinal oximetry. In retinal oximetry, retinal image quality is an important factor. Whereas, in case of red-eye choroidal oximetry, recording the reflection is quite simple and does not require elaborate imaging setup or training. Unlike retinal oximetry it is also possible to simultaneously perform oximetry in both the eyes using red-eye reflection.

The measurement of oxygen saturation using reflected light from the human fundus was first demonstrated by Broadfoot et al [159] in 1961. In their study, they measured amount of light of different colour reflected by the fundus using photodiodes and photomultiplier. They showed that the fundus reflection of red light changed significantly when the choroidal oxygenation was altered in subjects by nitrogen breathing or by apnea. They established that fundus reflection changes with choroidal oxygenation and can be used to measure the same. In another study Laing et al [160], developed a 'Choroidal Eye Oximeter' that measured the amount of light reflected from the fundus at two wavelengths (650 nm and 805 nm) and were able to determine the oxygen saturation in the choroidal blood. They changed the oxygen saturation of subjects by nitrogen breathing and measured a change in oxygenation with their device. Both these techniques are described in detail in Chapter 1.

In this chapter, we present a new improved spectral imaging method for choroidal oximetry using the reflected light from the fundus based on the early works by Broadfoot [159] and Laing [160]. We also demonstrate the sensitivity of our technique with a change in oxygenation in healthy human volunteers.

7.2. Methods

7.2.1. Wavelength Selection for Red-Eye

To determine the wavelength to be used for imaging the choroidal reflections, a range of wavelengths were assessed. This was done by estimating the amount of light transmitted through the choroid using the Lambert-Beer law. A simulation was run in Matlab to ascertain the amount of transmitted light at any given wavelength.

According to the Lambert-Beer law, at any given wavelength of light its absorption is dependent on the extinction coefficient and concentration of the solution and the path length travelled by the light.

$$I_T = I_0 * 10^{-\varepsilon c d} \qquad (7.1)$$

Where

I_T = Amount of light transmitted through solution

I_0 = Amount of incident light

ε = Extinction coefficient of blood solution

c = Concentration (haematocrit) of blood

d = Distance through the solution

Using equation 7.1, the amount of transmitted light (I_T) at a wavelength range of 550 nm to 850 nm was calculated for the choroid with an average thickness of 400µm [4]. The extinction coefficient value of blood depends on oxygenated (HbO_2) and deoxygenated (Hb) haemoglobin, and the values were taken from data compiled by Prahl [136].

Figure 7.4 shows the light transmission values for wavelength range of 550 nm to 850 nm for fully oxygenated blood (red line) and completely deoxygenated blood (blue line) in choroid.

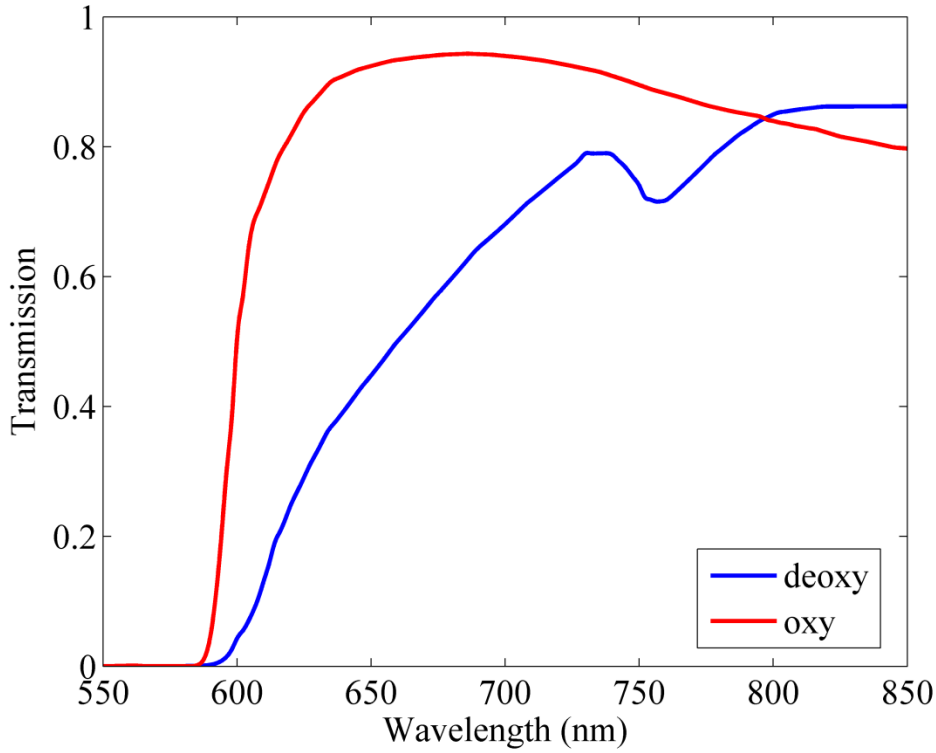

Figure 7.4: The amount of light transmission through choroid between wavelengths of 560 nm to 850 nm (simulated data). The red line represents 100% oxygenated blood in choroid and the blue line represents 0% oxygenation.

Based on figure 7.4, it is clear that the choroid is very less transmissive for visible light at a wavelength range between 550 nm to 590 nm. The choroidal transmission increases above 590 nm and transmission is quite high for near infra-red and infra-red region of the spectrum. As transmission is higher in infra-red region, 800 nm and 780 nm were selected as two wavelengths to record the red-eye reflection. The 800 nm was selected as it is an isosbestic wavelength and absorbance coefficient value of Hb and HbO_2 is the same. 780 nm was selected as oxygen sensitive wavelength as it was available with the IRIS system. Both of these wavelengths were available with our snapshot IRIS system when used with a narrow band pass filter (788/25 nm) with the fundus camera.

7.2.2. Imaging Setup

The red-eye images were acquired using the IRIS snapshot multispectral fundus camera, as described in Chapter 2. The IRIS snapshot enabled us to capture images at different desired wavelengths in a single snapshot. The same imaging system was used in previous chapters to acquire images for retinal oximetry. The imaging setup was slightly modified to acquire

images at infra-red wavelengths. To achieve this narrow band pass filter (788/25 nm) was used in front of the illumination lamp and the flash of the fundus camera. The subjects were seated 10 cm (approx) away from the fundus camera with the head resting on a headrest to minimise any movement. Figure 7.5 shows the setup to capture the red-eye reflection. The eyes of the subjects were illuminated with the filtered infra-red light and the reflected light from the fundus and choroid was captured via the imaging plane of the fundus camera after it passed through the IRIS system on to an sCMOS camera (Zyla, Andor; Belfast, U.K.).

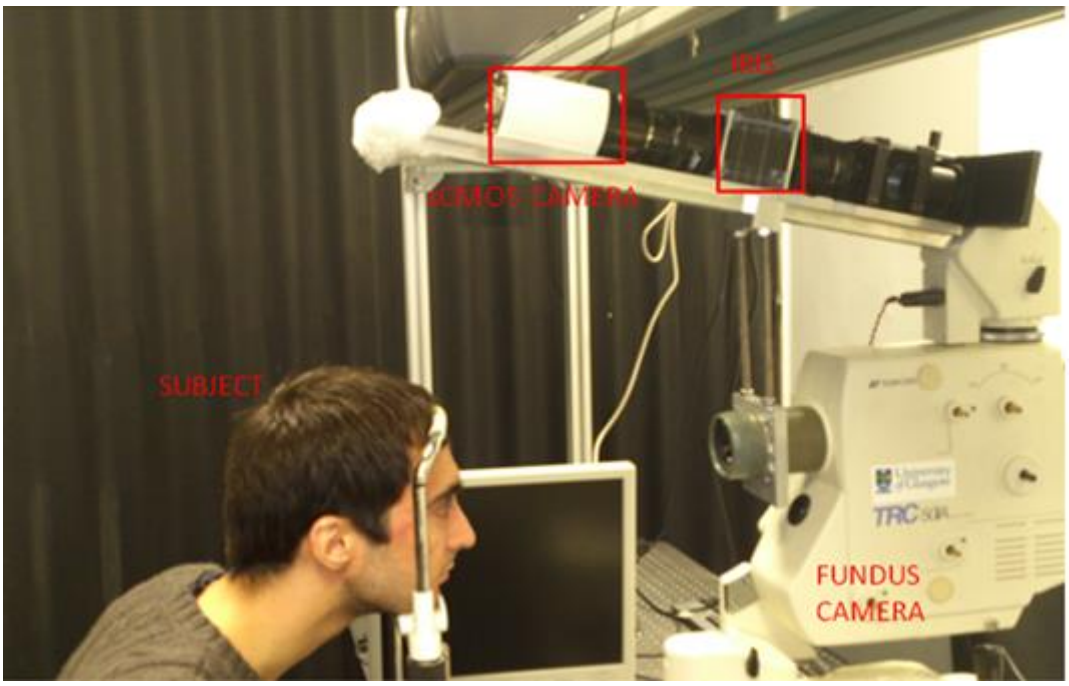

Figure 7.5: Fundus camera setup to record the red-eye reflection, the subject is seated approx 10 cm away from the objective of the fundus camera to record the red-eye reflection of both the eyes.

The spectral transmission of all of the 8 sub-images from the IRIS system for the infra-red region is shown in the Figure 7.6. The two sub-images used for red-eye choroidal oximetry (highlighted in red) had the spectral transmission peaks at 780 nm and 800 nm. An example of red-eye raw image is shown in Figure 7.7.

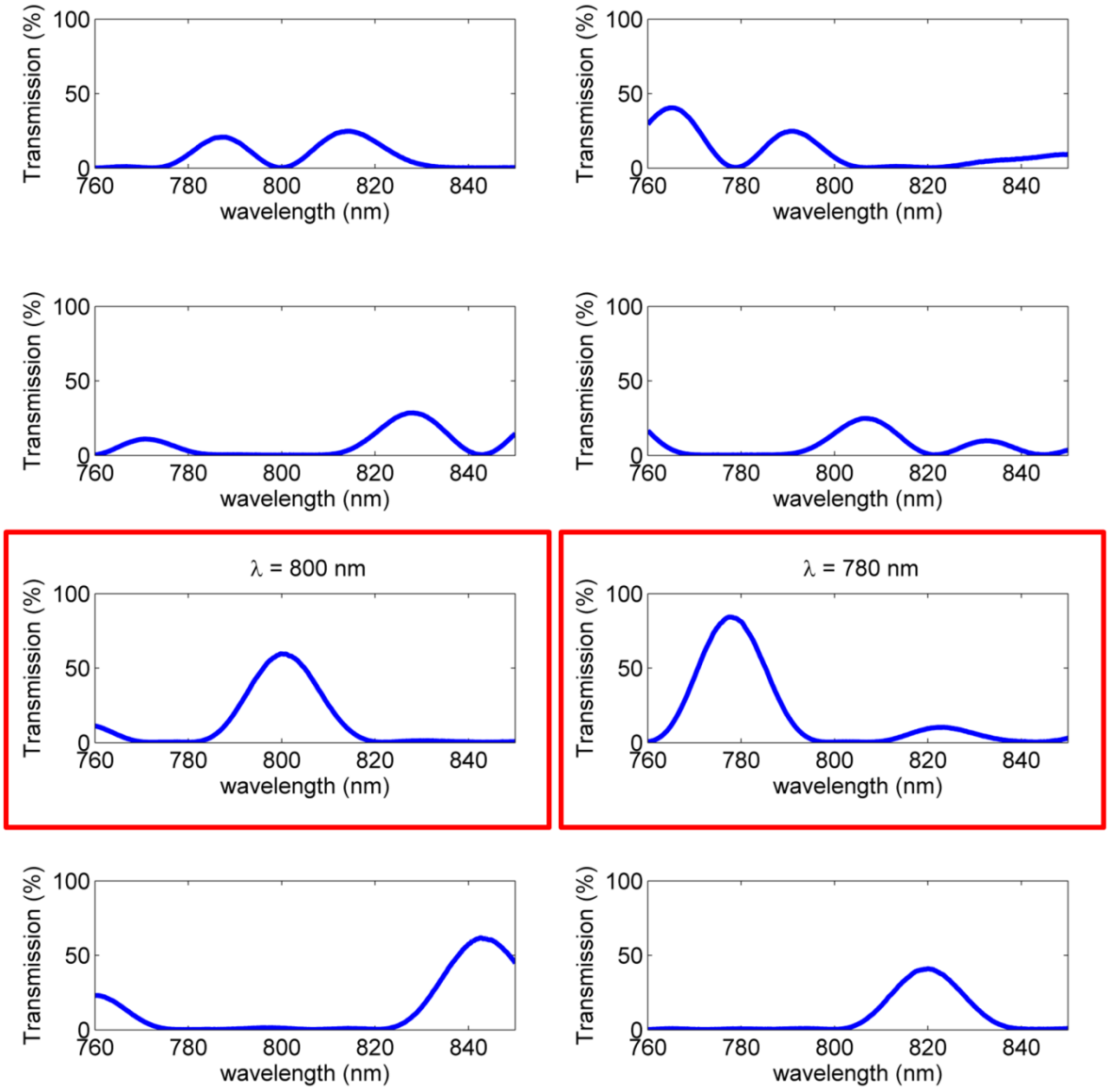

Figure 7.6: Spectral transmissions of 8 sub-images from an infra-red IRIS raw image. The two bands used for red-eye reflection choroidal oximetry were (highlighted in red) 800 nm and 780 nm

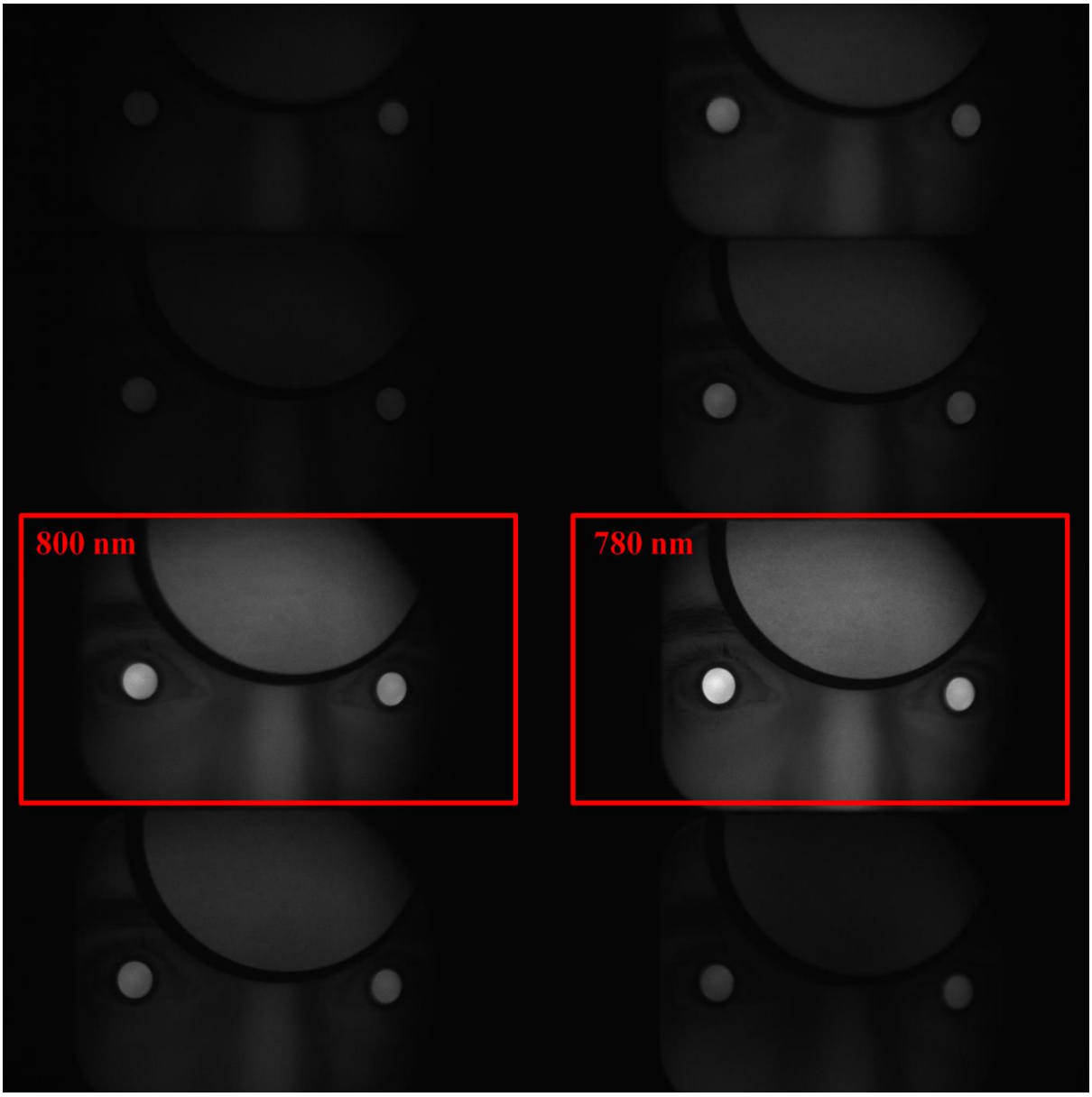

Figure 7.7: A raw red-eye image captured by IRIS system. The two sub-images used for red-eye choroidal oximetry were 800 nm as isosbestic and 780 nm as oxygen sensitive.

7.2.3. Image Analysis

Images were co-registered to ensure pixels of the same pupil area were included to calculate the intensity of red-eye reflection at both the wavelengths. The registration process was same as used for retinal oximetry images described in Chapter 5.

For both the wavelengths the average intensity value of the reflected light was calculated. Then intensity ratio (R) of reflected light at 780 nm and 800 nm was subsequently calculated.

$$R = I_{780}/I_{800} \qquad (7.2)$$

Where

R = Intensity Ratio

I_{780} = Intensity of reflected light at 780 nm

I_{800} = Intensity of reflected light at 800 nm

The red-eye intensity ratio (R) depends on the blood oxygen saturation of the choroid.

7.2.4. Red-Eye Reflection with Different Angle of Gaze

The angle of gaze is an important factor to consider when using the red-eye reflections from the choroid to determine the oxygen saturation because the angle of gaze determines which part of fundus is being sampled. When the eye was gazing straight in to the objective of the camera (or the light source) the macular region of fundus was in view (see Figure 7.8 (A)). As the angle of gaze of the eye moved towards nasal side or the temporal side, the different region of the fundus comes into view (Figure 7.8).

Red-eye reflection depends on which part of the fundus it is coming from, hence on the angle of gaze. The effect of the angle of gaze on red-eye ratio was analysed by imaging different angle of gaze in two subjects. Subjects angle of gaze in one eye were changed from extreme nasal side to extreme temporal side with the use of a fixation light. Five images at each angle of gaze were acquired and analysed for red-eye ratio. The effect of angle of gaze on red-eye ratio is presented in the result section.

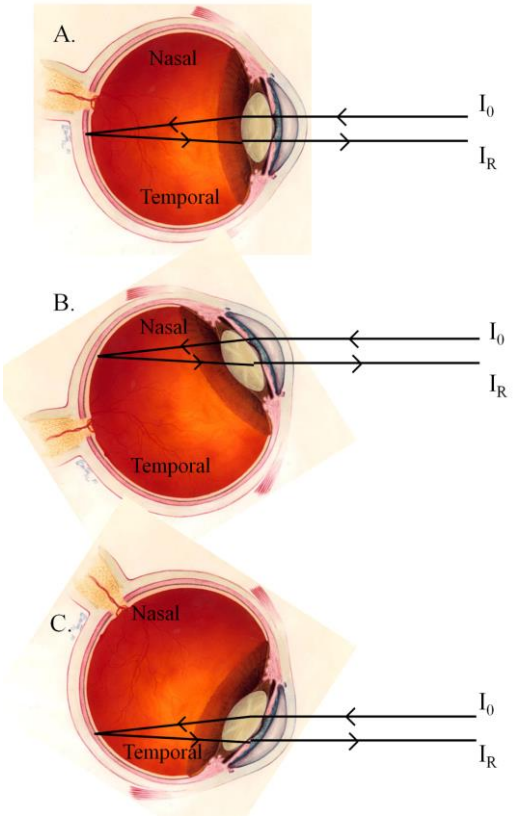

Figure 7.8: The effect of the different angle of gaze, (A) when angle of gaze is straight ahead macular region is in focus, as the gaze shifts towards nasal side (B) or temporal side (C) a different region of fundus will be in focus. I_0 is the incident light and I_R is the reflected light from the fundus.

When the eye gaze was towards the nasal side, nasal side of the fundus was sampled and when the gaze was towards the temporal side, temporal fundus was sampled. For straight gaze, the macular region of fundus was being sampled, which is relatively free of retinal blood vessels and the red-eye reflection from this area was mainly due to choroidal blood. For choroidal oximetry red-eye reflection of all the subjects were measured with straight gaze looking directly into objective of the fundus camera (light source).

7.2.5. Red-Eye Reflection with Varying Optical Power of Eye Lens

The effect of the optical power of the eye lens on red-eye reflection was also determined. A commercially available artificial eye (HEINE Ophthalmoscope Trainer, HEINE Optotechnik GmbH & Co., Germany) was used for this experiment (Figure 7.9).

Figure 7.9: A commercially available artificial eye (HEINE Ophthalmoscope Trainer)

The artificial eye had a front lens, a chamber filled with fluid, which mimicked aqueous and vitreous humour and an artificial retinal background. The background of the artificial eye was reflective and mimicked the red-eye reflection when imaged with the IRIS snapshot multispectral fundus camera. The artificial eye provided the option to change the optical power of the lens from -10 dioptre to +10 dioptre. Red-eye images were recorded for a range of -10 dioptre to +10 dioptre in step of one dioptre. The images were then analysed to calculate the red-eye ratio.

7.2.6. Red-Eye Reflection with Change in Inspired Oxygen in Healthy Human Subjects

Ten healthy subjects were recruited (age 27 ± 9 years; eight males and two females) to this study. A written informed consent was obtained from all the subjects. The subjects were briefed about the experimental procedure and were asked to refrain from consuming any alcohol or caffeinated drink on the day of the experiment. All the subjects recruited were healthy, non-smokers, without history of any respiratory disorder and were taking no medication.

On the day of study, they were once again briefed about the experimental protocol. Age, sex, weight were recorded. Tropicamide (1%, Bausch & Laumb, Chauvin Pharmaceuticals, Ltd., U.K.) was used to dilate the pupil. After about ten to fifteen minutes maximum dilation of pupil was achieved, and the subjects were ready to be imaged.

Red-eye reflection images were acquired for all the subjects under normoxia (21% inspired oxygen). Hypoxia was then induced by changing the inspired oxygen to 15% using a hypoxia

generator (as described in Chapter 6). Red-eye reflection images were acquired under hypoxic conditions. In total five sets of images were acquired- three under normoxia and two under hypoxia. The peripheral arterial oxygen saturation was monitored using fingertip pulse oximeter during both normoxia and hypoxia conditions. All images were then analysed to calculate the red-eye ratio at different inspired oxygen levels.

7.3. Results

7.3.1. Effect of Angle of Gaze on Red-Eye Reflection

The effect of the angle of gaze on red-eye reflection was analysed in two subjects. Figure 7.10 shows the effect of the angle of gaze on red-eye reflection of two subjects. As the angle of gaze is shifted from extreme temporal to extreme nasal, reflection samples of the temporal fundus, macular region, optic disc and nasal side of the fundus were obtained. The plateau region in the intensity ratio represents the optic disc reflection, which is higher in scale when compared with either the nasal or temporal regions of the fundus.

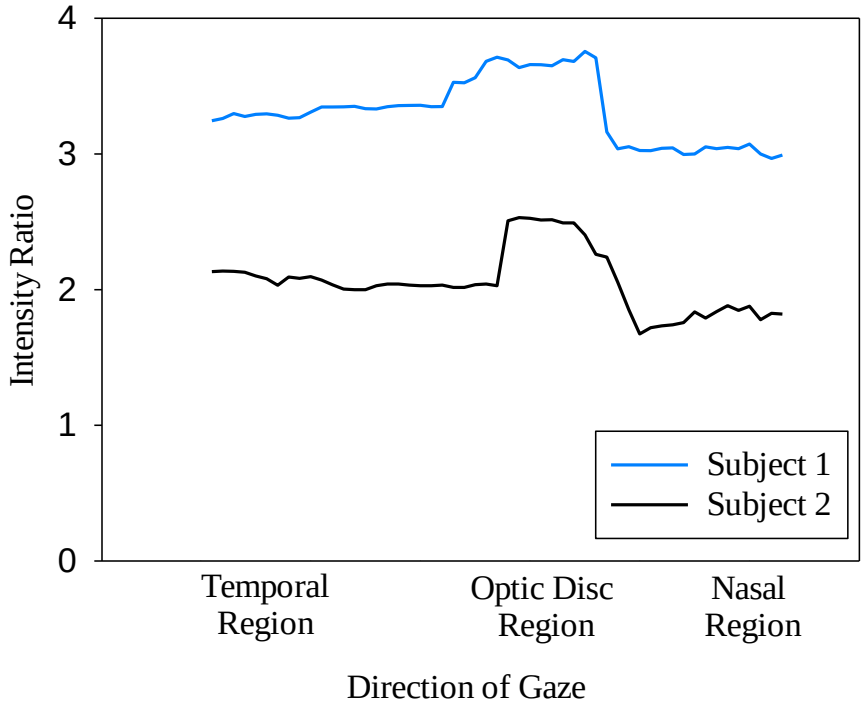

Figure 7.10: Red-eye reflection intensity ratio with the angle of gaze. The high intensity ratio plateau region corresponds to optic disc which is more reflective than the rest of the fundus.

7.3.2. Effect of Optical Power of Eye Lens on Red-Eye Reflection

To assess the effect of eye lens optical power on the intensity of the red-eye reflection a model eye was used for the range of -10 dioptre to +10 dioptre with gradual increment of 1 dioptre and the images recorded. Figure 7.11 shows the effect of varying lens power on intensity of red-eye reflection at 780 nm and 800 nm. The intensity of red-eye gradually increases from -10 D to -5 D and then the intensity gradually declines and as it goes from -5 D to +10 D for both the wavelengths.

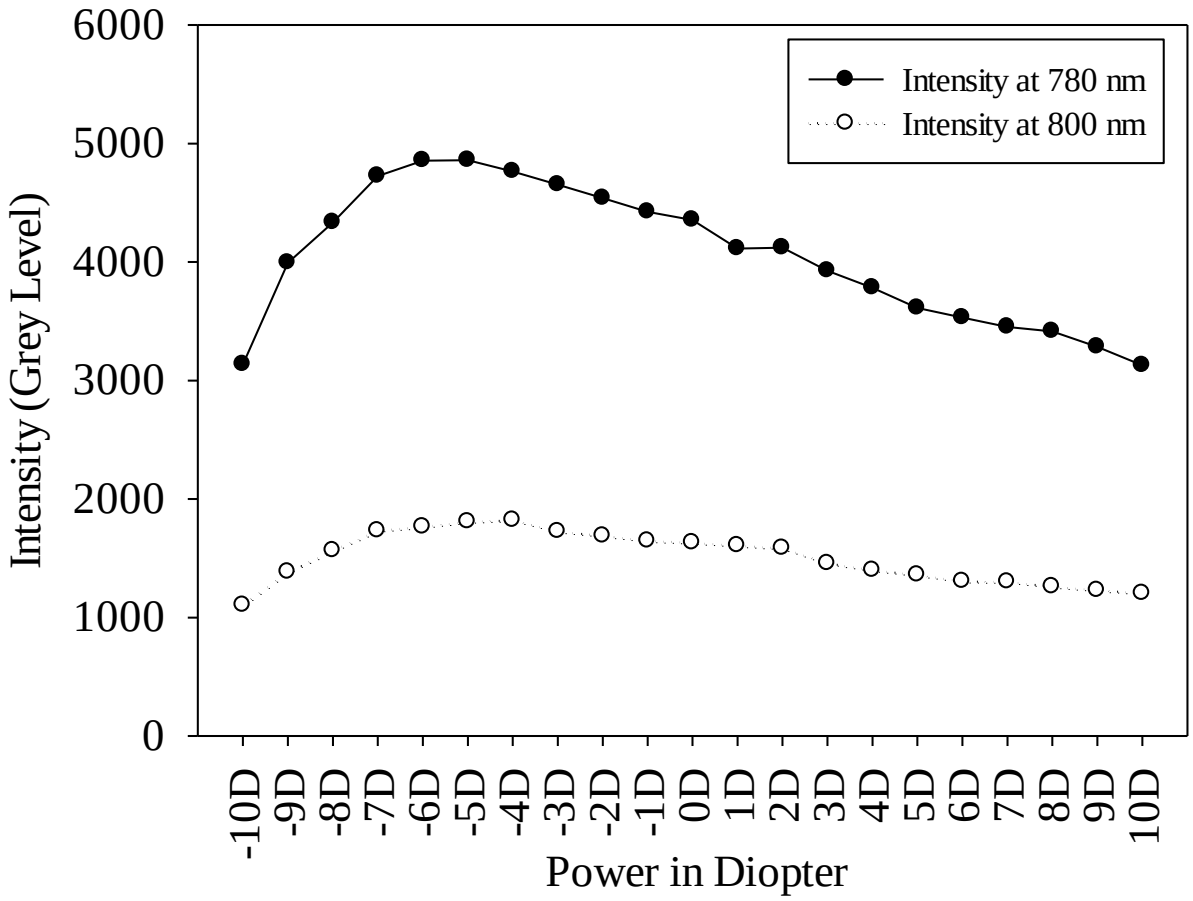

Figure 7.11: Effect of power of eye lens on red-eye reflection intensity

Figure 7.12 shows the intensity ratio of red-eye reflection at 780 nm and 800 nm for the range of -10 D to +10 D. In contrast to the effect of lens power on the intensity of reflection, the intensity ratio did not vary across the dioptre range -10 D to +10 D and remains almost constant with a change in optical power of the eye lens.

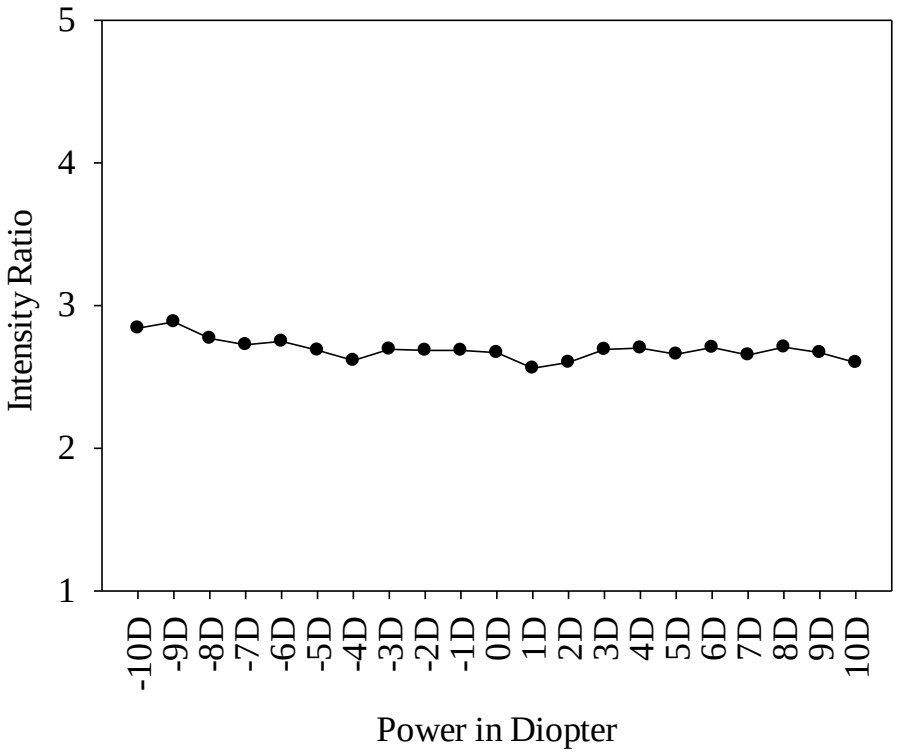

Figure 7.12: Red-eye reflection intensity ratio (780 nm / 800 nm) with change in power of the eye lens

7.3.3. Red-Eye Reflection with Change in Inspired Oxygen in Healthy Human Subjects

Figure 7.13 shows the oscillation in intensity ratio of the red-eye reflection at wavelengths 780 nm and 800 nm first with normoxia (21% FiO_2, O_2 Saturation 100%) and then hypoxia (15% FiO_2, O_2 Saturation 85%) repeated three times in ten subjects.

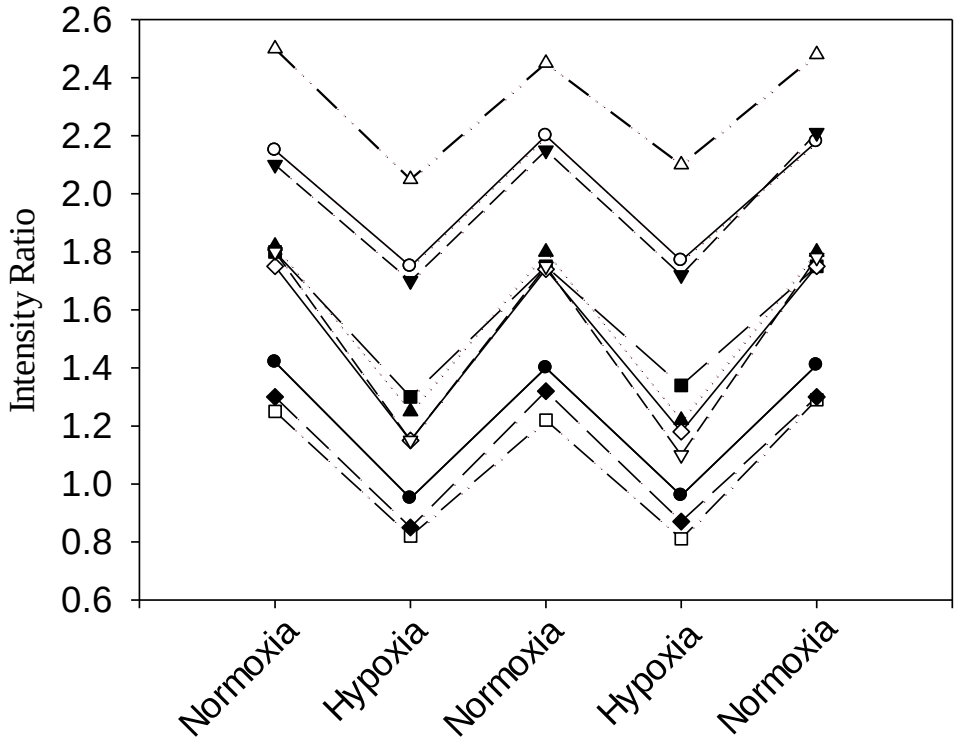

Figure 7.13: Changes in red-eye reflection intensity ratio as a function of either normoxia (21% FiO_2, O_2 Saturation 100%) or hypoxia (15% FiO_2, O_2 Saturation 85%) in ten subjects.

A reduction in red-eye reflection intensity ratio was observed during hypoxia. Paired t-test between each levels of normoxia and hypoxia intensity ratio was found to be statistically significant ($P < 0.001$).

To assess the repeatability and stability of the device, red-eye reflection was recorded in two subjects for 60 seconds at room air and the results are shown in figure 7.14.

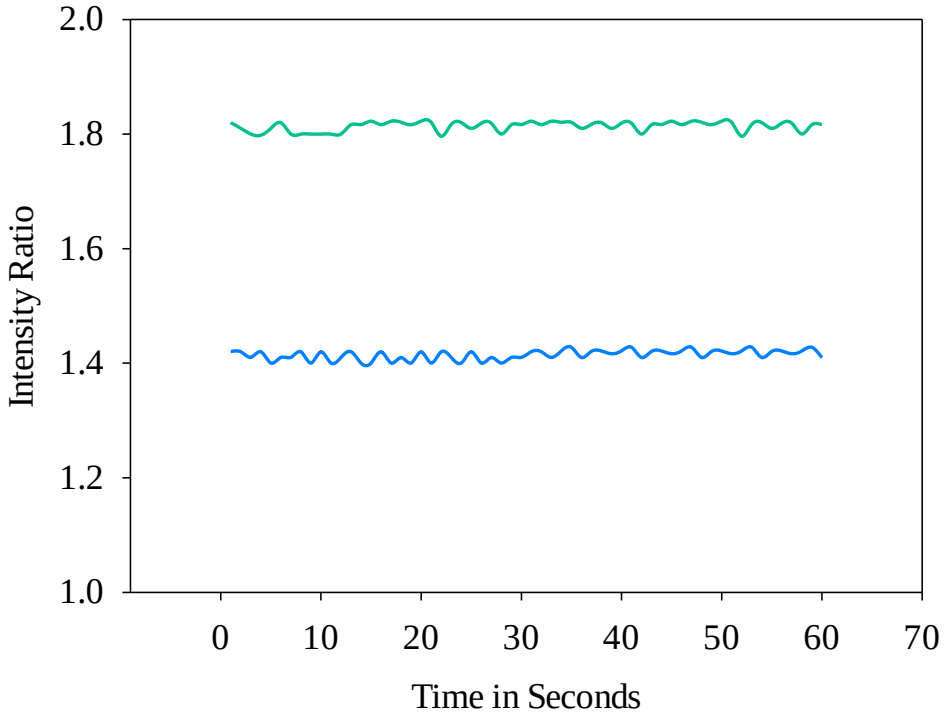

Figure 7.14: Red-eye reflection intensity ratio of two subjects at room air with respect to time.

It is clear from the figure 7.16 that the red-eye reflection intensity ratio remained stable with time (60 seconds) and the decrease in intensity that was observed during hypoxic exposure was due to a decrease in oxygen saturation of the blood.

7.4. Discussion

In this chapter, a non-invasive method to assess oxygen saturation in choroidal blood is presented. Red-eye reflection intensity ratio is sensitive to blood oxygenation and decreases with decrease in blood oxygenation, was demonstrated in human subjects.

The red-eye reflection intensity ratio was assessed in healthy human subjects. The red-eye reflection-intensity ratio decreased significantly ($P < 0.001$) when compared with normoxia and hypoxia. The red-eye reflection was recorded for normoxia (room air) and with mild hypoxia (15% inspired oxygen). At both normoxia and hypoxia arterial blood-oxygen saturation was monitored with a finger-tip pulse oximeter. Red-eye reflection was recorded alternatively for three normoxia stage and two hypoxia stage for each subject. The red-eye reflection intensity ratio decreased significantly between each stages of normoxia and

hypoxia (Figure 7.13) for all the ten subjects. Red-eye reflection intensity ratio was also recorded for 60 seconds at room air, and it was found to be stable with time (Figure 7.14).

The results presented in this chapter agrees with the results obtained by Broadfoot[159] and by Laing[160]. They both reported a decrease in the reflection intensity with decrease in blood oxygenation. The imaging and recording setup presented here is much simpler and has advantages over the methods used by Broadfoot and Laing. Both Broadfoot and Laing, their imaging setup comprised of a fundus camera to image the eye, and an elaborate electronic system with photomultipliers and photodiodes to record the intensity of the reflections from the eye. Broadfoot used a filter wheel assembly to record the intensity at different wavelengths and Laing apparatus used dual spectral beam of light and dichroic mirrors to separate reflections at each wavelengths and was then recorded onto a photodiode. The setup presented here has a fundus camera fitted with IRIS device, which enables recording of the spectral images at different wavelengths in a single snapshot onto a sCMOS detector. The use of snapshot imaging ensured that reflections at different wavelengths were captured at the same point of time and removed any variability due to difference in time of recordings. Our device recorded the spectral images and the reflection intensity was calculated from the images, any eye movement was then easily corrected by image registration process. Any faulty image frame or eye-blinks could also be easily identified and removed from the data. Whereas, in Broadfoot and Laing setup, the reflection intensity was directly recorded onto a photodiode and these corrections were not possible. The other advantage of the technique presented here is that it can image both the eyes simultaneously.

One of the potential applications of this technique can be in the detection of carotid artery stenosis. Stenosis is in turn a risk factor for stroke[205]. The current method for diagnosis of stenosis is Doppler ultrasound, which has its limitations [206, 207]. If one of the internal carotid arteries is stenosed the blood will take longer time to reach the eye it supplies as compared to the other eye supplied by stenosis free other internal carotid artery. If the stenosis is severe, then the blood takes alternate and longer route to supply the eye [208, 209]. With the technique presented here, we have shown that we can measure the desaturation pulse of deoxygenated blood coming from lungs in the choroid. The principle of measurement is to produce a transient deoxygenation of arterial blood leaving the lungs (by taking a single breath of deoxygenated air) and to measure the time delay for this deoxygenation pulse to arrive at the choroid. As we can image both the eyes simultaneously, we can detect any time difference between the eyes for the arrival of desaturation pulse.

While using red-eye reflection for oxygen saturation calculation, it is important to know which region of the fundus (and choroid underneath) is being sampled. This depends mainly on the direction of gaze as described earlier in the method section (7.2.4). The effect of direction of the gaze on red-eye reflection was also assessed (Fig 7.10). From these results we have shown that the optic disc is more reflective than rest of the fundus. To use red-eye reflections for oximetry purposes, it is very important to sample the same region of fundus for each individual and to avoid imaging the optic disc. Consequently it was decided that sampling the macula region during recording of red-eye reflection in the experiments would avoid these issues. The other reason to use macular region is due to its avascular nature, having no retinal vasculature structure provides a better view of the choroid and the reflections recorded in this region are mainly due to blood in the choroidal circulation.

We also evaluated the effect of optical power of eye lens on red-eye reflection intensity. As this technique is based on the reflection intensity, any change in intensity due to optical power of lens because of refractive error of eye will produce an error. Although the intensity of reflection changed with change in dioptre at both the wavelengths of 780 nm and 800 nm but the resultant red-eye ratio remained almost constant with a change in optical power of the eye lens. An artificial eye, with the option of changing the lens power was used for this experiment.

We successfully demonstrated in human subjects that red-eye reflection ratio is sensitive and directly proportional to changes with change in blood oxygenation and can be used to calculate choroidal oxygenation. The next step is to translate this ratio into oxygen saturation values. The first challenge towards this is variations in pigmentation of choroid and retinal pigment epithelium (RPE) amongst humans. Due to this difference in pigmentation, the red-eye reflection ratio varies between subjects. One way to characterise the fundus and choroidal pigmentation is to record iris colour and skin colour and estimate the choroidal pigmentation based on that[210]. The results described in this chapter were based on a small number of subjects (n = 10). A study based on larger subject number with different iris and skin colour is needed.

There are certain advantages of using red-eye reflection oximetry over retinal oximetry. A good quality of retinal image is crucial to perform retinal oximetry which requires proper imaging technique and training, whereas red-eye images are easy to acquire. Retinal oximetry image analysis is lengthy and complex process as compared to red-eye reflection oximetry.

The other unique advantage is that unlike retinal oximetry, red-eye reflection oximetry can be performed in both the eyes simultaneously.

Choroidal-oxygenation measurement allows direct measurement of oxygen saturation in central vasculature. It will be very useful in understanding pathophysiology of diseases like age-related macular degeneration[211, 212], diabetic retinopathy[213, 214] etc in which choroidal blood flow plays an important role.[215] Other potential application includes blood loss and internal bleeding assessment in trauma victim. Using this technique, we could also detect arrival of de-saturation signal from lungs to the blood circulation of both the eyes. This could be useful in detecting stenosis of carotid artery.

In conclusion, the technique presented in this chapter can be used to determine the reflective intensity ratio of blood in the choroidal circulation. With subsequent development this simple technique could be employed to determine the absolute value of blood oxygenation in the choroidal circulation.

Chapter 8

General Discussion and Future Work

8.1. General Discussion

This thesis investigated use of the IRIS snapshot multispectral fundus camera to non-invasively measure oxygen saturation in the retinal and choroidal blood vessels in humans. The IRIS snapshot multispectral fundus camera was validated *in vitro* (model eye) and *in vivo* (animal model) demonstrating its ability to perform retinal oximetry. After successful validation of the device and the oximetry algorithms, retinal oximetry was performed in human subjects, which led to the human hypoxia trial. The human hypoxia trial was one of the first studies to assess the effect of acute mild hypoxia on retinal oxygenation. A new method to calculate choroidal oxygenation using fundus reflection is also presented in this thesis.

The model eye experiment was conducted to determine the ability of the oximetry technique to distinguish the difference between different blood oxygen saturation. The oxygen saturation of blood samples were calculated by the oximetry technique and compared with the known values and were found to be in close agreement. The use of a model eye for validation of retinal oximetry model has been reported in many previous studies [19, 139, 140, 149, 156, 164-167]. The model eye simulates optical environment very similar to human eye and provide an informative first step validation for oximetry system and algorithms but the human eye is far more complex optical system.

In vivo validation in animal (pig) model provided the opportunity to assess the oximetry system at a broad range of blood oxygenation and compare the result to the gold standard measurement (blood gas analysis). The retinal arterial oxygen saturation measured by the oximetry system significantly correlated with the blood gas analysis values for femoral arterial oxygen saturation ($r = 0.90$, $P < 0.0001$, Spearman's rank correlation test). This is in agreement with previous studies on pigs, which have found that femoral arterial oxygen saturation correlates significantly with retinal arterial oxygen saturation [188, 216]. The pig eye provided a closer environment to human eye than the model eye to validate the oximetry system and a broader range of blood oxygenation can be tested than is possible in humans.

Retinal oximetry was then performed in human subjects to evaluate the oximetry system and algorithms for human use. Oxygen saturation measured in retinal arterioles was found to be 96.08 % ± 1.9 % and 68.04 % ± 2.1 % in retinal venules. The calculated retinal arteriovenous oxygen saturation difference was 28.04 % ± 1.8 %. A significant correlation was found between pulse oximeter oxygen saturation values and measured retinal arterioles oxygen saturation. The reported oxygen saturation values for retinal arterioles and venules were within the normal physiological range and in agreement to the values reported by other groups [18, 137, 151, 154, 157]. Previous retinal oximetry studies have reported arterial oxygen saturation in the range of 92 % to 98 % and venular saturation oxygen saturation in the range of 52 % to 70 % [18, 151, 153, 154, 157, 217]. Few studies [18, 155, 218] have also reported arterial oxygen saturation above 100 %, which is physiologically not possible. Retinal oxygen saturation calculated from the measured optical density ratio (ODR) by two-wavelength oximetry depends on the calibration and is not an absolute measurement. Different studies apply different calibration, which is the main reason for a wide range of venous oxygen saturation values reported in the literature.

After successfully testing the oximetry system on humans, human hypoxia trial was conducted. The main purpose of the trial was to study the effect of acute mild hypoxia (lasting for 10 minutes) on retinal oxygenation and autoregulation. This was one of the first studies to assess effect of acute mild hypoxia on retinal oxygenation. The main findings of this study was that a reduction in inspired oxygen resulted in the reduction of retinal arterial and venular oxygen saturation but the arteriovenous oxygen saturation difference remained unchanged during hypoxia when compared with normoxia. We also observed increase in arterial and venular vessel diameter during hypoxia. Our results are in agreement with previous studies, which examined effect of severe and chronic hypoxia on retinal oxygenation and reported increased vessel diameter and retinal blood flow [28-34]. Frayser et al. [34] reported an increase in the retinal arterial and venous diameter by 18% and 21% respectively at 10% inspired oxygen within 2 hours of exposure. We observed an increment in retinal arterial and venular diameter by 4% and 3% respectively. The lower degree of vasodilation reported in our study as compared to Frayser et al. is due to lower level of hypoxia (15% as compared to 10% inspired oxygen) and smaller duration of hypoxic exposure (10 minutes as compared to 2 hours). In a recent study by Traustason et al. [219] the effect of chronic systemic hypoxemia on retinal oxygenation was assessed in patients with Eisenmenger syndrome. They reported a lower arterial and venular oxygen saturation in the

patients with Eisenmenger syndrome as compared with healthy individuals but the arteriovenous oxygen saturation difference was comparable between both the groups. Their result supports our finding as we also observed unchanged arteriovenous oxygen saturation difference between hypoxic and normoxic conditions. Unchanged arteriovenous oxygen saturation difference along with increase in retinal vessel diameter suggests that the effect of hypoxia was compensated by autoregulation. Autoregulatory process exists in retinal vessels but choroidal circulation has only limited degree of autoregulatory mechanism [21-23]. Retinal circulation is more sensitive to changes in oxygen saturation whereas choroid has reported to be insensitive to changes in oxygen saturation [26, 27]. The results suggest that retinal circulation compensated for reduced contribution from choroid, by autoregulation during hypoxia.

We also assessed the reproducibility of the oximetry system in repeated measurements of the same vessel. The standard deviation for repeated measurement was 1% for both arterioles and venules, which is comparable to other available oximetry systems [18, 153]. Hardarson et al. [151] reported a standard deviation of 3.7% and 5.3% for arterioles and venules respectively for 5 repeated measurements. In later studies, after improving their device, the same group reported a standard deviation of 1% and 1.4% for arterioles and venules respectively [153]. A standard deviation of 2.5% and 3.2% for repeated measurements in arterioles and venules respectively has been reported by Hammer et al. for their oximetry system [18].

There are few limitations associated with the oximetry method used in this thesis. Limitations associated with each experiment are discussed in detail at end of each chapter. The main limitation is the use of two-wavelength oximetry method. As this is a calibration based method, absolute oximetry cannot be achieved. The oximetry system, used in this thesis has shown to produce repeatable results. In this thesis, the results of most of the retinal oximetry studies are based on changes in measured blood oxygenation and these conclusions are unaffected by a scaling or offset of oximetry with respect to absolute values.

In this thesis, we also present a non-invasive spectral imaging technique that utilises red-eye reflection to determine blood oxygen saturation in choroidal circulation. This technique is based on and an improvement of the work by Broadfoot [159] and Laing [160]. We successfully demonstrated that our system can detect a decrease in red-eye reflection with reduction in blood oxygen saturation in human subjects. The results agrees with the result previously reported by Broadfoot [159] and Laing [160]. This initial work provided the proof

of concept that this technique, with subsequent development may provide a new way to measure and assess oxygen saturation in choroid. Choroidal oxygenation measurement allows direct measurement of oxygen saturation in central vasculature and may provide useful information about pathophysiology of diseases like age-related macular degeneration [211, 212], diabetic retinopathy[213, 214] in which choroidal blood flow plays an important role [215]. This technique also has some unique advantages over retinal oximetry. It is simple to implement and does not require any imaging training, and the data analysis is less tedious as compared to retinal oximetry. The other advantage is that using red-eye reflection choroidal oximetry; both eyes can be imaged and assessed simultaneously whereas retinal oximetry can be performed one eye at a time.

8.2. Retinal Oximetry: Future Work

This thesis demonstrated that IRIS snapshot multispectral fundus camera can be used for retinal oximetry and is reliable and sensitive to small changes in oxygen saturation. The retinal oximetry used in this thesis is based on calibration based two-wavelength oximetry method. The device used in this thesis is capable of taking images at eight wavelengths in one snapshot. Algorithms exploiting optical absorption measurements in all eight spectral bands are under development and offer the future prospect of robust, calibration-free oximetry. The work for developing calibration free multi-wavelength oximetry already has been started by Mr. Javier Fernandez (PhD Student, Andy Harvey's Group). Some of the already planned future works leading from this study are described in the following sections.

8.2.1. Treatment of Advanced Glaucoma Study

This project is in collaboration with Prof. Andy McNaught, Cheltenham General Hospital and the author. Retinal oximetry will be performed using the retinal oximetry device developed and described in this thesis to monitor the progression of glaucoma. Oximetry study will also be performed before and after glaucoma treatment to monitor the changes/improvements due to the intervention. The main aim of this study is to assess the usefulness of retinal oximetry in a clinical setting for disease diagnosis and prognosis.

8.2.2. Multicentre Central Retinal Vein Occlusion (CRVO) Oximetry Study

The general purpose of the study is to gain more insight into how retinal oxygenation is related to the severity of CRVO and to determine if retinal oximetry can be useful in the clinical management of the disease. More specifically, the research questions are:

1. Is retinal oximetry related to severity as judged by clinical signs at first visit?
2. Does retinal oximetry at first visit predict the visual outcome and neovascularisation?

This study is in collaboration with many different oximetry groups working across the globe. Although different oximetry devices will be used to collect the data, the analysis protocol will be uniform for easy comparison. Data from the different centre will be pooled together.

8.3. Red-Eye Reflection (Choroidal) Oximetry: Future Work

The work described in this thesis demonstrated that red-eye reflection can be used to measure blood oxygen saturation in choroidal circulation. A validation study in humans established that red-eye reflection ratio is sensitive to change in oxygen saturation and changes with change in blood oxygenation. The future work will be to translate this ratio into oxygen saturation values. As described in earlier chapter, this ratio is affected by difference in choroidal and fundus pigmentation; a multiethnic subject trial will be the logical next step. One of the planned studies for application of this technique is detailed below.

8.3.1. Measurement of propagation delay for transient deoxygenation of the blood using Red-Eye Reflection (Choroidal) Oximetry

The purpose of the research is to conduct a proof-of-concept study into the feasibility of using red-eye reflection (choroidal) oximetry to independently measure the propagation delay for a transient deoxygenation of blood to travel from the lungs to each eye. It is expected that the propagation delay increases with stenosis of the carotid arteries, and furthermore that, in general, asymmetry in the stenosis between left and right carotid arteries that often/normally accompanies stenosis, will be manifest by a differential delay of deoxygenated blood arriving at each eye. This may promises a more sensitive detection of stenosis.

This study will be conducted in collaboration with Institute of Cardiovascular and Medical Sciences, University of Glasgow. The technique involves transient deoxygenation of air in the lungs, and hence of the blood leaving the lungs and the recording of the delay in the deoxygenated blood arriving in the eyes. The arrival of the deoxygenation pulse is recorded using, the red-eye reflection simultaneously for each pupil. Deoxygenation of blood is achieved by inhaling a single breath of medical-grade nitrogen.

References

1. in *Neuroscience*, A.G. Purves D, Fitzpatrick D, et al., Editor. 2001, Sinauer Associates: Sunderland (MA).
2. *Webvision: The Organization of the Retina and Visual System [Internet]*. 1995: Salt Lake City (UT).
3. Hogan, M.J. and J. JA Weddell, *Histology of the human eye: an atlas and textbook.* 1971.
4. Spaide, R.F., H. Koizumi, and M.C. Pozzoni, *Enhanced depth imaging spectral-domain optical coherence tomography.* Am J Ophthalmol, 2008. **146**(4): p. 496-500.
5. Brown, J.S., et al., *In vivo human choroidal thickness measurements: evidence for diurnal fluctuations.* Investigative ophthalmology & visual science, 2009. **50**(1): p. 5-12.
6. Nickla, D.L., C.F. Wildsoet, and D. Troilo, *Diurnal rhythms in intraocular pressure, axial length, and choroidal thickness in a primate model of eye growth, the common marmoset.* Invest ophthalmol & vis sci, 2002. **43**(8): p. 2519-2528.
7. Troilo, D., D.L. Nickla, and C.F. Wildsoet, *Choroidal thickness changes during altered eye growth and refractive state in a primate.* Investigative ophthalmology & visual science, 2000. **41**(6): p. 1249-1258.
8. Fitzgerald, M.E., C.F. Wildsoet, and A. Reiner, *Temporal relationship of choroidal blood flow and thickness changes during recovery from form deprivation myopia in chicks.* Experimental eye research, 2002. **74(**5): p. 561-570.
9. Remington, L.A., *Clinical anatomy of the visual system*. 2011: Elsevier Health Sciences.
10. Nickla, D.L. and J. Wallman, *The multifunctional choroid.* Progress in Retinal and Eye Research, 2010. **29**(2): p. 144-168.
11. Wise, G.N., C.T. Dollery, and P. Henkind, *The retinal circulation.* 1971, New York: Harper & Row.
12. Takayama, S., et al., *Evaluation of the effects of acupuncture on blood flow in humans with ultrasound color Doppler imaging.* Evid Based Complement Alternat Med, 2012. **2012**: p. 513638.
13. Kur, J., E.A. Newman, and T. Chan-Ling, *Cellular and physiological mechanisms underlying blood flow regulation in the retina and choroid in health and disease.* Progress in Retinal and Eye Research, 2012. **31**(5): p. 377-406.

14. Anand-Apte, B. and J. Hollyfield, *Developmental anatomy of the retinal and choroidal vasculature.* Encyclopedia of the Eye, 2010. **48**(8-9): p. 9-15.
15. Okada, S. and Y. Ohta, *Microvascular pattern of the retina in the Japanese monkey (Macaca fuscata fuscata).* Scanning microscopy, 1994. **8**(2): p. 415-427.
16. Engerman, R.L., *Development of the macular circulation.* Invest Ophthalmol & Vis Sci, 1976. **15**(10): p. 835-40.
17. Ruskell, G.L., *Peripapillary venous drainage from the choroid: a variable feature in human eyes.* Br J Ophthalmol, 1997. **81**(1): p. 76-9.
18. Hammer, M., et al., *Retinal vessel oximetry-calibration, compensation for vessel diameter and fundus pigmentation, and reproducibility.* Journal of Biomedical Optics, 2008. **13**(5): p. 054015-054015-7.
19. Schweitzer, D., et al., *In vivo measurement of the oxygen saturation of retinal vessels in healthy volunteers.* IEEE Trans Biomed Eng, 1999. **46**(12): p. 1454-65.
20. Alm, A. and A. Bill, *Blood Flow and Oxygen Extraction in the Cat Uvea at Normal and High Intraocular Pressures.* Acta Physiologica Scandinavica, 1970. **80**(1): p. 19-28.
21. Bill, A. and G.O. Sperber, *Control of retinal and choroidal blood flow.* Eye (Lond), 1990. **4 (Pt 2)**: p. 319-25.
22. Kiel, J.W. and A.P. Shepherd, *Autoregulation of choroidal blood flow in the rabbit.* Investigative Ophthalmology & Visual Science, 1992. **33**(8): p. 2399-410.
23. Schmidl, D., G. Garhofer, and L. Schmetterer, *The complex interaction between ocular perfusion pressure and ocular blood flow – Relevance for glaucoma.* Experimental Eye Research, 2011. **93**(2): p. 141-155.
24. Guyton, A.C., C.E. Jones, and T.G. Coleman, *Cardiac output and its regulation*. 1973: Saunders Philadelphia.
25. Pournaras, C.J., et al., *Regulation of retinal blood flow in health and disease.* Progress in Retinal and Eye Research, 2008. **27**(3): p. 284-330.
26. Schmetterer, L., et al., *The Effect of Inhalation of Different Mixtures of O2and CO2on Ocular Fundus Pulsations.* Experimental Eye Research, 1996. **63**(4): p. 351-355.
27. Geiser, M.H., et al., *Response of choroidal blood flow in the foveal region to hyperoxia and hyperoxia-hypercapnia.* Current eye research, 2000. **21**(2): p. 669-676.
28. Eperon, G., M. Johnson, and N.J. David, *The effect of arterial PO2 on relative retinal blood flow in monkeys.* Investigative Ophthalmology & Visual Science, 1975. **14**(5): p. 342-52.

29. Pournaras, C., M. Tsacopoulos, and P. Chapuis, *Studies on the role of prostaglandins in the regulation of retinal blood flow.* Experimental Eye Research, 1978. **26**(6): p. 687-697.
30. Papst, N., E. Demant, and G. Niemeyer, *Changes in pO_2 induce retinal autoregulation in vitro.* Graefes Arch Clin Exp Ophthalmol, 1982. **219**(1): p. 6-10.
31. Tachibana, H., F. Gotoh, and Y. Ishikawa, *Retinal vascular autoregulation in normal subjects.* Stroke, 1982. **13**(2): p. 149-55.
32. Bosch, M.M., et al., *New insights into ocular blood flow at very high altitudes.* Journal of Applied Physiology, 2009. **106**(2): p. 454-460.
33. Frayser, R., G.W. Gray, and C.S. Houston, *Control of the retinal circulation at altitude.* J Appl Physiol, 1974. **37**(3): p. 302-4.
34. Frayser, R., et al., *The response of the retinal circulation to altitude.* Archives of Internal Medicine, 1971. **127**(4): p. 708-711.
35. Kety, S.S. and C.F. Schmidt, *The effects of altered arterial tensions of carbon dioxide and oxygen on cerebral blood flow and cerebral oxygen consumption of normal young men 1.* The Journal of Clinical Investigation, 1948. **27**(4): p. 484-492.
36. Kogure, K., et al., *Mechanisms of cerebral vasodilatation in hypoxia.* Journal of Applied Physiology, 1970. **29**(2): p. 223-229.
37. Riva, C.E., S.H. Sinclair, and J.E. Grunwald, *Autoregulation of retinal circulation in response to decrease of perfusion pressure.* Investigative Ophthalmology & Visual Science, 1981. **21**(1): p. 34-8.
38. Grunwald, J.E., C.E. Riva, and D.M. Kozart, *Retinal circulation during a spontaneous rise of intraocular pressure.* Br J Ophthalmol, 1988. **72**(10): p. 754-8.
39. Dumskyj, M.J., et al., *Autoregulation in the human retinal circulation: assessment using isometric exercise, laser Doppler velocimetry, and computer-assisted image analysis.* Microvasc Res, 1996. **51**(3): p. 378-92.
40. Feke, G.T., et al., *Response of human retinal blood flow to light and dark.* Investigative Ophthalmology & Visual Science, 1983. **24**(1): p. 136-41.
41. Riva, C.E., J.E. Grunwald, and B.L. Petrig, *Reactivity of the human retinal circulation to darkness: a laser Doppler velocimetry study.* Invest Ophthalmol Vis Sci, 1983. **24**(6): p. 737-40.
42. Polak, K., L. Schmetterer, and C.E. Riva, *Influence of flicker frequency on flicker-induced changes of retinal vessel diameter.* Invest Ophthalmol Vis Sci, 2002. **43**(8): p. 2721-6.

43. Riva, C.E., B. Falsini, and E. Logean, *Flicker-evoked responses of human optic nerve head blood flow: luminance versus chromatic modulation.* Invest Ophthalmol Vis Sci, 2001. **42**(3): p. 756-62.
44. Falsini, B., C.E. Riva, and E. Logean, *Flicker-evoked changes in human optic nerve blood flow: relationship with retinal neural activity.* Invest Ophthalmol Vis Sci, 2002. **43**(7): p. 2309-16.
45. Longo, A., M. Geiser, and C.E. Riva, *Subfoveal choroidal blood flow in response to light-dark exposure.* Invest Ophthalmol Vis Sci, 2000. **41**(9): p. 2678-83.
46. Fuchsjager-Mayrl, G., et al., *Unilateral light-dark transitions affect choroidal blood flow in both eyes.* Vision Res, 2001. **41**(22): p. 2919-24.
47. Garhofer, G., et al., *Influence of diffuse luminance flicker on choroidal and optic nerve head blood flow.* Curr Eye Res, 2002. **24**(2): p. 109-13.
48. Klein, R., et al., *The Wisconsin Epidemiologic Study of Diabetic Retinopathy: IV. Diabetic Macular Edema.* Ophthalmology, 1984. **91**(12): p. 1464-1474.
49. Arun, C.S., et al., *Effectiveness of screening in preventing blindness due to diabetic retinopathy.* Diabet Med, 2003. **20**(3): p. 186-90.
50. Scanlon, P.H., *The English national screening programme for sight-threatening diabetic retinopathy.* Journal of Medical Screening, 2008. **15**(1): p. 1-4.
51. Roy, S., et al., *Vascular basement membrane thickening in diabetic retinopathy.* Curr Eye Res, 2010. **35**(12): p. 1045-56.
52. Cogan, D.G. and T. Kuwabara, *CAPILLARY SHUNTS IN THE PATHOGENESIS OF DIABETIC RETINOPATHY.* Diabetes, 1963. **12**: p. 293-300.
53. Garner, A., *Histopathology of diabetic retinopathy in man.* Eye, 1993. **7**(2): p. 250-253.
54. Imesch, P.D., C.D. Bindley, and I.H. Wallow, *Clinicopathologic correlation of intraretinal microvascular abnormalities.* Retina, 1997. **17**(4): p. 321-9.
55. Cai, J. and M. Boulton, *The pathogenesis of diabetic retinopathy: old concepts and new questions.* Eye, 2002. **16**(3): p. 242-260.
56. Alder, V.A., et al., *Diabetic retinopathy: early functional changes.* Clin Exp Pharmacol Physiol, 1997. **24**(9-10): p. 785-8.
57. Sone, H., et al., *Ocular vascular endothelial growth factor levels in diabetic rats are elevated before observable retinal proliferative changes.* Diabetologia, 1997. **40**(6): p. 726-730.

58. Smith, G., et al., *Immunolocalisation of the VEGF receptors FLT-1, KDR, and FLT-4 in diabetic retinopathy.* Br J Ophthalmol, 1999. **83**(4): p. 486-94.
59. Williams, B., *Vascular permeability/vascular endothelial growth factors: a potential role in the pathogenesis and treatment of vascular diseases.* Vasc Med, 1996. **1**(4): p. 251-8.
60. Aiello, L.P., et al., *Vascular endothelial growth factor in ocular fluid of patients with diabetic retinopathy and other retinal disorders.* New England Journal of Medicine, 1994. **331**(22): p. 1480-1487.
61. Ferrara, N., *Role of vascular endothelial growth factor in the regulation of angiogenesis.* Kidney Int, 1999. **56**(3): p. 794-814.
62. Linsenmeier, R.A., et al., *Retinal hypoxia in long-term diabetic cats.* Invest Ophthalmol Vis Sci, 1998. **39**(9): p. 1647-57.
63. Wangsa-Wirawan ND, L.R.A., *Retinal oxygen: Fundamental and clinical aspects.* Archives of Ophthalmology, 2003. **121**(4): p. 547-557.
64. Quigley, H.A., *Glaucoma.* Lancet, 2011. **377**(9774): p. 1367-77.
65. Flammer, J., et al., *The impact of ocular blood flow in glaucoma.* Progress in Retinal and Eye Research, 2002. **21**(4): p. 359-393.
66. Sigal, I.A. and C.R. Ethier, *Biomechanics of the optic nerve head.* Exp Eye Res, 2009. **88**(4): p. 799-807.
67. Glucksberg, M.R. and R. Dunn, *Direct Measurement of Retinal Microvascular Pressures in the Live, Anesthetized Cat.* Microvascular Research, 1993. **45**(2): p. 158-165.
68. Leske, M.C., *Ocular perfusion pressure and glaucoma: clinical trial and epidemiologic findings.* Current Opinion in Ophthalmology, 2009. **20**(2): p. 73-78.
69. Tezel, G. and M.B. Wax, *Hypoxia-inducible factor 1alpha in the glaucomatous retina and optic nerve head.* Arch Ophthalmol, 2004. **122**(9): p. 1348-56.
70. Quigley, H.A., et al., *The prevalence of glaucoma in a population-based study of hispanic subjects: Proyecto ver.* Archives of Ophthalmology, 2001. **119**(12): p. 1819-1826.
71. Leske, M.C., et al., *Risk factors for incident open-angle glaucoma: the Barbados Eye Studies.* Ophthalmology, 2008. **115**(1): p. 85-93.
72. *Natural history and clinical management of central retinal vein occlusion. The Central Vein Occlusion Study Group.* Arch Ophthalmol, 1997. **115**(4): p. 486-91.

73. *Risk factors for branch retinal vein occlusion. The Eye Disease Case-control Study Group.* Am J Ophthalmol, 1993. **116**(3): p. 286-96.
74. Hayreh, S., W. March, and C.D. Phelps, *Ocular hypotony following retinal vein occlusion.* Archives of Ophthalmology, 1978. **96**(5): p. 827-833.
75. Williamson, T.H. and G.M. Baxter, *Central retinal vein occlusion, an investigation by color Doppler imaging. Blood velocity characteristics and prediction of iris neovascularization.* Ophthalmology, 1994. **101**(8): p. 1362-72.
76. Williamson, T., et al., *Measurement of PO2 during vitrectomy for central retinal vein occlusion, a pilot study.* Graefe's Archive for Clinical and Experimental Ophthalmology, 2009. **247**(8): p. 1019-1023.
77. Prisco, D. and R. Marcucci, *Retinal vein thrombosis: risk factors, pathogenesis and therapeutic approach.* Pathophysiology of Haemostasis and Thrombosis, 2002. **32**(5-6): p. 308-311.
78. Bhagat, N., et al., *Central retinal vein occlusion: review of management.* European journal of ophthalmology, 1999. **9**(3): p. 165-180.
79. Cugati, S., et al., *Treatment options for central retinal artery occlusion.* Curr Treat Options Neurol, 2013. **15**(1): p. 63-77.
80. Hayreh, S.S., *Acute retinal arterial occlusive disorders.* Progress in Retinal and Eye Research, 2011. **30**(5): p. 359-394.
81. Mangat, H.S., *Retinal artery occlusion.* Surv Ophthalmol, 1995. **40**(2): p. 145-56.
82. Sharma, S., G.C. Brown, and A.F. Cruess, *Accuracy of visible retinal emboli for the detection of cardioembolic lesions requiring anticoagulation or cardiac surgery.* British journal of ophthalmology, 1998. **82**(6): p. 655-658.
83. Brown, G.C. and L.E. Magargal, *Central retinal artery obstruction and visual acuity.* Ophthalmology, 1982. **89**(1): p. 14-9.
84. Hayreh, S.S. and M.B. Zimmerman, *Central Retinal Artery Occlusion: Visual Outcome.* American Journal of Ophthalmology, 2005. **140**(3): p. 376.e1-376.e.
85. Hayreh, S.S., et al., *Central retinal artery occlusion.: Retinal survival time.* Experimental Eye Research, 2004. **78**(3): p. 723-736.
86. Flick, C.S., *Centenary of Babbage's ophthalmoscope.* Optician, 1947. **113**(2925): p. 246.
87. Keeler, C.R., *150 years since Babbage's ophthalmoscope.* Arch Ophthalmol, 1997. **115**(11): p. 1456-7.

88. Helmholtz, v.H., *Beschreibung eines Augens-Spiegels zur Untersuchung der Netzhaut im lebenden Auge.* Foerstner Berlin, 1851.
89. Gerloff, O., *Über die Photographie des Augenhintergrundes.* Klin Monbl Augenheilkd, 1891. **29:397**.
90. Dimmer, F., *Atlas photographischer Bilder des Menschlichen Augenhintergrundes.* Leipzig, Germany: F Deuticke, 1927.
91. Keeler, C., *THe ophthalmoscope in the lifetime of hermann von helmholtz.* Archives of Ophthalmology, 2002. **120**(2): p. 194-201.
92. Abramoff, M.D., M.K. Garvin, and M. Sonka, *Retinal Imaging and Image Analysis.* Biomedical Engineering, IEEE Reviews in, 2010. **3**: p. 169-208.
93. Blair, N.P., *Ocular oxygen consumption during vitreoperfusion in the cat.* Transactions of the American Ophthalmological Society, 2000. **98**: p. 305.
94. Cringle, S.J., et al., *Intraretinal oxygen consumption in the rat in vivo.* Investigative ophthalmology & visual science, 2002. **43**(6): p. 1922-1927.
95. Robinson, F., et al., *Retinal blood flow autoregulation in response to an acute increase in blood pressure.* Investigative Ophthalmology & Visual Science, 1986. **27**(5): p. 722-6.
96. Arjamaa, O. and M. Nikinmaa, *Oxygen-dependent diseases in the retina: Role of hypoxia-inducible factors.* Experimental Eye Research, 2006. **83**(3): p. 473-483.
97. Vandewalle, E., et al., *Oximetry in glaucoma: correlation of metabolic change with structural and functional damage.* Acta Ophthalmol, 2013.
98. Stefánsson, E., M.L. Wolbarsht, and M.B. Landers Iii, *In vivo O2 consumption in rhesus monkeys in light and dark.* Experimental Eye Research, 1983. **37**(3): p. 251-256.
99. Hardarson, S.H., et al., *Oxygen Saturation in Human Retinal Vessels Is Higher in Dark Than in Light.* Investigative Ophthalmology & Visual Science, 2009. **50**(5): p. 2308-2311.
100. Linsenmeier, R.A., *Effects of light and darkness on oxygen distribution and consumption in the cat retina.* The Journal of general physiology, 1986. **88**(4): p. 521-542.
101. Birol, G., et al., *Oxygen distribution and consumption in the macaque retina.* American Journal of Physiology-Heart and Circulatory Physiology, 2007. **293**(3): p. H1696-H1704.

102. Falsini, B., C.E. Riva, and E. Logean, *Flicker-Evoked Changes in Human Optic Nerve Blood Flow: Relationship with Retinal Neural Activity.* Investigative Ophthalmology & Visual Science, 2002. **43**(7): p. 2309-2316.
103. Bill, A. and G.O. Sperber, *Aspects of oxygen and glucose consumption in the retina: effects of high intraocular pressure and light.* Graefes Arch Clin Exp Ophthalmol, 1990. **228**(2): p. 124-7.
104. Falsini, B., C.E. Riva, and E. Logean, *Relationship of blood flow changes of the human optic nerve with neural retinal activity: a new approach to the study of neuro-ophthalmic disorders.* Klin Monbl Augenheilkd, 2002. **219**(4): p. 296-8.
105. Hammer, M., et al., *Retinal Venous Oxygen Saturation Increases by Flicker Light Stimulation.* Investigative Ophthalmology & Visual Science, 2011. **52**(1): p. 274-277.
106. Hickam, J.B., H.O. Sieker, and R. Frayser, *Studies of retinal circulation and A-V oxygen difference in man.* Am Clin Clim atol Assoc., 1959. **71**(34): p. 44.
107. Schweitzer, D., et al., *[Change of retinal oxygen saturation in healthy subjects and in early stages of diabetic retinopathy during breathing of 100% oxygen]*. Klin Monbl Augenheilkd, 2007. **224**(5): p. 402-10.
108. Khoobehi, B., et al., *Retinal arterial and venous oxygen saturation is altered in diabetic patients with and without retinopathy.* Investigative Ophthalmology & Visual Science, 2013.
109. Hammer, M., et al., *Diabetic patients with retinopathy show increased retinal venous oxygen saturation.* Graefe's Archive for Clinical and Experimental Ophthalmology, 2009. **247**(8): p. 1025-1030.
110. Hardarson, S.H. and E. Stefánsson, *Retinal oxygen saturation is altered in diabetic retinopathy.* Br J of Ophthalmol, 2011.
111. Tiedeman, J.S., et al., *Retinal oxygen consumption during hyperglycemia in patients with diabetes without retinopathy.* Ophthalmology, 1998. **105**(1): p. 31-36.
112. Harris, A., et al., *Hyperoxia improves contrast sensitivity in early diabetic retinopathy.* Br J Ophthalmol, 1996. **80**(3): p. 209-13.
113. Dean, F.M., G.B. Arden, and A. Dornhorst, *Partial reversal of protan and tritan colour defects with inhaled oxygen in insulin dependent diabetic subjects.* Br J Ophthalmol, 1997. **81**(1): p. 27-30.
114. Kurtenbach, A., et al., *Hyperoxia, hyperglycemia, and photoreceptor sensitivity in normal and diabetic subjects.* Visual neuroscience, 2006. **23**(3-4): p. 651-661.

115. Arden, G.B., J.E. Wolf, and Y. Tsang, *Does dark adaptation exacerbate diabetic retinopathy?: Evidence and a linking hypothesis.* Vision Research, 1998. **38**(11): p. 1723-1729.
116. Arden, G.B., et al., *A preliminary trial to determine whether prevention of dark adaptation affects the course of early diabetic retinopathy.* Eye, 2010. **24**(7): p. 1149-1155.
117. Mandecka, A., et al., *Influence of Flickering Light on the Retinal Vessels in Diabetic Patients.* Diabetes Care, 2007. **30**(12): p. 3048-3052.
118. Nguyen, T.T., et al., *Flicker Light–Induced Retinal Vasodilation in Diabetes and Diabetic Retinopathy.* Diabetes Care, 2009. **32**(11): p. 2075-2080.
119. Garhöfer, G., et al., *Reduced response of retinal vessel diameters to flicker stimulation in patients with diabetes.* British Journal of Ophthalmology, 2004. **88**(7): p. 887-891.
120. Hammer, M., et al., *Retinal Vessel Oxygen Saturation under Flicker Light Stimulation in Patients with Nonproliferative Diabetic Retinopathy.* Investigative Ophthalmology & Visual Science, 2012. **53**(7): p. 4063-4068.
121. Poulaki, V., *Hypoxia in the Pathogenesis of Retinal Disease*, in *Retinal Vascular Disease*, A. Joussen, et al., Editors. 2007, Springer Berlin Heidelberg. p. 121-138.
122. Bojić, L., et al., *The effect of hyperbaric oxygen breathing on the visual field in glaucoma.* Acta Ophthalmologica, 1993. **71**(3): p. 315-319.
123. Olafsdottir, O.B., et al., *Retinal Oximetry in Primary Open-Angle Glaucoma.* Investigative Ophthalmology & Visual Science, 2011. **52**(9): p. 6409-6413.
124. Vandewalle, E., et al., *Oximetry in glaucoma: correlation of metabolic change with structural and functional damage.* Acta Ophthalmologica, 2014. **92**(2): p. 105-110.
125. Olafsdottir, O.B., et al., *Retinal oxygen metabolism in healthy subjects and glaucoma patients.* British Journal of Ophthalmology, 2014. **98**(3): p. 329-333.
126. Pournaras, C.J., et al., *Scatter photocoagulation restores tissue hypoxia in experimental vasoproliferative microangiopathy in miniature pigs.* Ophthalmology, 1990. **97**(10): p. 1329-1333.
127. Hardarson, S.H. and E. Stefansson, *Oxygen saturation in central retinal vein occlusion.* Am J Ophthalmol, 2010. **150**(6): p. 871-5.
128. Hardarson, S.H., et al., *Retinal oximetry in central retinal artery occlusion.* Acta Ophthalmol, 2013. **91**(2): p. 189-90.

129. Jaime, G.R.L., et al., *Acute Variations in Retinal Vascular Oxygen Content in a Rabbit Model of Retinal Venous Occlusion.* PLoS One, 2012. **7**(11): p. e50179.
130. Mishra, A., A. Hamid, and E.A. Newman, *Oxygen modulation of neurovascular coupling in the retina.* Proceedings of the National Academy of Sciences, 2011. **108**(43): p. 17827-17831.
131. Denninghoff, K.R., et al., *Retinal Large Vessel Oxygen Saturations Correlate with Early Blood Loss and Hypoxia in Anesthetized Swine.* Journal of Trauma and Acute Care Surgery, 1997. **43**(1): p. 29-34.
132. Lo, L.W., C.J. Koch, and D.F. Wilson, *Calibration of oxygen-dependent quenching of the phosphorescence of Pd-meso-tetra (4-carboxyphenyl) porphine: a phosphor with general application for measuring oxygen concentration in biological systems.* Anal Biochem, 1996. **236**(1): p. 153-60.
133. Shonat, R.D., et al., *Oxygen distribution in the retinal and choroidal vessels of the cat as measured by a new phosphorescence imaging method.* Applied Optics, 1992. **31**(19): p. 3711-3718.
134. Zuckerman, R., J.E. Cheasty, and Y. Wang, *Optical mapping of inner retinal tissue PO2.* Current Eye Research, 1993. **12**(9): p. 809-825.
135. Duong, T.Q., et al., *Functional Magnetic Resonance Imaging of the Retina.* Investigative Ophthalmology & Visual Science, 2002. **43**(4): p. 1176-1181.
136. Prahl, S., *Optical absorption of hemoglobin*. 1999.
137. Beach, J.M., et al., *Oximetry of retinal vessels by dual-wavelength imaging: calibration and influence of pigmentation.* Journal of Applied Physiology, 1999. **86**(2): p. 748-758.
138. Hickam, J.B., R. Frayser, and J.C. Ross, *A study of retinal venous blood oxygen saturation in human subjects by photographic means.* Circulation, 1963. **27**: p. 375-85.
139. Hickam, J.B. and R. Frayser, *Spectrophotometric determination of blood oxygen.* Journal of Biological Chemistry, 1949. **180**(1): p. 457-465.
140. Delori, F.C., *Noninvasive technique for oximetry of blood in retinal vessels.* Applied Optics, 1988. **27**(6): p. 1113-1125.
141. Pittman, R.N. and B.R. Duling, *Measurement of percent oxyhemoglobin in the microvasculature.* J Appl Physiol, 1975. **38**(2): p. 321-7.

142. Schweitzer, D., et al., *Spectrometric investigations in ocular hypertension and early stages of primary open angle glaucoma and of low tension glaucoma--multisubstance analysis.* Int Ophthalmol, 1992. **16**(4-5): p. 251-7.
143. Thamm, E., D. Schweitzer, and M. Hammer, *A data reduction scheme for improving the accuracy of oxygen saturation calculations from spectrometric in vivo measurements.* Phys Med Biol, 1998. **43**(6): p. 1401-11.
144. Michelson, G. and M. Scibor, *Intravascular oxygen saturation in retinal vessels in normal subjects and open-angle glaucoma subjects.* Acta Ophthalmol Scand, 2006. **84**(3): p. 289-95.
145. Hammer, M., E. Thamm, and D. Schweitzer, *A simple algorithm for in vivo ocular fundus oximetry compensating for non-haemoglobin absorption and scattering.* Phys Med Biol, 2002. **47**(17): p. N233-8.
146. Drewes, J.J., et al. *Instrument for the measurement of retinal vessel oxygen saturation*. 1999.
147. Smith, M.H., *Optimum Wavelength Combinations for Retinal Vessel Oximetry.* Applied Optics, 1999. **38**(1): p. 258-267.
148. Denninghoff, K.R. and M.H. Smith, *Optical model of the blood in large retinal vessels.* J Biomed Opt, 2000. **5**(4): p. 371-4.
149. Drewes, J.J., et al. *An instrument for the measurement of retinal vessel oxygen saturation*. in *Proc. SPIE*. 1999.
150. Denninghoff, K.R., et al., *Retinal oximeter for the blue-green oximetry technique.* J Biomed Opt, 2011. **16**(10): p. 107004.
151. Hardarson, S.H., et al., *Automatic Retinal Oximetry.* Invest Ophthalmol & Vis Sci, 2006. **47**(11): p. 5011-5016.
152. Harris, A., et al., *A review of methods for human retinal oximetry.* Ophthalmic Surg Lasers Imaging, 2003. **34**(2): p. 152-64.
153. Palsson, O., et al., *Retinal Oximetry Images Must Be Standardized: A Methodological Analysis.* Investigative Ophthalmol & Vis Sci, 2012. **53**(4): p. 1729-1733.
154. Jani, P.D., et al., *Normative Values And Predictors Of Retinal Oxygen Saturation.* Retina, 2013.
155. Mordant, D.J., et al., *Spectral imaging of the retina.* Eye, 2011. **25**(3): p. 309-320.
156. Mordant, D.J., et al., *Validation of human whole blood oximetry, using a hyperspectral fundus camera with a model eye.* Invest Ophthalmol Vis Sci, 2011. **52**(5): p. 2851-9.

157. Geirsdottir, A., et al., *Retinal vessel oxygen saturation in healthy individuals.* Investigative Ophthalmology & Visual Science, 2012. **53**(9): p. 5433-5442.
158. Gloster, J., *Fundus oximetry.* Experimental Eye Research, 1967. **6**(3): p. 187-212.
159. Broadfoot, K.D., J. Gloster, and D.P. Greaves, *Photoelectric method of investigating the amount and oxygenation of blood in the fundus oculi.* British Journal of Ophthalmology, 1961. **45**(3): p. 161-182.
160. Laing, R.A., L.A. Danisch, and L.R. Young, *The choroidal eye oximeter: an instrument for measuring oxygen saturation of choroidal blood in vivo.* Biomedical Engineering, IEEE Transactions on, 1975(3): p. 183-195.
161. Gorman, A., D.W. Fletcher-Holmes, and A.R. Harvey, *Generalization of the Lyot filter and its application to snapshot spectral imaging.* Optics Express, 2010. **18**(6): p. 5602-5608.
162. Harvey, A. and D. Fletcher-Holmes, *Imaging Spectrometer*. 2003, WO Patent 2,003,089,890.
163. Alabboud, I., *Human retinal oximetry using hyperspectral imaging*, in *School of Engineering and Physical Sciences*. 2009, Heriot Watt University.
164. Ramella-Roman, J.C., et al., *Measurement of oxygen saturation in the retina with a spectroscopic sensitive multi aperture camera.* Opt Express, 2008. **16**(9): p. 6170-82.
165. Hirohara, Y., et al., *Validity of retinal oxygen saturation analysis: Hyperspectral imaging in visible wavelength with fundus camera and liquid crystal wavelength tunable filter.* Optical Review, 2007. **14**(3): p. 151-158.
166. Smith, M.H., et al., *Effect of Multiple Light Paths on Retinal Vessel Oximetry.* Applied Optics, 2000. **39**(7): p. 1183-1193.
167. de Kock, J.P., et al., *Reflectance pulse oximetry measurements from the retinal fundus.* IEEE Trans Biomed Eng, 1993. **40**(8): p. 817-23.
168. Saebvarnothing, K.B. and A. Bjvarnothingrnerud, *Accurate de-oxygenation of ex vivo whole blood using sodium Dithionite.* Proc. Intl. Soc. Mag. Reson. Med., 2000. **8**.
169. Crane, N.J., Z.D. Schultz, and I.W. Levin, *Contrast enhancement for in vivo visible reflectance imaging of tissue oxygenation.* Appl Spectrosc, 2007. **61**(8): p. 797-803.
170. Asakura, T. and J. Mayberry, *Relationship between morphologic characteristics of sickle cells and method of deoxygenation.* J Lab Clin Med, 1984. **104**(6): p. 987-94.
171. Thulborn, K.R., et al., *Oxygenation dependence of the transverse relaxation time of water protons in whole blood at high field.* Biochimica et Biophysica Acta (BBA) - General Subjects, 1982. **714**(2): p. 265-270.

172. in *http://webvision.med.utah.edu/2011/06/astrocyteblood-vessel-relationships*.
173. Suzuki, Y. and M. Yoshisuji, *[Retinal blood vessel measurement using a line sensor]*. Nihon Ganka Gakkai Zasshi, 1994. **98**(1): p. 92-7.
174. Baskurt, O.K., R.A. Farley, and H.J. Meiselman, *Erythrocyte aggregation tendency and cellular properties in horse, human, and rat: a comparative study.* Am J Physiol, 1997. **273**(6 Pt 2): p. H2604-12.
175. Barman, B.N., E.R. Ashwood, and J.C. Giddings, *Separation and Size Distribution of Red Blood Cells of Diverse Size, Shape, and Origin by Flow/Hyperlayer Field-Flow Fractionation.* Analytical Biochemistry, 1993. **212**(1): p. 35-42.
176. Clerbaux, T., et al., *Comparative study of the oxyhaemoglobin dissociation curve of four mammals: Man, dog, horse and cattle.* Comparative Biochemistry and Physiology Part A: Physiology, 1993. **106**(4): p. 687-694.
177. Nishi, O., et al., *Capsular bag refilling using a new accommodating intraocular lens.* J Cataract Refract Surg, 2008. **34**(2): p. 302-9.
178. Fernandez-Bueno, I., et al., *Muller and macrophage-like cell interactions in an organotypic culture of porcine neuroretina.* Mol Vis, 2008. **14**: p. 2148-56.
179. Ruiz-Ederra, J., et al., *The pig eye as a novel model of glaucoma.* Experimental Eye Research, 2005. **81**(5): p. 561-569.
180. Sanchez, I., et al., *The parameters of the porcine eyeball.* Graefe's Archive for Clinical and Experimental Ophthalmology, 2011. **249**(4): p. 475-482.
181. De Schaepdrijver, L., et al., *Morphologic and clinical study of the retinal circulation in the miniature pig. B: Fluorescein angiography of the retina.* Experimental Eye Research, 1992. **54**(6): p. 975-985.
182. Rootman, J., *Vascular system of the optic nerve head and retina in the pig.* Br J Ophthalmol, 1971. **55**(12): p. 808-19.
183. Simoens, P., L. De Schaepdrijver, and H. Lauwers, *Morphologic and clinical study of the retinal circulation in the miniature pig. A: Morphology of the retinal microvasculature.* Exp Eye Res, 1992. **54**(6): p. 965-973.
184. Bloodworth, J.M., Jr., H.P. Gutgesell, Jr., and R.L. Engerman, *Retinal vasculature of the pig. Light and electron microscope studies.* Exp Eye Res, 1965. **4**(3): p. 174-8.
185. Fischer, M.J., S. Uchida, and K. Messlinger, *Measurement of meningeal blood vessel diameter in vivo with a plug-in for ImageJ.* Microvasc Res, 2010. **80**(2): p. 258-66.

186. Hickam, J.B. and R. Frayser, *Studies of the Retinal Circulation in Man: Observations on Vessel Diameter, Arteriovenous Oxygen Difference, and Mean Circulation Time.* Circulation, 1966. **33**(2): p. 302-316.
187. Hannon, J.P., C.A. Bossone, and C.E. Wade, *Normal physiological values for conscious pigs used in biomedical research.* Lab Anim Sci, 1990. **40**(3): p. 293-8.
188. Traustason, S., et al., *Spectrophotometric Retinal Oximetry in Pigs.* Investigative Ophthalmology & Visual Science, 2013. **54**(4): p. 2746-2751.
189. Jeppesen, P., C. Aalkjaer, and T. Bek, *Myogenic response in isolated porcine retinal arterioles.* Curr Eye Res, 2003. **27**(4): p. 217-22.
190. Robinson, B.J., et al., *Mechanisms whereby propofol mediates peripheral vasodilation in humans. Sympathoinhibition or direct vascular relaxation?* Anesthesiology, 1997. **86**(1): p. 64-72.
191. Klockgether-Radke, A.P., et al., *Propofol and thiopental attenuate the contractile response to vasoconstrictors in human and porcine coronary artery segments.* Eur J Anaesthesiol, 2000. **17**(8): p. 485-90.
192. Kolh, P., et al., *Comparison of the effects of propofol and pentobarbital on left ventricular adaptation to an increased afterload.* J Cardiovasc Pharmacol, 2004. **44**(3): p. 294-301.
193. Garhofer, G., et al., *Retinal blood flow in healthy young subjects.* Invest Ophthalmol Vis Sci, 2012. **53**(2): p. 698-703.
194. Choudhary, T.R., et al., *Assessment of acute mild hypoxia on retinal oxygen saturation using snapshot retinal oximetry.* Invest ophthalmol & vis sci, 2013. **54**(12).
195. Lipowsky, H.H., S. Kovalcheck, and B.W. Zweifach, *The distribution of blood rheological parameters in the microvasculature of cat mesentery.* Circulation Research, 1978. **43**(5): p. 738-49.
196. Hardy, P., D.R. Varma, and S. Chemtob, *Control of cerebral and ocular blood flow autoregulation in neonates.* Pediatric Clinics of North America, 1997. **44**(1): p. 137-152.
197. Lassen, N.A., *Autoregulation of Cerebral Blood Flow.* Circ Res., 1964. **15**: p. SUPPL:201-4.
198. Patton, N., et al., *Retinal vascular image analysis as a potential screening tool for cerebrovascular disease: a rationale based on homology between cerebral and retinal microvasculatures.* J Anat, 2005. **206**(4): p. 319-48.

199. Paulson, O.B., S. Strandgaard, and L. Edvinsson, *Cerebral autoregulation.* Cerebrovasc Brain Metab Rev, 1990. **2**(2): p. 161-92.
200. Fog, M., *Cerebral circulation: The reaction of the pial arteries to a fall in blood pressure.* Archives of Neurology & Psychiatry, 1937. **37**(2): p. 351-364.
201. Fog, M., *Cerebral circulation: II. reaction of pial arteries to increase in blood pressure.* Archives of Neurology & Psychiatry, 1939. **41**(2): p. 260-268.
202. Aaslid, R., et al., *Cerebral autoregulation dynamics in humans.* Stroke, 1989. **20**(1): p. 45-52.
203. Ainslie, P.N., et al., *Dynamic cerebral autoregulation and baroreflex sensitivity during modest and severe step changes in arterial PCO_2.* Brain Research, 2008. **1230**(0): p. 115-124.
204. Iwasaki, K.-I., et al., *Acute exposure to normobaric mild hypoxia alters dynamic relationships between blood pressure and cerebral blood flow at very low frequency.* J Cereb Blood Flow Metab, 2006. **27**(4): p. 776-784.
205. Siebler, M., et al., *Cerebral Microembolism and the Risk of Ischemia in Asymptomatic High-Grade Internal Carotid Artery Stenosis.* Stroke, 1995. **26**(11): p. 2184-2186.
206. Bornstein, N.M., Z.G. Beloev, and J.W. Norris, *The limitations of diagnosis of carotid occlusion by Doppler ultrasound.* Ann Surg, 1988. **207**(3): p. 315-7.
207. Alexandrov, A.V., et al., *Measuring carotid stenosis. Time for a reappraisal.* Stroke, 1993. **24**(9): p. 1292-6.
208. Viedma, A., C. Jimenez-Ortiz, and V. Marco, *Extended Willis circle model to explain clinical observations in periorbital arterial flow.* J Biomech, 1997. **30**(3): p. 265-72.
209. Hendrikse, J., et al., *Collateral Ability of the Circle of Willis in Patients With Unilateral Internal Carotid Artery Occlusion: Border Zone Infarcts and Clinical Symptoms.* Stroke, 2001. **32**(12): p. 2768-2773.
210. Franssen, L., J.E. Coppens, and T.J.T.P. van den Berg, *Grading of Iris Color with an Extended Photographic Reference Set.* Journal of Optometry, 2008. **1**(1): p. 36-40.
211. Pournaras, C.J., et al., *Regulation of Subfoveal Choroidal Blood Flow in Age-Related Macular Degeneration.* Investigative Ophthalmology & Visual Science, 2006. **47**(4): p. 1581-1586.
212. Friedman, E., *A hemodynamic model of the pathogenesis of age-related macular degeneration.* American journal of ophthalmology, 1997. **124**(5): p. 677-682.
213. Nagaoka, T., et al., *Alteration of choroidal circulation in the foveal region in patients with type 2 diabetes.* British Journal of Ophthalmology, 2004. **88**(8): p. 1060-1063.

214. Schocket, L.S., et al., *Foveolar choroidal hemodynamics in proliferative diabetic retinopathy.* International ophthalmology, 2004. **25**(2): p. 89-94.
215. Kristjansdottir, J.V., et al., *Choroidal Oximetry With a Noninvasive Spectrophotometric Oximeter.* Investigative Ophthalmology & Visual Science, 2013. **54**(5): p. 3234-3239.
216. Denninghoff, K.R., et al., *Retinal large vessel oxygen saturations correlate with early blood loss and hypoxia in anesthetized swine.* J Trauma, 1997. **43**(1): p. 29-34.
217. Olafsdottir, O.B., et al., *Retinal oxygen metabolism in healthy subjects and glaucoma patients.* Br J Ophthalmol, 2014.
218. Lim, L.S., L. Tan, and S.A. Perera, *Retinal vessel oxygen saturation increases after vitrectomy.* Investigative Ophthalmology & Visual Science, 2014.
219. Traustason, S., et al., *Retinal Oxygen Saturation in Patients with Systemic Hypoxemia.* Investigative Ophthalmology & Visual Science, 2011. **52**(8): p. 5064-5067.